Postsynthetic Modification of Nucleic Acids and Generation of Nucleoside Supramolecular Synthons by Palladium-Mediated Reactions

A thesis submitted in partial fulfilment of the requirements

for the degree of

Doctor of Philosophy

by

Manisha Balasaheb Walunj

20143327

Research Supervisor

Prof. Seergazhi G. Srivatsan

Indian Institute of Science Education and Research, Pune

2020

This thesis is dedicated to my parents

INDIAN INSTITUTE OF SCIENCE EDUCATION AND RESEARCH (IISER),
(An Autonomous Institution, Ministry of Human Resource Development, Govt. of India)
Dr. Homi Bhabha Road, Pashan, Pune–411 008

Prof. Seergazhi G. Srivatsan
Department of Chemistry
Wellcome Trust DBT-India Alliance Senior Fellow

CERTIFICATE

Certified that the work incorporated in the thesis entitled *"**Postsynthetic Modification of Nucleic Acids and Generation of Nucleoside Supramolecular Synthons by Palladium-Mediated Reactions"*** submitted by Miss. Manisha Balasaheb Walunj was carried out by the candidate under my supervision. The work presented here or any part of it has not been included in any other thesis submitted previously for the award of any degree or diploma from any other University or Institution.

S.G. Srivatsan

Date: May 20, 2020
Place: Pune

Professor Seergazhi G. Srivatsan

Tel.: +91-20-25908086 E-mail: srivatsan@iiserpune.ac.in

Declaration

I declare that this written submission entitled " **Postsynthetic Modification of Nucleic Acids and Generation of Nucleoside Supramolecular Synthons by Palladium-Mediated Reactions"** submitted for Doctor of Philosophy in Chemistry at Indian Institute of Science Education and Research, Pune, represents my ideas in my own words and wherever other's ideas have been included; I have adequately cited and referenced the original sources. I also declare that I have adhered to all the principles of academic honesty and integrity and have not misrepresented or fabricated or falsified any idea/data/fact/source in my submission. The reported work in this thesis was carried out at the Indian Institute of Science Education and Research, Pune, India, under the guidance of Professor Seergazhi G. Srivatsan.

Date: May 20, 2020 **Manisha Balasaheb Walunj**

Place: Pune Reg. No: 20143327

Acknowledgement

Foremost, I would like to express my deepest gratitude to my thesis supervisor, prof. Seergazhi G. Srivatsan. His immense knowledge, valuable guidance and encouragement were the key motivations during my PhD years. I highly admire his way of analysing data, approaching and designing the new experiments. Along with a good mentor, he is a good human being, and that's what makes him more lovable. I cannot think of better supervisor to have.

I sincerely thank Prof. Jayant B. Udgaonkar (present director, IISER Pune) and Prof. K. N. Ganesh (former director, IISER Pune) for providing the excellent infrastructure and facilities to pursue my doctoral research. I would like to express my sincere gratitude to my research advisory committee RAC members Dr. B. Gnanaprakasam and Dr. H. V. Thulasiram for providing critical suggestion during RAC meeting. I want to thank Prof. H. N Gopi, Chair Chemistry for all departmental facilities. I appreciate all non-teaching and technical staffs, particularly Chinmay, Swati, Mahesh, Mayuresh, Tushar, Sayalee, and Sandeep for their help. I particularly thank Rupam from Prof. Jayant B. Udgaonkar's lab for his extensive help in ESI-MS analysis of DNA ONs which I have used in chapter 3. I am thankful to Council of Scientific and Industrial Research (CSIR) India for a research fellowship and IISER Pune Infosys foundation for travel support to attend an international conference.

It's my great pleasure to acknowledge my former and present labmates Dr.Maroti, Dr. Anupam, Dr. Arun, Dr. Pramod, Dr. Ashok, Dr.Sudeshna, Dr.Vyankat, Dr. Cornelia, Dr.Jerrin, Pankaj, Saddam, Pulak, Akanksha, Sarupa, Swagata, Samiksha, Uddhav and Sangamesh. Their help during my lab work and improving my presentations skills made my PhD journey smoother.

I am forever debited to my parents (Aai-Aappa) for their unconditional love and unbreakable support—the unsung warrior of my life, my father (Aappa), who is always there to support my opinion and decision about my career. My mother (Aai), she played multiple roles in my life, she is my wonder woman, my teacher, my friend and many more. She has raised her two daughters, along with her teaching career with so much perfection. This skill of her is always going to boost me to accomplish my professional as well as personal life. I want to thank a brilliant person with whom I share an unbreakable childhood-bond, my soul-sister Sujata, who always stood by my side, no matter what. I am forever grateful to her for making me a steadfast person to tackle the hurdles in my path. Most of all, I owe my deepest

gratitude to love of my life, my husband, Pavan, for his enduring love and patience. His help in correcting the drafts for the paper and thesis helped me a lot to improve my writing skill. He has stood by me through my fits of anger and impatience. He gave me complete support and help, discussed ideas and prevented several wrong turns in my life.

Manisha Balasaheb Walunj

Table of contents

Abbreviations

2-AP	2-Aminopurine
A	Adenosine
ACN	Acetonitrile
ADHP	2-aminopyrimidine-4,6-diol
ATP	Adenosine Triphosphate
BrU	5-bromouridine
C	Cytosine
CD	Circular Dichroism
CGC	Critical gelation concentration
CTP	Cytidine Triphosphate
DMADHP	2-Dimethylaminopyrimidine-4,6-diol
DMAP	4-Dimethylaminopyridine
DMF	Dimethylformamide
DMSO	N, N-dimethyl sulfoxide
DMT	Dimethoxytrityl
DNA	Deoxyribonucleic acid
dNTP	Deoxynucleoside Triphosphate
3D	Three Dimensional
ds	Double-stranded
dU	2′-deoxyuridine
dA	2′-deoxyadenosine
dG	2′-deoxyguanosine
dT	Thymidine
EDC	1-(3-Dimethylaminopropyl)-3-ethylcarbodiimide
EDTA	Ethylenediaminetetraacetic Acid
em	Emission
EPR	Electron Paramagnetic Resonance
ESI-MS	Electrospray Ionization Mass Spectroscopy
ex	Excitation
FDA	Food Drug Administration
FESEM	Field Emission Scanning Electron Microscopy

G	Guanosine
GFP	Green Fluorescence Protein
GQ	G-quadruplex
HPA	Hydroxyl picolinic Acid
HPLC	High Performance Liquid Chromatography
H-Telo	Human Telomeric
Hz	Hertz
IdU	5-iodo-2′-deoxyuridine
IEDDA	Inverse electron-demand Diels–Alder
in vitro	Outside living organism
in vivo	Inside living organism
IU	5-iodouridine
IUTP	5-iodouridine-5′-triphosphate
LMWG	Low Molecular Weight Gel
MALDI-TOF	Matrix Assisted Laser Desorption Ionisation-Time of flight
max	Maximum
MeOH	Methanol
mg	Milligram
MHz	Megahertz
mM	Milimolar
NBD-Cl	4-Chloro-7-nitrobenzo-2-oxa-1,3-diazole
nm	Nanometer
nM	Nanomolar
NMR	Nuclear Magnetic Resonance
NOESY	Nuclear Overhauser Effect Spectroscopy
NTP	Nucleoside Triphosphate
ON	Oligonucleotide
Pa	Pascal
PAGE	Polyacrylamide Gel Electrophoresis
PBH	Pinacolborane
PCR	Polymerase Chain Reaction
Pd	Palladium
PDB	Protein Data Bank

PEG200	Polyethylene glycol 200
PELDOR	Pulse Electron Double Resonance
PG	Protecting groups
ppm	Parts per million
PXRD	Powder X-ray Diffraction
R_f	Retention factor
RNA	Ribonucleic acid
RNase	Ribonuclease
ss	Single-stranded
SSB	Single-strand binding
T	Thymine
TCA	Trichloroacetic acid
TEAA	Triethylammonium acetate
THF	Tetrahydrofuran
TLC	Thin layer chromatography
Tm	Thermal melting
TMEDA	*N*,*N*,*N*′,*N*′-Tetramethylethylenediamine
TMS	Tetramethylsilane
TPA	2,2,5,5-tetramethyl-pyrrolin-1-yloxyl-3-acetylene
TPPTS	triphenylphosphan-3,3′,3″-trisulfonate
Tris	Tris (hydroxymethyl) Amino Methane
U	Uridine
UTP	Uridine 5′-triphosphate
UV	Ultraviolet
WC	Watson-Crick
ε	Molar extinction coefficient
μL	Microliter
μM	Micromolar

Synopsis

Postsynthetic Modification of Nucleic Acids and Generation of Nucleoside Supramolecular Synthons by Palladium-Mediated Cross-Coupling Reactions

Background and Aim

Probing the structure of nucleic acids is paramount in understanding their recognition properties and ensuing functions. Nucleic acids are commonly studied by biophysical techniques like fluorescence, NMR, EPR and X-ray crystallography, to name a few.[1–4] The majority of these techniques use DNA and RNA oligonucleotides (ONs) labeled with appropriate biophysical probes as components of nucleic acids do not contain intrinsic labels such as fluorophores, NMR isotopes, paramagnetic and heavy atoms that are suitable for efficient analysis. Labeled ONs are commonly synthesized by either solid-phase ON synthesis or enzymatic methods. While solid-phase protocol is a convenient approach to construct site-specifically labeled ON sequences, longer nucleic acids are made by using nucleic acid processing enzymes such as polymerases[5–8] and nucleotide transferase.[9–11] In case of chemical method, certain modified amidites show poor coupling efficiency or they do not survive harsh conditions employed in solid-phase method. On the other hand, enzymatic incorporation works under mild conditions, but in several instance the unnatural substrates are not well accepted by the enzymes.[12] Hence, there is constant demand for the development of new labeling strategies that will provide access to a wide variety of labeled ONs.

In this direction, postsynthetic chemical modification strategies using chemoselective reactions have emerged as powerful tools to label proteins, glycans, lipids and nucleic acids.[13] In these methodologies, an ON is synthesized with a small reactive group, which is then functionalized with desired biophysical tags by using chemoselective reactions. Copper-catalyzed azide-alkyne cycloaddition, strain promoted azide-alkyne cycloaddition, Staudinger ligation, inverse electron demand Diels–Alder, to name a few, are used in labeling DNA and RNA ONs that are suitable for *in vitro* and in cell nucleic acid analysis.[14–18] However, some of these methods use bulky activated building blocks (e.g., cyclooctyne, tetrazine), which could affect the original function of the nucleic acid, and also the synthesis of many of these building blocks is tedious and involves multiple steps.[19–21] The use of linkers to span the reactive handle and bulky building blocks could serve as a solution, but this would not allow direct attachment of environment-sensitive nucleoside probes to nucleic acids. Therefore,

development of a modular labeling strategy to directly install microenvironment-sensitive probes onto ONs postsynthetically will complement existing tools in probing nucleic acid structure and function.

Modified nucleoside and nucleotide analogs have greatly aided the understanding of nucleic acid structure-function relationship and in developing nucleic acid-based diagnostic tools and supramolecular assemblies. A key chemical transformation, which has been a backbone in preparing such nucleoside analogs is C-C bond formation using palladium-catalyzed cross-coupling reactions.[22] While this methodology has been implemented in synthesizing various nucleoside probes, which are then incorporated into nucleic acids, their implementation in directly introducing functional tags on nucleic acid is quite a challenge for the following reasons.

i. Palladium can coordinate to the nitrogenous bases present in the ON, thereby compromising the catalytic activity.
ii. Steric hindrance could also play a significant role in the reaction efficiency at the ON level.
iii. Most of the Pd-mediated cross-coupling reactions demands alkaline conditions. Thus carrying out Pd-mediated transformations on nucleic acid, especially RNA, is challenging owing to its inherent instability in alkaline conditions.

Hence, the development of postsynthetic Pd-mediated reactions to label RNA ONs remains a major challenge.

This doctoral dissertation describes the (i) development of a modular postsynthetic modification method to label DNA/RNA ONs and (ii) generation of nucleoside supramolecular synthons by using palladium-mediated cross-coupling reactions. In the first part, we illustrate the development of a Pd-mediated posttranscriptional Suzuki–Miyaura cross-coupling reaction to label RNA with various biophysical probes. This method is highly chemoselective and offers direct access to RNA ONs labeled with commonly used fluorescent and affinity tags and new fluorogenic environment-sensitive nucleoside probes in a ligand-controlled stereoselective fashion. Further, we explored the influence of nucleic acid conformations on the Suzuki–Miyaura cross-coupling reaction using polymorphic G-quadruplex forming sequences as the study model. We observed that the cross-coupling reaction works in a conformation-dependent manner and conformational selectivity of the reaction decreased in the order of – GQ topology > single-stranded DNA and no reaction with double-stranded DNA. In the second part of the doctoral dissertation, we describe the

utility of Pd-mediated cross-coupling reaction to develop environment-sensitive fluorescent deoxyguanosine nucleolipids. These fluorescent nucleolipids support gel formation and show interesting chemo- and thermo-responsive behaviour upon self-assembling. Taken together, the results presented in this thesis highlight the potential of Pd-mediated cross-coupling reactions in generating functionalized nucleic acids for biophysical analysis and supramolecular assemblies for material applications.

The thesis is organized into following four Chapters:

Chapter 1: Application of Palladium-Mediated Transformations in Generating Labeled Nucleic Acids and Nucleoside Supramolecular Synthons

In this chapter, a comprehensive discussion on how chemists have developed and judiciously applied palladium-mediated cross-coupling reactions like Suzuki–Miyaura, Sonogashira, Stille and Heck to synthesize modified nucleoside and nucleotide analogs suitable for labeling of nucleic acids is discussed. Following this, applications of Pd-mediated cross-coupling reactions to postsynthetically functionalize DNA/RNA ONs with various biophysical reporters are presented. In the second part of this chapter, applications of various nucleoside supramolecular synthons and architectures, particularly related to guanine derivatives are presented. The motivation behind developing efficient and robust palladium-mediated cross-coupling reaction to label nucleic acids and further utilization of the cross-coupling reaction to develop a new class of guanosine-based supramolecular synthons is discussed.

Chapter 2: Posttranscriptional Labeling by Using Suzuki–Miyaura Cross-Coupling Generates Functional RNA probes

Pd-catalyzed C-C bond formation, an important vertebra in the spine of synthetic chemistry, is emerging as a valuable chemoselective transformation for postsynthetic functionalization of biomacromolecules. While methods are available for labeling protein and DNA, development of an analogous procedure to label RNA by cross-coupling reactions remains a major challenge. In chapter 2, we describe a new Pd-mediated RNA oligonucleotide (ON) labeling method that involves posttranscriptional functionalization of iodouridine (IU)-labeled RNA transcripts by using Suzuki–Miyaura cross-coupling reaction.[23] 5-Iodouridine triphosphate (IUTP) is efficiently incorporated into RNA ONs at one or more sites by T7 RNA polymerase. Further, using a catalytic system made of $Pd(OAc)_2$ and 2-

aminopyrimidine-4,6-diol (ADHP) or dimethylamino-substituted ADHP (DMADHP), we established a modular method to functionalize iodouridine-labeled RNA ONs in the presence of various boronic acid and ester (**2**–**10**) substrates under very mild conditions (37 °C and pH 8.5) (Figure 1).

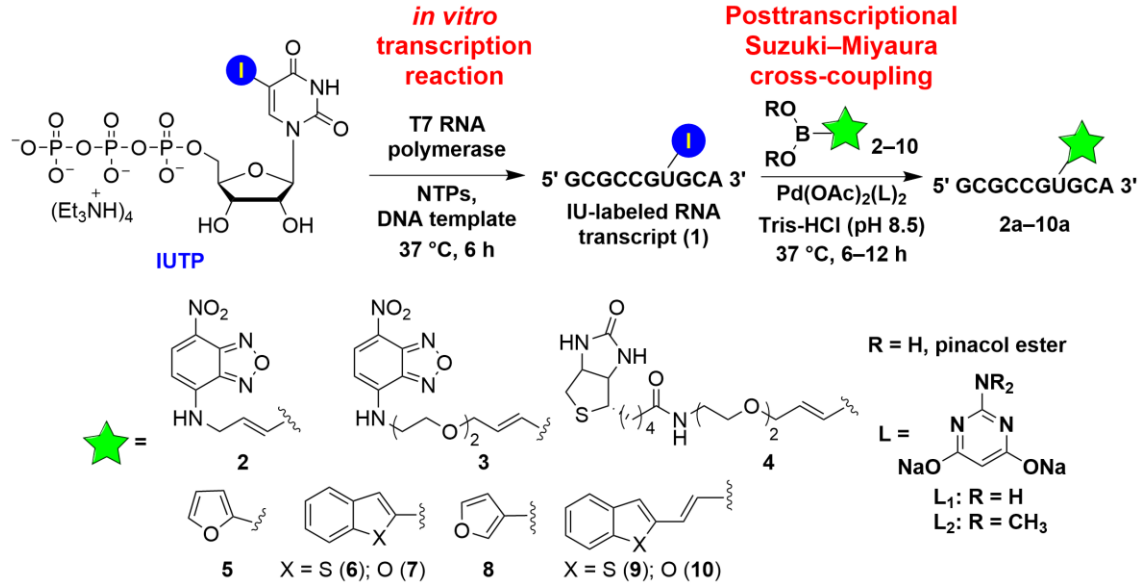

Figure 1. Incorporation of iodo-modified uridine triphosphate (IUTP) into RNA transcript by *in vitro* transcription, followed by posttranscriptional functionalization of IU-labeled RNA transcript **2** by using Suzuki–Miyaura cross-coupling reaction to generate RNA labeled with various functional probes (**2a**−**10a)**.

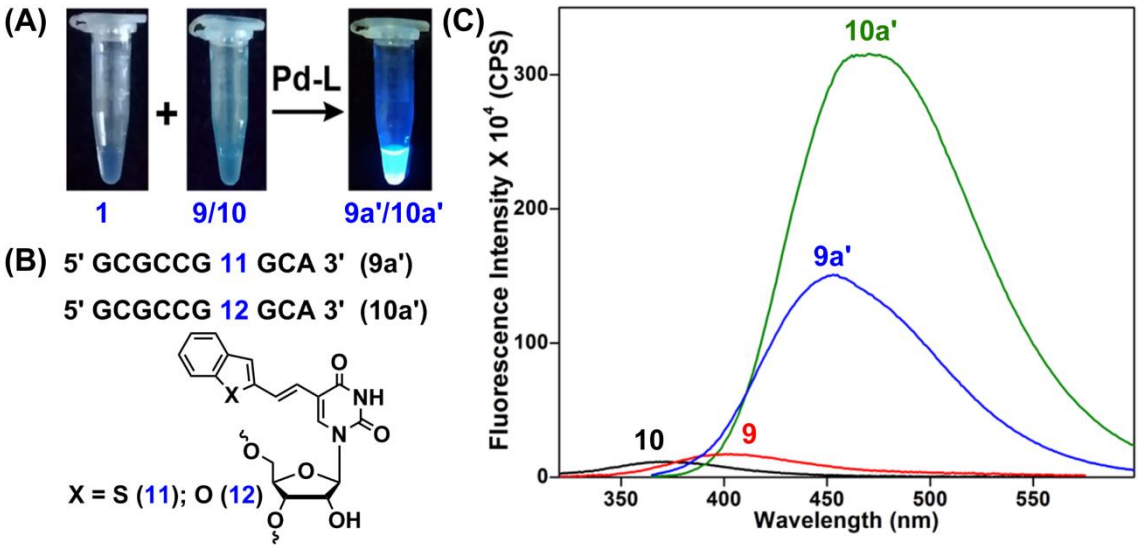

Figure 2. (**A**) Image showing the fluorogenic Suzuki coupling of IU-labeled RNA transcript **1** with boronic ester **9** and **10**. The samples were irradiated using 365 nm light source. (**B**) Structures of **11** and **12** modified RNA transcripts **9a'**and **10a'**, respectively. (**C**) Emission spectra (1 µM) of substrates (very weakly emissive) and RNA ON cross-coupled products **9a'** and **10a'** (highly emissive).

Further, the coupling of nonemissive IU-labeled RNA **1** with very weakly emissive boronic ester **9** and **10** gave highly fluorescent RNA products **9a'** and **10a'**, respectively (Figure 2). In particular, 5-(benzofuran-2-yl)vinyluridine (**12**)-modified RNA ON **10a'** displayed more than 25-fold enhancement in fluorescence intensity as compared to boronic ester **10**.

This method is highly chemoselective, and offers direct access to RNA ONs labeled with commonly used fluorescent and affinity tags and new fluorogenic environment-sensitive nucleoside probes in a ligand-controlled stereoselective fashion. Taken together, this simple approach of generating functional RNA ON probes by Suzuki–Miyaura coupling will be a very important addition to the resources and tools available for analyzing RNA motifs.

Chapter 3: Effect of nucleic acid conformation on the efficiency of Suzuki–Miyaura cross-coupling reaction: Polymorphic G-quadruplex structure as a study model

We have successfully developed the posttranscriptional Suzuki–Miyaura cross-coupling reaction to label the RNA molecules in chapter 2. Herein, we explore the influence of nucleic acid conformational space on the efficiency of postsynthetic Suzuki–Miyaura cross-coupling reaction. 5-Iodo-2′-deoxyuridine (IdU) is incorporated site-specifically into various H-Telo G-rich DNA sequences, which upon annealing in different ionic conditions and in the presence of a synthetic molecular crowding agent (PEG) form different GQ structures (Figure 3). Next, we have performed postsynthetic Suzuki–Miyaura cross-coupling reaction on respective IdU-modified DNA conformations using benzofuran boronic acid in presence of Pd catalyst. To perform postsynthetic Suzuki–Miyaura reaction we have used similar reaction conditions which is described in chapter 2 (Tris-HCl pH = 8.5, 20% DMSO). Importantly, CD and thermal melting analysis of IdU-modified and control unmodified H-Telo DNA GQ revealed the IdU incorporation and Suzuki–Miyaura coupling reaction conditions did not affect the GQ structure and stability.

All the ONs used in this study form a random unfolded structure in the presence of LiCl[24], antiparallel GQ topology in the presence of NaCl and hybrid-type topology (hybrid 1 and hybrid 2) in KCl solution (Figure 3B).

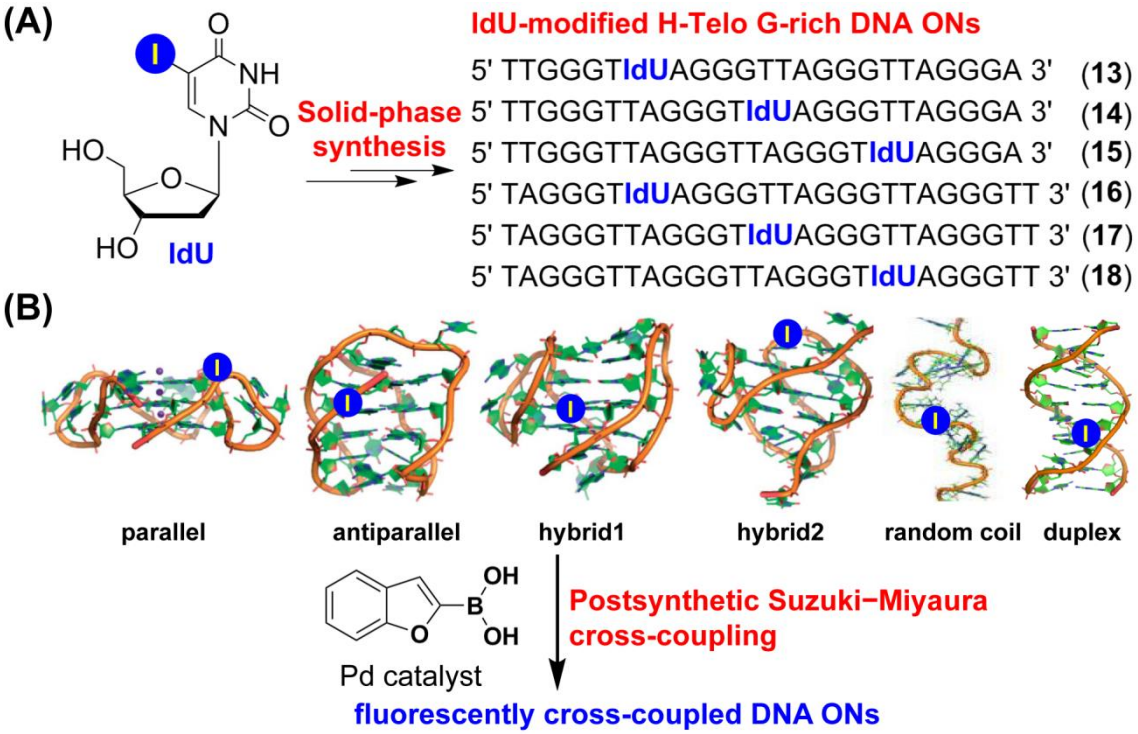

Figure 3. (**A**) Incorporation of 5-iodo-2′-deoxyuridine (IdU) into the G-rich H-Telo DNA sequence (5′-d[$T_2G_3(T_2AG_3)_3A$]-3′ (24-mer) and 5′-d[$TAG3(T_2AG_3)_3T_2$]-3′) (25-mer); the dT residues in the first (**13** and **16**), second (**14** and **17**) and third (**15** and **18**) loops of H-Telo DNA ONs were replaced with IdU. (**B**) A schematic illustration of the different conformations formed by IdU-modified H-Telo DNA ONs upon annealing in presence of different ionic conditions or in the presence of a synthetic molecular crowding agent (PEG) or in presence of complimentary c-rich DNA strand followed by postsynthetic Suzuki–Miyaura cross-coupling reaction using benzofuran boronic acid and Pd catalyst.

Rewardingly, HPLC analysis of reaction mixture shows, when the reactions were performed with G-quadruplex structures the yields of the cross-coupled ON products were considerably higher than when the reactions were performed with the random unfolded structures formed by the same sequences (Figure 4). We found when the IdU was placed at the second thymidine residue of the first, second or third loop **(**ONs **13**–**18**), the reaction efficiency was found to vary with the position of iodo modification (Figure 4). Interestingly, an antiparallel GQ topology formed by 24-mer DNA ON **15** in which IdU is present in the third loop gave 2 to 3-fold higher yields of the product than ONs **13** and **14** in which the modification is present in the first and second loop, respectively (Figure 4A). For the same set of sequences (ONs **13–15**) in the presence of K^+ ions, the yields for the cross-coupled product was very similar irrespective of the position of iodo modification. However, reactions with 25-mer ON sequences **16**–**18** the trend was reversed. In Li^+ and Na^+ ionic conditions, the ONs gave similar amounts of the coupled ON products irrespective of position of

modification (Figure 4B). However, for the same ONs (**16**–**18)** in presence of K^+ ions showed difference in cross-coupling efficiency. There was a progressive increase in the product yield as the iodo position was moved from first (**16**) to second (**17**) and to the third loop (**18**). Apart from labeling random unfolded and H-Telo DNA GQ structures with benzofuran probes, the Suzuki coupling reaction did not work on the corresponding duplex form, suggesting a conformational dependence of the reaction.

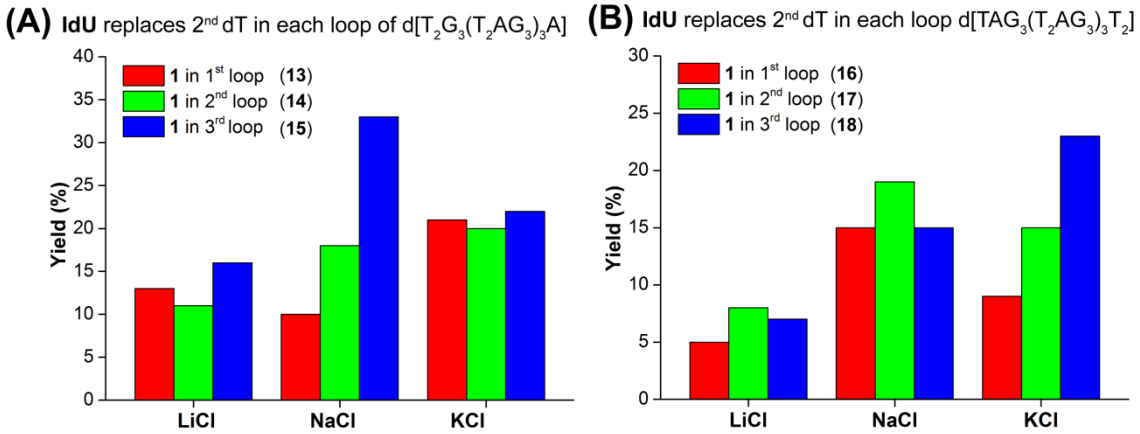

Figure 4. Bar diagram for isolated yields of fluorescently labelled DNA ONs after Suzuki cross-coupling when IdU in first, second and third loop in the presence of LiCl, NaCl and KCl. (**A**) **13**, **14** and **15**. (**B**) **16**, **17** and **18**.
Figure 4A shows the preferential formation of cross-coupled product in the lateral (third) loop of GQ formed by 5′-d[$T_2G_3(T_2AG_3)_3A$]-3′(24-mer) DNA sequences in Na^+ solution.
Figure 4B shows the preferential formation of cross-coupled product in the double chain reversal (third) loop of GQ formed by 5′-d[TAG3$(T_2AG_3)_3T_2$]-3′ (25-mer) DNA sequences in K^+ solution.

Altogether, in this chapter we have shown that postsynthetic Suzuki–Miyaura cross-coupling reaction exhibits both the chemo- and conformational selectivity and isolated yields for GQ topology > random unfolded strand DNA and no reaction with double-stranded DNA. Analysis of available 3D structures for hybrid and antiparallel GQ[25–27] reveals, electronic and steric effects originating from the nucleotide conformation results in differences in reactivity exhibited by the ONs adopting different conformations. We believe that this approach might apply to the conformational sampling of cellular DNA as well as different GQ topologies through C-C bond formation.[28]

Chapter 4: Supramolecular synthons made of an environment-sensitive fluorescent nucleoside exhibits interesting emission properties upon self-assembly

Despite the immense progress in the area of guanine-based supramolecular self-assembly, use of fluorescently modified lipophilic guanine derivatives in developing responsive fluorescent organogel has not been well explored. Attachment of aryl groups onto

guanine can be a convenient choice to create such fluorescently modified synthons for constructing the fluorescent supramolecular assemblies, which can also provide an additional noncovalent interaction such as π–π stacking. To accomplish this, we envisioned to incorporate suitable aryl moieties, which could impart fluorescence as well as offer the opportunity to modulate the self-assembly using external stimuli. In chapter 2 and 3, we have described the usefulness of palladium-mediated cross-coupling reaction in developing fluorescent environment-sensitive nucleoside scaffolds. While, in this chapter we have utilized the similar scaffolds for developing fluorescent environment-sensitive deoxyguanosine nucleolipids. Herein, lipophilic fluorescent deoxyguanosine molecules (OAcBFVdG, OmyrBFVdG and OpalBFVdG) were synthesized by using Pd-mediated Suzuki-Miyaura cross-coupling reaction followed by alcohol-acid coupling (Figure 5).

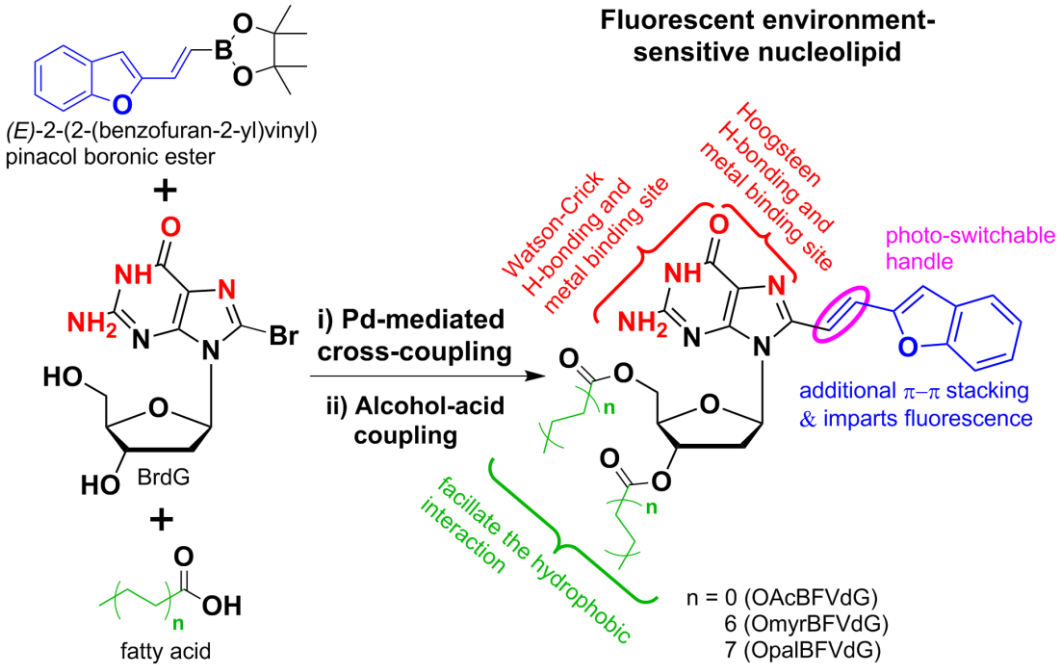

Figure 5. Design of self-assembling lipophilic fluorescent environment-sensitive deoxyguanosine.

We show that simple mixing of a non-gelling guanosine derivative OAcBFVdG with the gelator guanosine in presence of 500 mM potassium chloride results in the formation of a stable cogel, which not only efficiently hindered the crystallization process in guanosine hydrogel but also modulated the mechanical properties as well as the morphology of the cogel (Figure 6A). The cogel shows very weak fluorescence in the assembled state with emission maximum around 510 nm (Figure 6B). When the temperature of the cogel is increased from 25 °C to 85 °C, non-covalent interactions break and the gel disassembles.

Interestingly, the disassembled gel shows very high fluorescence with a hypsochromic shift from 510 nm to 474 nm. We believe that the ability to access fluorescent cogel of guanosine with nongelator opens the door for tailoring the properties of guanosine gels

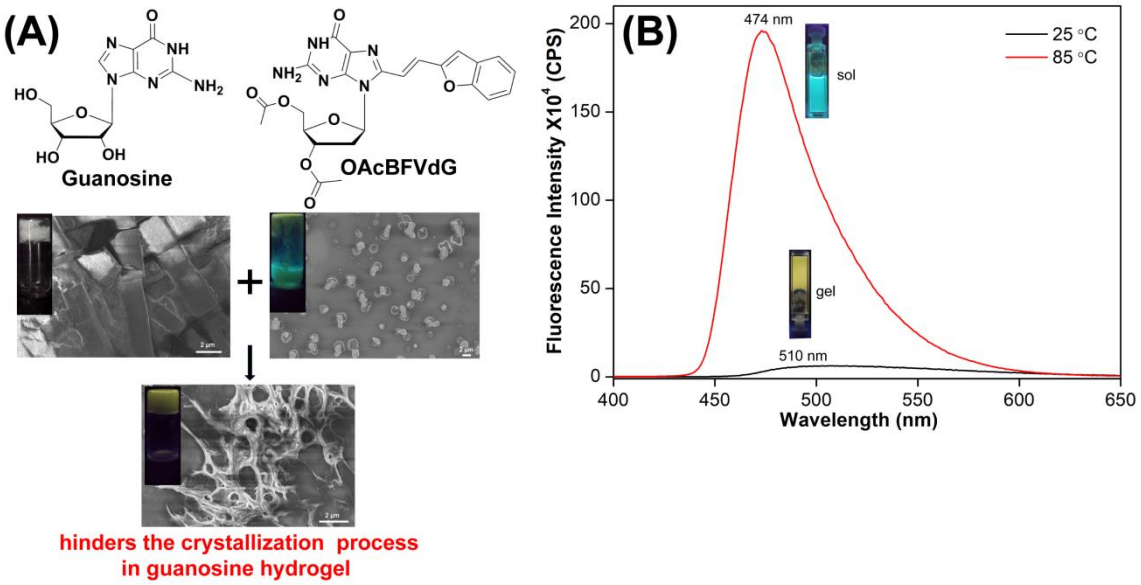

Figure 6. (**A**) FESEM images of guanosine, OAcBFVdG and cogel obtained by mixing guanosine and OAcBFVdG, vials shadowed at 365 nm wavelength. (**B**) Fluorescence spectra for cogel made up 35 wt% of OAcBFVdG and 65 wt% guanosine in DMSO:H_2O (at CGC concentration) at two different temperature 25 °C (gel state, λ_{em} = 510 nm) 85 °C (sol state, λ_{em} = 474 nm). The samples were excited at 387 nm with an excitation and emission slit width of 1 nm and 2 nm, respectively.

Following this, we also synthesized lipophilic deoxyguanosine molecules containing longer alkyl chains like myristoyl (C14, OmyrBFVdG) and palmitoyl (C16, OpalBFVdG), respectively (Figure 5). These nucleolipids form stable fluorescent organogel in DMSO and show remarkable self-assembly properties. Notably, when complementary nucleolipid cytidine dimyristate is added to the fluorescent organogel formed by OmyrBFVdG, the original emission wavelength shifts from 497 nm to the 543 nm (green to yellow fluorescent, Figure 7). Furthermore, the emission properties of cogel, which is made of a nucleolipid OmyrBFVdG and dimyristate cytidine, is responsive to changes in temperature. When the temperature of the cogel is increased from 25 °C to 75 °, the fluorescence intensity increases with a blue-shift from 543 nm to 486 nm (Figure 7B). Such multi-stimuli responsive fluorescent organogels can be employed in constructing chemical and temperature sensors.[29]

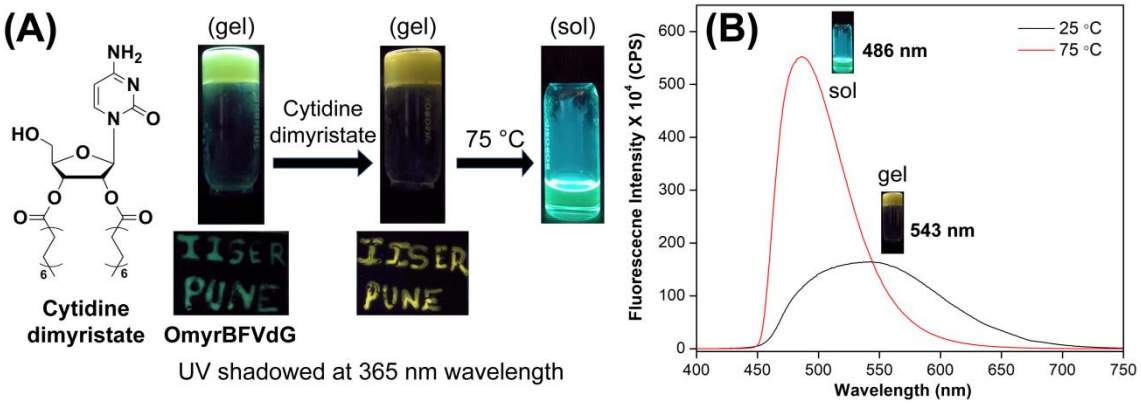

Figure 7. (A) Structure of nucleolipid cytidine dimyristate and picture of vials showing changes in emission colour after the addition of cytidine dimyristate to the organogel made up of OmyrBFVdG. **(B)** Fluorescence spectra for cogel made up of OmyrBFVdG and cytidine dimyristate (1:5 millimolar ratio) in DMSO (at CGC concentration of OmyrBFVdG) at two different temperature 25 °C (gel state, λ_{em} = 543 nm) 75 °C (sol state, λ_{em} = 486 nm). The samples were excited at 387 nm with an excitation and emission slit width of 2 nm and 3 nm, respectively.iv

References

1. Tanpure, A. A.; Pawar, M. G.; Srivatsan, S. G. Fluorescent nucleoside analogs: Proves for investigating nucleic acid structure and function. *Isr. J. Chem.* **2013**, *53*, 366–378.
2. Carlomagno, T. Present and future of NNR for RNA-protein complexes: A perspective of integrated structural biology. *Journal of Magnetic Resonance* **2014**, *241*, 126–136.
3. Zhang, W.; Szostak, J. W.; Huang, Z. Nucleic acid crystallization and X-ray crystallography facilitated by single selenium atom. Front. *Chem. Sci. Eng.* **2016**, *10*, 196–202.
4. Sowa, G. Z.; Qin, P. Z. Site-directed spin labeling studies on nucleic acid structure and dynamics. *Progress in nucleic acid research and molecular biology* **2008**, *82*, 147–197.
5. Rao, H.; Tanpure, A. A.; Sawant, A. A.; Srivatsan, S. G. Enzymatic incorporation of an azide-modified UTP analog into oligoribonucleotides for post-transcriptional chemical functionalization. *Nat. Protoc.* **2012**, *7*, 1097–1112.
6. George, J. T.; Srivatsan, S. G. Vinyluridine as a versatile chemoselective handle for the posttranscriptional chemical functionalization of RNA. *Bioconjug. Chem.* **2017**, *28*, 1529–1536.
7. Hocek, M. Synthesis of base-modified 2′-deoxyribonucleoside triphosphates and their use in enzymatic synthesis of modified DNA for applications in bioanalysis and chemical biology. *J. Org. Chem.***2014**, *79*, 9914–9921.
8. Ménová, P.; Vrábel, M.; Cahová, H.; Hocek, M. Synthesis of base-modified dNTPs through cross-coupling reactions and their polymerase incorporation to DNA (Book Chapter), in Non-Natural Nucleic Acids: Methods and Protocols, *Methods in Molecular Biology* (N. Shank ed.), Humana Press, New York, NY, **2019**, *1973*, 39–57.
9. Winz, M. -L.; A. Samanta, A.; Benzinger, D.; Jäschke, A. Site-specific terminal and internal labeling of RNA by poly(A) polymerase tailing and copper-catalyzed or copper-free strain-promoted click chemistry. *Nucleic Acids Res.* **2012**, *40*, e78.
10. Holstein, J. M.; Rentmeister, A. Current covalent modification methods for detecting RNA in fixed and living cells. *Methods* **2016**, *98*, 18–25.
11. Muthmann, N.; Hartstock, K.; Rentmeister, A. Chemo-enzymatic treatment of RNA to facilitate analyses. *Wiley Interdiscip. Rev. RNA* **2019**, https://doi.org/10.1002/wrna.1561

12. Beaucage, S. L.; Reese, C. B. Recent advances in the chemical synthesis of RNA. *Curr.Protoc. Nucleic Acid Chem*. **2009**, *38*, 2.16.1–2.16.31.
13. Merkel, M.; Peewasan, K.; Arndt, S.; Ploschik, D.; Wagenknecht, H. -A. Copper-free postsynthetic labeling of nucleic acids by means of bioorthogonal reactions. *Chembiochem.* **2015**, *16*, 1541–1553.
14. Saxon, E.; Bertozzi, C. R. Cell surface engineering by a modified Staudinger reaction. *Science* **2000**, *287*, 2007–2010.
15. Asare-Okai, P. N.; Agustin, E.; Fabris, D.; Royzen, M. Site-specific fluorescence labeling of RNA using bio-orthogonal reaction of trans-cyclooctene and tetrazine. *Chem. Commun.* **2014**, *50*, 7844–7847.
16. Kath-Schorr, S. Cycloadditions for studying nucleic acids. *Top. Curr. Chem.* **2016**, 374, 4.
17. Sawant, A. A.; Tanpure, A. A.; Mukherjee, P. P.; Athavale, S.; Kelkar, A.; Galande, S.; Srivatsan, S. G. A versatile toolbox for posttranscriptional chemical labeling and imaging of RNA. *Nucleic Acids Res.* **2016**, *44*, e16.
18. Someya, T.; Ando, A.; Kimoto, M.; Hirao, I. Site-specific labeling of RNA by combining genetic alphabet expansion transcription and copper-free click chemistry. *Nucleic Acids Res.* **2015**, *43*, 6665−6676.
19. Agard, N. J.; Prescher, J. A.; Bertozzi, C. R. A strain-promoted [3+2] azide-alkyne cycloaddition for covalent modification of biomolecules in living systems. *J. Am. Chem. Soc.* **2004**, *126*, 15046–15047.
20. Rieder, U; Luedtke, N. W. Alkene–tetrazine ligation for imaging cellular DNA. *Angew. Chem. Int. Ed.* **2014**, *53*, 9168–9172.
21. Oliveira, B. L.; Guo, Z.; Bernardes, G. J. L. Inverse electron demand Diels–Alder reactions in chemical biology. *Chem. Soc. Rev.* **2017**, *46*, 4895–4950.
22. Shaughnessy, K. H. Palladium-Catalyzed Modification of Unprotected Nucleosides, Nucleotides, and Oligonucleotides. *Molecules* **2015**, *20*, 9419–9454.
23. Walunj, M. B.; Tanpure, A. A.; Srivatsan, S. G. Posttranscriptional labeling by using Suzuki–Miyaura cross-coupling generates functional RNA probes. *Nucleic Acids Res.* **2018**, *46*, e65.
24. Dumas, A.; Luedtke, N. W. Cation-Mediated Energy Transfer in G-Quadruplexes Revealed by an Internal Fluorescent Probe. *J. Am. Chem. Soc.* **2010**, *132*, 18004–18007.
25. Wang, Y.; Patel, D. J. Solution structure of the human telomeric repeat d[AG3(T2AG3)3] G-tetraplex. *Structure* **1993**, *1*, 263–282.
26. Luu, K. N.; Phan, A.T.; Kuryavyi, V.; Lacroix, L.; Patel, D. J. Structure of the human telomere in K^+ solution: an intramolecular (3+1) G-quadruplex scaffold. *J. Am. Chem. Soc.* **2006**, *128*, 9963–9970.
27. Dai, J.; Carver, M.; Punchihewa, C.; Jones, R. A.; Yang, D. Structure of the Hybrid-2 type intramolecular human telomeric G-quadruplex in K^+ solution: insights into structure polymorphism of the human telomeric sequence. *Nucleic Acids Res.* **2007**, *35*, 4927–4940.
28. Walunj, M. B.; Srivatsan, S. G (*Manuscript under preparation*).
29. Walunj, M. B.; Srivatsan, S. G (*Manuscript under preparation*).

List of publications

1. **Walunj, M. B.**; Tanpure, A. A.; Srivatsan, S. G. Posttranscriptional labeling by using Suzuki-Miyaura cross-coupling generates functional RNA probes. *Nucl. Acid. Res*. **2018**, *46*, e65. DOI: 10.1093/nar/gky185.
2. **Walunj, M. B.**; Sabale, P. M.; Srivatsan, S. G. Advances in the application of Pd-mediated transformations in nucleotides and oligonucleotides: Palladium-catalyzed modification of nucleosides, nucleotides and oligonucleotides. *Elsevier Inc*, **2018**, 269–293.
3. Nuthankanthi, A.; **Walunj, M. B.**; Torris, A.; Badiger, M.V.; Srivatsan, S.G. Self-assemblies of nucleolipid supramolecular synthons show unique self-sorting and cooperative assembling process. *Nanoscale*, **2019**, *11*, 11956–11966.
4. **Walunj, M. B.**; Srivatsan, S. G. Posttranscriptional Suzuki-Miyaura cross-coupling yields labeled RNA for conformational analysis and imaging. *Methods in Molecular Biology* **2020**, *2166*, 473–486. DOI: 10.1007/978-1-0716-0712-1.
5. **Walunj, M. B.**; Srivatsan, S. G. Nucleic acid conformation influences postsynthetic Suzuki–Miyaura labeling of oligonucleotide (*submitted).*
6. **Walunj, M. B.**; Srivatsan, S. G. Supramolecular synthons made of an environment-sensitive fluorescent nucleoside exhibits interesting emission properties upon self-assembly (*manuscript under preparation*).

Chapter 1

Applications of Palladium-Mediated Transformations in Generating Labeled Nucleic Acids and Nucleoside Supramolecular Synthons*

1.1 Introduction

For long, different chemical modification strategies have been developed to synthesize functionalized nucleosides and nucleotides as many of them serve as pharmaceutical candidates and chemical probes to analyze the structure, dynamics and function of nucleic acids.[1–3] Modification strategies have also enabled the development of nucleoside and nucleotide derivatives, which serve as supramolecular synthons to construct programed nanoarchitectures.[4] Many such supramolecular structures have been used as delivery vehicles, and as smart optical and sensing materials.[5] Notably, most of the initial work was dedicated towards developing nucleoside and nucleotide analogs, which mimic their native counterparts in terms of recognition and reactivity.[6] Many of these analogs serve as good substrates in the metabolic pathways involving nucleosides and nucleotides, and some even effectively inhibit cellular division and viral replication processes. Currently there are a notable number of FDA approved nucleoside analogs for the treatment of certain cancers and infections, and several newer analogs are in the various stages of clinical evaluation.[7] Conventional approaches and recent advances in the development of nucleoside and nucleotide analogs for therapeutic applications have been comprehensively reviewed elsewhere,[2,7] and hence, will not be discussed in details in this Chapter.[1]

During the course of these developments in the therapeutic front, chemical modification of nucleic acids for diagnostic and antisense applications became one of the main stream programs in the nucleic acid research. The reason is twofold. Nucleic acids, as we know, perform their cellular function by interacting with various biomolecules and by folding into complex secondary and tertiary structures.

---

* *A part of this work presented in this chapter is published*: Walunj, M. B.; Sabale, P. M.; Srivatsan, S. G. Advances in the application of Pd-mediated transformations in nucleotides and oligonucleotides: Palladium-catalyzed modification of nucleosides, nucleotides and oligonucleotides. *Elsevier Inc*, **2018**, 269–293.

To understand the structure and folding dynamics, several biophysical tools based on fluorescence, NMR, EPR, X-ray diffraction techniques, to name a few, have been developed.[9–12] Needless to say, these investigations greatly rely on nucleic acid labeling methods as natural nucleosides are practically non-fluorescent and do not contain intrinsic labels (e.g., isotopes like $^{13}C/^{15}N$ for NMR, spin labels like nitroxide radicals for EPR and heavy atoms like Se/I for X-ray crystallography), which would allow the effective analysis by these techniques.[13] On the other hand, antisense technology has immensely benefited from a portfolio of chemistries for the design of clinically productive antisense ONs.[14] Typically, a combination of sugar, phosphate backbone, base and 3′- and 5′- modification methods is now being used to develop antisense ONs with stability, binding strength, specificity and biodistribution suitable for silencing disease-associated genes in clinics.[15] In all these applications, the major theme has been to incorporate one or more functionalities into an ON sequence without affecting its primary recognition property.

Conventionally, base-, sugar- and phosphate backbone-modified DNA and RNA ONs are prepared by using solid-phase ON synthesis protocols.[16] In this method, base- or sugar-modified phosphoramidite or phosphorothioate substrates are site-specifically incorporated into DNA and RNA ONs. Alternatively, DNA and RNA polymerases and other nucleic acid processing enzymes, which are promiscuous and have the ability to accept modified nucleotide substrates, have been utilized in labeling DNA and RNA ONs with a wide variety of biophysical probes.[17] However, some shortcomings in both the methods present challenges when incorporating certain modifications. For example, synthesis of functionalized phosphoramidite substrate may involve cumbersome and elaborate synthetic steps, and in many cases, the phosphoramidite substrates may not survive the solid-phase ON synthesis cycle or exhibit poor coupling efficiency. Although enzymatic labeling methods allow the introduction of sensitive functional groups as these reactions work under very mild conditions,[18] introduction of large functionality and effecting site-specific labeling of ONs is not straight forward.[19] These limitations have been largely addressed by the development of postsynthetic chemical modification strategy based on bioorthogonal reactions.[20] In this technique, a small reactive group, which is amenable to incorporation by either chemical or enzymatic methods, is introduced into DNA and RNA ONs, and further functionalization is accomplished by treating the labeled ON with its reactive counterpart containing the desired biophysical tag. Of course, all these methods require modified nucleoside, nucleoside

phosphoramidite or nucleotide substrates in order to label nucleic acids by any of the methods mentioned above. Consequently, depending on the downstream biophysical or therapeutic application, several chemical strategies have been adopted to synthesize building blocks suitable for incorporation by either chemical or enzymatic means.

Among the various methods, metal-mediated modification strategies, particularly involving palladium, have provided access to a variety of base-functionalized nucleosides, nucleotides and ONs. Over the years, the development in Pd-mediated cross-coupling reactions in the context of nucleic acid labeling has taken a progressive path. Pd-catalyzed cross-coupling reactions such as Suzuki–Miyaura, Sonogashira, Stille and Heck have been initially applied in the synthesis of a wide variety of base-modified nucleoside analogs, and more recently, nucleotide analogs.[21] The coupling reactions can be performed with protected and unprotected halogenated purine and pyrimidine nucleosides in the presence of ligand-free Pd catalysts or Pd-ligand complexes. However, coupling reactions, particularly with nucleotides, pose two problems−solubility of the substrates and ligands in organic solvents and the ability of nitrogenous bases to coordinate with metal catalysts and deactivate them. These challenges have led to the development of new Pd-ligand catalytic systems, which are not only soluble in aqueous buffers but also significantly accelerate the coupling reactions under mild conditions.[22] These developments further encouraged the design of labeling methods to directly install reporters onto ONs postsynthetically by using various Pd-mediated cross-coupling reactions.[23] In this chapter, first we provide a general overview of different methods to label ONs by Pd-mediated reactions. Following this, a detailed discussion on the various protocols that have been developed to label ONs postsynthetically by using Pd-mediated cross-coupling reactions is presented.

1.2 Labeling ONs using Pd-mediated reactions

General scheme to label ONs by using Pd-mediated cross-coupling reactions is provided as a flowchart in Figure 1.1. Conventionally, the halogenated nucleoside is base-functionalized by any one of the Pd-mediated reactions, which is then converted into phosphoramidite building block required for the incorporation by solid-phase ON synthesis protocol. Synthesis of such nucleoside analogs, their incorporation and applications are reviewed in the preceding chapters and elsewhere,[9b,21,24] and hence, are not discussed here. In an alternative approach, modifications are directly installed onto the halogenated nucleotide triphosphates, which are

then incorporated enzymatically into ONs by using polymerases.[21c,25] However, this approach greatly relies on the efficiency of the enzyme to incorporate such modified nucleotides into ONs. More recently, postsynthetic ON modification approaches based on chemo-selective reactions, which overcome the limitation of solid-phase and enzymatic methods, have gained significant attention.[23] In the context of Pd-catalyzed reactions, a halogen-modified phosphoramidite or nucleotide is chemically or enzymatically incorporated into an ON, and further functionalization is achieved by performing a chemo-selective reaction in the presence of an appropriate reactive counterpart depending on which Pd-mediated reaction is chosen. Although in infancy, a notable number of examples have been put forward to label ONs by using this strategy.

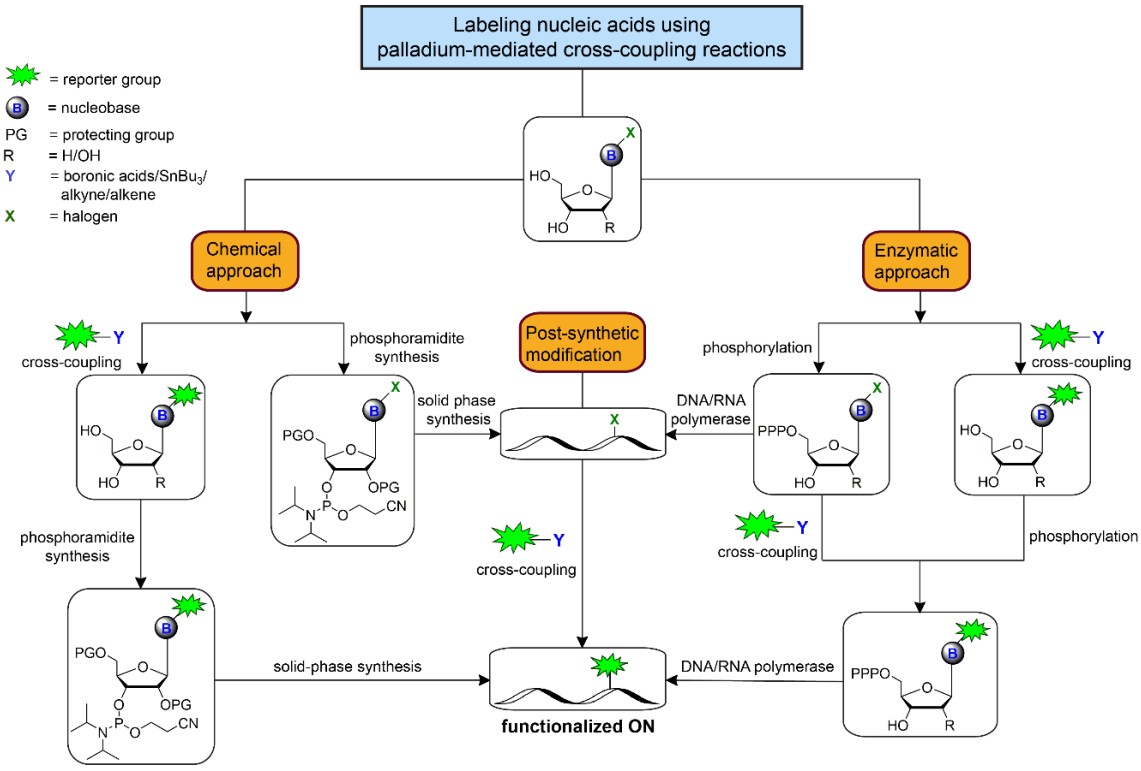

Figure 1.1. Flowchart explaining the various strategies to functionalize nucleic acid using Pd-mediated cross-coupling reactions.

1.3 Pd-based catalytic systems for aqueous-phase cross-coupling of nucleosides and nucleotides

In general, modified nucleotides suitable for incorporation into DNA and RNA by primer extension reaction, PCR and transcription reactions are synthesized by Ludwig's method.[26] Typically, the modified nucleoside is triphosphorylated at the 5′-OH position by using $POCl_3$

and bis-tributylammonium pyrophosphate in a one-pot two step reaction. Most nucleosides can be directly phosphorylated without base and sugar protection (Figure 1.2). However, certain relatively more reactive nucleophilic groups (e.g., aliphatic NH_2, guanidine, etc.) require appropriate orthogonal protection such that under deprotection conditions the triphosphate is stable. Alternatively, methods to directly conjugate functional moieties onto halogenated nucleoside 5′-*O*-triphosphates have been successfully established using Pd-catalyzed reactions (Figure 1.2, Figure 1.3). This has been possible due to the development of aqueous-phase cross-coupling reactions using water-soluble ligands. A common approach to design water-soluble ligands was to attach hydrophilic functionality to ligand scaffolds (e.g., triphenylphosphine) regularly used in Pd-catalyzed cross-coupling reactions (Figure 1.4).[27]

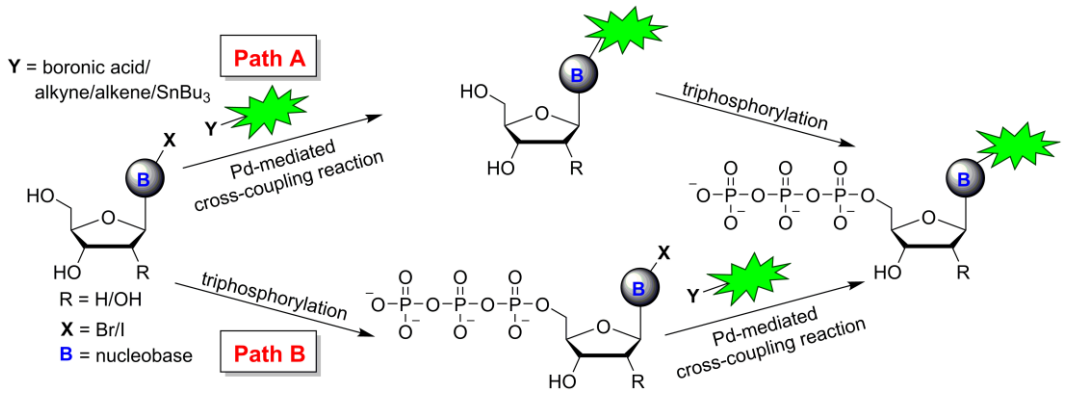

Figure 1.2. General scheme for the synthesis of base-modified nucleotide analogs, suitable for enzymatic incorporation into DNA and RNA, by Pd-mediated reactions. Path A: halogenated nucleosides are functionalized by using an appropriate cross-coupling reaction, which are then phosphorylated to produce nucleotides. Path B: halogenated nucleotides are directly cross-coupled to give modified nucleotides

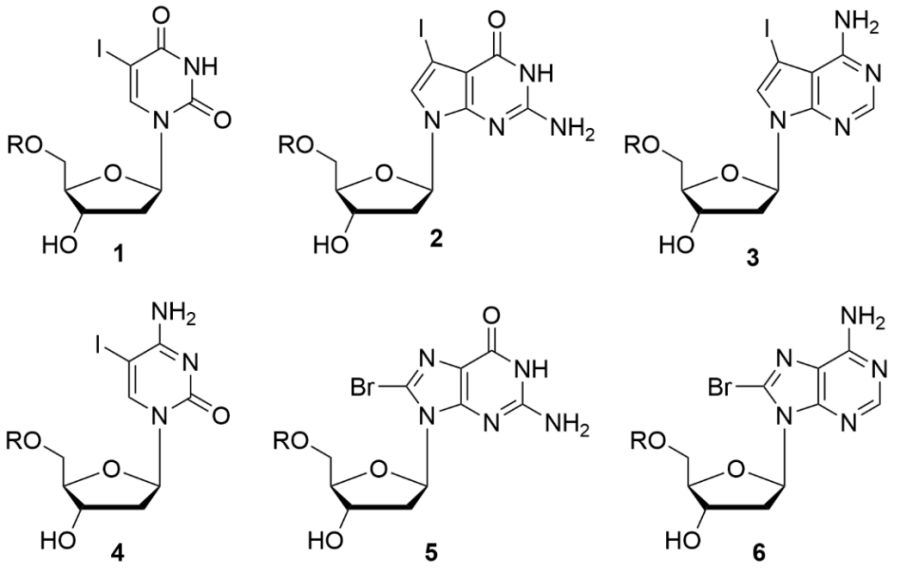

Figure 1.3. Chemical structure of various halogen-labeled 2′-deoxynucleosides (R = H, dN) and 2′-deoxynucleotides (R = $P_3O_9^{3-}$, dNTP) used in the Pd-mediated reactions to generate functionalized nucleosides or nucleotides.

Casalnuovo and Calabrese for the first time used a Pd-phosphine catalyst $Pd(TPPMS)_3$, TPPMS = sodium diphenyl(3-sulfonatophenyl)phosphine) to carry out Sonogashira and Heck coupling reactions on 5-iodo-modified pyrimidine nucleosides in aqueous acetonitrile.[28] More than a decade later, Shaughnessy group revisited this nucleoside modification strategy and developed a general approach to install functionalities on nucleosides by performing Suzuki and Sonogashira reactions on halogenated purine and pyrimidine nucleosides in the presence of $Pd(OAc)_2$ and triphenylphosphan-3,3′,3″-trisulfonate (TPPTS, **10**).[29] Following this, Burgess and coworkers reported the first example on the direct Sonogashira alkynylation of dUTP in aqueous phase to afford fluorescent nucleotides.[30] Subsequently, Hocek and Wagner groups reported the arylation of halogenated dNTPs by Suzuki–Miyaura reaction using palladium(II) salt and TPPTS.[31,32] Although elevated temperatures and basic conditions were employed in these transformations, the cross-coupled nucleotide products were reasonably stable and yields were moderate. Except for few examples, most of the modifications have been performed on unprotected halogenated 2′-deoxy NTPs. Excellent reviews thoroughly discussing the use of Pd-mediated cross-coupling reactions in modifying nucleotides have been published.[17b,21c,22,25] Hence, in this section, we restrict our discussion to the applications of modified nucleotide analogs derived by Pd-mediated cross-coupling reactions on halogenated nucleoside and nucleotides, and set the stage for the detailed discussion on postsynthetic ON modification strategies.

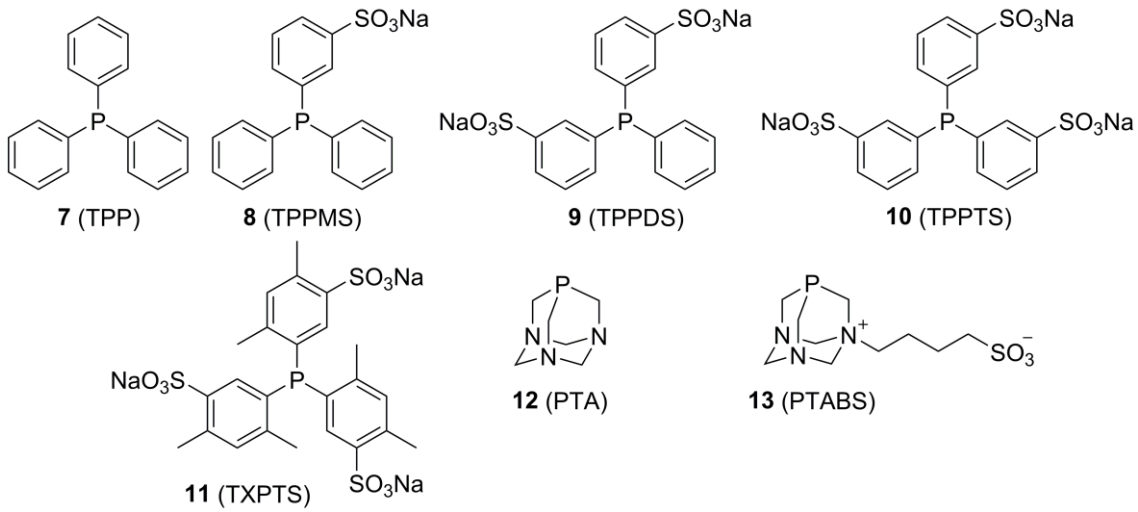

Figure 1.4. Examples of triphenylphosphine- and adamantane-based ligands.

1.3.1 Functionalized nucleoside and nucleotide analogs derived by Pd-mediated reactions

Biophysical platforms based on environment-sensitive fluorescent nucleoside analogs have been very useful in advancing our understanding of the nucleic acid structure, dynamics and recognition properties.[9] Many such environment sensitive-fluorescent analogs are prepared by using Pd-mediated cross-coupling reaction like Stille, Suzuki-Miyaura, Sonogashira etc. (Figure 1.5). Some of the examples of such environment-sensitive fluorescent nucleoside are given in figure 1.5.

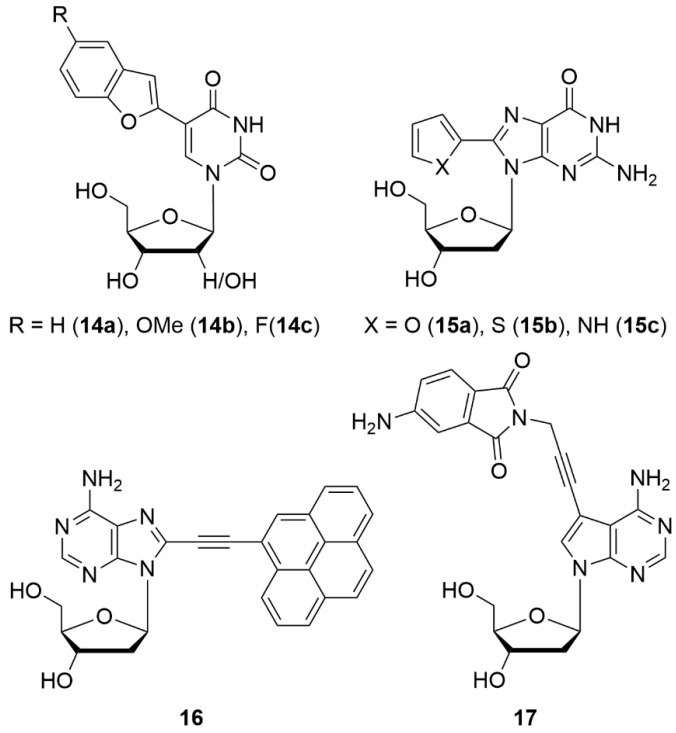

Figure 1.5. Examples of fluorescently modified nucleoside analogs synthesized by Suzuki-Miyaura and Sonogashira reactions.

Srivatsan and coworkers reported the various fluorescent heterobicyclic-modified uridine analog (**14a**–**14c**) as probes to study nucleic acids in a cell-like environment or cellular environment. Importantly, all the nucleoside analogs displayed excellent fluorescence properties like emission wavelength, quantum yield, lifetime and anisotropy, and these emissive nucleosides were sensitive to the surrounding solvent polarity and viscosity. For example, depending on the fluorescence outcome nucleoside **14a** was suitably utilized in designing assays to detect abasic sites in DNA[33a] and RNA ONs.[33b] Also **14a** was employed in studying the ON dynamics in a confined cell-like environment.[34] The fluorescent probe **14b** is used in the detection of dT-dT mismatch and Hg^{2+}-ion-mediated base pairing in RNA-

DNA and RNA-RNA duplexes.[35] From the same group, dual-app nucleoside probe **14c** containing fluorine label was also developed, which successfully indicates the formation of hybrid 2 G-quadruplex topology in live *Xenopus laevis* oocytes by using ^{19}F-NMR spectroscopy.[36]

Manderville and coworkers developed a series of environment-sensitive fluorescent C8-heteroaryl-2′-deoxyguanosine analogs–furyl (FurdG, **15a**), thienyl (ThdG, **15b**), pyrrolyl (PyrdG, **15c**).[37] Notably; probe **15a** is used as tools to detect the GQ folding of a 15-mer (5′-GGTTGGTGTGGTTGG-3′) thrombin-binding aptamer.[38] The pyrene fluorophore appended on adenine (**16**) *via* Sonogashira cross-coupling reaction has been used to probe the charge transfer within the double helix DNA.[39] The same probe was utilized to distinguish the structure-switching between the mixed and antiparallel structure.[40] Hocek and coworkers constructed solvatochromic nucleoside analogs by conjugating aminophthalimide (e.g., **17**) via an alkyne linker.[41] They enzymatically incorporated the corresponding triphosphates into DNA oligonucleotide and established fluorescence assays to detect the binding of DNA to p53, which is an important tumor suppressor protein. Also, this probe detects a non-specific single-strand binding (SSB) protein, which stabilizes DNA in single-stranded form.

To synthesize the environment-sensitive fluorescent triphosphate, in most of the methods, the fluorescently modified nucleoside is first prepared and then phosphorylated (Figure 1.2, Path A). However, advancement in the water-soluble Pd-catalyst allows the access to perform such Pd-mediated reactions directly onto halogenated nucleotides in the aqueous medium (Figure 1.2, Path B). As a practice, the first course of action was to evaluate the ability of base-modified dNTPs to serve as a good substrate for DNA polymerases in primer extension reaction or PCR. This is usually tested by performing polymerization reactions in the presence of various DNA polymerases. In most cases the thermostable polymerases such as KOD XL, Vent (exo-) and Pwo were found to be highly efficient in introducing the modified nucleotides into the DNA during polymerization reactions.[42] Engineered proteins from Holliger and Marx groups displayed discernibly improved efficiency of incorporation of certain modified nucleotides.[43] Important observations, which were made during the course of these studies, are (i) DNA polymerases prefer to incorporate 5-substituted pyrimidine dNTPs and 7-substituted 7-deazapurine dNTPs efficiently as the modifications in these positions project into the vacant pocket of the major groove, and (ii)

baring few examples, 8-substituted purine dNTPs are not good substrates for DNA polymerases as these modifications prefer to adopt unfavorable *syn* conformation.[44]

Burgess and coworkers synthesized a small series of fluorescein-modified 2′-deoxy and 2′,3′-dideoxy-uridine 5′-triphosphates (e.g., **18**) by reacting alkyne-tagged fluorescein with respective 5-iodo-modified uridine nucleotides under Sonogashira reaction conditions (Figure 1.6).[30]Among these 2′-dUTP and 2′,3′-ddUTP tethered to fluorescein via a long linker were found to be good substrates for thermostable polymerase *TaqF*S. Hocek and coworkers developed a series of bifunctional dNTPs containing a fluorophore and NMR active label, ^{19}F. Several fluorine-containing heterocycles were coupled to iodinated triphosphate via Suzuki reaction in the presence of $Pd(OAc)_2$ and TPPTS (e.g., **19**, Figure 1.6).[45] The biaryl-modified dNTPs were efficiently incorporated into DNA by KOD XL polymerase. Photophysical and NMR analyses of labeled DNA revealed that these modifications could allow two-channel detection of structural changes in DNA, for example from a hairpin to duplex structure. In a similar approach, dNTPs containing GFP-like fluorophores (e.g., **20**) and viscosity-sensitive probe based on benzylidene cyanoacetamide were synthesized and enzymatically introduced into DNA ONs.[46,47] More recently, a BODIPY-labeled nucleotide **21** was developed, which could be incorporated into DNA by using DNA polymerases.[48] This environment-sensitive fluorescent label enabled the fluorescence-lifetime imaging of DNA interactions in live cells by microscopy.[49]

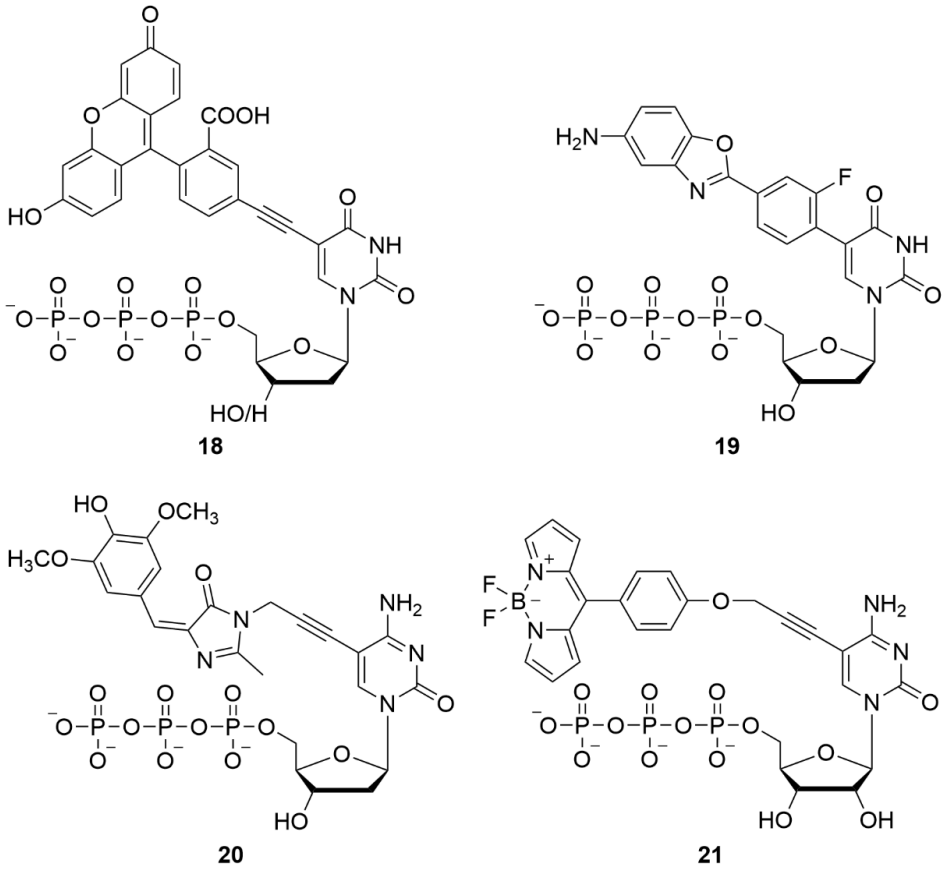

Figure 1.6. Examples of fluorescently modified nucleotide analogs synthesized by Suzuki–Miyaura and Sonogashira reactions.

1.4 Pd-mediated postsynthetic functionalization of ONs

Palladium-catalyzed cross-coupling reactions like Suzuki–Miyaura, Sonogashira, Stille etc. afford a powerful passageway to attach a variety of biophysical probe to nucleoside or nucleotide structures. Later, the modified nucleosides can effectively be incorporated into oligonucleotides using enzymatic or solid-phase DNA synthesis methods (Figure 1.1). Although this method has been significantly adapted to modify the oligonucleotides, the methodology still has some limitations. For example, C-8 aryl modified purines are more susceptible to acidic hydrolysis and oxidation than native nucleoside.[50] In case of enzymatic polymerase approaches, the steric group on triphosphate can decrease the incorporation efficiency of polymerase enzyme. To incorporate the modifications as mentioned above (Figure 1.5 and 1.6) into an oligonucleotide either by solid-phase DNA synthesis or enzymatic methods, one has to synthesize their individual modified phosphoramidite/triphosphate. This could make the synthetic strategy more laborious.

A more general approach based on postsynthetic method which would provide the attachment of the various fluorescent environment-sensitive probe and other biophysical tags to the nucleic acid using a common precursor such as halo-modified nucleic acid is needed. In which, halo modified nucleoside is incorporated into the nucleic acid either by enzymatic or solid-phase DNA synthesis methods. Further, the halo group is reacted with its cognate partner such as $SnBu_3$, boronic acid/ester, alkyne to generate the nucleic acid labeled with environment-sensitive nucleoside probe (Figure 1.1).

Performing metal-mediated cross-coupling reactions on ONs is not straightforward as several considerations have to be taken into account. Metals can coordinate to the nitrogenous bases and kill the catalytic activity or form adducts with the ON. Redox environment can also damage the ON. Unlike in nucleosides and nucleotides, steric hindrance also plays a major on the reaction efficiency at the ON level.[51]Nevertheless, the applicability of Pd-mediated cross-coupling reactions to directly functionalize ONs has been realized recently. Notably, the developments in the design of catalytic system, especially in the context of ligand development, and optimization of cross-coupling reaction conditions suitable for biopolymers, especially for peptides and proteins, have essentially laid the foundation for the implementation of Pd-mediated postsynthetic functionalization strategies to ONs.[52]

In general, postsynthetic modification of halogenated ONs by using Pd catalyst is accomplished in two ways. The halogenated nucleoside phosphoramidite (usually iodo-modified nucleoside phosphoramidite) is incorporated into a DNA or RNA ON at desired position(s) by solid-phase ON synthesis chemistry, and the cross-coupling reaction is performed on the protected ON attached to the solid-support. In this case, conventional Pd-catalyzed reactions can be performed in a polar organic solvent such DMF or DMSO to install the modification. Further, cleavage from the solid-support and global deprotection afford the desired functionalized ON. However, the stability of the nucleoside protecting groups under cross-coupling reactions conditions (elevated temperatures and basic conditions) and that of modification under strong deprotection conditions used in the ON synthesis protocols will majorly influence the yield of the ON product. In the second approach, an ON labeled with halogenated nucleoside is subjected to Pd-mediated reaction in aqueous solution. In this case, the choice of Pd-ligand catalytic system becomes crucial. As mentioned in the previous section, ligands suitable for Pd-mediated coupling reactions of biomolecules in aqueous-phase were initially based on triphenylphosphine scaffold (Figure

1.4). Cage-like ligands such as 1,3,5-triaza-7-phosphaadamantane (PTA) and its derivatives have also been developed to effect cross-coupling reactions in aqueous condition.[53] Although phosphine-based ligands, particularly TPPTS, have been highly useful in designing catalytic systems for modifying nucleosides and nucleotides, their application at the ON level is very limited as they are prone to oxidation, and require elevated temperature and longer reaction time. The deiodination of substrates was also a major concern in these reaction conditions.[23]

Several *N*-heterocyclic compounds have severed as good ligands in Pd-catalyzed cross-coupling reactions. After evaluating various *N*-heterocyclic compounds, Li and coworkers identified 2-aminopyrimidine-4,6-diol (ADHP) as one of the best ligands for such reactions (Figure 1.7).[54] The advantage of this scaffold is that the diol and exocyclic amino groups can be derivatized to modulate the electron density and solubility of the ligand. Davis and coworkers used a catalytic system made of sodium salt of ADHP and $Pd(OAc)_2$ to setup aqueous-phase Suzuki–Miyaura reaction on an iodo-labeled protein substrate.[55] This catalytic system was also used in the fluorescence labeling of bacterial cell surface, wherein p-iodophenylalanine-labeled OmpC, a protein highly expressed on *Escherichia coli* surface, was coupled with a fluorescent boronic acid substrate.[56] Meanwhile, Lin and coworkers developed a series of ligands by derivatizing ADHP to perform Sonogashira reaction on protein substrates (Figure 1.7). Notably, $Pd(OAc)_2$ and dimethylamino-substituted ADHP (DMADHP) combination was found to be highly robust in cross-coupling homopropargylglycine-encoded ubiquitin protein with various aryl iodides.[57]

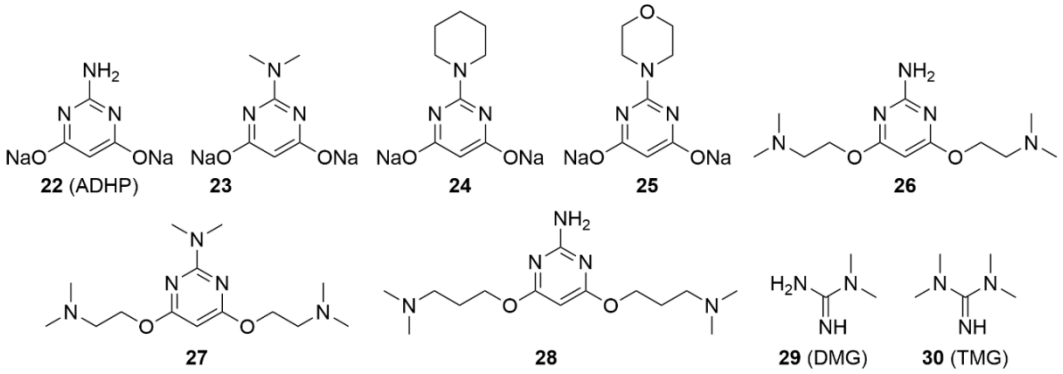

Figure 1.7. Ligands based on *N*-heterocyclic compound ADHP for aqueous-phase Pd-catalyzed reactions. DMG and TMG represent the minimal motif of ADHP.

Interestingly, guanidine-based ligands **29** and **30**, which represent the minimal motif of ADHP, also showed similar efficiency as the parent ligand in Suzuki–Miyaura coupling of

a protein substrate.[58] It is important to mention here that the coupling reactions using these ADHP-based ligands work under mild (37 °C) and buffered (pH ~ 8.5) conditions. Consequently, these catalytic systems and conditions have also been applied to develop Pd-mediated labeling strategies for nucleic acids.

1.4.1 Functionalization of ONs by Suzuki–Miyaura reaction

Manderville and coworkers, for the first time, demonstrated the utility of Suzuki–Miyaura reaction in functionalizing DNA ONs.[50] DNA ONs were first labeled with 8-bromoguanosine by using solid-phase ON synthesis protocol. The coupling reaction was performed with various arylboronic acid substrates in the presence of $Pd(OAc)_2$/TPPTS catalytic system and Na_2CO_3 at 70 °C for 24 h (Figure 1.8). The coupling of arylboronic acid substrates produced DNA ONs labeled with environment-sensitive fluorescent reporters and C^8-Ar-dG adducts in good yields.

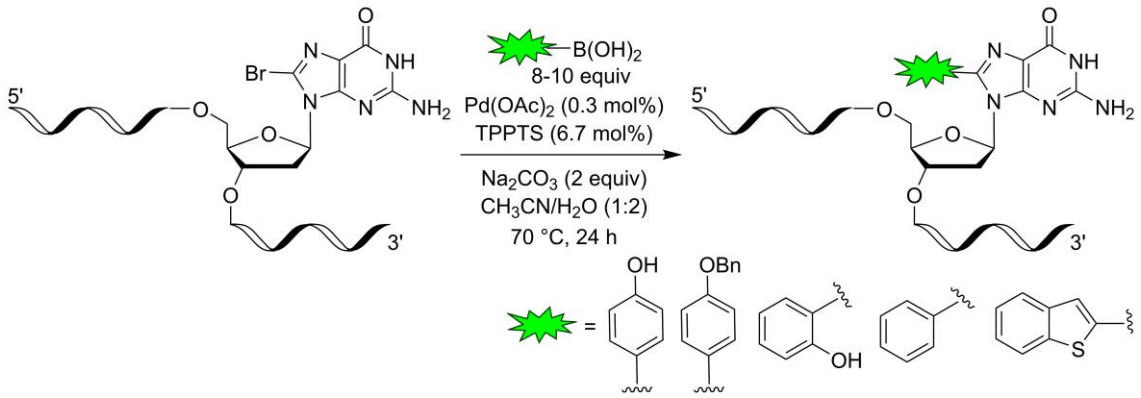

Figure 1.8. Postsynthetic modification of 8-bromoguanosine-modified DNA ONs by aqueous-phase Suzuki–Miyaura reaction.[50]

Cahová and Jäschke installed a new type of nucleoside-based diarylethene photoswitches onto DNA ONs by employing postsynthetic Suzuki–Miyaura reaction.[59] DNA ONs containing 5-iodo-dC or 5-iodo-dU were prepared and reacted with 2-[2-methyl-5-phenylthien-3-yl]cyclopent-1-ene boronic ester (**31**) under the conditions optimized by Manderville and coworkers. However, under these conditions no detectable amount of the photoswitch-modified DNA ON product was observed. Subsequently, the authors used the coupling conditions employed for sensitive nucleotides (Cs_2CO_3, water/acetonitrile mixture, argon atmosphere, 120 °C, 60 min) to achieve cross-coupling between the bulky boronic ester substrate **34** and iodo-labeled ONs. The reaction with ONs containing 5-iodo-pyrimidine

nucleosides at various positions produced the coupled product in moderate yields. Substantial amount of deiodinated ONs was also formed. Upon irradiation, the photoswitch-modified DNA ONs were found to undergo efficient and reversible electrocyclic rearrangement reaction to produce the open and closed forms (Figure 1.9). It has been proposed that this approach of assembling photoswitch-modified ONs could have potential applications in biology and nanotechnology.

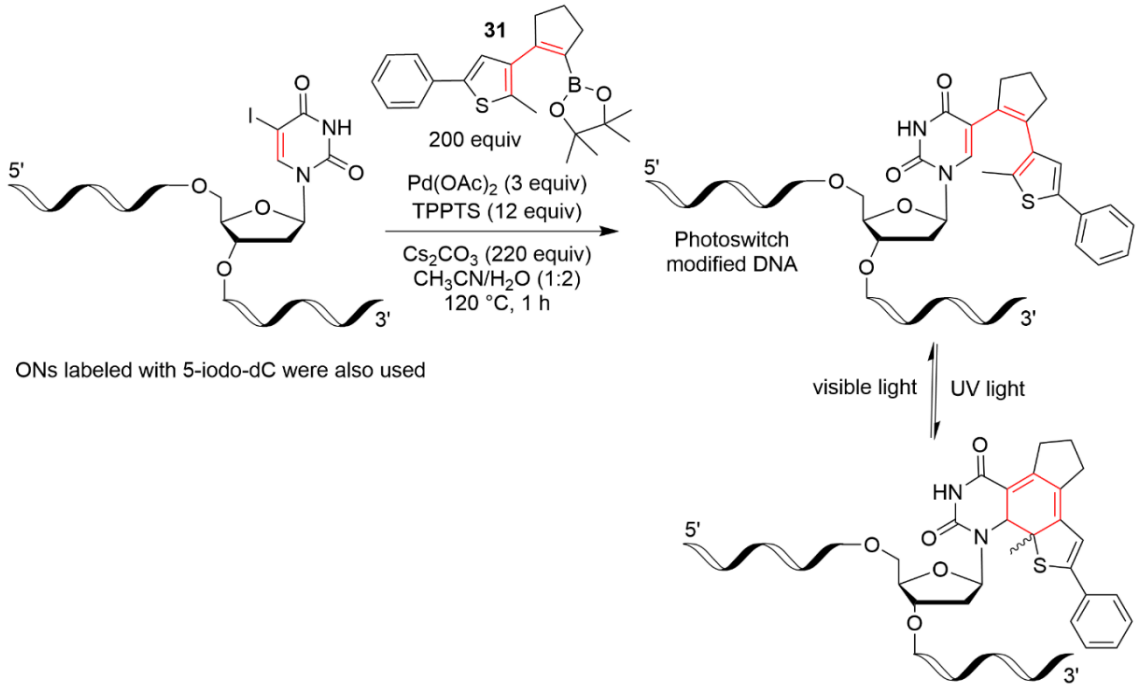

Figure 1.9. Synthesis of photoswitch-modified DNA ONs by postsynthetic modification of iodo-labeled DNA ONs with 2-[2-methyl-5-phenylthien-3-yl]cyclopent-1-ene boronic ester **31**. Reversible electrocyclic rearrangement reaction at the ON level was possible by irradiating with a light source of different wavelength.[59]

Davis group came up with a milder and more efficient postsynthetic DNA ON labeling strategy based on Suzuki–Miyaura coupling reaction.[60] In this method, a combination of sodium salt of ADHP/DMADHP and $Pd(OAc)_2$ was used as the catalytic system. 5-Iodo-dU-modified DNA ONs were subjected to coupling reaction with various boronic ester substrates in Tris buffer (pH 8.5) at 37 °C for 4–16 h (Figure 1.10). Pinacol boronic esters used in this study include photocrosslinking agents (diazirine and benzophenone), photoswitch label (azobenzene), fluorescent and sugar tags. Using these substrates and above reaction conditions, functional ON probes were prepared in very good yields. Subsequently, three different tags, namely hydroxymethylcytosine (hmC, natural

modification), diazirine and biotin were introduced into DNA strands. This combination allowed the profiling of proteins associated with hmC versus cytosine by first photocrosslinking the DNA with proteins by using the diazirine tag followed by pull-down by using biotin tag.

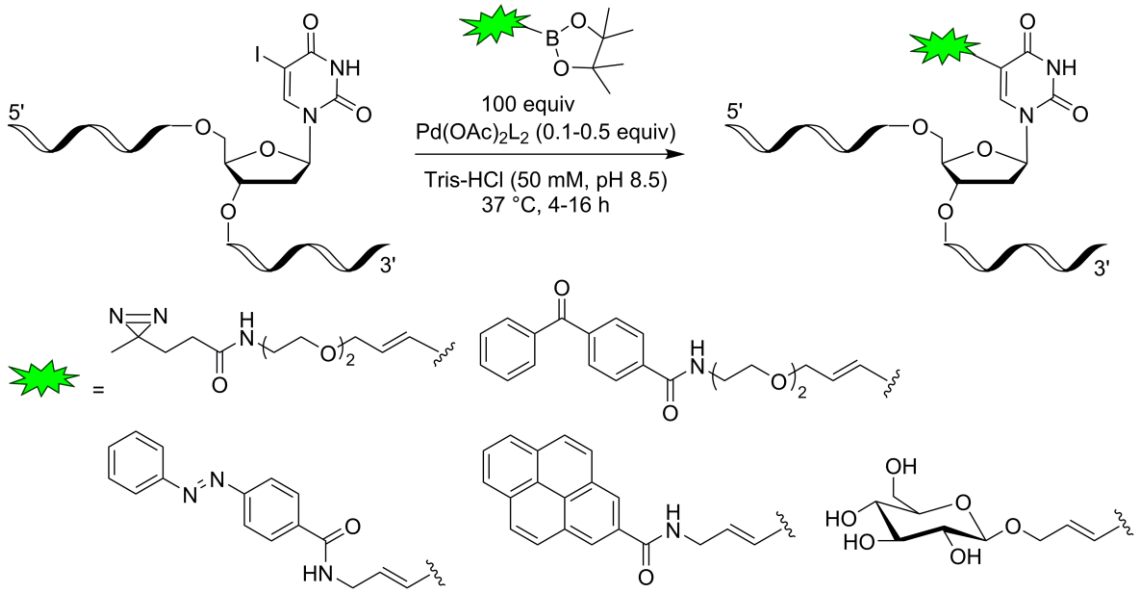

Figure 1.10. Postsynthetic modification of DNA ONs by using Suzuki–Miyaura reaction in the presence of Pd(II) salt and ADHP/DMADHP ligand. These Pd-ligand catalytic systems have enabled the modification of iodo-labeled DNA ONs with a variety of biologically useful tags under mild conditions.[60]

Recently, Okamoto and coworkers used diazirine photocrosslinking chemistry to study the recognition of N^6-methyladenosine (m^6A) modification on RNA by the fat mass and obesity associated (FTO) demethylase.[61] This modification of RNA is regulated by m^6A methyltransferases and plays important roles in posttranscriptional regulation processes. FTO is a nonheme Fe(II) α–ketoglutarate-dependent dioxygenase protein, which demethylates m^6A to A. A highly photo-reactive diazirine group was placed next to m^6A of an RNA strand by performing Suzuki–Miyaura reaction between a diazirine-modified boronic ester and 5-iodouridine-modified RNA (Figure 1.11). The photocrosslinking experiments revealed enrichment of activated FTO based on m^6A recognition, which was found to depend on Fe(II) cofactor and α–ketoglutarate activity.

Ding and Clark generated DNA-encoded libraries containing variety of functionalities at the duplex terminus by performing Suzuki–Miyaura reaction between DNA-linked aryl halides and various boronic acid/ester substrates in the presence of $Pd(PPh_3)_4$ catalyst.[62]

Following this report, Ding group introduced a new catalytic system based on $[(t\text{-Bu})_2\text{P-(OH)}]_2PdCl_2$ (POPd) and a biphenyl ligand **32** for postsynthetic DNA modification by Suzuki–Miyaura reaction (Figure 1.12). This catalytic system was found to be highly active in coupling challenging pyrimidinyl and phenyl chlorides with boronic acids.[63]

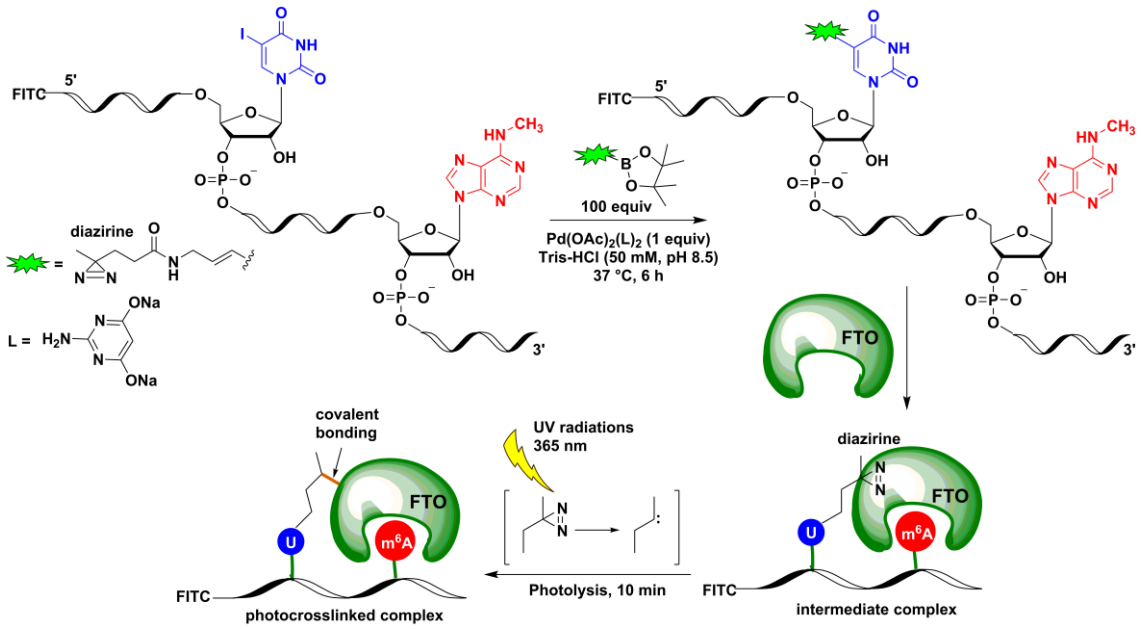

Figure 1.11. Schematic diagram showing the use of postsynthetic ON modification strategy to study RNA-protein interaction. RNA labeled with a diazirine photocrosslinking agent next to an m^6A residue was prepared by postsynthetic Suzuki–Miyaura reaction. RNA was selectively photocrosslinked to a FTO protein (binds to m^6A and demethylates) based on m^6A recognition event.[61]

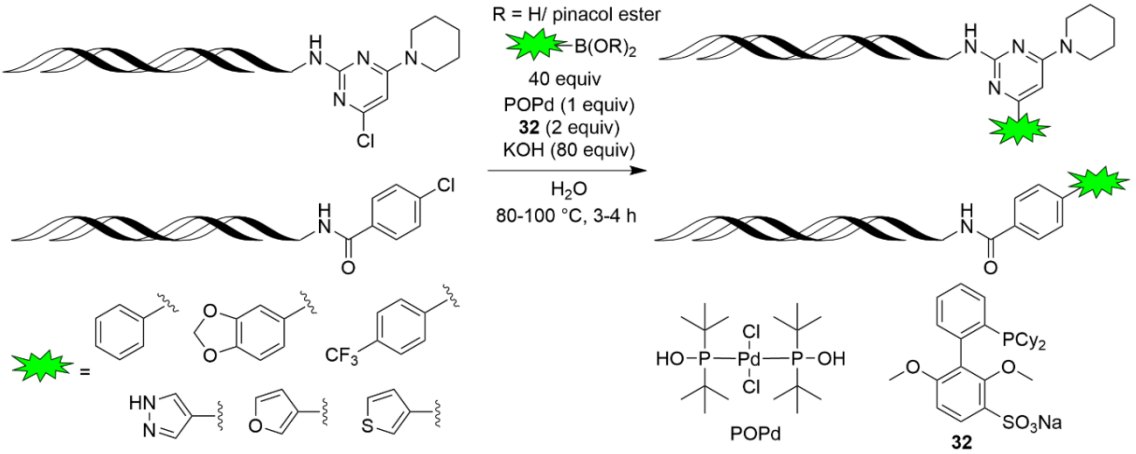

Figure 1.12. Suzuki–Miyaura reaction on double-stranded DNA ONs. A combination of POPd and ligand **32** enabled the postsynthetic modification of duplexes containing challenging pyrimidinyl and phenyl chlorides with different boronic acid substrates.[63]

1.4.2 Functionalization of ONs by Sonogashira reaction

Unlike Suzuki–Miyaura reaction, only few examples are available on the postsynthetic functionalization of ONs by using Sonogashira reaction. In particular, aqueous-phase modification of ONs by Sonogashira reaction has remained elusive, and hence, on-column Sonogashira reaction was used in following examples. In one of the first examples, Khan and Grinstaff used Pd-catalyzed Sonogashira reaction during automated solid-phase synthesis to modify ONs. In this approach, after incorporating the protected 5-iodo-dU residue, the ON attached to the column was coupled successfully to alkyne-derivatized substrates in DMF in the presence of $Pd(Ph_3P)_4$, CuI, and Et_3N.[64] Using a similar strategy, Wagenknecht and coworkers prepared 1-ethynylpyrene-modified DNA ONs and studied the electron-transfer property of pyrene in DNA.[65]Richert and coworkers wanted to study the stabilization/destabilization effect of alkynyl substituents projected in the major of DNA duplexes. For this purpose, they resorted to on-column Sonogashira reaction to introduce various alkynyl-substituents onto DNA ONs.[66] 5-Iodo-dU was incorporated into short DNA ON sequences and was further subjected to on-support Sonogashira reaction with various alkynyl substrates in the presence of $Pd(PPh_3)_2Cl_2$, PPh_3, and CuI in THF and Et_3N. Global deprotection gave the desired ON products in moderate yields. Thermal denaturation experiments indicated the modifications either destabilized or stabilized the duplex, and in particular, pyrenylbutyramidopropyne was found to significantly stabilize the duplex, possibly by intercalation. Engels and colleagues used on-column Sonogashira coupling to introduce a rigid spin label (2,2,5,5-tetramethyl-pyrrolin-1-yloxyl-3-acetylene, TPA) into DNA and RNA ONs for EPR analysis.[67] In one of the examples, the spin-labeled RNA ONs were subjected to 4-Pulse Electron Double Resonance (PELDOR) analysis, which enabled the differentiation of the A- and B-form of duplexes (Figure 1.13).[68]

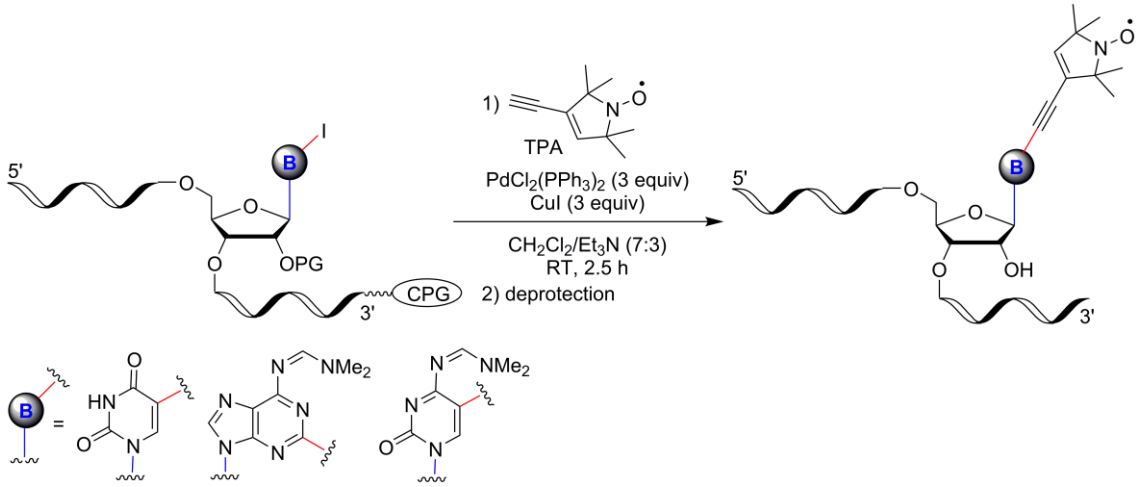

Figure 1.13. On-column modification of ONs by using Sonogashira reaction. Here, an iodo-labeled ON attached to the solid-support is functionalized by a reaction with alkyne-modified spin label.[67,68]

1.4.3 Functionalization of ONs by Stille- and Heck-type reactions

Engels group extended their on-column Sonogashira strategy to modify RNA ONs by Stille coupling reaction. 5-Iodouridine or 2-iodoadenosine in the form of phosphoramidite was incorporated into short RNA ONs, which were then coupled with various stannylated heterocycles in the presence of $Pd_2(dba)_3$ and P(furyl)$_3$ to produce fluorescent RNA ONs.[69] Jäschke and coworkers established a convenient postsynthetic DNA and RNA labeling method using Stille-Migita chemistry. The authors used $Pd_2(dba)_3$ and $AsPh_3$ as the catalytic system to effect cross-coupling reaction in solution by using halogenated dinucleotide substrates and in solid-support by using iodopyrimidine-labeled DNA and RNA ONs. The coupling reactions were performed in DMF at 60 °C with various stannylated substrates to generate fluorescent- and azide-labeled ONs (Figure 1.14).[70]

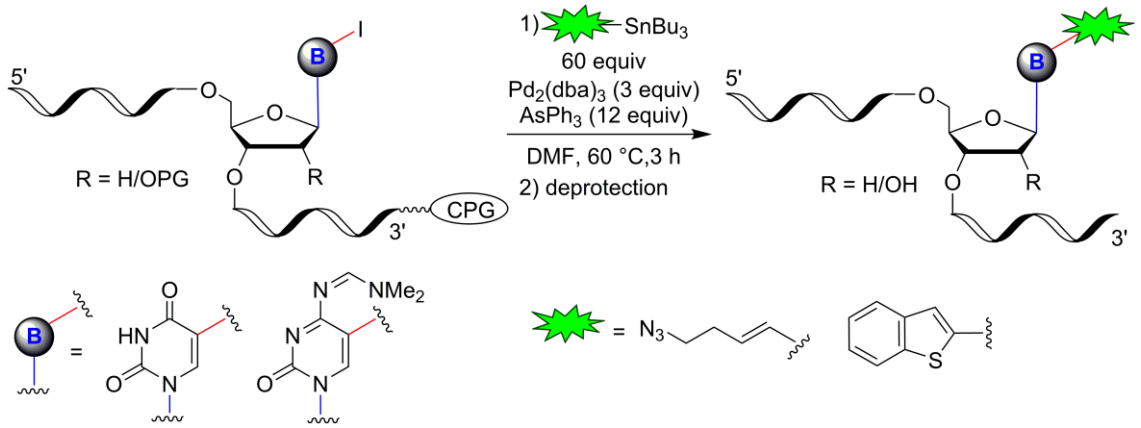

Figure 1.14. On-column modification of ONs by using Stille-Migita reaction.[70]

Vinyl-labeled biomolecules serve as good bioorthogonal reactive partners in photoclick, inverse electron demand Diels-Alder (IEDDA) and oxidative Heck reactions.[71–73] However, the versatility of vinyl label has not been well explored in the context of labeling RNA until recently. George and Srivatsan developed a modular posttranscriptional RNA labeling method by using IEDDA and oxidative Heck reactions.[74] In this method, 5-vinyluridine triphosphate (VUTP **33**) was prepared and incorporated into RNA ONs by *in vitro* transcription reaction in the presence of T7 RNA polymerase. VUTP could be incorporated into RNA ONs at one or more sites and also into longer RNA transcripts with very good efficiency. The vinyl-labeled RNA transcript was then subjected to oxidative Heck reaction with various heterocycle boronic acid/ester substrates in the presences of Pd-EDTA complex in aqueous buffer (Figure 1.15). The coupling reaction proceeded reasonably well and produced fluorescent RNA ONs. In particular, benzothiophene-coupled and benzothiophene-alkene-coupled RNA products exhibited remarkable enhancement in fluorescence intensity as compared to its corresponding boronic acid substrate. It is suggested this novel approach of functionalizing RNA posttranscriptionally by fluorogenic Heck-type coupling reaction could offer direct access to fluorescent RNA reporters.

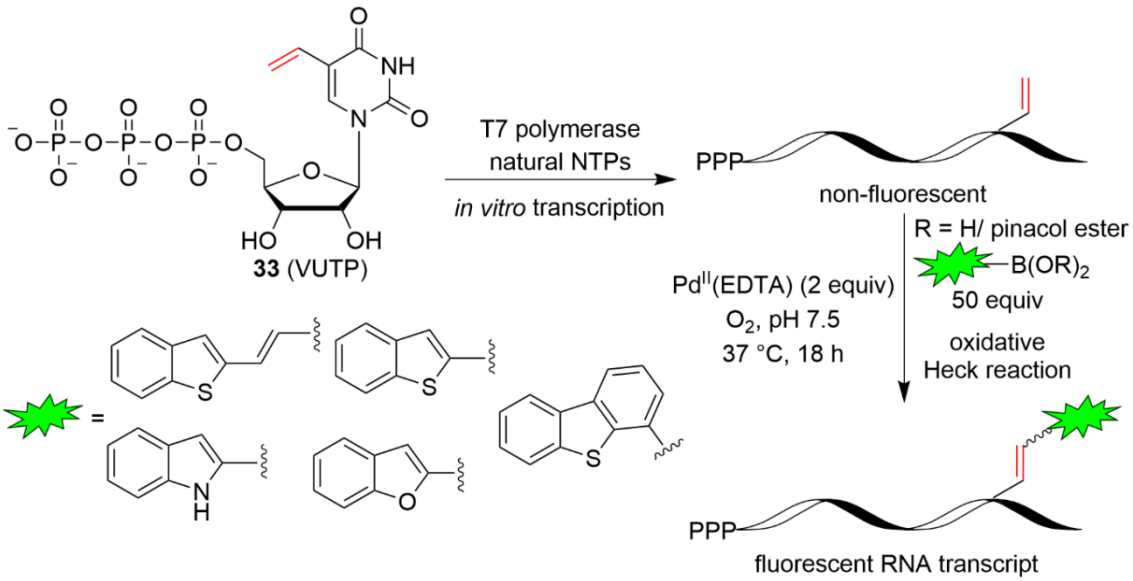

Figure 1.15. Posttranscriptional modification of vinyl-labeled RNA transcripts by using oxidative Heck reaction. Vinyl-labeled RNA was reacted with various heterocyclic boronic acid substrates in the presences of Pd-EDTA complex to produce fluorescent RNA.[74]

1.5 Functionalized nucleoside as supramolecular synthons

Supramolecular assemblies based on nucleobases, nucleosides, nucleotides and nucleic acids are useful for various biomedical and material applications.[75] Nucleic acids have received much attention as a unique material for constructing supramolecular motifs.[76] However, the major limitation associated with them is the scalability. On the other hand, supramolecular synthons based on nucleic acid components (nucleobase, nucleoside and nucleotide) are readily scalable and sustainable to generate the perfect balance between hydrophilicity and hydrophobicity.[77] Pyrimidne and purine can form non-covalent interactions like hydrogen bonding and π-π stacking. Purine bases, in particular guanine derivatives have potential to self-assemble more extensively compared to the pyrimidine nucleobase. The high propensity of guanine to self-assemble originates due to the presence of additional hydrogen bonding face (Hoogsteen) and expanded surface area for π-π stacking interaction. The self-assemblies formed by guanine derivatives and their applications are discussed in the following section.

Usually, derivatization of nucleobase, nucleoside and nucleotides with a hydrophobic group (e.g., fatty acid chain) is required to induce the gelation process (except guanine derivatives). Typically, hydrophobic tail or linker is attached either to sugar or nucleobase to achieve the necessary balance of hydrophobic character. The resulting derivatized product is commonly known as nucleolipid. There are several examples of nucleolipids based on pyrimidine-fatty acid conjugates, which have been published earlier in various reviews.[78] Here we have shown some of the examples of pyrimidine-nucleolipids that serves as low molecular weight gelators (LMWGs) (Figure 1.16).

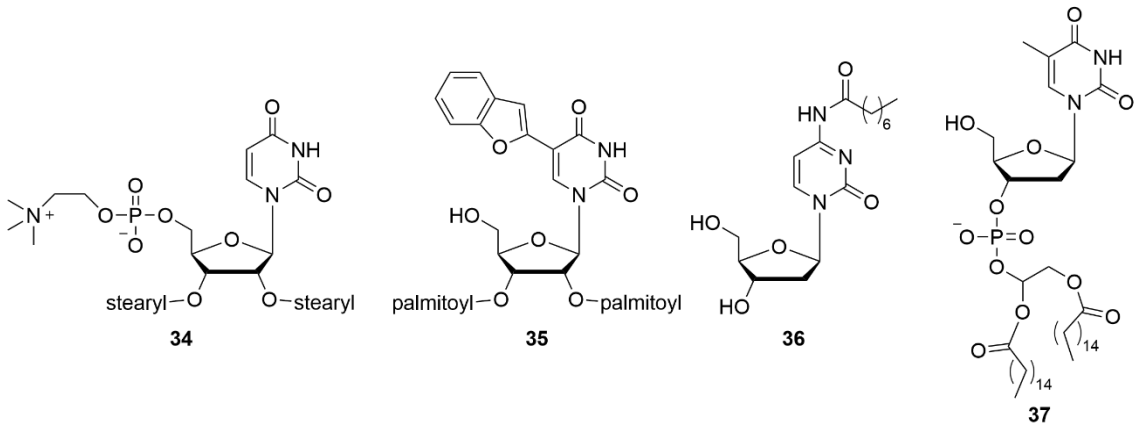

Figure 1.16. Chemical structures of synthetic pyrimidine-based nucleolipid.

Grinstaff and coworker reported the diacylated uridinophosphocholine derivative **34**, which forms stable and opaque hydrogels consisting of entangled helical nanofibers. The authors stated that the helical structure is formed by π-π stacking interaction between the nucleobases and hydrophobic interaction of stearyl group. The 5′-phosphocholine group in **34** provides solubility in aqueous media. Further, the hydrogels formed by the nucleolipid **34** are of potential use for the delivery of therapeutically relevant DNA or RNA.[79] Fluorescently modified nucleolipids synthon are less commonly reported. Our group developed an environment-sensitive fluorescent supramolecular synthon by attaching benzofuran-2-yl and benzothiophen-2-yl moieties at the C-5 position of uridine (e.g., **35** Figure 1.16). These fluorescent nucleoside–lipid hybrids form organogels in DMSO, which is driven by hierarchical structures such as fibres, twisted ribbons, helical ribbons and nanotubes. Morphological architecture is found to be depended on the nature of fatty acid chain and nucleobase modification. Most importantly, these nucleolipids retains their fluorescence even in the gel state and displayed aggregation induced enhanced emission (AIEE) after gelation.[80] Zelzer and coworkers reported a cytidine-based gelator by attaching octanoyl chain at the N4-position of the cytosine ring.[81] Novel supramolecular gelator, *N4*-octanoyl-2′-deoxycytidine **36** forms a transparent gel at 0.6 %w/v in binary systems of water and ethanol. Molecular dynamics (MD) simulations study suggest that gelators arrange themselves into a cylindrical fibre in such a way that the aliphatic chains face towards the inside core and cytosine ring stacked together and the hydrophilic sugars remain at the external surface of the fibre. The author claims that, this architecture present in cytidine based gel gives a promising opportunity for the encapsulation of therapeutically relevant DNA or protein or small bioactive molecules in drug delivery applications. Barthélémy and coworkers reported the synthesis of a nucleotide lipid which contains thymidine as a head group and 1,2-dipalmitoyl-sn-glycerol phosphate (diC16dT) as a tail (**37**).[82] In the presence of monovalent cations (Li^+, Na^+, K^+, NH_4^+ and $NHEt_3^+$) this nucleotide lipid spontaneously forms an opaque hydrogel. Further, the resultant hydrogel in the presence of alkali metal ions (Li^+, Na^+, K^+) can be safely injected into mice without any adverse effects. These hydrogels also allow the gradual release of proteins (e.g., bovine serum albumin) into the bloodstream *in vivo*.

While several pyrimidine-based LMWGs have been reported, supramolecular assemblies generated by the purine derivatives, especially guanine, require special mention. Guanine derivatized supramolecular synthons are the most fascinating among other

derivatized nucleosides due to their tendency to self-assemble into different forms of architectures including linear G-ribbon and cyclic G4-quartet (Figure 1.17).[83] Guanine can self-assemble into two different ribbon structures, where hydrogen bonds are formed in between amide proton at the N1, the amide oxygen O6, the amino protons at N2 and the lone pair at either the N7 (G-ribbon I) or the N3 (G-ribbon II) (Figure 1.17).On the other hand, G4-quartet is composed of four guanine units linked together by eight intermolecular hydrogen bonds in presence of metal ions (e.g., K^+, Na^+). However, there are some exceptions where G-quartet can form even in the absence of any added cation, for example, G-quartet formed by 8-aryl-substituted guanosine derivatives.[84] Further, these G-ribbons and G-quartets self-assemble extensively to form G-sheets and G-quadruplex, respectively. At certain concentrations these G-sheets or G-quadruplexes aggregate to form supramolecular gels.

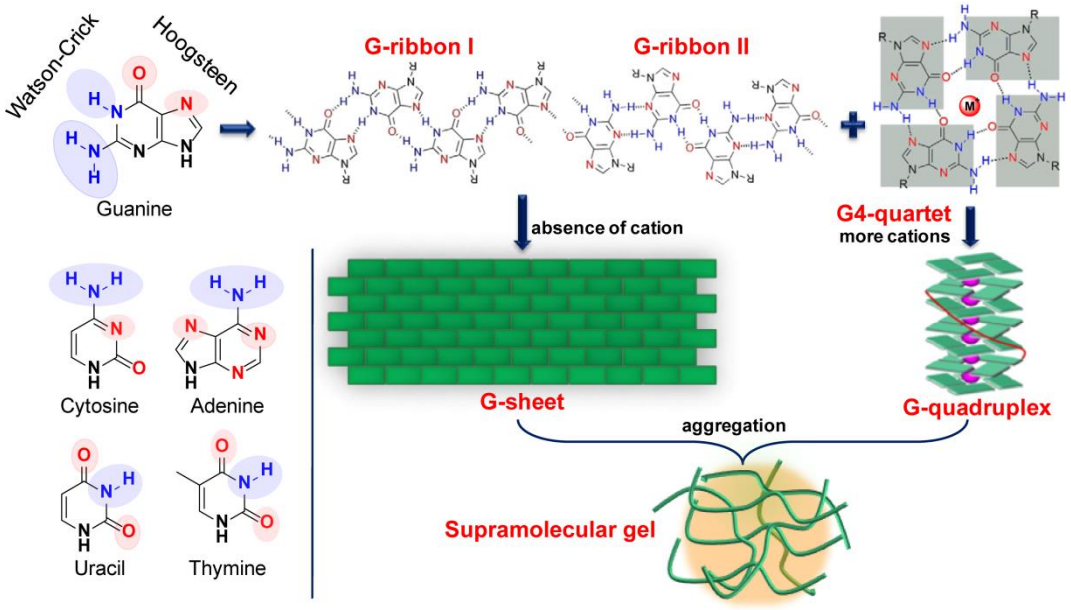

Figure 1.17. Guanine-containing derivatives self-assembled into different kind of motifs, including linear G-ribbon I, G-ribbon II and the cyclic G4-quartet, which further forms the supramolecular gel.

Usually, in the presence of cation, the guanine derivatives without fatty acid chain form a hydrogel, where G-quartet is the basic unit in the gel network. Guanosine and deoxyguanosine are insoluble in organic solvents and derivatization of them with fatty acid is useful in inducing gelation process. Lipophilic guanine derivatives form organogel even in the absence of added cations. Fortunately, the hydroxyl groups of sugar residues provide an excellent way to attach a fatty acid chain *via* alcohol-acid coupling. Also, functionalization at

the C-8 position can used to provide additional properties to the supramolecular gel. Thus, in recent years, various guanine-based organogelators have been developed. Some examples of lipophilic guanine derivatives are shown in Figure 1.18.

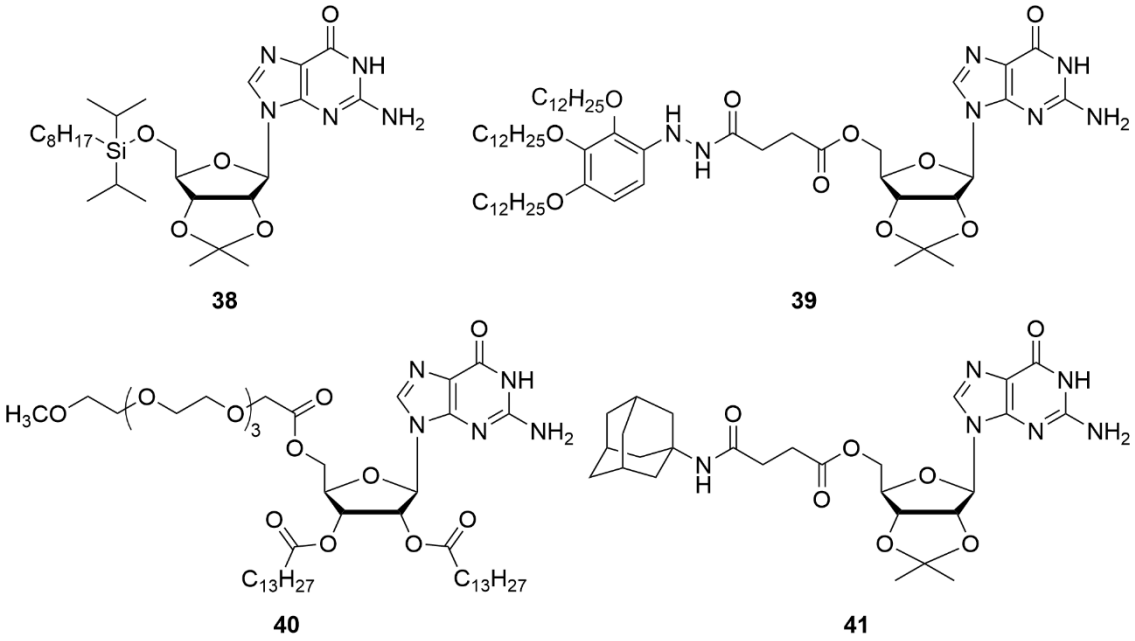

Figure 1.18. Examples of lipophilic guanine based supramolecular synthons which forms organogels.

Araki reported a series 2′, 3′-O-isopropylideneguanosine derivatives (e.g., **38**), which show excellent gelation ability in alkane solvent (e.g., n-Dexane).[85] Also, the addition of complimentary nucleolipid cytidine derivative, which itself is non-gelator suppressed the gelation ability of **38**. This suggests that the Watson–Crick G–C base pair was quite stronger compared to the G–G base pair in the gel network, indicating the G-G hydrogen bonding plays a crucial role in the gelation process. CD and IR analysis further confirmed the involvement of G–G base pair in the gelation process. Liu and coworkers reported reversible organogel, which can be triggered by the addition and removal of K^+ ions.[86] Lipophilic guanosine derivative **39** can immobilise both chloroform and toluene. This organogelator forms stable ribbon-like structure. The authors suggested that there could be π-π stacking interaction between aromatic hydrocarbon solvent (toluene) and guanine moiety. Interestingly, ribbon-like structure in organogel **39** was able to change to G-quartets after addition of K^+ ion. This led to the transformation from a gel to a sol state. Upon addition of cryptand [2.2.2], which can efficiently chelate K^+ ions, again G-quartets reverted to the ribbon-like structure and reformed the gel. Such an approach proves that the gel-sol transition

can be controlled by using external stimuli. Montesarchio and coworkers reported acylated polyether functionalized guanosine derivatives **40**. Lipophilic guanosine derivative **40** gave stable organogel in polar solvents, such as methanol, ethanol and acetonitrile. The authors suggested that the two bi-tailed alkyl chains at 2′- and 3′-OH is essential for the gelation process due to a balanced lipophilicity.[87] Yi and coworkers reported guanine nucleolipid **41**, which is derivatized with adamantane moiety.[88] Interestingly **41** forms G-quadruplex structure at low concentration in acetonitrile solution without any templating ions. Further, at higher concentration, the G-quadruplex from convert into a linear G-ribbon which next transformed into a gel network. Organogel formed by **41** was sensitive to sonication, and FESEM images showed that the morphology of the gel changes from a columnar structure to a flower-like structure after sonication. Moreover, this study shows that conversion between G-quartets and the G-ribbon structure could be reversibly controlled by just varying the concentration of the gelator.

1.6 Applications of guanine-based supramolecular synthons

1.6.1 Drug delivery

"Self-destroying" guanine-based hydrogels have been used in the controlled release of bioactive compounds. For example, the release of guanine-containing antiviral drugs acyclovir and ganciclovir have been achieved using hydrogels based on 5′-deoxy-5′-iodoguanosine (**42**) (Figure 1.19).[89]

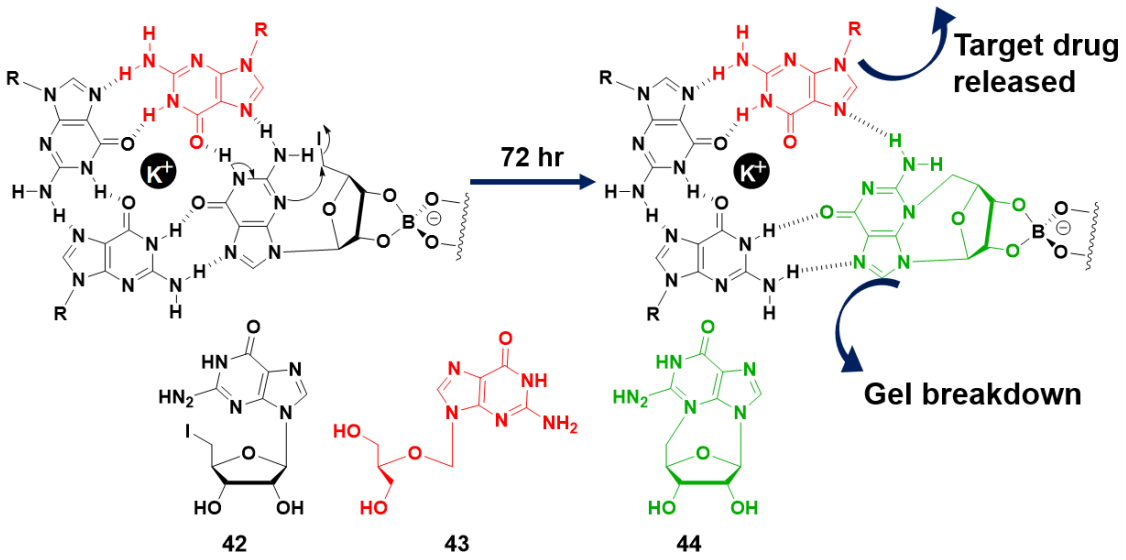

Figure 1.19. The cyclization of (**42**) to (**44**) triggers weakening and disruption of the gel, allowing the controlled release of acyclovir drug which was pre-incorporated into the stacked guanosine (G)-quartet assemblies. This schematic illustration is adapted from ref. 89.

Here, **42** and guanine-containing antiviral drug acyclovir (**43**) forms hydrogels with 2 equivalent $KB(OH)_4$. Over time, **42** undergoes *in situ* intramolecular cyclization to form a non-gelling compound (**44**), leading to breakdown of the gel. Disruption of the gel eventually releases pre-incorporated acyclovir drug (>80% release after 72 h). This ability of self-destroyinghydrogels could be potentially applied in controlled release of the various drugs *in vivo*, provided that the gelator and cyclized side product are non-toxic to the cell.

1.6.2 Scaffold for tissue engineering

Rowan and coworkers have used hydrogel made from 8-methoxy-2′,3′,5′-tri-*O*-acetylguanosine (8OMeTAcG, **45**) as a scaffold for tissue engineering.[90] Compound **45** can gel aqueous media at a low concentration of 0.5 wt% of **45** and 100 mM NaCl (Figure 1.20). The authors suggested that this is due to a shift in the conformational preference of **45** from anti to syn. Further, the hydrogel network formed by **45** supports cell culture. GFP-labeled C166 endothelial cells in DMEM solution were injected in 2 wt % of **45** + 1 wt % gelatin (which increases the adhesion of the cell). This cogel provided 3D gel network within which the cells incorporated and proliferated with little-to-no cytotoxicity. Microscopy analysis showed that the cells are quite healthy with good morphology, and they are present inside the gel network. This shows the gel formed by the combination of **45** with adhesive agent gelatin is suitable for growing the cells inside the gel network and can be used as a tissue engineering scaffold.

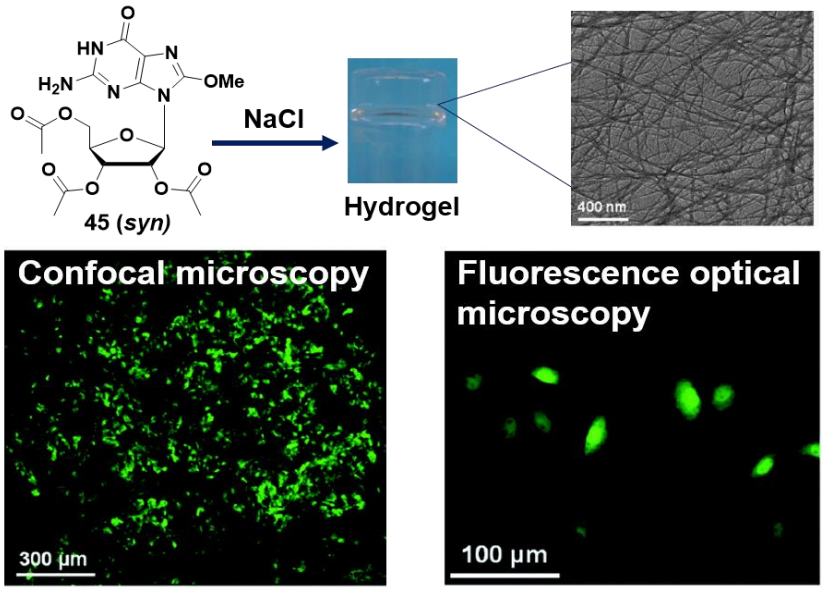

Figure 1.20. 2 wt% 8OMeTAcG/DMEM gel (with added 1 wt% gelatin) forms the hydrogel at 100 mM NaCl and shows the ability to culture the GFP +C166 cells inside its gel network as seen in the

confocal microscopy and fluorescence optical microscopy. This schematic illustration is adapted from ref. 90.

1.6.3 Environmental remediation

Davis and coworkers reported a hydrogel made of a binary mixture of 1:1 guanosine (G, **46**) and 8-aminoguanosine (8AmG, **47**) in the presence of a stoichiometric amount of either K^+ or Ba^{2+} ion (Figure 1.21).[91] These hydrogels show the ability to selectively adsorb the anionic dye from the bulk solution with the help of electrostatic interactions. Three dyes were used to study the uptake by the binary hydrogel: Naphthol blue black (NBB), rose bengal (RB) and safranin O (SO). It was found that the hydrogels in the presence of KCl adsorbs more of the anionic dyes (RB at 58% and NBB at 37%) than the cationic SO (22%). Most importantly, binary gel in the presence of a divalent cation Ba^{2+} shows higher selectivity towards the anionic dye over cationic dye**.** NBB and RB (89% and 75%, respectively) as compared to 15% of SO. These hydrogels are promising in the context of environmental remediation such as removing the pollutants from industrial wastes.

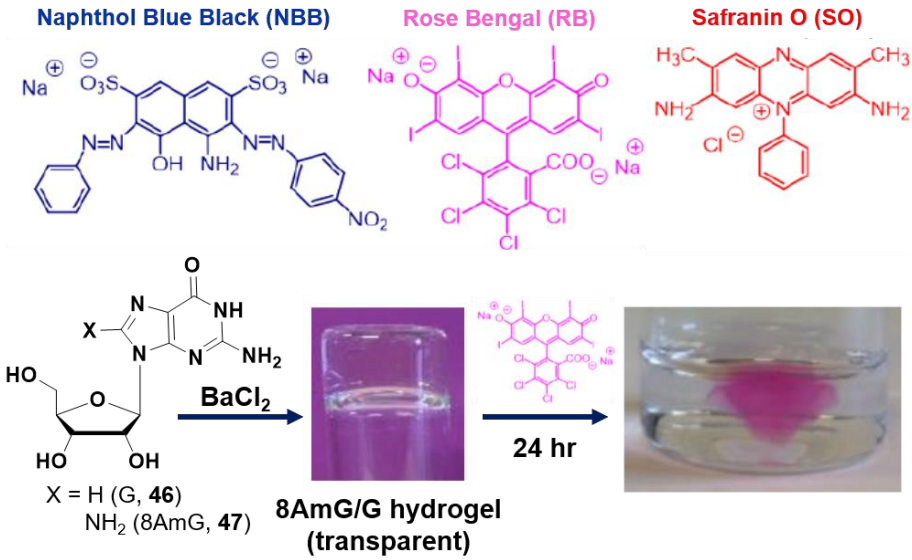

Figure 1.21. Binary mixture of G (**46**) and 8AmG (**47**) with Ba^{2+} give G-quartet structures that lead to the formation of transparent hydrogels. This hydrogel extracts selectively anionic dye NBB and RB from an aqueous phase into the gel network. This schematic illustration is adapted from ref. 91.

1.6.4 Ion channels

The lipophilic supramolecular assemblies have been widely used as frameworks to construct synthetic ion channels.[92] Davis and coworkers developed ionophores based on supramolecular assembly formed by lipophilic guanine core. These ionophores were

constructed by self-assembly of 5′-(3,5-bis(allyloxy)benzoyl)-2′,3′-isopropylidene guanosine (**48**) in the presence of potassium picrate, followed by crosslinking of neighbouring guanine units within the formed G-quadruplex using ruthenium-catalyzed ring-closing metathesis (Figure 1.22).[93]This approach of using the olefin metathesis to crosslink the guanine units within the G-quadruplex architectures helps to avoid the dynamics between self-assembly and disassembly of formed G-quadruplex. Thus making the stable and unimolecular G-quadruplex based-ionophore that would remain functional and integral when incorporated into the hydrophobic phospholipid membrane. CD analysis shows that the formed metathesis product $[G]_{16}$ **2** found to be stable and intact when added to an aqueous solution of EYPC liposomes. Further, both base-pulse assay and ^{23}Na NMR spectroscopic experiments show the $[G]_{16}$ **2** can selectively transport Na^+ over the K^+ ions across phospholipid bilayer membranes.

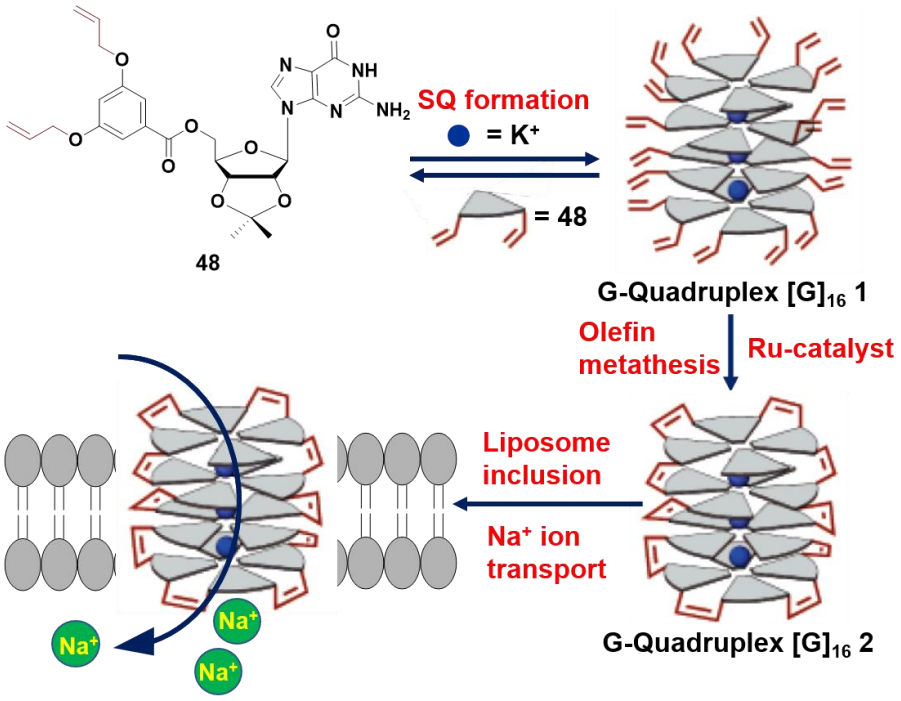

Figure 1.22. Schematic illustration showing the formation of G-quadruplex $[G]_{16}$ **1** by the 16 units of the **48**, followed by the formation of G-quadruplex $[G]_{16}$ **2***via* olefin metathesis. The formed supramolecular structure $[G]_{16}$ **2** acts as a Na^+ transporter through inclusion in a liposome membrane. This schematic illustration is adapted from ref. 93.

1.7 Research statement

It is clear from the above studies that a variety of Pd-mediated cross-coupling reactions have been established to functionalize DNA ONs in solution as well on solid-support. However, similar reaction conditions do not necessarily work for RNA due to its inherent instability.

Therefore, there is a significant demand for the development of robust and modular Pd-mediated cross-coupling reactions that will be suitable for labeling RNA ONs. Notably, studies also show (Section 1.3.1) that Pd-mediated cross-coupling reactions could be utilized in generating environment-sensitive fluorescent nucleoside probes through direct C-C bond formation. In addition to developing Pd-mediated RNA labeling strategies, we sought to harness the potential of this C-C bond formation reaction in designing environment-sensitive fluorescent supramolecular synthons that would self-assemble and enable construct responsive architectures.

a) Suzuki–Miyaura cross-coupling reaction generates functional nucleic acid probes: We describe the first example of an efficient and modular chemical functionalization methodology to label RNA transcripts with biophysical probes by using Suzuki–Miyaura cross-coupling reaction (Figure 1.23A). To set up the labeling technique, 5-iodo UTP analog was synthesized and enzymatically incorporated into RNA transcripts *in vitro* by using T7 RNA polymerase. Further, iodo-modified RNA transcripts werefunctionalized posttranscriptionally by Suzuki–Miyaura cross-coupling reaction with commonly used fluorescent and affinity tags, and new fluorogenic environment-sensitive nucleoside probes. After successfully establishing Suzuki–Miyaura cross-coupling reaction on RNA, we extended its utility in probing different nucleic acid conformations based on their reactivity (Figure 1.23B). For this purpose, polymorphic G-quadruplex forming human telomeric repeat sequence was used as a study system. The effect of various DNA conformations and position of iodo group on each loop on the efficiency of the Suzuki–Miyaura reaction was studied systematically.

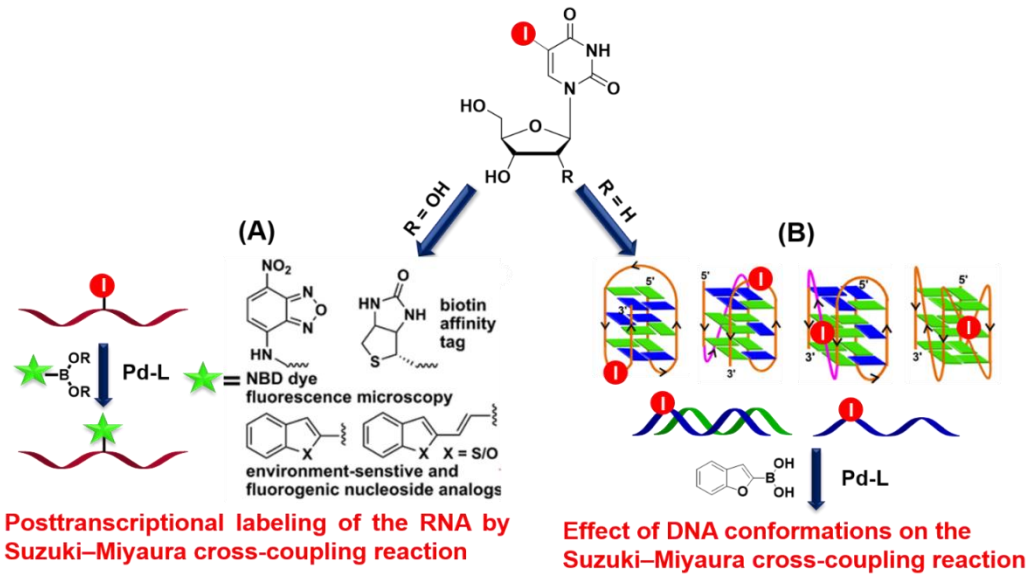

Figure 1.23. Use of iodo-modified uridine and deoxyuridine for postsynthetic Suzuki–Miyaura cross-coupling reaction (**A**) to label the RNA with fluorescent, fluorogenic environment-sensitive and affinity label biotin. (**B**) to study the effect of DNA conformations on reaction efficiency.

b) Environment-sensitive fluorescent nucleolipid supramolecular synthons: To construct fluorescent guanine-based synthons, we attached 2-vinylbenzofuran moiety at the C-8 position and long chain alkyl groups at 3′-*O*- and 5′-*O*- positions of 2′-deoxyguanosine (Figure 1.24). To attach the fluorophore unit at the C-8 position, we have taken advantage of Pd-mediated Suzuki–Miyaura cross-coupling reaction. Depending upon the nature of alkyl chain, the nucleolipid exhibits interesting fluorescence properties upon self-assembly. A combination of guanosine and fluorescent guanosine derivative, containing a methyl ester at 3′-*O*- and 5′-*O*- positions, hindered the crystallization process observed in simple guanosine gels and formed a stable cogel with modulated mechanical properties and morphological features. Further, the nucleolipids containing longer alkyl chain (R = myristyl and palmityl) formed green fluorescent organogels and exhibited chemo- and thermo-responsive behaviour after addition of a complimentary nucleolipid.

Collectively, the results presented in this thesis underscore the potential of Pd-mediated cross-coupling reactions in generating functionalized RNA oligonucleotides for biophysical analysis and functionalized supramolecular assemblies for material applications.

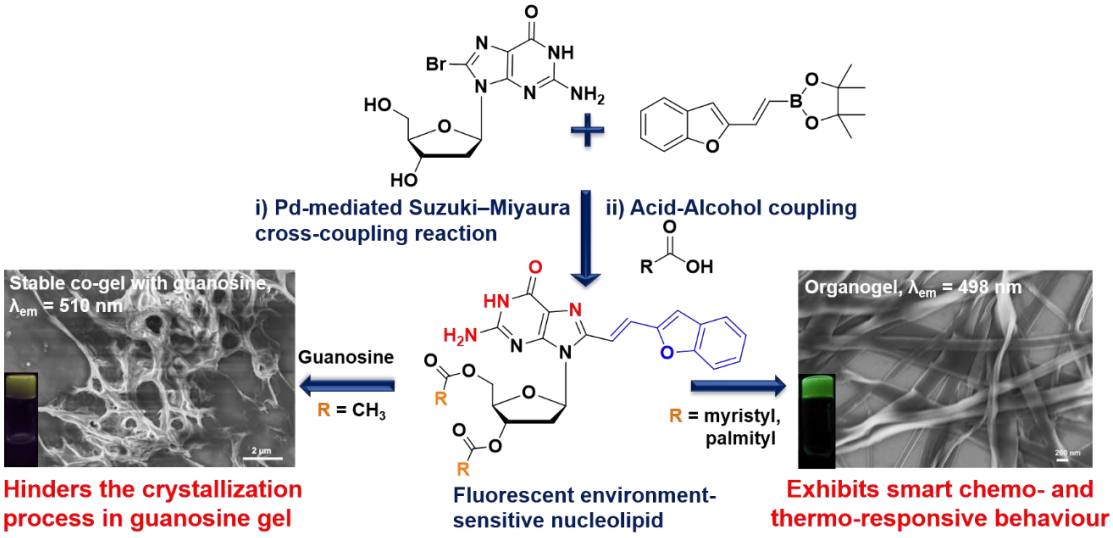

Figure 1.24. Application of Pd-mediated Suzuki-Miyaura cross-coupling reaction to generate the fluorescent environment-sensitive nucleolipids for supramolecular assembly.

1.8 References

1. (a) Hollenstein, M. *Molecules* **2012**, *17*, 13569–13591. (b) Kore, A. R.; Yang, B.; Srinivasan, B. *Curr. Org. Chem.* **2014**, *18*, 2072–2107. (c) Lapponi, M. J.; Rivero, C. W.; Zinni, M. A.; Britos, C. N.; Trelles, J. A. *Journal of Molecular Catalysis B: Enzymatic* **2016**, *133*, 218–233.
2. (a) Périgaud, C.; Gosselin, G.; Imbach, J. L. *Nucleos. Nucleot. Nucl. Acids* ***1992***, *11*, 903–945. (b) Galmarini, C. M.; Mackey, J. R.; Dumontet, C. *Lancet Oncol.* **2002**, *3*, 415–424. (c) De Clercq, E. *Annu. Rev. Pharmacol. Toxicol.* **2011**, *51*, 1–24.
3. (a) Verma, S.; Jäger, S.; Thum, O.; Famulok, M. *Chem Rec*. **2003**, *3*,51–60. (b) Martí, A. A.; Jockusch, S.; Stevens, N.; Ju, J.; Turro, N. J. *Acc. Chem. Res.* **2007**, *40*, 402–409. (c) Xia, T. *Curr. Opin. Chem. Biol.* **2008**, *12*, 604–611.
4. (a) Kwak, M.; Herrmann, A. *Chem. Soc. Rev*. **2011**, *40*, 5745–5755. (b) Peters, G. M.; Davis, J. T. *Chem. Soc. Rev*. **2016**, *45*, 3188–3206.
5. (a) Gissot, A.; Camplo, M.; Grinstaffd, M. W.; Barthélémy, P. *Org. Biomol. Chem.* **2008**, *6*, 1324–1333. (b) Yuan, D.; Du, X.; Shi, J.; Zhou, N.; Zhou, J.; Xu, B. *Angew. Chem. Int. Ed.* **2015**, *54*, 5705–5708. (c) Nuthanakanti, A.; Srivatsan, S. G. *Nanoscale* **2016**, *8*, 3607–3619. (d) Nuthanakanti, A.; Srivatsan, S. G. *ACS Appl. Mater. Interfaces* **2017**, doi: 10.1021/acsami.7b06037.
6. Ewald, B.; Sampath, D.; Plunkett, W. *Oncogene* **2008**, *27*, 6522–6537.
7. (a) Elion, G. B. *J. Med. Virol.* **1993**, *41*, 2–6. (b) Jordheim, L. P.; Durantel, D.; Zoulim, F.; Dumontet, C. *Nat. Rev. Drug Discov* .**2013**, *12*, 447–464.
8. (a) Neidle, S. *Principles of Nucleic Acid Structure*; Academic Press, Elsevier Inc., London, **2008**. (b) Egli, M.; Pallan, P. S. *Curr. Opin. Struct. Biol.* **2010**, *20*, 262–275. (c) Mortimer, S. A.; Kidwell, M. A.; Doudna, J. A. *Nat. Rev. Genet.* **2014**, *15*, 469–479.
9. (a) Wilson, J. N.; Kool, E. T. *Org. Biomol. Chem.* **2006**, *4*, 4265–4274. (b) Sinkeldam, R. W.; Greco, N. J.; Tor, Y. *Chem. Rev.* **2010**,*110*, 2579–2619. (c) Wilhelmsson, L. M. *Quart. Rev. Biophy*. **2010**, *43*, 159–183. (d) Srivatsan, S. G.; Sawant, A. A. *Pure Appl. Chem*. **2011**, *83*, 213–232. (e) Phelps, K.; Morris, A.; Beal, P. A. *ACS Chem. Biol.* **2012**, *7*, 100–109.
10. (a) Dethoff, E. A.; Chugh, J.; Mustoe, A. M.; Al-Hashimi, H. M. *Nature* **2012**, *482*, 322–330. (b) Bardaro Jr., M. F.; Varani, G. *WIREs RNA* **2012**, *3*, 122–132.
11. (a) Nguyen, P.; Qin, P. Z. *WIREs RNA* **2012**, *3*, 62–72. (b) Shelke, S. A.; Sigurdsson, S. T. *Springer*, **2016**, 159–187.
12. (a) Ogle, J. M.; Carter, A. P.; Ramakrishnan, V. *Trends Biochem. Sci*. **2003**, *28*, 259–266 (b) Holbrook, S. R. *Annu. Rev. Biophys*. **2008**, *37*, 445–464. (c) Serganov, A.; Patel, D. J. *Curr. Opin. Struct. Biol*. **2012**, *22*, 279–286.
13. (a) Wachowius, F.; Höbartner, C. *ChemBioChem* **2010**, *11*, 469–480. (b) Khakshoor, O.; Kool, E. T. *Chem. Commun*. **2011**, *47*, 7018–7024.
14. (a) Campbell, M. A.; Wengel, J. *Chem. Soc. Rev.* **2011**, *40*, 5680–5689. (b) Deleavey, G. F.; Damha, M. J. *Chem. Biol.* **2012**, *19*, 937–954. (c) Khvorova, A.; Watts, J. K. *Nat. Biotechnol.* **2017**, 35, 238–248.
15. (a) Sharma, V. K.; Watts, J. K. *Future Med. Chem*. **2015**, *7*, 2221–2242. (b) Brad Wan, W.; Seth, P. P. *J. Med. Chem.* **2016**, *59*, 9645–9667.
16. Blackburn, G. M.; Gait, M. J.; Loakes, D.; Williams, D. M. *Nucleic Acids in Chemistry and Biology*, third ed. Royal Society of Chemistry publishing, **2006**.

17. (a) Jung, K.-H.; Marx, A. *Cell. Mol. Life Sci.* **2005**, *62*, 2080–2091. (b) Hocek, M. *J. Org. Chem.* **2014**, *79*, 9914–9921. (c) Holstein, J. M.; Rentmeister, A. *Methods* **2016**, *98*, 18–25.
18. (a) Rao, H.; Tanpure, A. A.; Sawant, A. A.; Srivatsan, S. G. *Nat. Protocols* **2012**, *7*, 1097–1112. (b) Neef, A. B.; Luedtke, N. W. *ChemBioChem* **2014**, *15*, 789–793. (c) Sawant, A. A.; Tanpure, A. A.; Mukherjee, P. P.; Athavale, S.; Kelkar, A.; Galande, S.; Srivatsan, S. G.; *Nucleic Acids Res*. **2016**, *44*, e16.
19. (a) Morohashi, N.; Kimoto, M.; Sato, A.; Kawai, R.; Hirao, I. *Molecules***2012**, *17*, 2855–2876. (b) Hottin. A.; Marx, A. *Acc. Chem. Res.***2016**, *49*, 418–427.
20. (a) Gramlich, P. M. E.; Wirges, C. T.; Manetto, A.; Carell, T. *Angew. Chem. Int. Ed.***2008**, *47*, 8350–8358. (b) Weisbrod, S. H.; Marx, A. *Chem. Commun.***2008**, 5675–5685. (c) El-Sagheer, A. H.; Brown, T. *Chem. Soc. Rev.* **2010**, *39*, 1388–1405. (d) Paredes, E.; Evans, M.; Das, S. R. *Methods***2011**, *54*, 251–259. (e) Wu, H.; Devaraj, N. K. *Top Curr. Chem. (Z)* **2016**, 374: 3. doi:10.1007/s41061-015-0005-z. (f) George, J. T.; Srivatsan, S. G. *Method s***2017**, *120*, 28–38.
21. (a) Agrofoglio, L. A.; Gillaizeau, I.; Saito, Y. *Chem. Rev.* **2003**, *103*, 1875–1916. (b) Lakshman, M. K. *Curr. Org. Synth.* **2005**, *2*, 83–112. (c) Shaughnessy, K. H. *Molecules* **2015**, *20*, 9419–9454.
22. (a) Hervé, G.; Sartori, G.; Enderlin, G.; Mackenzie, G.; Len, C. *RSC Adv*. **2014**, *4*, 18558–18594. (b) Hervé, G.; Len, C. *Sustain. Chem. Process***2015**, 3: 3. doi:10.1186/s40508-015-0029-2.
23. Defrancq, E.; Messaoudi, S. **2017**, *18*, 426–431.
24. Tanpure, A. A.; Pawar, M. G.; Srivatsan, S. G. *Isr. J. Chem.* **2013**, *53*, 366–378.
25. Hocek, M.; Fojta, M. *Org. Biomol. Chem.* **2008**, *6*, 2233–2241.
26. Ludwig, J. *Biochim. Biophys. Acad. Sci. Hung.* **1981**, *16*, 131–133.
27. Shaughnessy, K. H. *Eur. J. Org. Chem.* **2006**, 1827–1835.
28. Casalnuovo, A. L.; Calabrese, J. C. *J. Am. Chem. Soc.* **1990**, *112*, 4324–4330.
29. (a) Shaughnessy, K. H.; Booth, R. S. *Org. Lett.* **2001**, *3*, 2757–2759. (b) Western, E. C.; Daft, J. R.; Johnson, II, E. M.; Gannett, P. M.; Shaughnessy, K. H. *J. Org. Chem.* **2003**, *68*, 6767–6774.
30. Thoresen, L. H.; Jiao, G.-S.; Haaland, W. C.; Metzker, M. L.; Burgess, K. *Chem. Eur. J.***2003**, *9*, 4603–4610.
31. (a) Čapek, P.; Pohl, R.; Hocek, M. *Org. Biomol. Chem.* **2006**, *4*, 2278–2284. (b) Čapek, P.; Cahová, H.; Pohl, R.; Hocek, M.; Gloeckner, C.; Marx, A. *Chem. Eur. J.***2007**, *13*, 6196– 6203.
32. Collier, A.; Wagner, G. *Org. Biomol. Chem.* **2006**, *4*, 4526–4532.
33. (a) Tanpure, A. A.; Srivatsan, S. G. *Chem. Eur. J.* **2011**, *17*, 12820–12827. (b) Tanpure, A. A.; Srivatsan, S. G. *Chembiochem.* **2012**, *13*, 2392–9156.
34. Manna, S.; Panse, C. H.; Sontakke, V. A.; Sangamesh, S.; Srivatsan, S. G. *ChemBioChem* **2017**, *18*, 1604–1615.
35. Manna, S.; Srivatsan, S. G.*Org. Lett.* 2019**,** *21*, 4646–4650.
36. Manna, S.; Sarkar, D.; Srivatsan, S. G. *J. Am. Chem. Soc.* **2018**, *140*, 12622–12633.
37. Rankin, K. M.; Sproviero, M.; Rankin, K.; Sharma, P.; Wetmore, S. D.; Manderville, R. A. *J. Org. Chem.* **2012**, *77*, 10498–10508.
38. Sproviero, M.; Fadock, K. L.; Witham, A. A.; Manderville, R. A.; Sharma, P.; Wetmore, S. D. *Chem. Sci.*2014**,***5* , 788–796.
39. Seo, Y .J.;Ryu, J. H.; Kim, B. H. *Org. Lett.* **2005**, *7*, 22, 4931–4933.

40. Seo, Y. J.; Lee, I. J.; Kim. B. H. *Bioorganic & Medicinal Chemistry Letters* **2008,** *18*, 3910–3913.
41. Riedl, J.; Pohl, R.; Ernsting, N. P.; Orság, P.; Fojta, M.; Hocek, M. *Chem. Sci.*, **2012**, *3*, 2797–2806.
42. Kuwahara, M.; Takano, Y.; Kasahara, Y.; Nara, H.; Ozaki, H.; Sawai, H.; Sugiyama, A.; Obika, S. *Molecules* **2010**, *15*, 8229–8240.
43. (a) Ramsay, N.; Jemth, A.-S.; Brown, A.; Crampton, N.; Dear, P.; Holliger, P. *J. Am. Chem. Soc.* **2010**, *132*, 5096–5104. (b) Steiger, N.; Marx, A. *ChemBioChem* **2010**, *11*, 1963–1966.
44. Hollenstein, M.; Hipolito, C.; Lam, C.; Dietrich, D.; Perrin, D. M. *Angew. Chem. Int. Ed.* **2008**, *47*, 4346–4350.
45. Riedl, J.; Pohl, R.; Rulíšek, L.; Hocek, M. *J. Org. Chem.* **2012**, *77*, 1026−1044.
46. Riedl, J.; Ménová, P.; Pohl, R.; Orság, P.; Fojta, M.; Hocek, M. *J. Org. Chem.* **2012**, *77*, 8287–8293.
47. Dziuba, D.; Pohl, P.; Hocek, M. *Chem. Commun.* **2015**, *51*, 4880–4882.
48. Dziuba, D.; Pohl, R.; Hocek, M. *Bioconjugate Chem.* **2014**, *25*, 1984–1995.
49. Dziuba, D.; Jurkiewicz, P.; Cebecauer, M.; Hof, M.; Hocek, M. *Angew. Chem. Int. Ed.* **2016**, *55*, 174–178.
50. Omumi, A.; Beach, D. G.; Baker, M.; Gabryelski, W.; Manderville, R. A. *J. Am. Chem. Soc.* **2011**, *133*, 42–50.
51. Naik, A.; Alzeer, J.; Triemer, T.; Bujalska, A.; Luedtke, N. W. *Angew. Chem. Int. Ed.* **2017**, *56*, 10850–10853.
52. (a) Spicer, C. D.; Davis, B. G. *Nat. Commun.* **2014**, *5*, 4740. (b) Yang, M.; Li, J.; Chen, P. R. *Chem. Soc. Rev.* **2014**, *43*, 6511–6526.
53. (a) Gayakhe, V.; Ardhapure, A.; Kapdi, A. R.;Sanghvi, Y. S.; Serrano, J. L.; García, L.; Pérez, J.; García, J.; Sánchez, G.; Fischer, C.; Schulzke, C. *J. Org. Chem.* **2016**, *81*, 2713–2729. (b) Bhilare, S.; Gayakhe, V.; Ardhapure, A. V.; Sanghvi, Y. S.; Schulzke, C.; Borozdina, Y.; Kapdi, A. R. *RSC Adv.* **2016**, *6*, 83820–83830. (c) Bhilare, S.; Shah, J.; Gaikwad, V.; Gupta, G.; Sanghvi, Y. S.; Bhanage, B. M.; Kapdi, A. R. *Synthesis* **2019**, *51*, 4239–4248. (d) Murthy Bandaru, S. S.; Bhilare, S.; Cardozo, J.; Chrysochos, N.; Schulzke, C.; Sanghvi, Y. S.; Gunturu, K. C.; Kapdi, A. R. *J. Org. Chem.* **2019**, *84*, 8921–8940.
54. Li, J.-H.; Zhang, X.-D.; Xie, Y.-X. *Eur. J. Org. Chem.* **2005**, 4256–4259.
55. Chalker, J. M.; Wood, C. S. C.; Davis, B. G. *J. Am. Chem. Soc.***2009**, *131*, 16346–16347.
56. Spicer, C. D.; Triemer, T.; Davis, B. G. *J. Am. Chem. Soc.* **2012**, *134*, 800–803.
57. Li, N.; Lim, R. K. V.; Edwardraja, S.; Lin, Q. *J. Am. Chem. Soc.* **2011**, *133*, 15316–5319.
58. Gao, Z.; Gouverneur, V.; Davis, B. G. *J. Am. Chem. Soc.* **2013**, *135*, 13612–13615.
59. Cahová, H.; Jäschke, A. *Angew. Chem. Int. Ed.* **2013**, *52*, 3186–3190.
60. Lercher, L.; McGouran, J. F.; Kessler, B. M.; Schofield, C. J.; Davis, B. G. *Angew. Chem. Int. Ed.***2013**, *52*, 10553–10558.
61. Jeong, H. S.; Hayashi, G.; Okamoto, A. *ACS Chem. Biol.* **2015**, *10*, 1450–1455
62. Ding, Y.; Clark, M. A. *ACS Comb. Sci.* **2015**, *17*, 1–4.
63. Ding, Y.; DeLorey, J. L.; Clark, M. A. *Bioconjugate Chem.* **2016**, *27*, 2597–2600.
64. Khan, S. I.; Grinstaff, M. W. *J. Am. Chem. Soc.***1999**, *121*, 4704–4705.
65. Rist, M.; Amann, N.; Wagenknecht, H.-A. *Eur. J. Org. Chem.* **2003**, 2498–2504.
66. Kottysch, T.; Ahlborn, C.; Brotzel, F.; Richert, C.*Chem. Eur. J.* **2004**, *10*, 4017–4028.

67. (a) Schiemann, O.; Piton, N.; Mu,Y.; Stock, G.; Engels, J. W.; Prisner, T. F. *J. Am. Chem. Soc.***2004**, *126*, 5722–5729. (b) Schiemann, O.; Piton, N.; Plackmeyer, J.; Bode, B. E.; Prisner, T. F.; Engels, J. W. *Nat. Protocols***2007**, *2*, 904–923.
68. Piton, N.; Mu,Y.; Stock,G.; Prisner, T. F.; Schiemann, O.; Engels, J. W. *Nucleic Acids Res.***2007**, *35*, 3128–3143.
69. Wicke, L.; Engels, J. W. *Bioconjugate Chem.* **2012**, *23*, 627–642.
70. Krause, A.; Hertl, A.; Muttach, F.; Jäschke, A. *Chem. Eur. J.* **2014**, *20*, 16613–16619.
71. Holstein, J. M.; Stummer, D.; Rentmeister, A. *Chem. Sci.* **2015**, *6*, 1362–1369.
72. (a) Rieder, U.; Luedtke, N. W. *Angew. Chem. Int. Ed.* **2014**, *53*, 9168–9172. (b) Bußkamp, H.; Batroff, E.; Niederwieser, A.; Abdel-Rahman, O. S.; Winter, R. F.; Wittmann, V.; Marx, A. *Chem. Commun.***2014**, *50*, 10827–10829.
73. Ourailidou, M. E.; van der Meer, J.-Y.; Baas, B.-J.; Jeronimus-Stratingh, M.; Gottumukkala, A. L.; Poelarends, G. J.; Minnaard, A. J.; Dekker, F. J. *ChemBioChem***2014**, *15*, 209–212.
74. George, J. T.; Srivatsan, S. G. *Bioconjugate Chem.* **2017**, *28*, 1529–1536.
75. (a) Davis, J. T.; Spada, G .P. *Chem. Soc. Rev.* **2007**, *36*, 296–313. (b) Spada, G .P.; Davis, J. T. *Chem. Soc. Rev.* **2016**, *45*, 3188–3206.
76. (a) Wang, Z.-G.; Ding, B. *Adv. Mater.* **2013**, *25*, 3905–3914. (b) Uzumcu, A. T.; Guney, O.; Okay, O. *ACS Applied Materials & Interfaces* **2018**, *10*, 8296–8306. (c) Yao, C.; Yuan, Y.; Yang, D.*ACS Applied Bio Materials* **2018**, *1*, 2012–2020.
77. (a) Llanes-Pallas,A.; Palma, C.-A.; Piot, L.; Belbakra, A.; Listorti, A.; Prato, M.; Samorì, P.; Armaroli, N.; Bonifazi, D. *J. Am. Chem. Soc.* **2009**, *131*, 509–520. (c) Li, X.; Kuang, Y.; Lin,H.-C.; Gao, Y.; Shi, J.; Xu, B. *Angew. Chem. Int. Ed* .**2011**, *50*, 9365–9369. (d) Wu, D.; Zhou, J.; Shi, J.; Du, X.; Xu, B.*Chem. Commun.* **2014**, *50*, 1992–1994.
78. Baillet, J.; Desvergnes, V.; Hamoud, A.; Latxague, L.; Barthélémy, P. *Adv. Mater.* **2018**, 1705078.
79. Moreau, L.; Barthélémy, P. Maataoui, M. E.; Grinstaff, M. W. *J. Am. Chem. Soc.***2004**, *126*, 7533–7539.
80. Nuthanakanti A.; Srivatsan. S. G. *Nanoscale*, **2016**, *8*, 3607–3619.
81. Angelerou, M.; W. J. M. Frederix, P.; Wallace, M.; Yang, B.; Rodger, A.; Adams, D. J.; Marlow, M.; Zelzer, M. *Langmuir* **2018**, *34*, 6912–6921.
82. Ramin, M. A.; Sindhu, K. R.; Appavoo, A.; Oumzil, K.; Grinstaff, M. W.; Chassande, O.; Barthélémy, P. *Adv. Mater.* **2017**, *29*, 1605227.
83. Davis, J. T. *Angew. Chem. Int. Ed.* **2004**, *43*, 668–698.
84. Sessler, J.; Sathiosatham, M.; *Angew. Chem., Int. Ed.* **2000**, *39*, 1300–1303.
85. Yoshikawa, I.; Yanagi, S.; Yamaji. Y.; Araki, K. *Tetrahedron* **2007**, *63*, 7474–7481.
86. Wang, X.; Zhou, L.; Wang, H.; Luo, Q.; Xu, J.; Liu, J. *J. Colloid Interface Sci.* **2011**, *353*, 412–419.
87. Simeone, L.; Milano, D.; De Napoli, L.; Irace, C.; Di Pascale, A.; Boccalon, M.; Tecilla, P.; Montesarchio, D. *Chem. Eur. J.* **2011**, *17*, 13854–13865.
88. Meng, L.; Liu, K.; Mo, S.; Mao, Y.; Yi, T.; *Org. Biomol. Chem.* **2013**, *11*, 1525–1532.
89. Plank, T. N.; Davis, J. T. *Chem. Commun.* **2016**, *52*, 5037–5040.
90. Buerkle, L. E.; von Recuma H. A.; Rowan, S. J. *Chem. Sci.* **2012**, *3*, 564–572.
91. Plank, T. N.; Skala, L. P.; Davis, J. T. *Chem. Commun.* **2017**, *53*, 6235–6238.
92. Davis, J. T.; Okunola, O.; Quesada, R. *Chem. Soc. Rev.* **2010**, *39*, 3843–3862.
93. Kaucher, M. S.; Harrell, Jr., W. A.; Davis, J. T. *J. Am. Chem. Soc.* **2006**, *128*, 38–39.

Chapter 2

Posttranscriptional Labeling by Using Suzuki–Miyaura Cross-Coupling Generates Functional RNA probes*

2.1. Introduction

Understanding of RNA structure and function, and its use in therapeutics are greatly aided by recent developments in the nucleic acid functionalization strategy based on bioorthogonal chemical reactions.[1–4] Traditional approaches like solid-phase synthesis and enzymatic methods are very useful in installing variety of probes onto RNA for various biophysical investigations. However, in several instances, elaborate chemical manipulations to synthesize the functionalized monomers (e.g., phosphoramidites and triphosphates) and challenges associated with their incorporation (e.g., stability under reaction conditions, poor coupling and enzymatic incorporation efficiency) limit the applications of these methods.[4] In this context, postsynthetic modification of RNA by using bioorthogonal reactions is proving as a valuable tool to generate functional RNA probes. In this method, an RNA ON is labeled with a small reactive handle by using solid-phase ON synthesis protocol or by using the substrate promiscuity of RNA polymerases and certain RNA processing enzymes (e.g., transferases).[4–6] Following this step, a chemoselective reaction with the cognate reactive partner is performed to introduce the desired functional modification into the RNA. Reactions like azide-alkyne cycloaddition,[7–22] Staudinger ligation,[21] inverse electron demand Diels– Alder,[23–28] to name a few, have emerged as valuable tools to label, image and profile RNA in cell-free and cellular environments. These methods often use bulky activated building blocks (e.g., cyclooctyne, tetrazine, norbornyl etc.) to promote efficient postsynthetic reaction under mild conditions. However, the synthesis of many of these building blocks is tedious involving multiple steps, and if commercially available are very expensive.[29–31] Therefore, establishment of new postsynthetic RNA modification strategies that allow direct introduction of various functionalities by using easily accessible tags and reporters remains a high priority.[2]

---

*_The work presented in this chapter is published:_ Walunj, M. B.; Tanpure, A. A.; Srivatsan, S. G. Posttranscriptional labeling by using Suzuki-Miyaura cross-coupling generates functional RNA probes. *Nucl. Acid. Res*. **2018**, *46*, e65. DOI: 10.1093/nar/gky185.

In this regard, Pd-mediated C-C bond formation, which is applied in almost all facets of chemistry, is proving useful as a valuable chemoselective transformation for synthetic modification of biomacromolecules.[32–36] This has been possible due to the development of new Pd-ligand catalytic systems, which appreciably accelerate the coupling reaction inaqueous buffer.[37–39] Manderville group first demonstrated the usefulness of Suzuki–Miyaura reaction in the postsynthetic functionalization of DNA oligonucleotides (ON).[40] ONs containing 8-bromoguanosine were reacted with arylboronic acids in the presence of a catalytic system made of $Pd(OAc)_2$ and a water-soluble triphenylphosphan-3,3',3''-trisulfonate ligand, which was used previously for nucleotide modification.[41,42] Using a similar method, a diarylethene photoswitch capable of undergoing reversible electrocyclic rearrangement was introduced into DNA ONs.[43] This catalytic system requires elevated temperature (>70 °C), long reaction time and alkaline conditions to generate coupled ON products in moderate yields. Meantime, Davis group used a combination of $Pd(OAc)_2$ and 2-aminopyrimidine-4,6-diol (ADHP) or dimethylamino-substituted ADHP (DMADHP), which was originally developed for labeling proteins by Suzuki and Sonogashira reactions,[44–46] to step up a milder route to directly install functional labels onto DNA ONs by using Suzuki–Miyaura reaction.[47] Despite these successes with protein and DNA, functionalization of RNA by Pd-mediated coupling reactions remains a major challenge as methods developed for protein and DNA mostly do not work for RNA due to inherently low stability of RNA.[28,48–49] Therefore, we embarked on establishing a milder and efficient method to modify RNA by first incorporating a halogenated nucleotide analog into RNA by transcription reaction, followed by a posttranscriptional Suzuki–Miyaura reaction in the presence of a cognate reactive partner labeled with a desired biophysical reporter or tag (Figure 2.1). Here, we demonstrate a posttranscriptional modification method to generate functional RNA probes by using Suzuki–Miyaura reaction under benign conditions (37 °C and pH 8.5). This method is modular, and offers direct access to RNA labeled with fluorogenic environment-sensitive nucleoside analogs for nucleic acid structure and recognition analysis, fluorescent probes for microscopy and an affinity tag for pull-down and immunoassay (Figure 2.1).

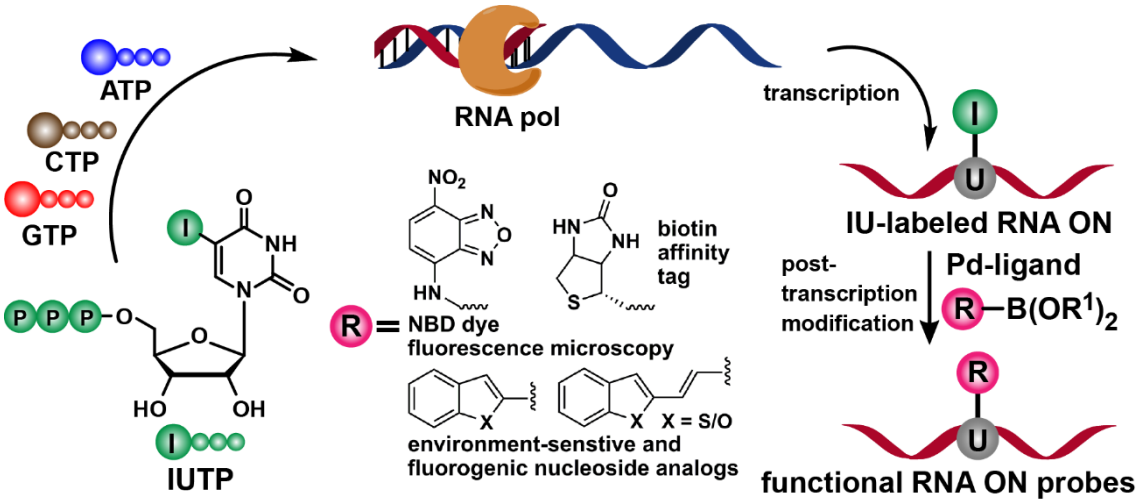

Figure 2.1. Design showing the posttranscriptional functionalization of iodouridine-labeled RNA transcripts by using Suzuki–Miyaura cross-coupling reaction to generate RNA labeled with functional probes.

Base-functionalized nucleoside analogs containing fluorescent, isotope, heavy atom or spin labels serve as excellent tools for biophysical investigation of nucleic acid structure, dynamics and function.[50–61] Many such modified nucleoside and nucleotide substrates, suitable for incorporation into ONs, are synthesized from halogenated nucleosides and nucleotides (e.g., iodo-labeled substrates) by using Pd catalyzed cross-coupling reaction as the key step.[62–64] However, necessity to prepare individual substrates, and the challenges associated with their synthesis and incorporation (vide supra) can be circumvented by developing a modular postsynthetic RNA labeling method, which would allow direct installation of the probes by Suzuki–Miyaura reaction between iodo-labeled RNA ONs with various easily accessible boronic acid/ester substrates (Figure 2.1).

2.2 Results and discussion

2.2.1 Enzymatic incorporation of 5-iodouridine 5′-triphosphate (IUTP 2) into RNA ON:

In order to setup an RNA functionalization method by Suzuki–Miyaura reaction, we chose to incorporate 5-iodouridine 5'-triphosphate (IUTP **2**) into RNA transcripts by in vitro transcription reaction.[65,66] Iodo-modified nucleoside phosphoramidites can also be used to incorporate the halogen label into RNA ONs by solid-phase method. IUTP was prepared by phosphorylating IU (**1**)[67] using $POCl_3$ and bis-tributylammonium pyrophosphate[68] by following the literature procedure (Scheme 2.1).[69]

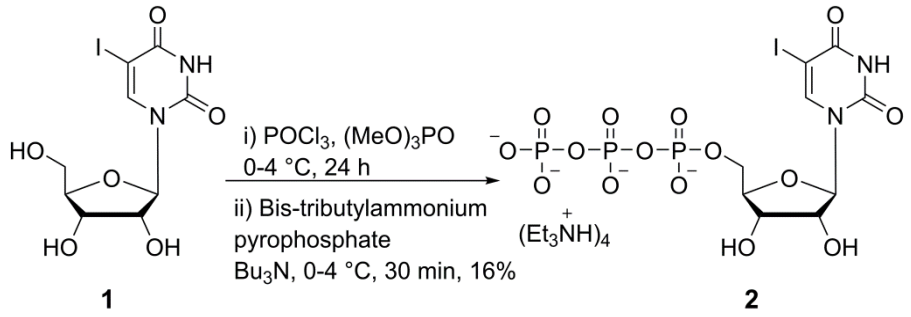

Scheme 2.1. Synthesis of 5-iodouridine triphosphate **2**.

The efficiency of IUTP incorporation by bacteriophage T7 polymerase was evaluated by performing in vitro transcription reactions with a series of T7 promoter-template DNA duplexes (Figure 2.2). The templates were designed to guide the incorporation of monophosphate of IUTP into RNA at one or two sites. The templates also contained a single dT residue at the 5'-end of the coding region so that a reaction performed in the presence of UTP/IUTP, GTP, CTP and α-^{32}P ATP, if successful, would result in the formation of the full-length transcripts containing a radioactive α-^{32}P A label at the 3'-end.

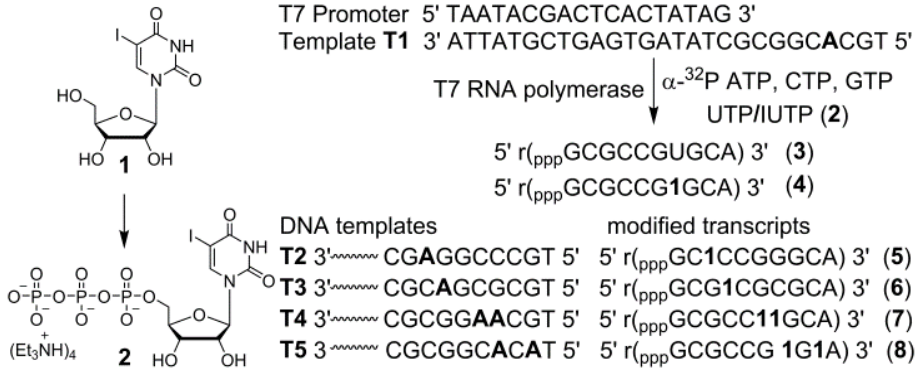

Figure 2.2. Incorporation of IUTP **2** (prepared from IU **1**) into RNA ONs by *in vitro* transcription reactions using T7 RNA polymerase and templates T1−T5. Transcripts **4**−**8** containing IU label at different sites are shown.

Reactions performed with template T1 and UTP/IUTP produced full-length transcripts **3** and **4**, respectively, with excellent efficiency and comparable yields (98%, Figure 2.3, lanes 1 and 2). Slower mobility of 4 compared to 3 indicated the incorporation of modified U into transcript **4**. The labeling of IU in the full-length transcript was confirmed by mass measurement of the purified transcript prepared from a large-scale reaction (Figure 2.4). A control reaction in the absence of UTP and IUTP did not yield full-length transcript, indicating that there was no misincorporation during the transcription process (lane 3).

Interestingly, in a reaction containing 1:1 molar ratio of UTP and IUTP, the RNA polymerase preferentially incorporated IUTP over UTP (lane 4). Reactions with other templates (T2−T5) indicated that IU can be introduced near the promoter region and at more than one site with very good efficiency (lanes 5−12).

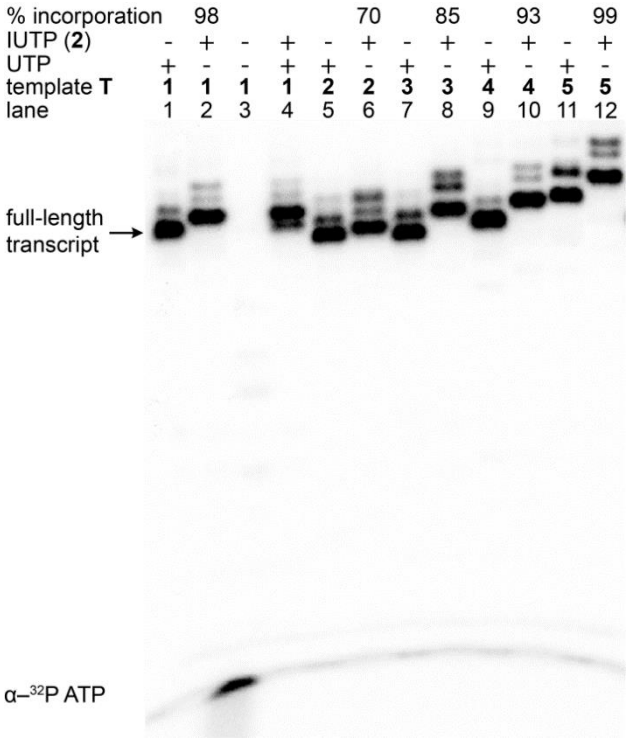

Figure 2.3. Phosphor image of transcripts obtained by *in vitro* transcription of DNA templates **T1**–**T5** in the presence of UTP/IUTP **2**. Incorporation efficiency of **2** is reported with respect to a control reaction with UTP. Trace amounts of non-templated products are formed along with full-length transcripts.

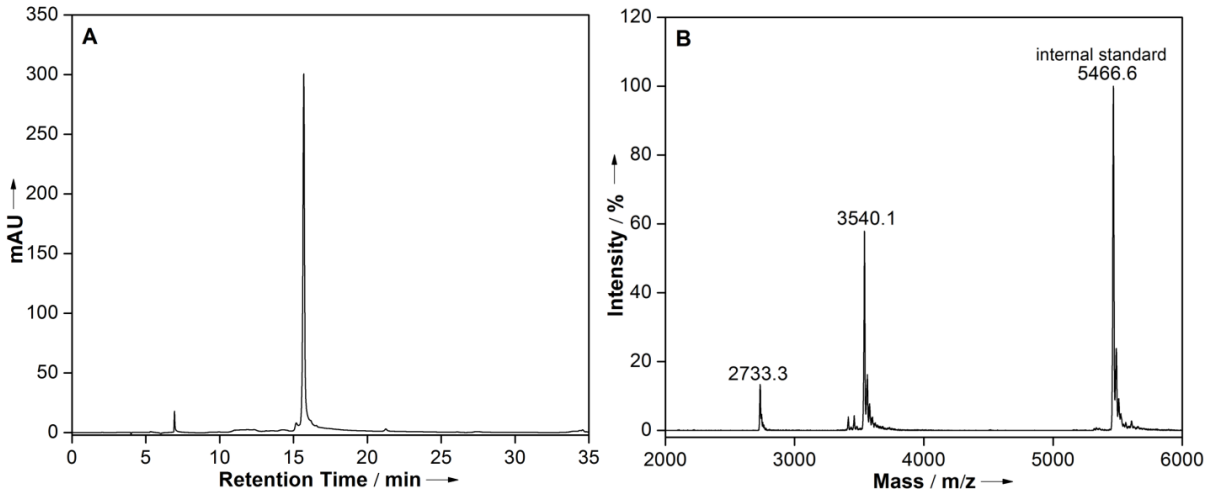

Figure 2.4. (**A**) HPLC chromatogram of PAGE purified IU-labeled RNA transcript **4** at 260 nm. Mobile phase A = 50 mM triethylammonium acetate buffer (TEAA, pH 7.0), mobile phase B =

acetonitrile. Flow rate = 1 mL/min. Gradient = 0−30% B in 35 min, 30−100% B in 10 min and 100% B for 5 min. HPLC analysis was performed using Phenomenex-Luna C18 column (250 x 4.6 mm, 5 micron).
(**B**) MALDI-TOF mass spectrum of RNA ON **4**. Spectrum is calibrated with respect to the +1 and +2 ion of an internal 18-mer DNA ON standard (m/z for +1 and +2 ion are 5466.6 and 2733.3 respectively). Calcd. mass for IU-modified RNA transcript **4**: $[M]^+$ 3540.8; found: $[M]^+$ 3540.1.

2.2.2 Synthesis of boronate ester and catalyst for Suzuki–Miyaura reaction

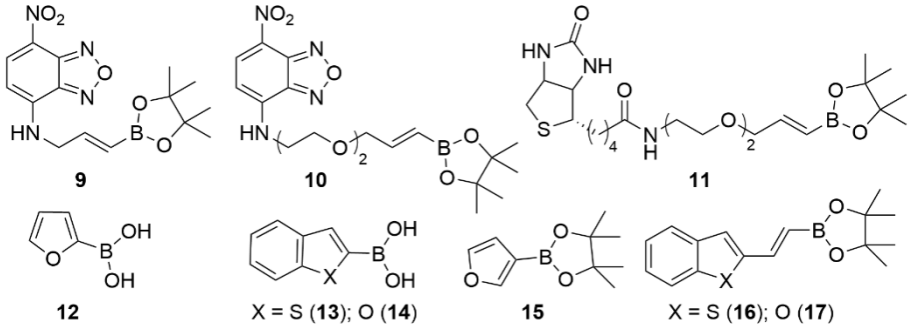

Figure 2.5. Substrates used in posttranscriptional Suzuki–Miyaura coupling.

For the synthesis of the different boronic esters (**9**-**11**, Figure 2.5), firstly two amine-containing boronic acid pinacol esters with different length linkers (with zero (**21**) or two (**22**) PEG units), starting from propargylamine or 2-(2-aminoethoxy)ethanol, were synthesized (Scheme 2.2 and Scheme 2.3).[47] The resulting amines **21** and **22** were coupled to NBD-Cl or biotin yielding the desired boronate esters (**9**–**11**, Figure 2.5).

2.2.2.1 Synthesis of boronate ester containing short and long amine linker (21 and 22)

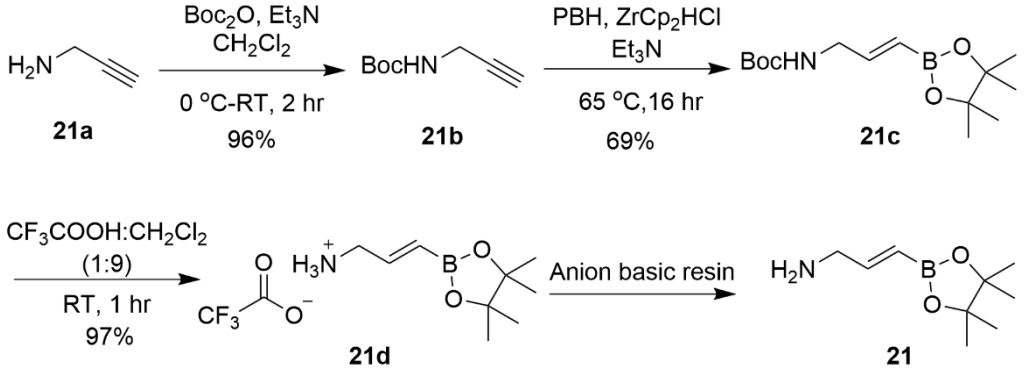

Scheme 2.2. Synthesis of (*E*)-3-(4,4,5,5-tetramethyl-1,3,2-dioxaborolan-2-yl)prop-2-en-1-amine amine linker **21.**

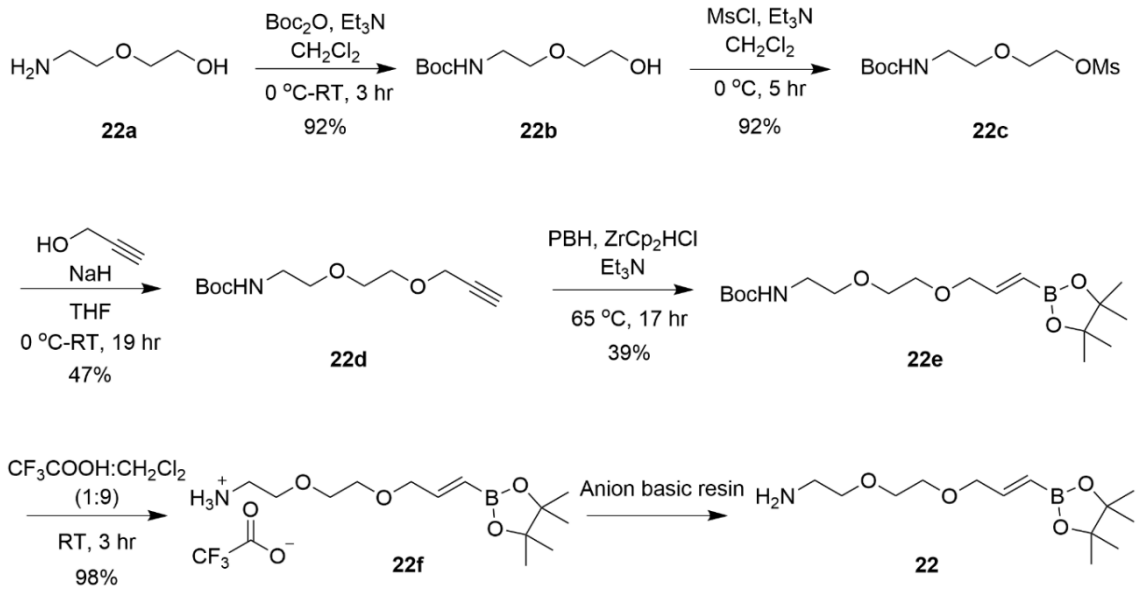

Scheme 2.4. Synthesis of (*E*)-2-(2-((3-(4,4,5,5-tetramethyl-1,3,2-dioxaborolan-2-yl)allyl)oxy)ethoxy) ethan-1-amine linker **22**.

2.2.2.2 Synthesis of NBD- and biotin-tagged pinacol boronate esters (9–11)

Linker **21** and **22** were reacted with NBD-Cl in presence of triethyl amine to yielding NBD modified boronate esters **9** and **10**, respectively. Amine linker **22** was coupled with activated biotin **11b**[70] to give biotin labelled boronate ester **11** (Scheme 2.4).

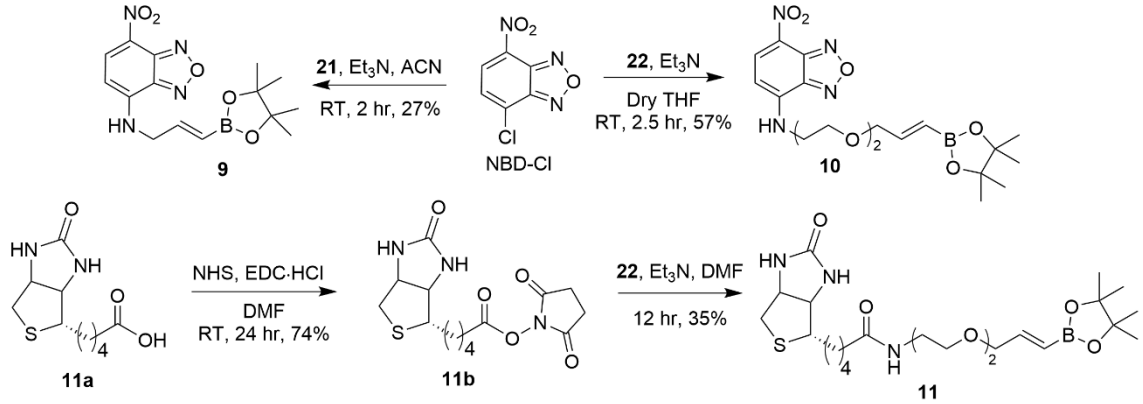

Scheme 2.4. Synthesis of NBD- and biotin-tagged pinacol boronate esters **9**–**11**.

2.2.2.3 Synthesis of 2-vinylbenzothiophene- and 2-vinylbenzofuran-boronic esters 16 and 17

Boronic esters **16** and **17** were synthesized using hydroboration reaction with 2-ethynyl benzothiophene[71] and 2-ethynyl benzofuran[72], respectively.

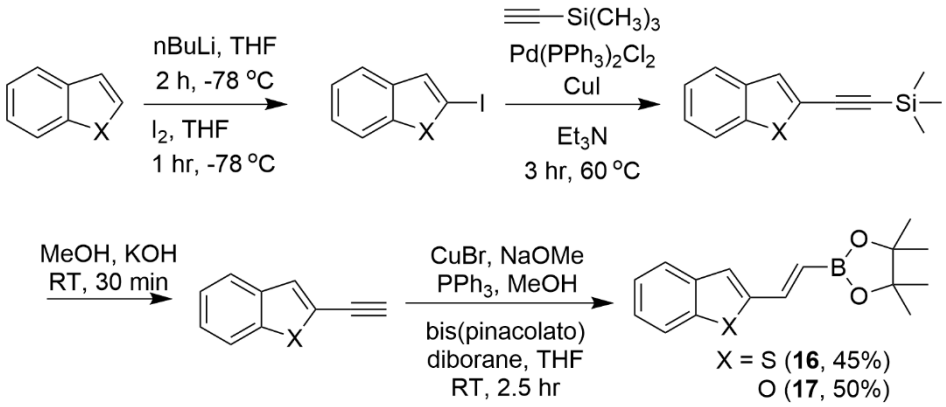

Scheme 2.5. Synthesis of 2-vinylbenzothiophene- and 2-vinylbenzofuran-boronic esters **16** and **17**.

2.2.2.4 Synthesis of *N,N*-dimethyl-4,6-dihydroxy pyrimidine ligand (L2) and catalyst preparation

Synthesis of ligand L2 and preparation of $Pd(OAc)_2(L)_2$ complex using either L1 or L2 ligand was completed by following the literature procedure.[73,47]

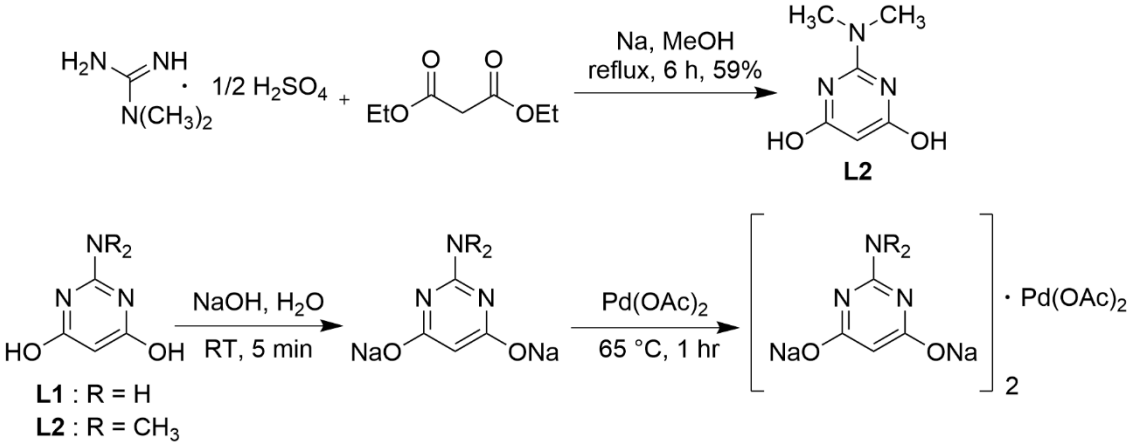

Scheme 2.6. Synthesis of ligand L2 and palladium complex.

2.2.3 Posttranscriptional Suzuki–Miyaura cross-coupling reaction

2.2.3.1 Optimization of coupling reaction conditions: IU-labeled RNA ON **4** was subjected to Suzuki–Miyaura cross-coupling at different stoichiometries of the substrate and reagents so as to achieve good conversion with minimum degradation of the coupled product. We preferred to use a combination of $Pd(OAc)_2$ and ADHP (L1) or DMADHP (L2) as this system has been shown to be efficient in the Pd-mediated functionalization of protein and DNA.[44–47] Coupling reaction was performed by incubating **4** (1 equiv) with $Pd(OAc)_2(L1)_2$ (1 equiv) and nitrobenzofurazan (NBD)-labeled boronic ester **9**/**10** (commonly used dye in fluorescence imaging, 100 equiv) in Tris–HCl buffer (50 mM, pH 8.5) at 37 °C (Figures 2.5

and 2.6). Aliquots of reaction mixture after 3, 6 and 9 h were resolved by analytical polyacrylamide gel electrophoresis under denaturing conditions, and analyzed by UV-shadowing. Rewardingly, reactions with boronic esters **9** and **10** resulted in the formation of respective coupled RNA product, which migrated slower compared to the substrate 4 (Figure 2.7A). A reaction with NBD dye (**10**) attached to boronic ester via a longer linker showed almost complete consumption of the substrate in 6 h as compared to **9**, which remained partially consumed after 9 h. When the amount of boronic ester **10** was reduced to 50 equivalents, the reaction required a slightly higher loading of Pd-L1 (2 equiv) to effect the coupling in 6h (Figure 2.7B). UV-shadowing the gel at longer wavelength (∼365 nm) further confirmed the fluorescence labeling of RNA with NBD. Importantly, under these conditions we observed no detectable degradation of the RNA product.

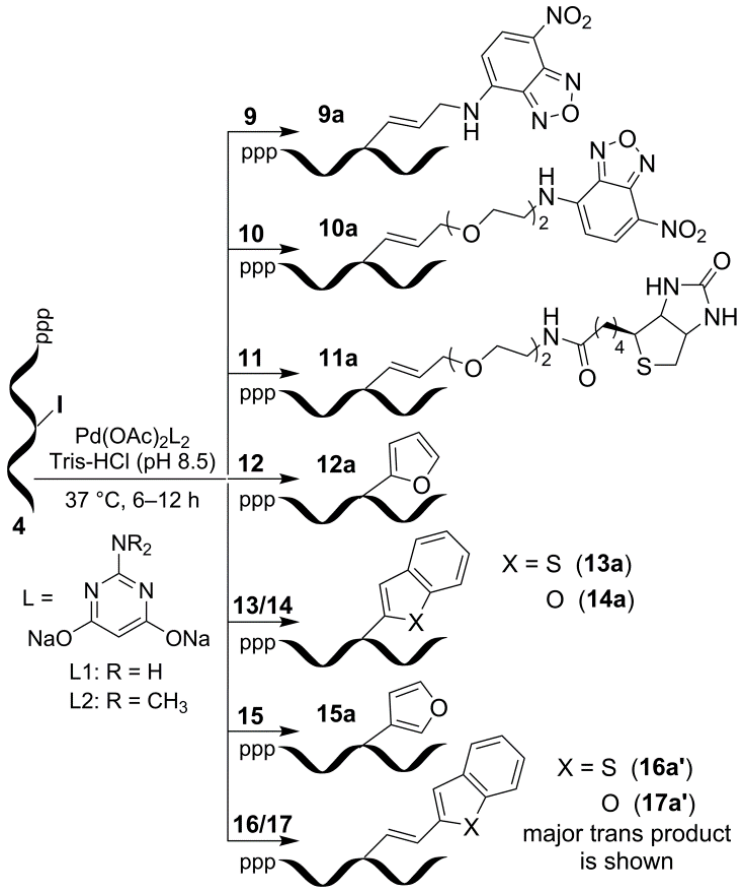

Figure 2.6. Posttranscriptional chemical functionalization of IU-labeled RNA transcript **4** with substrates **9**–**17** by using Suzuki–Miyaura reaction.

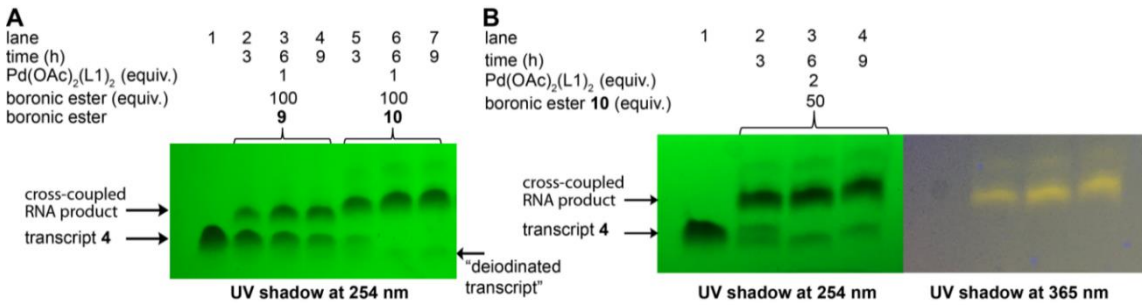

Figure 2.7. (**A**) Suzuki reaction on iodo-labeled RNA ON **4** using 1 equivalent of Pd-catalyst and 100 equivalents of boronic ester **9**/**10**. UV-shadow of the gel (short wave UV, 254 nm). (**B**) Suzuki reaction on IU-labeled RNA ON **4** using 2 equivalents of Pd-catalyst and 50 equivalents of boronic ester **10**. UV-shadow of the gel at 254 nm (left) and at 365 nm (right).

2.2.3.2 Posttranscriptional coupling of RNA with fluorescent and affinity tags: Based on these preliminary results, transcript **4** (5 nmol, 1 equiv) was then subjected to posttranscriptional coupling reaction with boronic esters **9**–**11** (50 equiv) using Pd-L1/L2 (2 equiv) catalytic systems. The reaction was monitored by High performance liquid chromatography (HPLC), and the peak corresponding to the product was isolated and characterized by mass analysis (Figure 2.8 and Table 2.1). While UV shadowing of the gel gave a qualitative understanding of the coupling reaction, HPLC analysis gave a better understanding of the reaction in terms of efficiency and isolated yields (Table 2.2). A reaction with NBD-boronic ester **9**, containing a short linker, in the presence of L1 gave 28% of the fluorescent RNA product **9a** in 12 h. However, a reaction with NBD-boronic ester 10, containing a longer linker, afforded 30% of the fluorescent RNA product **10a** within 6 h. Under similar conditions, biotin-coupled RNA product **11a** was isolated in 28% yield from a reaction with biotinylated boronic ester substrate **11**. HPLC chromatogram of reactions with substrates **9**–**11** revealed the formation of noticeable amount of deiodinated transcript along with unreacted transcript **4**, and hence, longer reaction times were not attempted with these substrates (Figure 2.8). Reactions using Pd-L2 system for above substrates were found to be less efficient as compared to Pd-L1 combination (Table 2.2 and Figure 2.9).

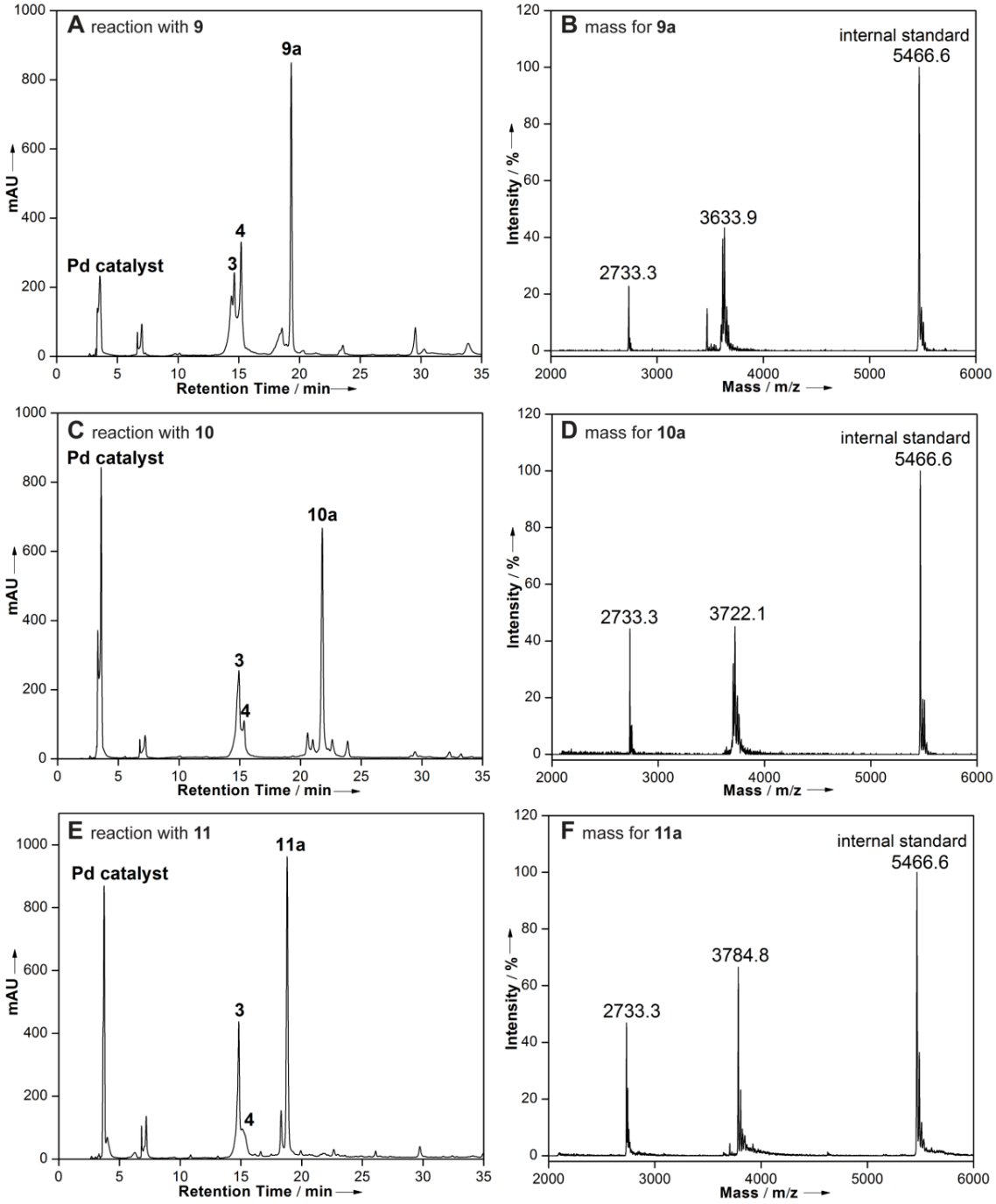

Figure 2.8. (**A**, **C**, **E**)RP-HPLC chromatogram of reaction mixture of Suzuki–Miyaura cross-coupling between IU-labeled transcript **4** and boronic esters **9**–**11**. **9a**–**11a** correspond to coupled RNA ON product; **3** is deiodinated transcript. Mobile phase A: 50 mM TEAA buffer (pH 7.0); mobile phase B: acetonitrile. Flow rate: 1 mL/min. Gradient: 0−30% B in 35 min, 30−100% B in 10 min and 100% B for 5 min.
(**B**, **D**, **F**) MALDI-TOF mass spectrum of coupled RNA ON products **9a**, **10a** and **11a** (HPLC fractions) obtained from reactions between transcript **4** and boronic esters **9**–**11**, respectively. See Figure 2.6 for the structure of the product. Spectrum is calibrated with respect to the +1 and +2 ion of an internal 18-mer DNA ON standard (m/z for +1 and +2 ion are 5466.6 and 2733.3 respectively). See Table 2.1 and Table 2.2 for isolated yield and mass data.

Table 2.1. Mass data of Suzuki–Miyaura cross-coupled RNA ON products obtained by posttranscriptional chemical modification of IU-labeled RNA ON transcripts.

Entry	Cross-coupled RNA ON product	MALDI-TOF analysis of product (m/z) $[M]^+$	
		Calculated	Observed
1	**9a**	3633.1	3633.9
2	**10a**	3721.2	3722.1
3	**11a**	3784.4	3784.8
4	**12a**	3481.0	3482.0
5	**13a**	3547.1	3546.6
6	**14a**	3531.0	3531.0
7	**15a**	3481.0	3481.1
8	**16a′**	3573.1	3573.3
9	**17a′**	3557.1	3556.8
10	**19a′**	3477.0	3476.4
11	**20a′**	3525.1	3524.6

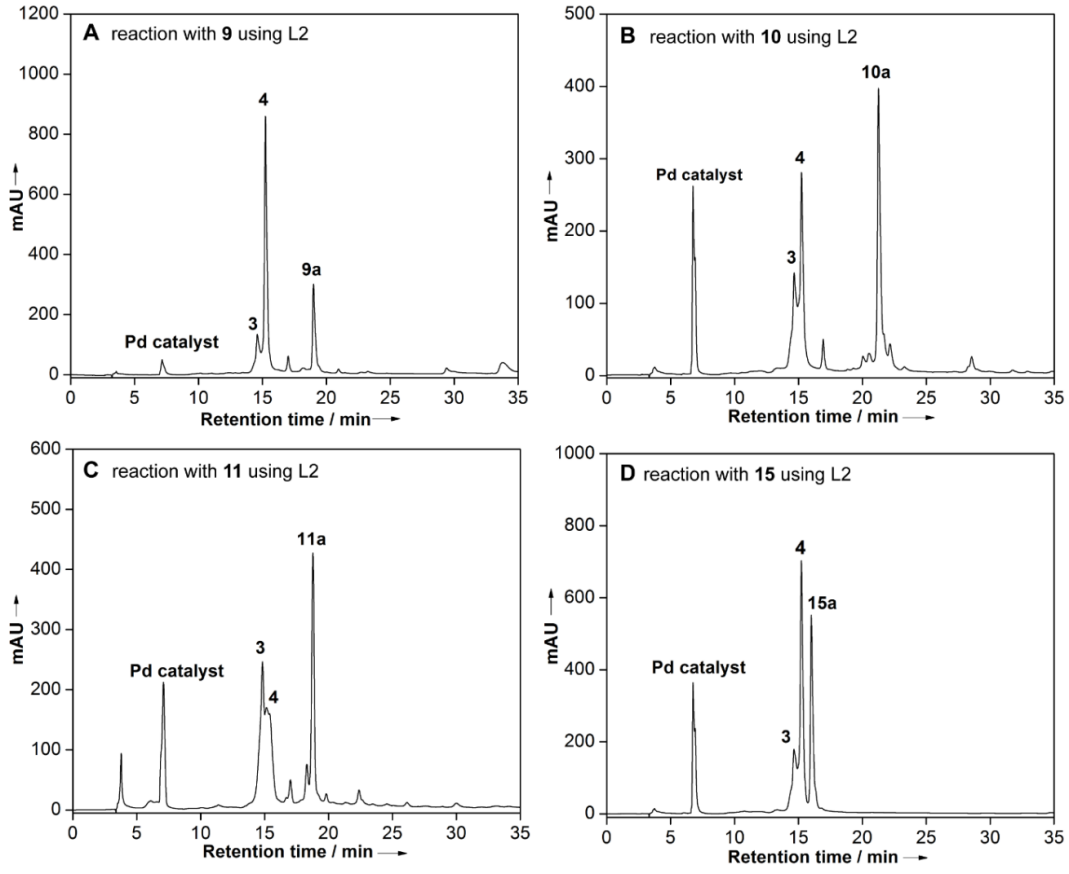

Figure 2.9. (**A**, **B, C, D**)RP-HPLC chromatogram of reaction mixture of Suzuki–Miyaura cross-coupling between IU-labeled transcript **4** and boronic esters **9**–**11** using ligand L2. **9a**–**11a** correspond to coupled RNA ON product; **3** is deiodinated transcript. Mobile phase A: 50 mM TEAA buffer (pH 7.0); mobile phase B: acetonitrile. Flow rate: 1 mL/min. Gradient: 0−30% B in 35 min, 30−100% B in 10 min and 100% B for 5 min.

2.2.3.3 Posttranscriptional coupling generates RNA labeled with fluorogenic environment-sensitive nucleoside analogs: Several examples including the ones reported from our laboratory indicate that responsive fluorescent nucleoside analogs can be assembled by conjugating heterocyclic rings onto nucleobases.[74–82] Such nucleosides incorporated into ONs by chemical or enzymatic means serve as excellent probes for studying nucleic acid structure and function, and in diagnostic applications. These strategies usually use modified nucleoside phosphoramidites or triphosphates, which involve elaborate chemical manipulations. Moreover, in several instances, the substrates (i) show poor coupling efficiency, (ii) do not survive the conditions used in the solid phase protocols and (iii) are not efficiently incorporated by polymerases.[4] In this context, posttranscriptional coupling of IU-labeled RNA ONs with heterocycle-containing boronic acids/esters should provide direct access to RNA functionalized with responsive nucleoside probes. This approach will avoid cumbersome synthesis and challenges in the incorporation of individual modified amidites and nucleotides.

First we focused on functionalizing RNA with some known environment-sensitive base-modified fluorescent nucleoside analogs. IU-labeled RNA ON 4 was reacted with commercially available heteroaryl boronic acid derivatives **12**−**15** in the presence of Pd-L1 (Figures 2.5 and 2.6). Reactions with these substrates gave fluorescent RNA ONs (**12a**−**15a**) labeled with furan-, benzothiophene- and benzofuran modified uridine (Table 2.1 and 2.2; Figure 2.10). These analogs have been successfully used in assays to probe nucleic acid structure, lesion, recognition and in setting up screening platforms.[83–87]

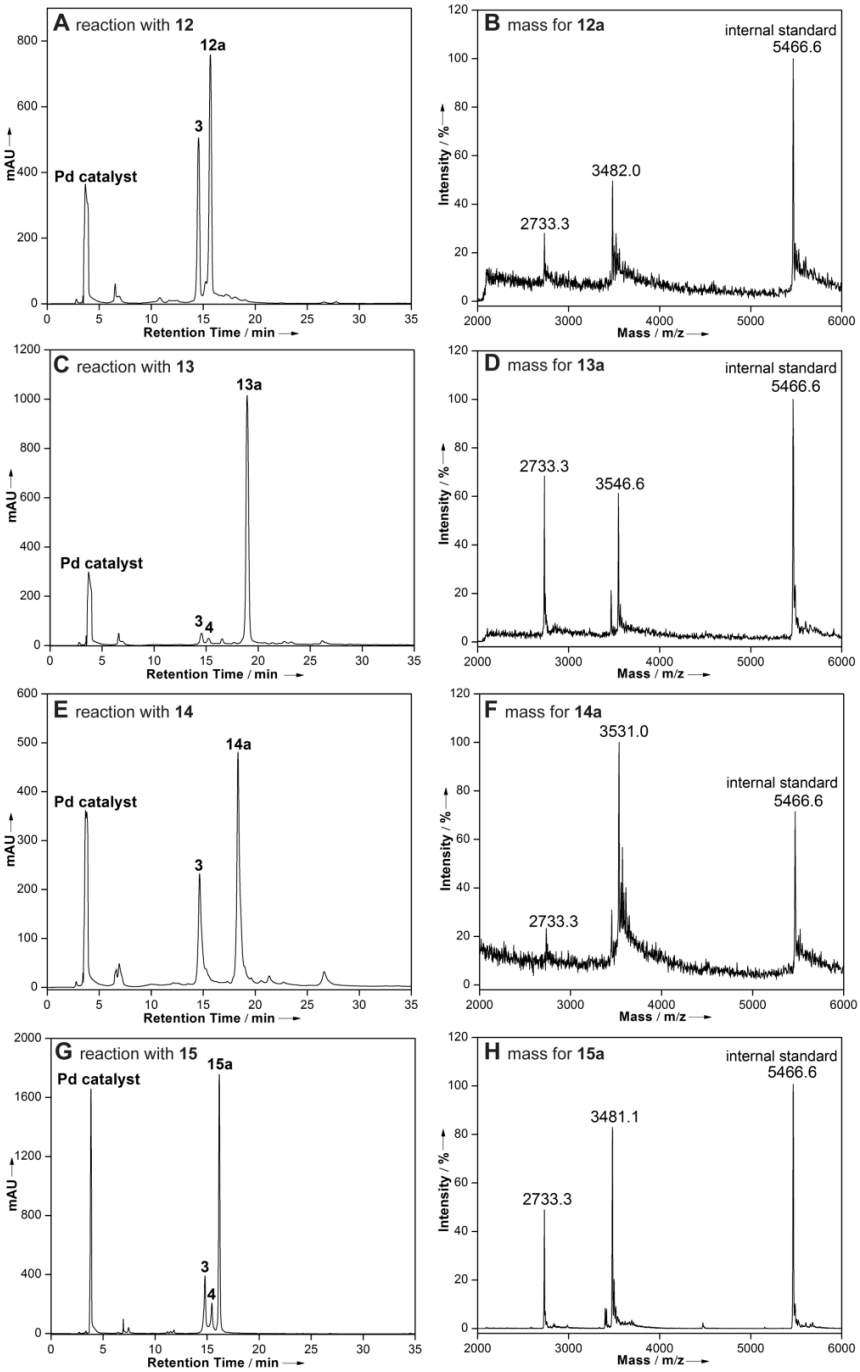

Figure 2.10. (**A**, **C**, **E**, **G**)RP-HPLC chromatogram of reaction mixture of Suzuki–Miyaura cross-coupling between IU-labeled transcript **4** and boronic acids/ester **12**–**15**. **12a**–**15a** correspond to coupled RNA ON product; **3** is deiodinated transcript. Mobile phase A: 50 mM TEAA buffer (pH 7.0); mobile phase B: acetonitrile. Flow rate: 1 mL/min. Gradient: 0−30% B in 35 min, 30−100% B in 10 min and 100% B for 5 min.
(**B**, **D**, **F, H**) MALDI-TOF mass spectrum of coupled RNA ON products **12a**, **13a**, **14a** and **15a** (HPLC fractions) obtained from reactions between transcript **4** and boronic acids/ester **12**–**15**, respectively. See Figure 5 for the structure of the product. Spectrum is calibrated with respect to the +1 and +2 ion of an internal 18-mer DNA ON standard (m/z for +1 and +2 ion are 5466.6 and 2733.3 respectively). See Table 2.1 and Table 2.2 for mass data and isolated yield.

Table 2.2. Yields of Suzuki–Miyaura cross-coupled RNA ON products obtained by posttranscriptional chemical modification of IU-labeled RNA ON transcripts.[a]

Entry	RNA ON	Boronate ester Substrate	Reaction time (h)	Cross-coupled product	ε_{260} $M^{-1}cm^{-1}$ [b]	Isolated yield (nmol) (with ligand L1)	Isolated yield (%) (with ligand L1)	Isolated yield (%) (with ligand L2)
1	**4**	**9**	12	**9a**	84740	1.4	28	11
2	**4**	**10**	6	**10a**	84740	1.5	30	24
3	**4**	**11**	6	**11a**	84740	1.4	28	23
4	**4**	**12**	6	**12a**	92420	1.8	36	-
5	**4**	**13**	6	**13a**	90340	1.5	30	-
6	**4**	**14**	6	**14a**	98553	1.6	32	-
7	**4**	**15**	6	**15a**	92420	2.5	50	25
8	**4**	**16**	6	**16a′(16 a″)**[c]	85020	3.1 (0.9)	62 + 18 = 80	46
9	**4**	**17**	6	**17a′ (17a″)**[c]	85400	2.6 (0.5)	52 + 10 = 62	43
10	**19**	**17**	12	**19a′ (19a″)**[c]	79400	0.9 (0.6)	18 + 12 = 30	-
11	**20**	**17**	6	**20a′ (20a″)**[c]	91800	1.8 (0.8)	36 + 16 = 52	-

[a] All reactions were performed on a 5 nmole scale of IU-labeled RNA transcripts. Yields reported are with respect to the RNA products isolated after HPLC purification. Concentration and yield of the product was calculated using the molar absorption coefficient (ε260) of the RNA product. See, 2.5 and 2.7, and Table 2.1 for mass spectra and data.
[b] ε260 of coupled RNAON products was determined by using OligoAnalyzer3.1.In case of **9a**–**11a**, ε260 of 5-vinyluridine[28] was used in place of uridine. For **12a**–**15a**, ε260 of corresponding 5-heterocycle coupled uridine was used in place of uridine.[83–85] For coupled RNA ON products using boronic esters 16 and 17, ε260 of 5-(benzothiophen-2-yl)vinyluridine (3820 $M^{-1}cm^{-1}$) and 5-(benzofuran-2-yl) vinyl uridine (4200 $M^{-1}cm^{-1}$) was determined, and used in place of uridine.
[c] **16a′**, **17a′**, **16a′** and **20a′** represent the trans isomer of cross-coupled product (major). **16a″**, **17a″**, **19a″**and **20a″**given in parenthesis represent the 'cis' isomer of cross-coupled product (minor). Isolated yields in nmoles and percentage for trans and 'cis' isomers products are also given.

Next, we sought to use this labeling approach to introduce new fluorescent nucleoside modifications into RNA ONs. Although predicting the fluorescence outcome based on the structure is difficult, we envisioned that coupling heterocycles onto nucleosides via an extended π system may impart interesting photophysical features to otherwise nonemissive

nucleosides.[88,89] In this regard, we chose to couple easily synthesizable hetero aryl vinyl boronic esters **16** and **17** with IU-labeled RNA ON **4** (Figure 2.5 and 2.6). Rewardingly, these substrates underwent facile coupling reaction to produce RNA ONs containing 5-(benzothiophen-2-yl)vinyl uridine and 5-(benzofuran-2-yl)vinyl uridine, respectively, in good yields (Figure 2.6, Table 2.1 and Table 2.2). The HPLC chromatogram of the reaction revealed the presence of major (designated as **16a′** and **17a′**) and minor (designated as **16a′′**and **17a′′**) peaks having the same mass; probably corresponding to trans and cis isomers, respectively (Figure 2.11, Figure 2.12 and Table 1.1). In order to ascertain the isomeric identity of the products formed, the major peak (**17a′**) was isolated and digested using a cocktail of enzymes, which would generate individual ribonucleosides. The HPLC chromatogram of the digest revealed the presence of native ribonucleosides (C, G and A) and trans form of 5-(benzofuran-2-yl)vinyl uridine, which matched well with the retention time of the authentic trans isomer (**18**) obtained from a control reaction between IU and ester **17** (Scheme 2.7 and Figure 2.13). Remarkably, reaction in the presence of Pd-L2 catalytic system yielded only the trans products **16a′** and **17a′**, suggesting that this posttranscriptional modification is an example of a ligand controlled stereoselective alkenylation process (Table 2.2 and Figure 2.11).

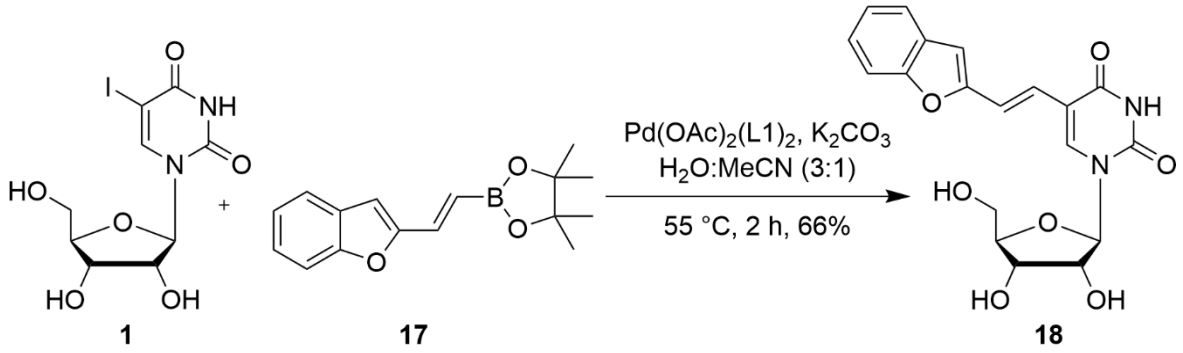

Scheme 2.7. Synthesis of *trans*form of 5-(benzofuran-2-yl)vinyl uridine (**18**).

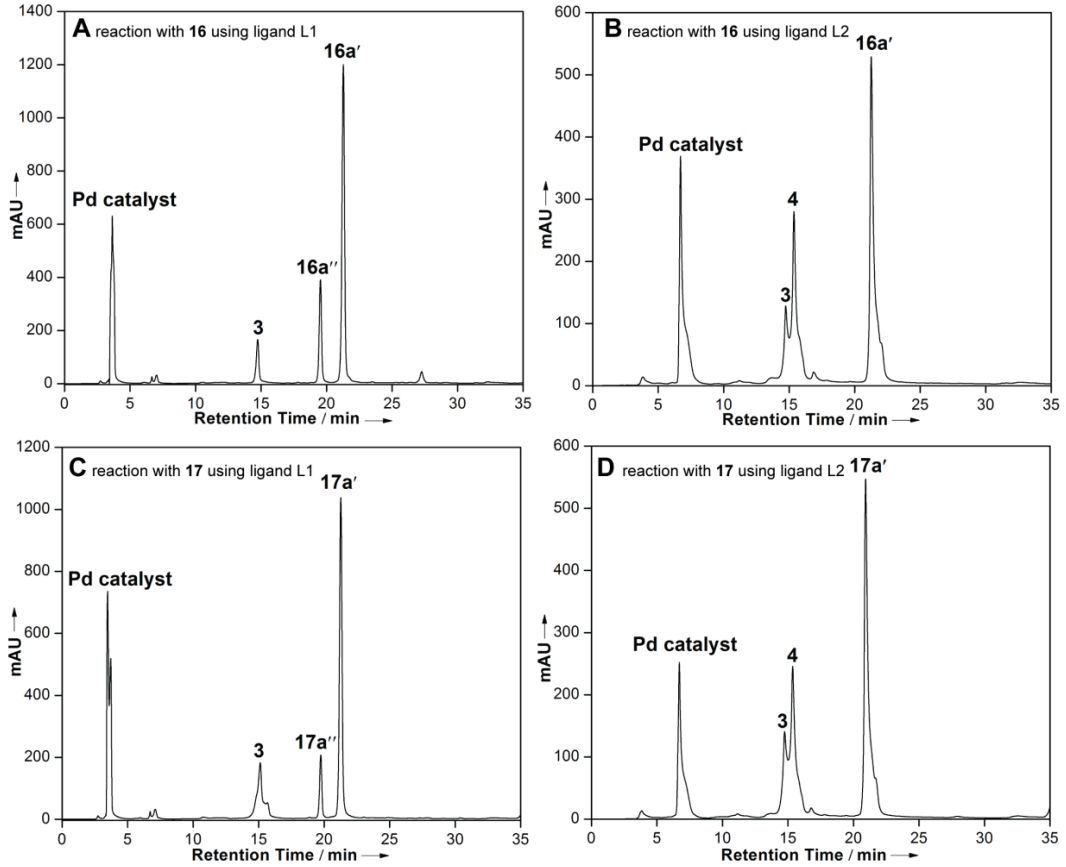

Figure 2.11. RP-HPLC chromatogram of reaction mixture of Suzuki–Miyaura cross-coupling between IU-labeled transcript **4** and boronic ester **16** and **17**. **A** and **B**: reaction with boronic ester **16** using ligand L1 and L2, respectively. **C** and **D**: reaction with **17** using ligand L1 and L2, respectively. While major peaks **16a′** and **17a′** correspond to the "*trans"* isomer product, minor peaks **16a″** and **17a″** correspond to the *"cis"* isomer product. See Table 2.1 for mass data.
Importantly, reaction in the presence of Pd-L2 catalytic system yielded only the *trans* products **16a′** and **17a′**, suggesting that this posttranscriptional modification is an example of a ligand-controlled stereoselective alkenylation process.
Mobile phase A: 50 mM TEAA buffer (pH 7.0), mobile phase B: acetonitrile. Flow rate: 1 mL/min. Gradient: 0−30 % B in 35 min, 30−100% B in 10 min and 100% B for 5 min.

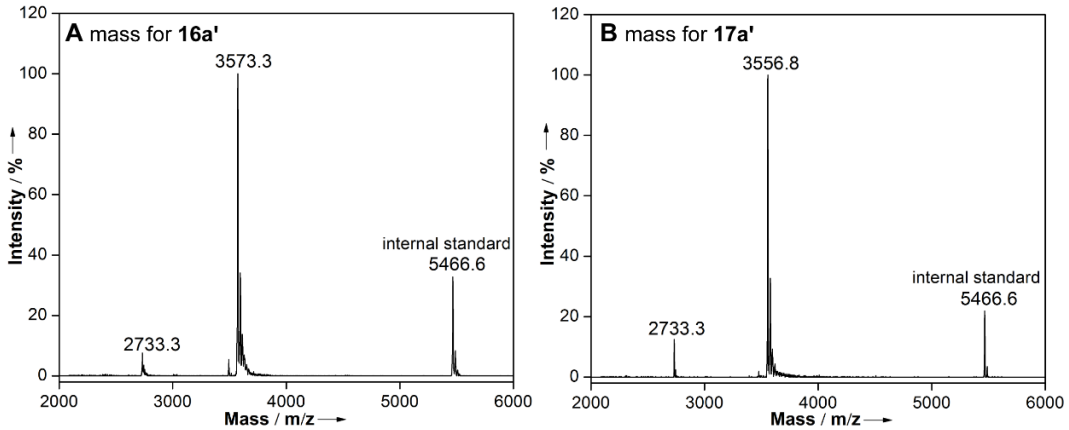

Figure 2.12. MALDI-TOF mass spectrum of coupled RNA ON products **16a′** and**17a′**. (HPLC fractions) obtained from reactions between transcript **4** and boronic ester **16** and **17**, See Figure 2.6 for

the structure of the product. Spectrum is calibrated with respect to the +1 and +2 ion of an internal 18-mer DNA ON standard (m/z for +1 and +2 ion are 5466.6 and 2733.3 respectively). See Table 2.1 and Table 2.2 for mass data and isolated yield.

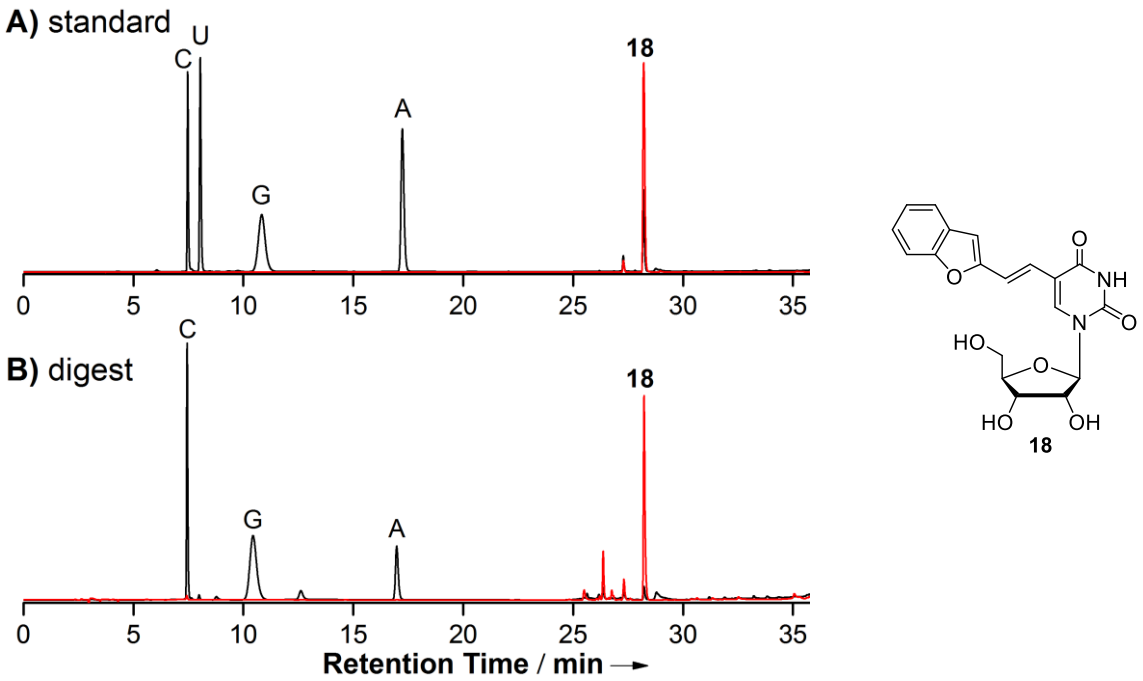

Figure 2.13. RP-HPLC profile of ribonucleoside products obtained after enzymatic digestion of Suzuki-coupled RNA ON **17a′**. (**A**) A mix of natural ribonucleosides (C, U, G, A) and 2-vinyl benzofuran modified-uridine **18** at 260 nm (black line) and 338 nm (red line). *Trans* form of 5-(benzofuran-2-yl)vinyl uridine (**18**) was synthesized by Suzuki coupling reaction between IU (**1**) and boronic ester **17**. **18** absorbs at 260 nm and 338 nm. (**B**) Transcript **17a′** digest at 260 nm (black line) and 338 nm (red line). The retention time and strong absorbance at 338 nm confirmed the presence of *trans* form of the modified nucleoside **18** in RNA ON **17a′**. Mass analysis of individual fractions of the digested RNA ON confirmed the identity of the natural and modified nucleosides (Table 2.3).

Table 2.3. MALDI-TOF mass analysis of HPLC fractions of RNA ON **17a′** digest.

HPLC fraction	Calculated mass for	Found
C	$C_9H_{13}N_3O_5K$ $[M+K]^+$: 282.3	282.0
G	$C_{10}H_{13}N_5O_5K$ $[M+K]^+$: 322.3	322.1
A	$C_{10}H_{13}N_5O_4Na$ $[M+Na]^+$: 290.2	290.1
18	$C_{19}H_{18}N_2O_7Na$ $[M+Na]^+$: 409.4	409.0

A 5 nmole reaction scale gave 1.4−4 nmole of the coupled RNA product, which is sufficient for subsequent biophysical analysis (Table 2.2). Similar yields are reported for postsynthetic click functionalization of RNA ONs.[12,17,21] It is worth mentioning here that dehalogenation is a common side reaction in Pd-catalyzed cross-coupling reactions, including

Suzuki–Miyaura reaction. The extent of deiodination of the substrate, and hence, the reduction in the reaction efficiency is known to vary with the reaction temperature, nature of the catalyst-ligand system and loading nature of boronic acid/ester substrates, solvent/buffer conditions and reaction time.[40,43,47] Hence, for a given boronic acid/ester substrate the deiodination can be potentially minimized by optimizing the reaction conditions in terms of catalyst loading and reaction time. In case more amount of the RNA product is required then a batch reaction is recommended, which can be pooled before purification, thereby avoiding multiple HPLC runs (data not shown). Control reactions with ON **4** in the presence of boronic acids/esters or $Pd(OAc)_2$ or Pd-ligand alone did not yield the coupled product (Figure 2.14). Similarly, an unmodified RNA ON **3** did not react under the coupling reaction conditions. These results indicate that Suzuki coupling on IU-labeled RNA is highly chemoselective.

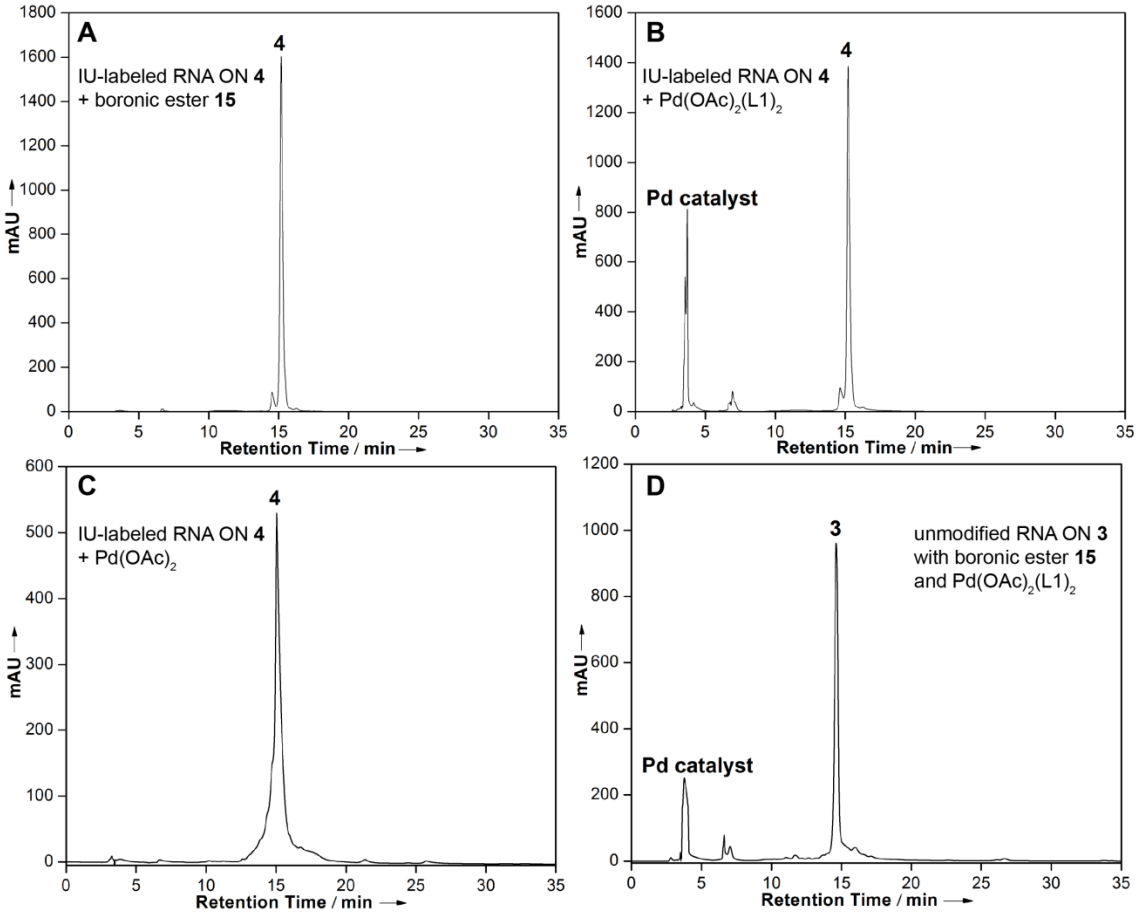

Figure 2.14. Control Suzuki coupling reactions with IU-labeled RNA ON **4** (5 nmol) and unmodified RNA ON **3** (5 nmol) were performed under similar conditions. (**A**) Reaction mix containing RNA ON **4** and boronic ester **15**. (**B**) Reaction mix containing RNA ON **4** and $Pd(OAc)_2(L1)_2$. (**C**) Reaction mix containing RNA ON **4** and $Pd(OAc)_2$. (**D**) Reaction of unmodified RNA ON **3** in the presence of boronic ester **15** and catalytic system $Pd(OAc)_2(L1)_2$. Formation of Suzuki coupled RNA ON product was not observed in all the cases.

2.2.2.4 Fluorogenic nature and environment-sensitivity of the coupled RNA products: Another very important and useful feature of this postsynthetic Suzuki coupling reaction is that it is fluorogenic in nature. Coupling of nonemissive IU-labeled RNA **4** with very weakly emissive boronates**16** and **17** gave highly fluorescent RNA products **16a′** and **17a′**, respectively (Figure 2.15A and B). In particular, 5-(benzofuran-2-yl)vinyl uridine (**18**)-modified RNA ON **17a′** displayed more than 25-fold enhancement in fluorescence intensity as compared to boronic ester **17**. The environment-sensitivity of this fluorescent label was evaluated at the nucleoside level (**18**) and by using **18**-containing RNA ONs (**17a′**, **19a′** and **20a′**, Figure 2.15C). These ONs in which the emissive nucleoside is placed in-between different flanking bases were prepared by posttranscriptional Suzuki coupling of IU-labeled RNA ONs **4**, **19** and **20**, respectively, with ester **17**. (Figure 2.15C, Figure 2.16, Table 2.1 and Table 2.2).

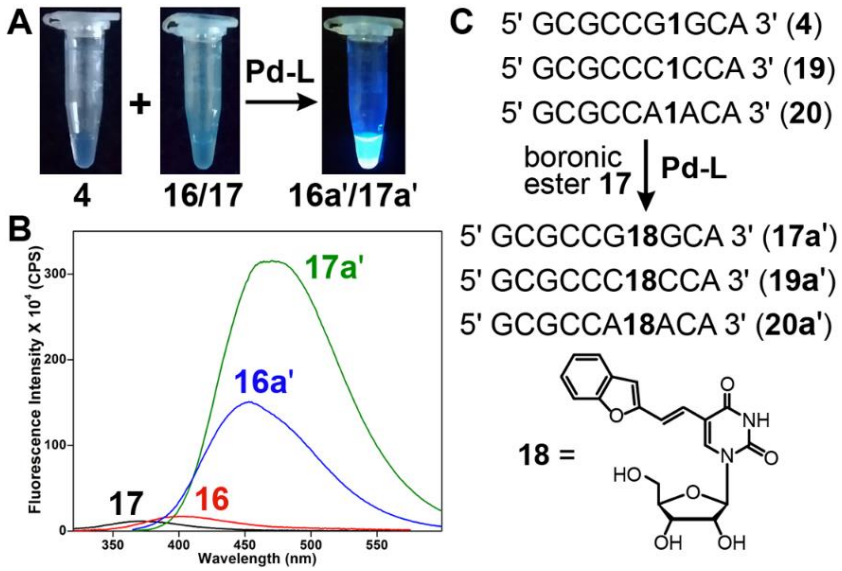

Figure 2.15. (**A**) Image showing the fluorogenic Suzuki coupling of IU-labeled transcript **4** with boronic esters **16** and **17**.The samples were irradiated using 365 nm light source. (**B**) Emission spectra (1 µM) of substrates (very weakly emissive) and RNA ON products **16a′** and **17a′** (highly emissive). (**C**) Synthesis of RNA ONs **17a′**, **19a′** and **20a′**, containing emissive nucleoside **18** in-between different flanking bases, from respective iodo-labeled RNA ON transcripts by posttranscriptional Suzuki coupling.

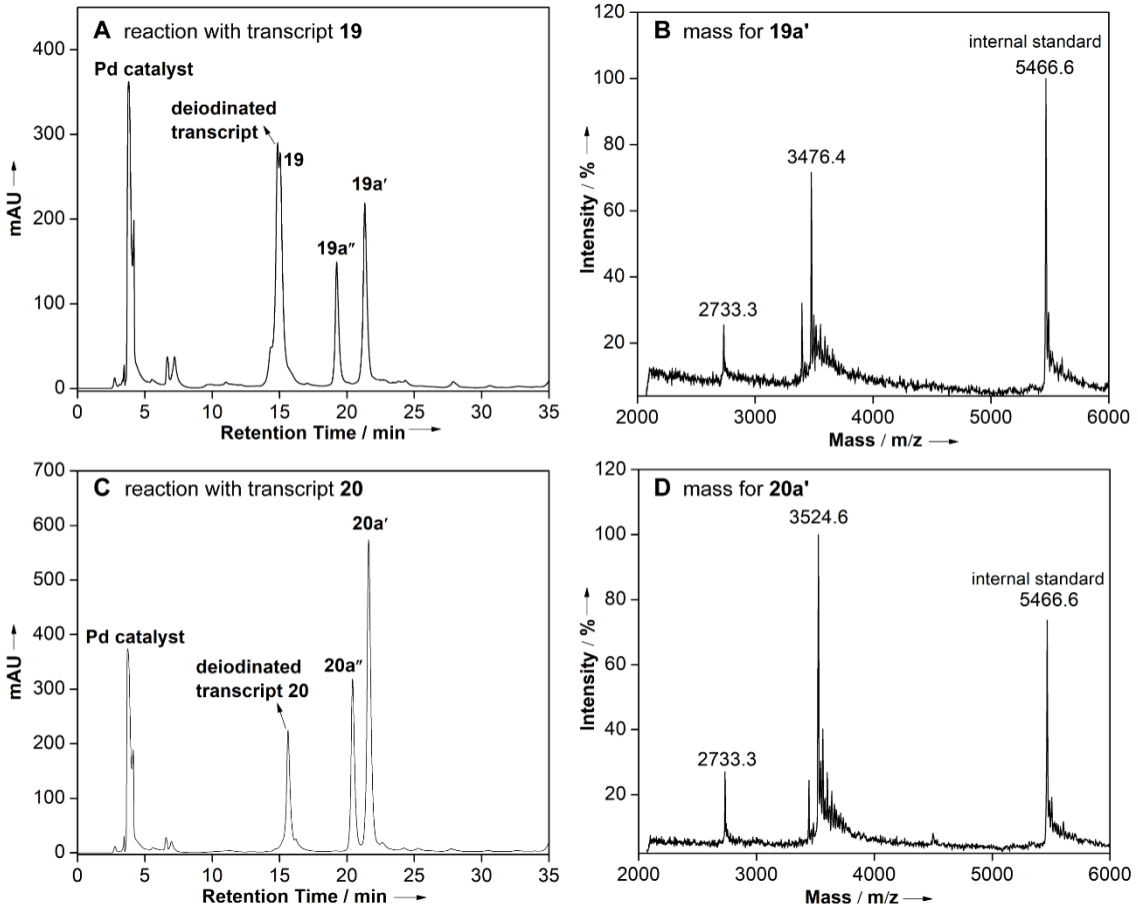

Figure 2.16. (**A**, **C**) RP-HPLC chromatogram of reaction mixture of Suzuki–Miyaura cross-coupling between IU-labeled transcripts **19**/**20** with boronic ester **17**. **19a′**and **20a′** correspond to *trans* coupled RNA ON product, **19a″**and **20a″** correspond to *cis* coupled RNA ON product. Mobile phase A: 50 mM TEAA buffer (pH 7.0); mobile phase B: acetonitrile. Flow rate: 1 mL/min. Gradient: 0−30% B in 35 min, 30−100% B in 10 min and 100% B for 5 min.
(**B**, **D**) MALDI-TOF mass spectrum of coupled RNA ON products **19a′** and **20a′** (HPLC fractions) obtained from reactions between boronic ester **17**andtranscript **19** and **20**, respectively. See Figure 15c for the reaction. Spectrum is calibrated with respect to the +1 and +2 ion of an internal 18-mer DNA ON standard (m/z for +1 and +2 ion are 5466.6 and 2733.3 respectively). See Table 2.1 and Table 2.2 for isolated yield and mass data.

The ground-state electronic spectrum of **18** was not significantly affected by changes in solvent polarity. However, the nucleoside exhibited excellent fluorescence solvatochromism, wherein the emission maximum, Stokes shift, intensity and quantum yield were significantly influenced by changes in the polarity of the medium (Figure 2.17 and Table 2.4). In water, **18** displayed a weak fluorescence band (λ_{em} = 483 nm) corresponding to a quantum yield of 0.028. As the polarity of the medium was decreased from water to methanol to dioxane, a significant enhancement in fluorescence efficiency (5-fold) accompanied by a blue-shifted emission maximum was observed (λ_{em} = 427 nm in dioxane).

Encouraged by these results, we next sought to study the responsiveness of the nucleoside analog to changes in neighbouring base environment.

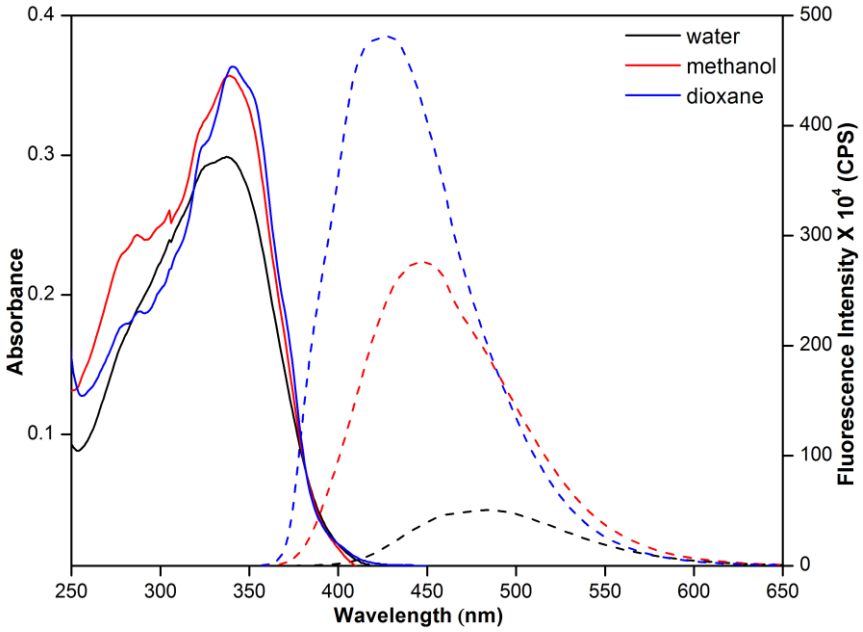

Figure 2.17. Absorption (25 μM, solid line) and emission (5.0 μM, dashed line) spectra of 5-(benzofuran-2-yl)vinyl uridine **18**in solvents of different polarity. For absorption and emission study, the samples contained 2.5 and 0.5% DMSO, respectively. The samples were excited at longest absorption maximum (Table 2.4) with an excitation and emission slit width of 2 nm and 3 nm, respectively.

Table 2.4. Photophysical properties of modified nucleoside **18** in different solvents.

Solvent	λ_{max}[a] (nm)	λ_{em} (nm)	I_{rel}[b]	Stokes shift (cm^{-1})	Φ[c]
Water	338	483	1.0	8882	0.028
methanol	339	447	5.0	7127	0.097
Dioxane	341	427	9.7	5906	0.149

[a] Longest absorption maximum is given. [b] Emission intensity relative to the intensity in water is given.
[c] Quantum yield of **18** in different solvents relative to 2-aminopurine as a standard was determined using the following equation.

$$\Phi_{F(x)} = (A_s/A_x)\,(F_x/F_s)\,(n_x/n_s)^2\,\Phi_{F(s)}$$

Where s is the standard, x is **18**, A is the absorbance at excitation wavelength, F is the area under the emission curve, *n* is the refractive index of the solvent, and Φ_F is the quantum yield.
Standard deviation for Φ is ≤0.004.

RNA ONs **17a′**, **19a′**and **20a′**were hybridized with DNA ONs such that the emissive analog **18** was paired opposite to complementary or mismatched bases (Figure 2.18A).

Typical of a responsive nucleoside probe, the emission maximum and intensity of the nucleoside were found to be sensitive to neighbouring base environment (Figure 2.18). **18** incorporated into single stranded RNA ONs and then into duplexes (matched or mismatched) showed a progressing increase in fluorescence intensity as compared to the free nucleoside analog. Notably, the emission maximum of duplexes (~455 nm) was significantly blue-shifted as compared to the nucleoside (483 nm). The enhancement in fluorescence and blue shifted emission indicate that the micropolarity around the emissive analog in duplexes is significantly lower than water. A comparison of emission maximum of the free nucleoside analog in different solvents and in duplexes suggest that the modification at the 5-position of uridine, which is projected in the major groove, experiences a polarity more close to methanol (Table 2.4). This result is consistent with the major groove polarity of the duplexes reported in the literature.[90,91] Further, among the duplexes, the emissive analog placed in the vicinity of guanine showed lower fluorescence intensity as compared to other bases, which is likely due to the known quenching effect of guanine by electron transfer process.[92] Taken together, these results underscore the potential of postsynthetic Suzuki coupling reaction in directly accessing RNA ONs labeled with fluorogenic and environment-sensitive nucleosides. Pd contamination in the labeled RNA product could potentially interfere with its application in cell-based and in vivo experiments due to the toxicity of Pd.[93] In the Suzuki-based protein labeling method, Davis *et al.* observed loss in signal in the mass spectra due to non-specific coordination of Pd to the protein.[94] This effect was significantly reduced by using 3-mercaptopropionic acid as a scavenger, which strongly binds to Pd as compared to the protein. However, when labeling DNA by Suzuki coupling such an effect was not observed.[47] Similarly, in our reaction conditions and purification method, we did not observe loss of mass signal from Suzuki-labeled RNA ON products. Nevertheless, it is suggested that a Pd scavenger can be used when preparing labeled RNA ONs for *in vivo* and therapeutic applications.

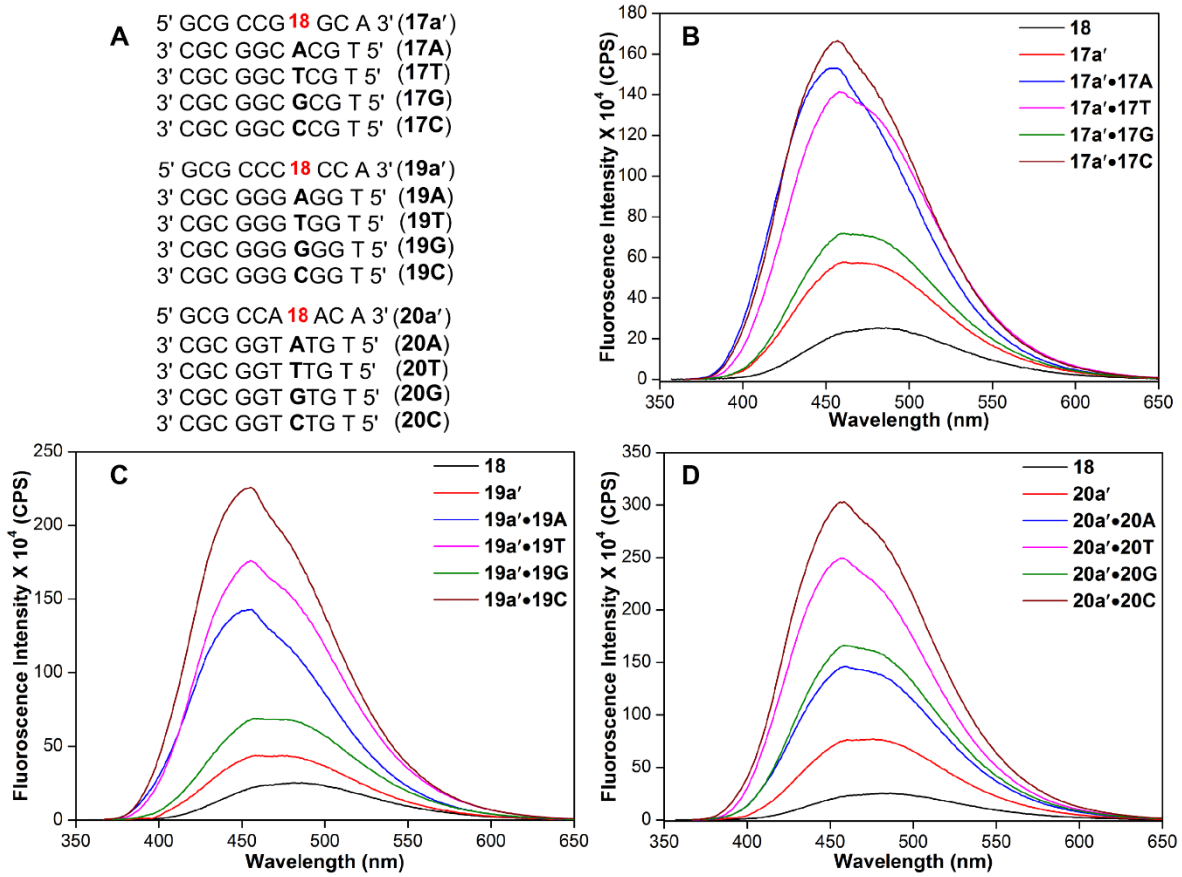

Figure 2.18. (**A**) Sequence of **18**-labeled RNA ONs **17a'**, **19a'** and **20a'** and custom DNA ONs. RNA ONs were hybridized to DNA ONs such that the emissive nucleoside was placed opposite to complementary base and mismatched bases. For example, hybridization of RNA ON **17a'** with DNA ONs **17A**, **17T**, **17G** and **17C** will place **18** opposite to complementary base dA and mismatched bases dT, dG and dC, respectively. (**B**–**D**) Emission spectra of RNA ONs and corresponding duplexes.

2.3 Conclusion

We have established an efficient method to label RNA ONs with functional probes by conceiving posttranscriptional Suzuki–Miyaura cross-coupling reaction under biocompatible conditions. This direct RNA labeling method can be used to install commonly used biophysical reporters as well as generate RNA ONs labeled with new fluorogenic and environment-sensitive nucleoside probes in a ligand controlled stereoselective fashion. Our results demonstrate that this RNA bioconjugation approach based on Suzuki–Miyaura coupling is a very powerful tool, which will complement existing methods to functionalize and study RNA ON motifs.

2.4 Experimental section

2.4.1 Materials: All chemicals and biochemicals purchased were used as supplied unless otherwise stated. 5-iodouridine (IU **1**) was prepared according to a literature report.[67] Boronic acids **12** and **15** were purchased from Sigma-Aldrich, whereas **13** and **14** were purchased from Alfa Aesar. 4-Chloro-7-nitrobenzofurazan, biotin, bis(pinacolato)diboron, 2-aminopyrimidine-4,6-diol (ADHP, L1) were purchased from Sigma-Aldrich. 2-(dimethylamino)pyrimidine-4,6-diol (DMADHP, L2) was prepared according to a literature report.[73] T7 RNA polymerase, ribonuclease inhibitor (RiboLock), NTPs, RNase A and RNase T1 were obtained from Fermentas, Thermo Fisher Scientific. DNA oligonucleotides (ONs) purchased from Integrated DNA Technologies, Inc., were purified by gel electrophoresis under denaturing condition and desalted using Sep-Pak Classic C18 cartridges (Waters Corporation). Calf intestinal alkaline phosphatase (CIP) and snake venom phosphodiesterase I were procured from Invitrogen and Sigma-Aldrich, respectively. $POCl_3$ was purchased from Across Organics and freshly distilled prior to use. Radiolabeled α-^{32}P ATP (2000 Ci/mmol) was purchased from the Board of Radiation and Isotope Technology, Government of India. Chemicals for preparing buffer solutions were purchased from Sigma-Aldrich (HPLC or BioUltra grade). Autoclaved water was used in all biochemical reactions.

2.4.2 Instrumentation: NMR spectra were recorded on a 400 MHz Jeol ECS-400 and Bruker Avance III HD Ascend 400 MHz spectrometer. Mass measurements were recorded on Applied Biosystems 4800 Plus MALDI TOF/TOF analyzer and Bruker Avance III HD Ascend 400 MHz mass spectrometer. Steady-state fluorescence experiments were carried out in a micro fluorescence cuvette (Hellma, path length 1.0 cm) on a Horiba JobinYvon, Fluorolog-3. Reversed-phase (RP) flash chromatographic (C18 Redi*SepRf*column) purifications were carried out using Teledyne ISCO, Combi Flash *Rf*. HPLC analysis was performed using Agilent Technologies 1260 Infinity.

2.4.3 Synthesis of 5-iodouridine 5′-triphosphate (IUTP 2): To an ice cold solution of 5-iodouridine **1** (96 mg, 0.26 mmol, 1 equiv) in trimethyl phosphate (1.20 mL) was added freshly distilled $POCl_3$ (61 µL, 0.65 mmol, 2.5 equiv). The solution was stirred for 24 at ~4 °C. TLC revealed only partial conversion of the ribonucleoside into the product. *Bis*-tributylammonium pyrophosphate[68] (0.5 M in DMF, 2.7 mL, 1.35 mmol, 5.2 equiv) and tributylamine (670 µL, 2.86 mmol, 11 equiv) were rapidly added simultaneously under ice-

cold conditions. The reaction was quenched after 30 min with 1 M triethylammonium bicarbonate buffer (TEAB, pH 7.5), and was extracted with distilled ethyl acetate. The aqueous layer was evaporated undervacuum and the residue was purified first on a DEAE sephadex-A25 anion exchange column (10 mM–1 M TEAB buffer, pH 7.5) followed by reversed-phase flash column chromatography (C18 Redi*SepRf*, 0–50% acetonitrile in 50 mM triethylammonium acetate buffer, pH 7.3, 45 min). Appropriate fractions were lyophilized to afford IUTP **2** as a tetratriethylammonium salt (61 mg, 16%); ^{1}H NMR (400 MHz, D_2O): δ (ppm) 8.24 (s, 1H), 5.89 (d, *J* = 5.2 Hz, 1H), 4.42–4.35 (m, 2H), 4.23–4.16 (m, 3H); ^{31}P NMR (162 MHz, D_2O): δ (ppm) -7.75 (br, P_γ), -11.10 (d, *J* = 18.31, P_α), -22.06 (br, P_β); HRMS: m/z Calcd. for $C_9H_{13}IN_2O_{15}P_3$ $[M-H]^-$ = 608.8573, found = 608.8574. Analytical data matches with the literature report.[69]

2.4.4 Synthesis of amine-containing pinacol boronate ester linkers 21 and 22

21 and **22** were prepared by following a literature procedure.[47] **21** and **22** were characterized by ^{1}H NMR, ^{13}C NMR and HRMS, which were consistent with reported data.

2.4.4.1 *tert*-Butyl prop-2-yn-1-ylcarbamate (21b): To a solution of di-*tert*-butyl dicarbonate (6.52 mL, 28.39 mmol, 1 equiv) in CH_2Cl_2 (30 mL) at 0 °C, propargylamine (**21a**, 2 mL, 31.22 mmol, 1.1 equiv) and Et_3N (7.90 mL, 56.78 mmol, 2 equiv) were added dropwise. The resulting solution was allowed to attain room temperature and stirred for 2 h. After completion, the reaction was quenched with saturated aq. NH_4Cl and diluted with EtOAc. The organic layer was washed with sat. NH_4Cl, sat. $NaHCO_3$ and brine solution. Then organic layer was dried over anhydrous Na_2SO_4, filtered. The filtrate was removed *in vacuo* to afford the crude product which was purified by silica gel column chromatography (3.32 g, 68%). TLC (EtOAc:pet ether = 40:60); R_f = 0.85; ^{1}H NMR (400 MHz, $CDCl_3$): δ (ppm) 4.77 (br, 1H), 3.92 (s, 2H), 2.22 (s, 1H), 1.45 (s, 9H); ^{13}C NMR (100 MHz, $CDCl_3$): δ(ppm) 155.38, 80.23, 80.17, 71.32, 30.50, 28.45; HRMS: m/z calculated for $C_8H_{13}NO_2Na$ $[M+Na]^+$ = 178.0857, found = 178.0842.

2.4.4.2 (E)-*tert*-Butyl 3-(4,4,5,5-tetramethyl-1,3,2-dioxaborolan-2-yl)allylcarbamate (21c): To *tert*-butyl prop-2-ynylcarbamate (1 g, 6.44 mmol) in pinacolborane (1.4 mL, 9.67 mmol), subsequently, Et_3N (90 µL, 0.644 mmol) and $ZrCp_2HCl$ (166 mg, 0.644 mmol) was added to it. The solution was stirred at 65 °C for 16 h. After completion, the reaction was allowed to attain room temperature and was diluted with EtOAc. The reaction was quenched

with saturated aq. NH_4Cl. The mixture was further diluted with EtOAc and organic layer was washed with sat. NH_4Cl, sat. $NaHCO_3$ and brine solution. The Organic layer was dried over anhydrous Na_2SO_4 and filtered. The filtrate was removed *in vacuo* to afford the crude product which was purified by silica gel column chromatography provided **21c** as yellowish oil (1.27 g, 69%). TLC (EtOAc:pet ether = 15:85); R_f = 0.58; ^{1}H NMR (400 MHz, $CDCl_3$) δ (ppm) 6.59 (dt, *J* = 18, 4.4 Hz, 1H), 5.57 (dt, *J* = 18, 1.6 Hz, 1H), 4.65 (br, 1H), 3.84 (s, 2H), 1.44 (s, 9H), 1.26 (s, 12H); ^{13}C NMR (100 MHz, $CDCl_3$) δ ppm 155.9, 149.5, 83.4, 83.3, 79.5, 44.1, 28.5, 24.9; HRMS: m/z calculated for $C_{14}H_{26}BNO_4Na$ $[M+Na]^+$ = 306.1852, found = 306.1857.

2.4.4.3 (E)-3-(4,4,5,5-*tetra*-Methyl-1,3,2-dioxaborolan-2-yl)prop-2-en-1-amine TFA salt (21d): (E)-*tert*-Butyl 3-(4,4,5,5-tetramethyl-1,3,2-dioxaborolan-2-yl)allylcarbamate (1.20 g, 4.22 mmol) dissolved in 1:9 TFA:CH_2Cl_2 (48 mL) and stirred at RT for 1 h. Then solvent was removed *in vacuo*. Excess TFA was co-evaporated with toluene and CH_2Cl_2 gave the compound **21d** as brown oil (1.22 g, 97%); ^{1}H NMR (400 MHz, $CDCl_3$) δ (ppm) 8.06 (br, 3H), 6.53 (dt, *J* = 18, 5.6 Hz, 1H), 5.74 (d, *J* = 18 Hz, 1H), 3.68 (br, 2H), 1.26 (s, 12H); ^{13}C NMR (100 MHz, $CDCl_3$) δ (ppm) 141.8, 124.7, 117.5, 84.2, 43.1, 24.7.

2.4.4.4 (E)-3-(4,4,5,5-*tetra*-Methyl-1,3,2-dioxaborolan-2-yl)prop-2-en-1-amine (21) : (E)-3-(4,4,5,5-*tetra*-Methyl-1,3,2-dioxaborolan-2-yl)prop-2-en-1-amine TFA salt was further neutralized by anion exchange resin to get the free amine **21** as a colorless oil.

2.4.4.5 *tert*-Butyl 2-(2-hydroxyethoxy)ethylcarbamate (22b): To a solution of di-*tert* butyl dicarbonate (9.06 g, 41.55 mmol, 1 equiv) in CH_2Cl_2 (30 mL) at 0 °C, 2-(2-aminoethoxy)ethanol (**22a**, 5 mL, 49.86 mmol, 1.2 equiv) and Et_3N (11.57 mL, 83.1 mmol, 2 equiv) were added. The resulting mixture was stirred at RT for 3 h. After completion, the reaction was quenched with saturated aq. NH_4Cl, and diluted with EtOAc. Organic layer was washed with sat. NH_4Cl and brine; dried using anhydrous Na_2SO_4, filtered. The filtrate was removed *in vacuo* to afford the crude product which was purified using silica gel column chromatography (7.90 g, 92%). TLC (100% EtOAc); R_f = 0.60; ^{1}H NMR (400 MHz, $CDCl_3$) δ (ppm) 5.07 (br, 1H) 3.75–3.73 (m, 2H), 3.59–3.54 (m, 4H), 3.36–3.32 (m, 2H), 2.53 (s, 1H), 1.45 (s, 9H); ^{13}C NMR (100 MHz, $CDCl_3$) δ (ppm) 156.3, 79.5, 72.3, 70.4, 61.8, 40.5, 28.5; HRMS: m/z calculated for $C_9H_{19}NO_4Na$ $[M+Na]^+$ = 228.1211, found = 228.1212.

2.4.4.6 2-(2-(*tert*-Butoxycarbonylamino)ethoxy)ethylmethanesulfonate (22c): To a solution of *tert*-Butyl 2-(2-hydroxyethoxy)ethylcarbamate (7.5 g, 36.52 mmol, 1 equiv) in CH_2Cl_2 (42 mL) was added Et_3N (11.18 mL, 80.35 mmol, 2.2 equiv) at 0 °C. Then methylsulfonyl chloride (3.10 mL, 40.18 mmol, 1.1 equiv) was added dropwise which results into yellow turbid solution. Reaction mixture was stirred at 0 °C for 5 h. After completion, the reaction was quenched with saturated aq. NH_4Cl, and was diluted with EtOAc. Organic layer was washed with sat NH_4Cl, sat. $NaHCO_3$ and brine, dried using anhydrous Na_2SO_4, filtered and filtrate was removed *in vacuo*. The crude product was purified by silica gel column chromatography to afford the compound **22c** as clear yellow oil (9.58 g, 92%). TLC (EtOAc:pet ether = 80:20); R_f = 0.76; ^{1}H NMR (400 MHz, $CDCl_3$) δ (ppm) 4.92 (br, 1H), 4.38–4.36 (m, 2H), 3.75–3.72 (m, 2H), 3.56 (t, *J* = 5.2 Hz, 2H), 3.35–3.31 (m, 2H), 3.07 (s, 3H), 1.45 (s, 9H); ^{13}C NMR (100 MHz, $CDCl_3$) δ (ppm) 155.9, 79.4, 70.4, 68.8, 68.7, 40.2, 37.7, 28.4; HRMS: m/z calculated for $C_{10}H_{21}NSO_6Na$ $[M+Na]^+$ = 306.0987, found = 306.0990.

2.4.4.7 *tert*-Butyl 2-(2-(prop-2-ynyloxy)ethoxy)ethylcarbamate (22d): To a solution of propargyl alcohol (5.63 mL, 97.6 mmol, 3 equiv) in dry THF (110 mL) at 0 °C was added NaH (2.34 g, 97.6 mmol, 3 equiv) portion wise. The resulting suspension was stirred at 0 °C for 30 min then 2-(2-(*tert*-butoxycarbonylamino)ethoxy)ethyl methanesulfonate (9.22 g, 32.53 mmol, 1 equiv) was added dropwise. The reaction mixture was stirred at RT for 19 h. After completion, the reaction was quenched with saturated aq. NH_4Cl and solvent was removed *in vacuo*. Ethyl acetate was added to the resultant red liquid. The organic phase was washed with sat. NH_4Cl, sat. $NaHCO_3$ and brine, dried over anhydrous Na_2SO_4, filtered. The filtrate was removed *in vacuo* to get the crude product which was purified by silica gel column chromatography to afford the pure compound **22d** as yellowish oil (3.67 g, 47%). TLC (EtOAc:pet ether = 50:50); R_f= 0.80; ^{1}H NMR (400 MHz, $CDCl_3$) δ (ppm) 4.20 (d, *J* = 2.4 Hz, 2H), 3.70–3.67 (m, 2H), 3.64–3.62 (m, 2H), 3.54 (t, *J* = 5.2 Hz, 2H), 3.31 (t, *J* = 5.2 Hz, 2H), 2.44 (t, *J* = 2.4 Hz, 1H), 1.43 (s, 9H); ^{13}C NMR (100 MHz, $CDCl_3$) δ (ppm) 156.1, 79.7, 79.4, 74.8, 70.4, 70.2, 69.2, 58.6, 40.6, 28.5; HRMS: m/z calculated for $C_{12}H_{21}NO_4Na$ $[M+Na]^+$ = 266.1367, found = 266.1367.

2.4.4.8 (E)-*tert*-Butyl-2-(2-(3-(4,4,5,5-tetramethyl-1,3,2-dioxaborolan-2-yl)allyloxy) ethoxy)ethylcarbamate (22e): To *tert*-butyl 2-(2-(prop-2-ynyloxy)ethoxy)ethylcarbamate

(2.35 g, 9.65 mmol, 1 equiv) was added pinacolborane (1.55 mL, 10.62 mmol, 1.1 equiv), Et_3N (134 µL, 0.965 mmol, 0.1 equiv) and $ZrCp_2HCl$ (249 mg, 0.965 mmol, 0.1 equiv).The solution was stirred at 65 °C for 17 h. After completion, the reaction was allowed to attain room temperature. Then, it was diluted with EtOAc and quenched with saturated aq. NH_4Cl. The mixture was further diluted with EtOAc. The organic layer was washed with sat. NH_4Cl, sat. $NaHCO_3$, brine and dried over anhydrous Na_2SO_4, filtered. The resultant filtrate was removed *in vacuo* to afford the crude product which was purified by silica gel column chromatography (1.38 g, 39%). TLC (EtOAc:pet ether = 20:80); R_f = 0.57; ^{1}H NMR (400 MHz, $CDCl_3$) δ (ppm) 6.63 (dt, *J* = 18, 4.8 Hz, 1H), 5.70 (d, *J* = 18 Hz, 1H), 5.04 (s, 1H), 4.10 (d, *J* = 4.4 Hz, 2H), 3.63–3.59 (m, 4H), 3.54 (t, *J* = 4.8 Hz, 2H), 3.34–3.31 (m, 2H), 1.44 (s, 9H), 1.27 (s, 12H); ^{13}C NMR (100 MHz, $CDCl_3$) δ (ppm) 156.2, 149.1, 83.4, 83.2, 79.3, 73.0, 70.5, 69.8, 40.5, 28.6, 24.9; HRMS: m/z calculated for $C_{18}H_{34}BNO_6Na$ $[M+Na]^+$ = 394.2376, found = 394.2379.

2.4.4.9 (E)-2-(2-(3-(4,4,5,5-tetramethyl-1,3,2-dioxaborolan-2-yl)allyloxy)ethoxy) ethanamine TFA salt (22f): (E)-*tert*-Butyl-2-(2-(3-(4,4,5,5-tetramethyl-1,3,2-dioxaborolan-2-yl)allyloxy)ethoxy) ethylcarbamate (1.38 g, 3.5 mmol) was dissolved in 22 mL of 10% TFA in CH_2Cl_2. The solution was then stirred for 3 h at RT. After completion, the solvent was removed *in* vacuo. Excess TFA was co-evaporated with toluene and CH_2Cl_2 gave desired product as brown oil (1.65 g, 97%), ^{1}H NMR (400 MHz, $CDCl_3$) δ (ppm) 7.81 (s, 3H), 6.58 (dt, *J* = 18, 4.8 Hz, 1H), 5.68 (d, *J* = 18 Hz, 1.6 Hz, 1H), 4.10 (dd, *J* = 4.8, 1.2 Hz, 2H), 3.74 (t, *J* = 4.4 Hz, 2H), 3.68–3.66 (m, 2H), 3.63–3.61 (m, 2H), 3.22 (s, 2H), 1.27 (s, 12H); ^{13}C NMR (100 MHz, $CDCl_3$) δ (ppm) 148.1, 83.6, 75.5, 72.6, 70.1, 69.5, 66.5, 46.2, 39.9, 31.0 24.7; HRMS: m/z calculated for $C_{13}H_{27}BNO_4$ $[M+H]^+$ = 272.2033, found = 272.2038.

2.4.4.10 (E)-2-(2-(3-(4,4,5,5-tetramethyl-1,3,2-dioxaborolan-2-yl)allyloxy)ethoxy) ethanamine (22): (E)-2-(2-(3-(4,4,5,5-tetramethyl-1,3,2-dioxaborolan-2-yl)allyloxy)ethoxy) ethanamine TFA salt was dissolved in MeOH. TFA salt was neutralized by anion exchange resin yielding free amine **22**.

2.4.5 Synthesis of NBD- and biotin-tagged pinacol boronate esters (9–11)

2.4.5.1 (E)-7-nitro-N-(3-(4,4,5,5-tetramethyl-1,3,2-dioxaborolan-2-yl)allyl)benzo[c] [1,2,5] oxadiazol-4-amine (9): 4-Chloro-7-nitrobenzofurazan (95 mg, 0.48 mmol, 1 equiv)

was dissolved in acetonitrile (4 mL). A solution of amine boronic ester **21** (176 mg, 0.96 mmol, 2 equiv) in acetonitrile (1 mL) was added dropwise. Reaction mixture was stirred at RT for 2 h. Solvent was evaporated and the residue was purified by silica gel column chromatography to afford NBD boronic ester **9** as an orange-brown solid (45 mg, 27%). TLC (EtOAc:pet ether = 30:70); R_f = 0.60. ^{1}H NMR (400 MHz, $CDCl_3$containing 0.03% (v/v) TMS) δ (ppm) 8.48 (d, *J* = 8.6 Hz, 1H), 6.65 (dt, *J* = 18, 4.6 Hz, 1H), 6.46 (br, 1H), 6.16 (d, *J* = 8.6 Hz, 1H), 5.75 (dt, *J* = 18, 1.6 Hz, 1H), 4.25–4.22 (m, 2H), 1.27 (s, 12H); ^{13}C NMR (100 MHz, $CDCl_3$ containing 0.03% (v/v) TMS) δ (ppm) 144.31, 144.27, 143.80, 143.43, 136.27, 124.63, 99.39, 83.79, 47.03, 24.78; HRMS: m/z Calcd. for $C_{15}H_{20}BN_4O_5$ $[M+H]^+$ = 347.1527, found = 347.1526.

2.4.5.2 (E)-7-nitro-N-(2-((3-(4,4,5,5-tetramethyl-1,3,2-dioxaborolan-2-yl)allyl)oxy)ethyl) benzo[c][1,2,5]oxadiazol-4-amine (10): A solution of amine boronic ester **22** (191 mg, 0.70 mmol, 1 equiv) in anhydrous THF (2 mL) was treated with Et_3N (195 µL, 1.40 mmol, 2 equiv). To this reaction mixture, a solution of 4-chloro-7-nitro benzofurazan (183 mg, 0.91 mmol, 1.3 equiv) in anhydrous THF (1 mL) was added dropwise. The resulting mixture was stirred at RT for 2.5 h. After completion, the reaction mixture was diluted with ethyl acetate and washed with saturated aq. NH_4Cl, saturated aq. $NaHCO_3$ and brine. The organic layer was dried over Na_2SO_4 and filtered. The resulting filtrate was evaporated and the obtained residue was purified by silica gel column chromatography to afford the pure product **10** as dark orange solid (175 mg, 57%). TLC (EtOAc:pet ether = 60:40); R_f = 0.67; ^{1}H NMR (400 MHz, $CDCl_3$containing 0.03% (v/v) TMS) δ (ppm) 8.49 (d, *J* = 8.6 Hz, 1H), 6.99 (br, 1H), 6.64 (dt, *J* = 18.4, 4.6 Hz, 1H), 6.19 (d, *J* = 8.6 Hz, 1H), 5.71 (dt, *J* = 18.4, 1.6 Hz, 1H), 4.16 (dd, *J* = 4.6, 1.6 Hz, 2H), 3.88 (t, *J* = 5.2 Hz, 2H), 3.75–3.73 (m, 2H), 3.71–3.65 (m, 4H), 1.26 (s, 12H); ^{13}C NMR (100 MHz, $CDCl_3$ containing 0.03% (v/v) TMS) δ (ppm) 148.6, 144.3, 144.2, 143.9, 136.4, 123.9, 98.8, 83.4, 72.8, 70.7, 69.9, 68.3, 43.7, 24.8; HRMS: m/z Calcd. for $C_{19}H_{28}BN_4O_7$ $[M+H]^+$ = 435.2051, found = 435.2069.

2.4.5.3 2,5-dioxopyrrolidin-1-yl-2-((4S)-2-oxohexahydro-1H-thieno[3,4-d]imidazol-4-yl)acetate (11b)[70]: A mixture of biotin (250 mg, 1.02 mmol, 1 equiv), N-hydroxysuccinimide (188 mg, 1.64 mmol, 1.6 equiv), and EDC (254 mg, 1.33 mmol, 1.3 equiv) was dissolved in DMF (10 mL) and stirred for 24 h at ambient temperature. The solution was poured onto crushed ice and the solid obtained was filtered, washed with water

and, dried to give compound **11b** as white solid (258 mg, 74%). TLC (MeOH:CH_2Cl_2 = 6:94); R_f = 0.31; ^{1}H NMR (d_6-DMSO, 400 MHz): δ 6.42 (br, 1H), 6.36 (br, 1H), 4.32–4.29 (m, 1H), 4.16–4.13 (m, 1H), 3.13–3.08 (m, 1H), 2.89–2.81 (m, 5H), 2.69–2.65 (m, 2H), 2.58 (d, 1H), 1.68–1.60 (m, 3H), 1.55–1.37 (m, 3H); ^{13}C NMR (d_6-DMSO, 100 MHz): δ 170.3, 168.9, 162.7, 61.0, 59.2, 55.2, 30.0, 27.7, 27.6, 25.4, 24.3.

2.4.5.4 5-((4S)-2-oxohexahydro-1H-thieno[3,4-d]imidazol-4-yl)-N-(2-(((E)-3-(4,4,5,5-tetramethyl-1,3,2-dioxaborolan-2-yl)allyl)oxy)ethyl)pentanamide (11): NHS-ester of biotin (**11b**, 200 mg, 0.59 mmol, 1 equiv) was dissolved in 3 mL of anhydrous DMF followed by addition of dry Et_3N (165 µL, 1.18 mmol, 2 equiv). A solution of amine boronic ester **22** (208 mg, 0.77 mmol, 1.3 equiv) in 2 mL dry DMF was added, and the reaction mixture was stirred at RT for 12 h. Solvent was evaporated and the residue was purified by silica gel column chromatography to afford the product **11** as a white solid (105 mg, 35%). TLC (MeOH:CH_2Cl_2 = 10:90); R_f = 0.60; ^{1}H NMR (400 MHz, $CDCl_3$ containing 0.03% (v/v) TMS) δ (ppm) 6.78 (t, *J* = 5.4 Hz, 1H), 6.62 (dt, *J* = 18, 4.6 Hz, 1H), 6.56 (s, 1H), 5.70 (dt, *J* = 18, 1.8 Hz, 1H), 5.62 (s, 1H), 4.52–4.48 (m, 1H), 4.33–4.10 (m, 1H), 4.10 (dd, *J* = 4.6, 1.8 Hz, 2H), 3.64–3.59 (m, 4H), 3.57 (t, *J* = 5 Hz, 2H), 3.49–3.39 (m, 2H), 3.16–3.11 (m, 1H), 2.90 (dd, *J* = 12.8, 4.8 Hz, 1H), 2.74 (d, *J* = 12.8 Hz, 1H), 2.27–2.20 (m, 2H), 1.81–1.61 (m, 4H), 1.48–1.40 (m, 2H), 1.27 (s, 12H); ^{13}C NMR (100 MHz, $CDCl_3$containing 0.03% (v/v) TMS) δ (ppm) 173.41, 164.09, 148.82, 83.38, 72.70, 70.18, 70.00, 69.57 , 61.74, 60.23, 55.54, 40.55, 39.15, 35.95, 28.14, 28.05, 25.57, 24.79; HRMS: m/z Calcd. for $C_{23}H_{41}BN_3O_6S$ $[M+H]^+$ = 498.2809, found = 498.2814.

2.4.6 Synthesis of 2-vinylbenzothiophene- and 2-vinylbenzofuran-boronic esters 16 and 17

2.4.6.1 General procedure for synthesis of 2-Ethynylbenzothiophene and 2-Ethynylbenzofuran[71,72]: tert-Butyl lithium (1.1 equiv) was added to a solution of benzothiophene/benzofuran (1 equiv) in THF (20 mL) at –78 °C. The mixture was stirred for 30 min and a solution of iodine (1.1 equiv) in THF (30 mL) was added. The mixture was stirred for another 30 min, allowed to warm to room temperature, diluted with saturated aq NH_4Cl, and extracted with ether. The organic solution was washed with $Na_2S_2O_3$ and water, dried over Na_2SO_4 and the solvent evaporated under reduced pressure, affording crude 2-iodobenzothiophene/2-iodobenzofuran as yellow oil in > 90% purity, which was confirmed

by ^{1}H NMR spectroscopy. To crude 2-iodobenzothiophene/2-iodobenzofuran was added CuI (1 mol %), $PdCl_2(PPh_3)_2$ (2 mol %), Et_3N (20 mL) and trimethylsilylacetylene (1.2 equiv). The mixture was flushed with Ar and heated at 60 °C for 3 h. The precipitate and solvent were filtered and evaporated, affording crude 2-(trimethylsilylethynyl) benzothiophene/2-(trimethylsilylethynyl) benzofuran as a yellow oil, which was then dissolved in CH_3OH (20 mL) containing KOH (1 equiv). The mixture was stirred at room temperature for 30 min. The solvent was evaporated by vacuum and the residue was purified by column chromatography using hexanes, affording 2-ethynylbenzothiophene as a yellow solid and 2-ethynylbenzofuran as a pale yellow oil.

2-ethynylbenzothiophene: ^{1}H NMR ($CDCl_3$) δ 7.80–7.74 (m, 2H), 7.52 (s, 1H), 7.41–7.35 (m, 2H), 3.45 (s, 1H).

2-ethynylbenzofuran: ^{1}H NMR (400 MHz, $CDCl_3$) δ (ppm) 3.51 (s, 1H), 7.02 (s, 1H), 7.26 (td, *J* = 8.4, 0.8 Hz, 1H), 7.36 (td, *J* = 8.4, 1.2 Hz, 1H), 7.47 (dd, *J* = 8.4, 0.8 Hz, 1H), 7.57 (d, *J* = 8.4 Hz, 1H).

2.4.6.2 General procedure for synthesis of boronic ester 16 and 17: A mixture of bis(pinacolato)diboron (1.1 equiv), sodium methoxide (0.20 equiv), triphenylphosphine (6 mol%) and copper bromide (5 mol%) were stirred under nitrogen for 30 min at RT in dry THF. To this mixture, 2-ethynylbenzothiophene/2-ethynylbenzofuran (1 equiv)[71,72] in methanol (2 equiv) was added. The reaction mixture was stirred for another 2 h at RT. After completion of reaction, solvent was evaporated. To the obtained residue, distilled hexane was added and filtered through celite pad. The filtrate was concentrated under reduced pressure. The residue was purified by silica gel column chromatography to afford the desired product as a yellow solid.

(E)-2-(2-(benzo[b]thiophen-2-yl)vinyl)-4,4,5,5-tetramethyl-1,3,2-dioxaborolane (16):

A mixture of 2-ethynylbenzothiophene (200 mg, 1.26 mmol, 1 equiv), bis(pinacolato)diboron (352 mg, 1.39 mmol, 1.1 equiv), sodium methoxide (14 mg, 0.25 mmol, 0.20 equiv), triphenylphosphine (20 mg, 0.076 mmol, 6 mol%) and copper bromide (9 mg, 0.06 mmol, 5 mol%) yielded **16** (160 mg, 45%). TLC (EtOAc:pet ether = 10:90); R_f = 0.37; ^{1}H NMR (400 MHz, $CDCl_3$) δ (ppm) 7.78–7.75 (m, 1H), 7.74–7.69 (m, 1H), 7.56 (d, *J* = 18 Hz, 1H), 7.33–7.29 (m, 2H), 7.26 (s, 1H), 6.01 (d, *J* = 18.0 Hz, 1H), 1.32 (s, 12H); ^{13}C NMR (100 MHz,

$CDCl_3$) δ (ppm) 144.1, 142.5, 140.1, 139.8, 125.4, 125.2, 124.6, 124.2, 122.5, 83.7, 25.0; HRMS: m/z Calcd. for $C_{16}H_{20}BO_2S$ $[M+H]^+$ = 287.1277, found = 287.1278.

(E)-2-(2-(benzofuran-2-yl)vinyl)-4,4,5,5-tetramethyl-1,3,2-dioxaborolane (17): A mixture of 2-ethynylbenzofuran (283 mg, 1.99 mmol, 1 equiv), bis(pinacolato)diboron (559 mg, 2.2 mmol, 1.1 equiv), sodium methoxide (22 mg, 0.40 mmol, 0.20 equiv), triphenylphosphine (32 mg, 0.12 mmol, 6 mol%) and copper bromide (14 mg, 0.10 mmol, 5 mol%) yielded **17** (270 mg, 50%). TLC (EtOAc:pet ether = 10:90); R_f = 0.50; ^{1}H NMR (400 MHz, $CDCl_3$) δ (ppm) 7.55–7.53 (m, 1H), 7.47–7.45 (m, 1H), 7.31–7.25 (m, 2H), 7.22–7.18 (m, 1H), 6.72 (s, 1H), 6.32 (d, *J* = 18.0 Hz, 1H), 1.32 (s, 12H); ^{13}C NMR (100 MHz, $CDCl_3$) δ (ppm) 155.3, 155.1, 136.6, 128.9, 125.4, 123.0, 121.5, 111.4, 107.3, 83.7, 24.9; HRMS: m/z Calcd. for $C_{16}H_{20}BO_3$ $[M+H]^+$ = 271.1505, found = 271.1509.

2.4.7 Synthesis of *trans*form of 5-(benzofuran-2-yl)vinyl uridine (18): 5-iodouridine **1** (229 mg, 0.62 mmol, 1 equiv), boronic ester **17** (250 mg, 0.93 mmol, 1.5 equiv), K_2CO_3 (257 mg, 1.86 mmol, 3 equiv) were taken in a round-bottomed flask containing H_2O (12 mL) and MeCN (4 mL). $Pd(OAc)_2(L1)_2$ (624 µL of a 50 mM stock, 5 mol%,) was added and the reaction mixture was heated at 55 °C for 2 h. After completion of the reaction, the reaction mixture was filtered through a Celite pad and was subsequently washed with MeOH. Solvent was evaporated under vacuum. The crude product was purified by silica gel column chromatography to afford the *trans* product as an off-white solid **18** (159 mg, 66%). Under these conditions *cis* isomer could not be isolated. TLC (MeOH:CH_2Cl_2 = 15:85); R_f = 0.48; ^{1}H NMR (400 MHz, d_6-DMSO) δ (ppm) 11.60 (br, 1H), 8.35 (s, 1H), 7.59–7.57 (m, 1H), 7.54–7.50 (m, 2H), 7.30–7.26 (m, 1H), 7.22 (td, *J* = 7.6, 0.8 Hz , 1H), 6.99 (d, *J* = 16 Hz, 1H), 6.88 (s, 1H), 5.82 (d, *J* = 4.8 Hz, 1H), 5.46 (br, 1H), 5.32 ($_{app}$t, *J* = 4.4 Hz, 1H), 5.11 (br, 1H), 4.11 (s, 1H), 4.04 ($_{app}$t, *J* = 4.6 Hz, 1H), 3.90–3.87 (m, 1H), 3.78–3.74 (m, 1H), 3.65–3.61(m, 1H); ^{13}C NMR (100 MHz, d_6-DMSO) δ (ppm) 162.1, 155.1, 154.1, 149.6, 139.8, 128.9, 124.6, 123.1, 123.0, 121.0, 115.8, 110.7, 110.0, 104.9, 88.3, 84.7, 73.8, 69.3, 60.5; HRMS: m/z Calcd. for $C_{19}H_{19}N_2O_7$ $[M+H]^+$ = 387.1192, found = 387.1189; ε_{260} = 4200 $M^{-1}cm^{-1}$, ε_{338} = 11960 $M^{-1}cm^{-1}$.

2.4.8 Synthesis of *N,N*-dimethyl-4,6-dihydroxy pyrimidine ligand (L2): Dimethylguanidine sulphate (1.5 g, 5.5 mmol) and sodium (253 mg, 11.00 mmol) in dry methanol (5 mL, 3.3 vol) was stirred for 30 minutes. Ethyl malonate (1.68 mL, 11.00 mmol)

was then added carefully and the reaction mixture was refluxed for 6 h. The resulting solution was allowed to attain room temperature and distilled H_2O was added to it. Further the solution was acidified with acetic acid to get the white crystalline solid of L2 (507 mg, 59%); ^{1}H NMR (400 MHz, $CDCl_3$) δ (ppm) 10.50 (br, 2H), 4.66 (s, 1H), 3.00 (s, 6H); ^{13}C NMR (100 MHz, $CDCl_3$) δ (ppm) 155.0, 167.9, 155.0, 78.3, 37.0; HRMS: m/z calculated for $C_6H_9N_3O_2K$ $[M+K]^+$ = 194.0332, found = 194.0847.

2.4.9. Incorporation of IUTP by *in vitro* transcription reaction

2.4.9.1 Radiolabel experiment: The promoter-template duplexes (5 µM) were assembled by heating a 1:1 mixture of DNA promoter of T7 RNA polymerase consensus sequence and DNA ON templates T1–T5 in annealing buffer (10 mM Tris–HCl, 1 mM ethylenediaminetetraacetic acid (EDTA), 100 mM NaCl, pH7.8) at 90 °C for 3min. The solution was allowed to attain room temperature slowly and then kept in an ice bath for 20 min followed by storing at −40°C. The transcription reactions were carried out at 37 °C in 40 mM Tris–HCl buffer (pH7.8) containing 250 nM annealed promoter-template duplexes, 10 mM MgCl2, 10 mM NaCl, 10 mM of dithiothreitol (DTT), 2 mM spermidine, 1 U/ µl RNase inhibitor (Riboblock), 1 mM guanosine triphosphate(GTP), cytidine triphosphate (CTP), uridine triphosphate (UTP) and or IUTP **2**, 20 µM adenosine triphosphate (ATP), 5 µCi α-^{32}P ATP and 3 U / µL T7 RNA polymerase in a 20 µL reaction volume. The reaction was quenched after 3.5 h by adding 20 µL of loading buffer (7 M urea in 10 mM Tris–HCl, 100 mM EDTA, 0.05% bromophenol blue, pH 8). Each sample was heated for 3 min at 75 °C and then cooled in an ice bath. The samples (4 µL) were loaded on an 18% denaturing polyacrylamide gel and were electrophoresed. The radioactive bands were phosphorimaged and then quantified by using GeneTools software from Syngene to determine the relative transcription efficiencies. Percentage incorporation of IUTP 2 is reported with respect to transcription efficiency in the presence of natural NTPs. All reactions were performed in duplicate and the errors in yields were <2%.

2.4.9.2 Large-scale transcription reaction using template T1 and IUTP 2. Transcription reaction was performed in 250 µL reaction volume using 2 mM of ATP, GTP, CTP and IUTP **2**, 20 mM $MgCl_2$ 2,10 mM DTT, 0.40U/µL RNase inhibitor (Riboblock), 300 nM promoter-template duplex and 800 units of T7 RNA polymerase. The reaction mixture was incubated at 37 °C for 6 h. The reaction volume was made one-third by speed vac followed by addition of

50 µL denaturing loading buffer (7 M urea in 10 mM Tris–HCl, 100 mM EDTA, pH 8) and the sample was loaded on a preparative 20% denaturing polyacrylamide gel. After running the gel for 6h, appropriate band was marked by UV shadowing and excised from the gel. In order to isolate the RNA, the band was extracted with 0.3 M sodium acetate and desalted using a Sep-Pak classic C18 cartridge. Under these conditions, an average of 10 nmole of the iodo-modified RNA transcript **4** was isolated ($\varepsilon 260 = 84300\ M^{-1}cm^{-1}$).

2.4.10 Suzuki–Miyaura reaction between transcript 4 and boronic ester (9–11, 15–17)/boronic acid (12–14)

2.4.10.1 Preparation of $Pd(OAc)_2(L)_2$ complex: To L1 (65mg, 0.5 mmol) or L2 (78 mg, 0.5 mmol) in a 5 mL round bottom flask was added autoclaved H_2O (3 mL) and NaOH (10 M stock,100 µL,1 mmol).The solution was stirred for 5 min at RT to obtain a clear solution. Then $Pd(OAc)_2$ (55 mg, 0.25 mmol) was added and the mixture was stirred at 65 °C for 1 h. Solution was taken in a 5 mL volumetric flask and the volume was adjusted to 5 ml with autoclaved H_2O to give a final stock solution of 50 mM.

2.4.10.2 Analytical-scale reaction with boronic ester 9 and 10: To a solution of iodo-modified RNA transcript **4** (200 µM, 1 equiv) in 10 µL of Tris–HCl buffer (50 mM, pH 8.5) was added boronic ester **9** or **10** (50 or 100 equiv) dissolved in dimethyl sulfoxide (DMSO). The coupling reaction was initiated by adding $Pd(OAc)_2(L1)_2$ catalyst (1 or 2 equiv). Final reaction volume was 50 µL containing 20% DMSO (v/v). The reaction mixture was incubated at 37 °C in thermoshaker. Aliquots of reaction mixture (16 µL) were taken at 3, 6 and 9 h, and 10 µL of denaturing loading buffer (7 M urea in 10 mM Tris–HCl, 100 mM EDTA, pH 8) was added to each aliquot. Samples were loaded on an analytical 20% denaturing polyacrylamide gel. Bands corresponding to the products were visualized by UV-shadowing method (shortwave UV 254 nm and long wave UV 365 nm).

2.4.10.3 Large-scale reaction: To a solution of iodo-modified RNA transcript **4** (5 nmol, 100 µM, 1 equiv) in 10 µL of Tris–HCl buffer (50 mM, pH 8.5) was added boronic acid/ester dissolved in DMSO (250 nmol, 5 mM, 50 equiv). The reaction was initiated by adding catalyst $Pd(OAc)_2(L)_2$ (10 nmol, 0.2 mM, 2 equiv). The final reaction volume was adjusted to 50 µl with water and DMSO such that the percentage of DMSO was 20% v/v. The reaction was incubated at 37 °C for 6−12 h. The reaction mixture was filtered using a spin filter (0.45

μm pore size) and was further washed with 40 μL of water. The filtrate was analyzed by RP-HPLC (Phenomenex-Luna C18 column, 250 × 4.6 mm, 5 micron). Mobile phase A: 50 mM triethylammonium acetate (TEAA) buffer (pH 7.0), mobile phase B: acetonitrile. Flow rate: 1 ml/min. Gradient: 0−30% B in 35 min, 30−100% B in 10 min and 100% B for 5 min. The run was monitored by UV absorption at 260 nm. Each peak was collected and freeze-dried. Similar procedure was used for posttranscriptional Suzuki coupling between IU-labeled transcripts **19** and **20** with ester **17**.

2.4.11 General procedure for the sample preparation for MALDI-TOF mass analysis of transcript and posttranscriptionally coupled RNA ON products: Sample for mass analysis was prepared by combining 1 μL of the transcript/coupled RNA product (~200 μM), 2.5 μL of DNA standard (100 μM, 18-mer) and 5 μL of a mixture of saturated 3-hydroxy picolinic acid and 100 mM ammonium citrate buffer (pH 9, in the ratio of 9:1). The sample was desalted using ion-exchange resin (Dowex 50W-X8, 100-200 mesh, ammonium cation form), spotted on the MALDI plate, and was air dried. The resulting spectrum was calibrated relative to an internal 18-mer DNA ON standard. Depending on the peak intensity the ratio of RNA ON and internal DNA standard was varied.

2.4.12 Enzymatic digestion of Suzuki-coupled RNA ON product 17a′: Enzymatic digestion of Suzuki-coupled RNA ON product **17a′**. A total of 3 nmol of RNA ON **17a′** was treated with snake venom phosphodiesterase I (10 μL, 0.01 U), calf intestinal alkaline phosphatase (10 μL, 1 U/μL) and RNase A (5 μL, 0.25 μg), $MgCl_2$ (20 μL, 40 mM), 10 μl of dephosphorylation buffer (50 mM Tris–HCl buffer, 40 mM $MgCl_2$, 0.1 mM EDTA pH 8.5) in a total volume of 100 μL for 12 h at 37 °C. Subsequently, RNase T1 (2 μL, 0.2 U/μL) was added and the sample was incubated for another 4 h at 37 °C. The ribonucleoside mixture obtained from the digest was analyzed by RP-HPLC using Phenomenex-Luna C18 column (250×4.6 mm, 5 micron) at 260 and 338nm. Mobile phase A: 50 mM TEAA buffer (pH7.0), mobile phase B:acetonitrile. Flow rate: 1 ml/min. Gradient: 0−10% B in 20 min, 10−100% B in 10 min, 0−100% B in 5 min. The fraction corresponding to the individual ribonucleosides was collected and analyzed by mass spectrometry, which also confirmed the identity of the natural ribonucleosides (C, G and A) and Suzuki-coupled ribonucleoside **18** (trans form).

2.4.13 Fluorescence of 5-(benzofuran-2-yl)vinyl uridine-modified RNA ONs obtained by posttranscriptional Suzuki coupling: RNA ONs **17a′**, **19a′** and **20a′** (10 μM) were hybridized to custom DNA ON (11 μM) by heating a mixture (1:1.1) of the ON in 20 mM cacodylate buffer (pH 7.1, 500 mM NaCl, 0.5 mM EDTA) at 90 °C for 3 min. Samples were cooled slowly to room temperature and incubated in crushed ice for 2 h. Samples were diluted to give a final concentration of 0.5 μM with respect to **17a′**, **19a′**and **20a′** in cacodylate buffer. Samples were excited at 350 nm with an excitation slit width of 4 nm and emission slit width of 5 nm. Fluorescence experiments were performed in triplicate in a micro fluorescence cuvette (Hellma, path length 1.0 cm) on a Horiba JobinYvon, Fluorolog-3 at 20 °C.

2.5 References

1. El-Sagheer, A. H. and Brown, T. (2012) Click nucleic acid ligation: applications in biology and nanotechnology. *Acc. Chem. Res*., **45**, 1258–1267.
2. Holstein, J. M. and Rentmeister, A. (2016) Current covalent modification methods for detecting RNA in fixed and living cells. *Methods*, **98**, 18–25.
3. Wu, H., and Devaraj, N. K. (2016) Inverse electron-demand Diels-Alder bioorthogonal reactions. *Top. Curr. Chem*., **374**, 3.
4. George, J. T. and Srivatsan, S. G. (2017) Posttranscriptional chemical labeling of RNA by using bioorthogonal chemistry. *Methods*, **120**, 28–38.
5. Deen, J., Vranken, C., Leen, V., Neely, R. K., Janssen, K. P. F. and Hofkens, J. (2017) Methyltransferase-directed labeling of biomolecules and its applications. *Angew. Chem. Int. Ed.*, **56**, 5182–5200.
6. Kath-Schorr, S. (2016) Cycloadditions for studying nucleic acids. *Top. Curr. Chem.*, **374**, 1–27.
7. Jao, C. Y. and Salic, A. (2008) Exploring RNA transcription and turnover *in vivo* by using click chemistry. *Proc. Natl. Acad. Sci. U.S.A.*, **105**, 15779–15784.
8. El-Sagheer, A. H. and Brown, T. (2010) New strategy for the synthesis of chemically modified RNA constructs exemplified by hairpin and hammerhead ribozymes. *Proc. Natl. Acad. Sci. U.S.A.*, **107**, 15329–15334.
9. Motorin, Y., Burhenne, J., Teimer, R., Koynov, K., Willnow, S., Weinhold, E. and Helm, M. (2011) Expanding the chemical scope of RNA:methyltransferases to site-specific alkynylation of RNA for click labeling. *Nucleic Acids Res*., **39**, 1943–1952.
10. Willibald, J., Harder, J., Sparrer, K., Conzelmann, K.-K. and Carell, T. (2012) Click-modified anandamide siRNA enables delivery and gene silencing in neuronal and immune cells. *J. Am. Chem. Soc.*, **134**, 12330–12333.
11. Paredes, E. and Das, S. R. (2012) Optimization of acetonitrile co-solvent and copper stoichiometry for pseudo-ligandless click chemistry with nucleic acids. *Bioorg. Med. Chem. Lett.*, **22**, 5313–5316.
12. Rao, H., Tanpure, A. A., Sawant, A. A. and Srivatsan, S. G. (2012) Enzymatic incorporation of an azide-modified UTP analog into oligoribonucleotides for posttranscriptional chemical functionalization. *Nat. Protoc*., **7**, 1097–1112.

13. Curanovic, D., Cohen, M., Singh, I., Slagle, C. E., Leslie, C. S. and Jaffrey, S. R. (2013) Global profiling of stimulus-induced polyadenylation in cells using a poly(A) trap. *Nat. Chem. Biol*., **9**, 671–675.
14. Santner, T., Hartl, M., Bister, K. and Micura, R. (2014) Efficient access to 3′-terminal azide-modified RNA for inverse click-labeling patterns. *Bioconjugate Chem.*, **25**, 188–195.
15. Samanta, A., Krause, A. and A. Jäschke, (2014) A modified dinucleotide for site-specific RNA-labeling by transcription priming and click chemistry. *Chem. Commun.*, 50 1313–1316.
16. Li, F., Dong, J., Hu, X., Gong, W., Li, J., Shen, J., Tian, H. and Wang, J. (2015) A covalent approach for site-specific RNA labeling in mammalian cells. *Angew. Chem. Int. Ed.*, **54**, 4597–4602.
17. Someya, T., Ando, A., Kimoto, M. and Hirao, I. (2015) Site-specific labeling of RNA by combining genetic alphabet expansion transcription and copper-free click chemistry. *Nucleic Acids Res*., **43**, 6665–6676.
18. Merkel, M., Peewasan, K., Arndt, S., Ploschik, D. and Wagenknecht, H.-A (2015) Copper-free postsynthetic labeling of nucleic acids by means of bioorthogonal reactions. *ChemBioChem*, **16**, 1541–1553.
19. Holstein, J. M., Anhäuser, L. and Rentmeister, A. (2016) Modifying the 5′-cap for click reactions of eukaryotic mRNA and to tune translation efficiency in living cells. *Angew. Chem. Int. Ed.*, **55**, 10899–10903.
20. Zheng, Y. and Beal, P. A. (2016) Synthesis and evaluation of an alkyne-modified ATP analog for enzymatic incorporation into RNA. *Bioorg. Med. Chem. Lett.*, **26**, 1799–1802.
21. Sawant, A. A., Tanpure, A. A., Mukherjee, P. P., Athavale, S., Kelkar, A., Galande, S. and Srivatsan, S. G. (2016) A versatile toolbox for posttranscriptional chemical labeling and imaging of RNA. *Nucleic Acids Res*., **44**, e16.
22. Nguyen, K., Fazio, M., Kubota, M., Nainar, S., Feng, C., Li, X., Atwood, S. X., Bredy, T. W. and Spitale, R. C. (2017) Cell-selective bioorthogonal metabolic labeling of RNA. *J. Am. Chem. Soc.*, **139**, 2148–2151.
23. Schoch, J., Ameta, S. and Jäschke, A. (2011) Inverse electron-demand Diels–Alder reactions for the selective and efficient labeling of RNA. *Chem. Commun*., **47**, 12536–12537.
24. Ameta, S., Becker, J. and Jäschke, A. (2014) RNA–peptide conjugate synthesis by inverse- electron demand Diels–Alder reaction. *Org. Biomol. Chem.*, **12**, 4701–4707.
25. Pyka, A. M., Domnick, C., Braun, F. and Kath-Schorr, S. (2014) Diels−Alder cycloadditions on synthetic RNA in mammalian cells. *Bioconjugate Chem.*,**25**, 1438−1443.
26. Domnick, C., Eggert, F. and Kath-Schorr, S. (2015) Site-specific enzymatic introduction of a norbornene modified unnatural base into RNA and application in posttranscriptional labeling. *Chem. Commun*., **51**, 8253–8256.
27. Asare-Okai, P. N., Agustin, E., Fabris, D. and Royzen, M. (2014) Site-specific fluorescence labeling of RNA using bio-orthogonal reaction of *trans*-cyclooctene and tetrazine. *Chem. Commun*., **50**, 7844–7847.
28. George, J. T. and Srivatsan, S. G. (2017) Vinyluridine as a versatile chemoselective handle for the posttranscriptional chemical functionalization of RNA. *Bioconjugate Chem*. **28**, 1529–1536.

29. Agard, N. J., Prescher, J. A. and Bertozzi, C. R. (2004) A strain-promoted [3 + 2] azide-alkyne cycloaddition for covalent modification of biomolecules in living systems. *J.Am. Chem. Soc.*, **126**, 15046–15047.
30. Rieder, U. and Luedtke, N. W. (2014) Alkene–tetrazine ligation for imaging cellular DNA. *Angew. Chem. Int. Ed.*, 53, 9168–9172.
31. Oliveira, B. L., Guo, Z. and Bernardes, G. J. L. (2017) Inverse electron demand Diels–Alder reactions in chemical biology. *Chem. Soc. Rev.*, **46**, 4895–4950.
32. Spicer, C. D. and Davis, B. G. (2014) Selective chemical protein modification. *Nat. Commun*., **5**, 4740.
33. Yang, M., Li, J. and Chen, P. R. (2014) Transition metal-mediated bioorthogonal protein chemistry in living cells. *Chem. Soc. Rev*., **43**, 6511–6526.
34. Shaughnessy, K. H. (2015) Palladium-catalyzed modification of unprotected nucleosides, nucleotides, and oligonucleotides. *Molecules*, **20**, 9419–9454.
35. Defrancq, E. and Messaoudi, S. (2017) Palladium-mediated labeling of nucleic acids. *ChemBioChem*, **18**, 426–431.
36. Jbara, M., Maity, S. K. and Brik, A. (2017) Palladium in the chemical synthesis and modification of proteins. *Angew. Chem. Int. Ed*., **56**, 10644–10655.
37. Shaughnessy, K. H. (2009) Hydrophilic ligands and their application in aqueous-phase metal-catalyzed reactions. *Chem. Rev*., **109**, 643–710.
38. Hervé, G. and Len, C. (2015) Heck and Sonogashira couplings in aqueous media–application to unprotected nucleosides and nucleotides. *Sustain. Chem. Process*, **3**, 3.
39. Ourailidou, M. E., Dockerty, P., Witte, M., Poelarends, G. J. and Dekker, F. J. (2015) Metabolic alkene labeling and *in vitro* detection of histone acylation *via* the aqueous oxidative Heck reaction. *Org. Biomol. Chem*., **13**, 3648–3653.
40. Omumi, A., Beach, D. G., Baker, M., Gabryelski, W. and Manderville, R. A. (2011) Postsynthetic guanine arylation of DNA by Suzuki−Miyaura cross-coupling. *J. Am. Chem. Soc*., **133**, 42–50.
41. Hollenstein, M. (2012) Synthesis of deoxynucleoside triphosphates that include proline, urea, or sulfonamide groups and their polymerase incorporation into DNA. *Chem. Eur. J*., **18**, 13320–13330.
42. Hocek, M. and Fojta, M. (2008) Cross-coupling reactions of nucleoside triphosphates followed by polymerase incorporation. Construction and applications of base-functionalized nucleic acids. *Org. Biomol. Chem.*,**6**, 2233–2241.
43. Cahová, H. and Jäschke, A. (2013) Nucleoside-based diarylethene photoswitches and their facile incorporation into photoswitchable DNA. *Angew. Chem. Int. Ed*., **52**, 3186–3190.
44. Chalker, J. M., Wood, C. S. C. and Davis, B. G. (2009) A convenient catalyst for aqueous and protein Suzuki–Miyaura cross-coupling. *J. Am. Chem. Soc*., **131**, 16346–16347.
45. Spicer, C. D., Triemer, T. and Davis, B. G. (2012) Palladium-mediated cell-surface labeling. *J. Am. Chem. Soc*., **134**, 800–803.
46. Li, N., Lim, R. K. V., Edwardraja, S. and Lin, Q. (2011) Copper-free Sonogashira cross-coupling for functionalization of alkyne-encoded proteins in aqueous medium and in bacterial cells. *J. Am. Chem. Soc*., **133**, 15316–15319.
47. Lercher, L., McGouran, J. F., Kessler, B. M., Schofield, C. J. and Davis, B. G. (2013) DNA modification under mild conditions by Suzuki–Miyaura cross-coupling for the generation of functional probes. *Angew. Chem. Int. Ed*., **52**, 10553–10558.

48. Wicke, L. and Engels, J. W. (2012) Postsynthetic on column RNA labeling via Stille coupling. *Bioconjugate Chem*., **23**, 627–642.
49. Jeong, H. S., Hayashi, G. and Okamoto, A. (2015) Diazirine photocrosslinking recruits activated FTO demethylase complexes for specific N^6-methyladenosine recognition. *ACS Chem. Biol*., **10**, 1450–1455.
50. Wachowius, F. and Höbartner, C. (2010) Chemical RNA modifications for studies of RNA structure and dynamics. *ChemBioChem*, **11**, 469–480.
51. Xu, W., Chan, K. M. and Kool, E. T. (2017) Fluorescent nucleobases as tools for studying DNA and RNA. *Nat. Chem*., **9**, 1043–1055.
52. Sholokh, M., Improta, R., Mori, M., Sharma, R., Kenfack, C., Shin, D., Voltz, K., Stote, R. H., Zaporozhets, O. A., Botta, M., Tor, Y. and Mély, Y. (2016) Tautomers of a fluorescent G surrogate and their distinct photophysics provide additional information channels. *Angew. Chem. Int. Ed.*, **55**, 7974–7978.
53. Rovira, A. R., Fin, A. and Tor, Y. (2017) Expanding a fluorescent RNA alphabet: synthesis, photophysics and utility of isothiazole-derived purine nucleoside surrogates. *Chem. Sci.*, **8**, 2983–2993.
54. Dumat, B., Larsen, A. F. and Wilhelmsson, L. M. (2016) Studying Z-DNA and B- to Z-DNA transitions using a cytosine analogue FRET-pair. *Nucleic Acids Res*., **44**, e101.
55. Nuthanakanti, A., Boerneke, M. A., Hermann, T., and Srivatsan, S. G. (2017) Structure of the ribosomal RNA decoding site containing a selenium-modified responsive fluorescent ribonucleoside probe. *Angew. Chem. Int. Ed.*, **56**, 2640–2644.
56. Puffer, B., Kreutz, C., Rieder, U., Ebert, M.-O., Konrat, R. and Micura, R. (2009) 5-Fluoro pyrimidines: labels to probe DNA and RNA secondary structures by 1D ^{19}F NMR spectroscopy. *Nucleic Acids Res*., **37**, 7728–7740.
57. Olszewska, A., Pohl, R. and Hocek, M. (2017) Trifluoroacetophenone-linked nucleotides and DNA for studying of DNA–protein interactions by ^{19}F NMR Spectroscopy. *J. Org. Chem.*, **82**, 11431–11439.
58. Salon, J., Jiang, J., Sheng, J., Gerlits, O. O. and Huang, Z. (2008) Derivatization of DNAs with selenium at 6-position of guanine for function and crystal structure studies. *Nucleic Acids Res.*, **36**, 7009–7018.
59. Piton, N., Mu, Y., Stock, G., Prisner, T. F., Schiemann, O. and Engels, J. W. (2007) Base-specific spin-labeling of RNA for structure determination. *Nucleic Acids Res*., **35**, 3128–3143.
60. Shelke, S. A. and Sigurdsson, S. T. (2010) Noncovalent and site-directed spin labeling of nucleic acids. *Angew. Chem. Int. Ed.*, **49**, 7984−7986.
61. Kerzhner, M., Abdullin, D., Więcek, J., Matsuoka, H., Hagelueken, G., Schiemann, O. and Famulok, M. (2016) Postsynthetic spin-labeling of RNA through click chemistry for PELDOR measurements.*Chem. Eur. J.*, **22**, 12113–12121.
62. Hocek, M. (2014) Synthesis of base-modified 2′-deoxyribonucleoside triphosphates and their use in enzymatic synthesis of modified DNA for applications in bioanalysis and chemical biology. *J. Org. Chem*., **79**, 9914–9921.
63. Collier, A. and Wagner, G. (2006) A facile two-step synthesis of 8-arylated guanosine mono- and triphosphates (8-aryl GXPs). *Org. Biomol. Chem.*, **4**, 4526–4532.
64. Čapek, P., Cahová, H., Pohl, R., Hocek, M., Gloeckner, C. and Marx, A. (2007) An efficient method for the construction of functionalized DNA bearing amino acid groups through cross-coupling reactions of nucleoside triphosphates followed by primer extension or PCR. *Chem. Eur. J.*, **13**, 6196–6203.

65. Vaught, J. D., Dewey, T. and Eaton, B. E. (2004) T7 polymerase transcription with 5-position modified UTP derivatives. *J. Am. Chem. Soc.*, **126**, 11231–11237.
66. Bley, C. J., Qi, X., Rand, D. P., Borges, C. R., Nelson, R. W. and Chen, J. J.-L (2011) RNA-protein binding interface in the telomerase ribonucleoprotein. *Proc. Natl. Acad. Sci. U.S.A.*, **108**, 20333–20338.
67. Flasche, W., Cismas, C., Herrmann, A. and Liebscher, J. (2004) Lipophilic nucleosides by Sonogashira coupling. *Synthesis*, **14**, 2335–2341.
68. Moffatt, J. G. (1964) A general synthesis of nucleoside-5′ triphosphates. *Can. J. Chem.*, **42**, 599–604.
69. Pesnot, T., Tedaldi, L. M., Jambrina, P. G., Rostac, E. and Wagner, G. K. (2013) Exploring the role of the 5-substituent for the intrinsic fluorescence of 5-aryl and 5-heteroaryl uracil nucleotides: a systematic study. *Org. Biomol. Chem.*, **11**, 6357–6371.
70. Kottani, R., Valiulin, R. A. and Kutateladze, A. G. (2006) Direct screening of solution phase combinatorial libraries encoded with externally sensitized photolabile tags. *Proc. Natl. Acad. Sci. U.S.A.*, **103**, 13917–13921.
71. Blanchard, D. J. M., Cservenyi, T. Z. and Manderville, R. A. (2015) Dual fluorescent deoxyguanosine mimics for FRET detection of G-quadruplex folding. *Chem. Commun.*, **51**, 16829–16831.
72. Zang, H. and Larock, R. C. (2002) Synthesis of β- and γ-carbolines by the Palladium/Copper-catalyzed coupling and cyclization of terminal acetylenes *J. Org. Chem.*, **67**, 7048–7056.
73. Boon, W. R. (1952) 6- Dichloro-2-dimethylamino pyrimidine *J. Chem. Soc*., 1532.
74. Sinkeldam, R. W., Greco, N. J. and Tor, Y. (2010) Fluorescent analogs of biomolecular building blocks: design, properties, and applications. *Chem. Rev*., **110**, 2579–2619.
75. Tanpure, A. A., Pawar, M. G. and Srivatsan, S. G. (2013) Fluorescent nucleoside analogs: probes for investigating nucleic acid structure and function. *Isr. J. Chem*., **53**, 366–378.
76. Mata, G. and Luedtke, N. W. (2015) Fluorescent probe for proton-coupled DNA folding revealing slow exchange of i-motif and duplex structures. *J. Am. Chem. Soc*., **137**, 699–707.
77. Kanamori, T., Ohzeki, H., Masaki, Y., Ohkubo, A., Takahashi, M., Tsuda, K., Ito, T., Shirouzu, M., Kuwasako, K., Muto, Y., Sekine, M. and Seio, K. (2015) Controlling the fluorescence of benzofuran-modified uracil residues in oligonucleotides by triple-helix formation. *ChemBioChem*, **16**, 167–176.
78. Dziuba, D., Jurkiewicz, P., Cebecauer, M., Hof, M. and Hocek, M. (2016) A rotational BODIPY nucleotide: an environment-sensitive fluorescence-lifetime probe for DNA interactions and applications in live-cell microscopy. *Angew. Chem. Int. Ed*., **55**, 174–178.
79. Wranne, M. S., Füchtbauer, A. F., Dumat, B., Bood, M., El-Sagheer, A. H., Brown, T., Gradén, H., Grøtli, M. and Wilhelmsson, L. M. (2017) Toward complete sequence flexibility of nucleic acid base Analogue FRET. *J. Am. Chem. Soc.*, **139**, 9271–9280.
80. Manna, S., Panse, C. H., Sontakke, V. A., Sangamesh, S. and Srivatsan, S. G. (2017) Probing human telomeric DNA and RNA topology and ligand binding in a cellular model by using responsive fluorescent nucleoside probes. *ChemBioChem*, 2017, **18**, 1604–1615.
81. Kimoto, M., Mitsui, T., Harada, Y., Sato, A., Yokoyama, S. and Hirao, I. (2007) Fluorescent probing for RNA molecules by an unnatural base-pair system. *Nucleic Acids Res.*, **35**, 5360–5369.

82. Siraiwa, S., Suzuki, A., Katoh, R. and Saito, Y. (2016) Design and synthesis of a novel fluorescent benzo[g]imidazo[4,5-c]quinoline nucleoside for monitoring base-pair-induced protonation with cytosine: distinguishing cytosine *via* changes in the intensity and wavelength of fluorescence. *Org. Biomol. Chem.*, **14**, 3934–3942.
83. Srivatsan, S. G. and Tor, Y. (2007) Fluorescent pyrimidine ribonucleotide: synthesis, enzymatic incorporation, and utilization. *J. Am. Chem. Soc.*, **129**, 2044–2053.
84. Pawar, M. G. and Srivatsan, S. G. (2011) Synthesis, photophysical characterization, and enzymatic incorporation of a microenvironment-sensitive fluorescent uridine analog. *Org. Lett.*, **13**, 1114–1117.
85. Tanpure, A. A. and Srivatsan, S. G. (2011) A microenvironment-sensitive fluorescent pyrimidine ribonucleoside analogue: synthesis, enzymatic incorporation, and fluorescence detection of a DNA abasic site. *Chem. Eur. J.*, **17**, 12820–12827.
86. Tanpure, A. A and Srivatsan, S. G. (2015) Conformation-sensitive nucleoside analogues as topology-specific fluorescence turn-on probes for DNA and RNA G-quadruplexes. *Nucleic Acids Res.*, **43**, e149.
87. Sproviero, M., Fadock, K. L., Witham, A. A. and Manderville, R. A. (2015) Positional impact of fluorescently modified G-tetrads within polymorphic human telomeric G-quadruplex structures. *ACS Chem. Biol*., **10**, 1311–1318.
88. Blanchard, D. J. M., Cservenyi, T. Z. and Manderville, R. A (2015) Dual fluorescent deoxyguanosine mimics for FRET detection of G-quadruplex folding. *Chem. Commun.*, **51**, 16829–16831.
89. Samanta, B., Seikowski, J. and Höbartner, C. (2016) Fluorogenic labeling of 5-formylpyrimidine nucleotides in DNA and RNA. *Angew. Chem. Int. Ed.*, **55**, 1912–1916.
90. Sinkeldam, R. W., Greco, N. J. and Tor, Y. (2008) Polarity of major grooves explored by using an isosteric emissive nucleoside. *ChemBioChem*, **9**, 706–709.
91. Jadhav, V. R., Barawkar, D. A. and Ganesh, K. N. (1999) Polarity sensing by fluorescent oligonucleotides: first demonstration of sequence-dependent microenvironmental changes in the DNA major groove. *J. Phys. Chem. B*, **103**, 7383–7385.
92. Doose, S., Neuweiler, H. and Sauer, M. (2009) Fluorescence quenching by photoinduced electron transfer: a reporter for conformational dynamics of macromolecules. *ChemPhysChem*, **10**, 1389–1398.
93. Garrett,C.E. and Prasad,K. (2004) The art of meeting palladium specifications in active pharmaceutical ingredients produced by Pd-catalyzed reactions. *Adv. Synth. Catal.*, **346**, 889–900.
94. Spicer,C.D. and Davis,B.G. (2011) Palladium-mediated site-selective Suzuki–Miyaura protein modification at genetically encoded aryl halides. *Chem. Commun.*, **47**, 1698–1700.

2.6 Appendix-I: Characterization data of synthesized compounds

^{1}H NMR of IUTP **2** in D_2O (400 MHz). Peaks corresponding to triethylammonium acetate buffer are present.

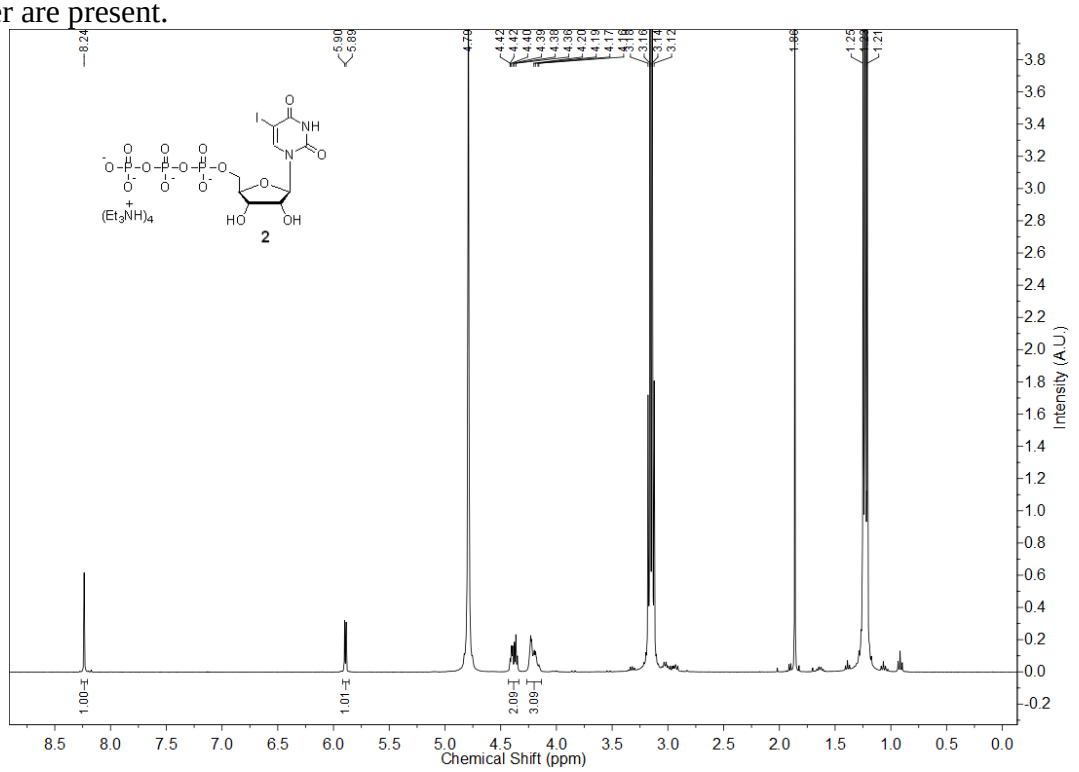

^{31}P NMR of IUTP **2** in D_2O (162 MHz)

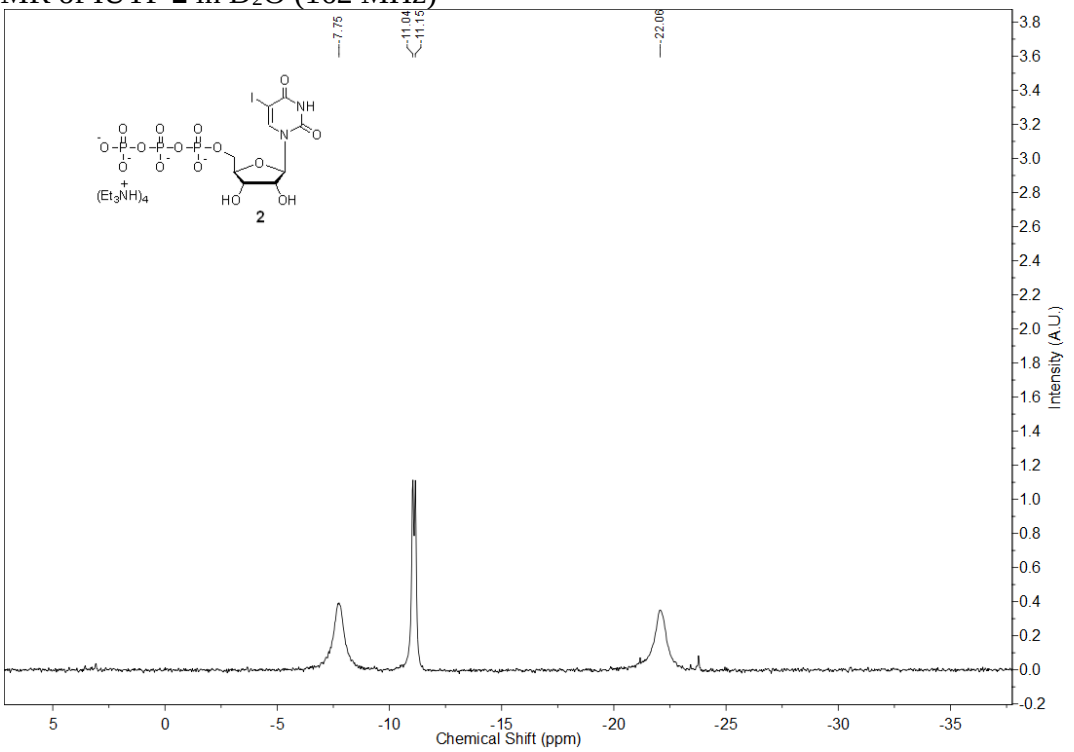

^{1}H NMR of the compound **9** in $CDCl_3$ containing 0.03% (v/v) TMS (400 MHz)

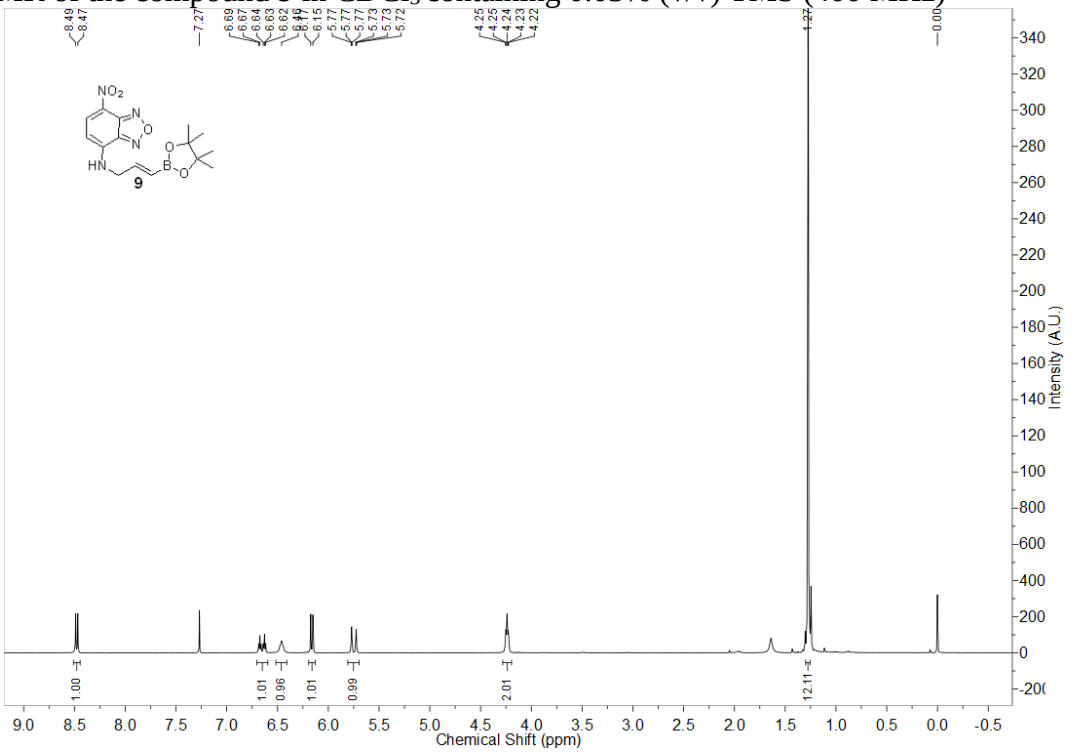

^{13}C NMR of the compound **9** in $CDCl_3$ containing 0.03% (v/v) TMS (100 MHz)

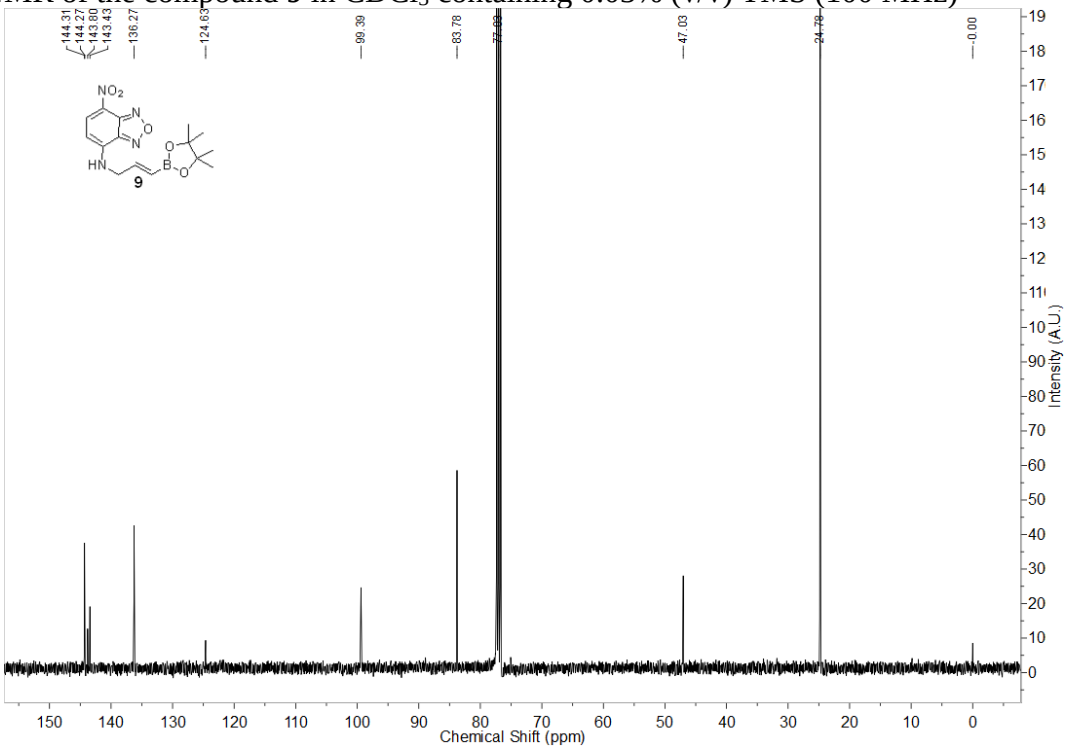

^{1}H NMR of the compound **10** in $CDCl_3$ containing 0.03% (v/v) TMS (400 MHz)

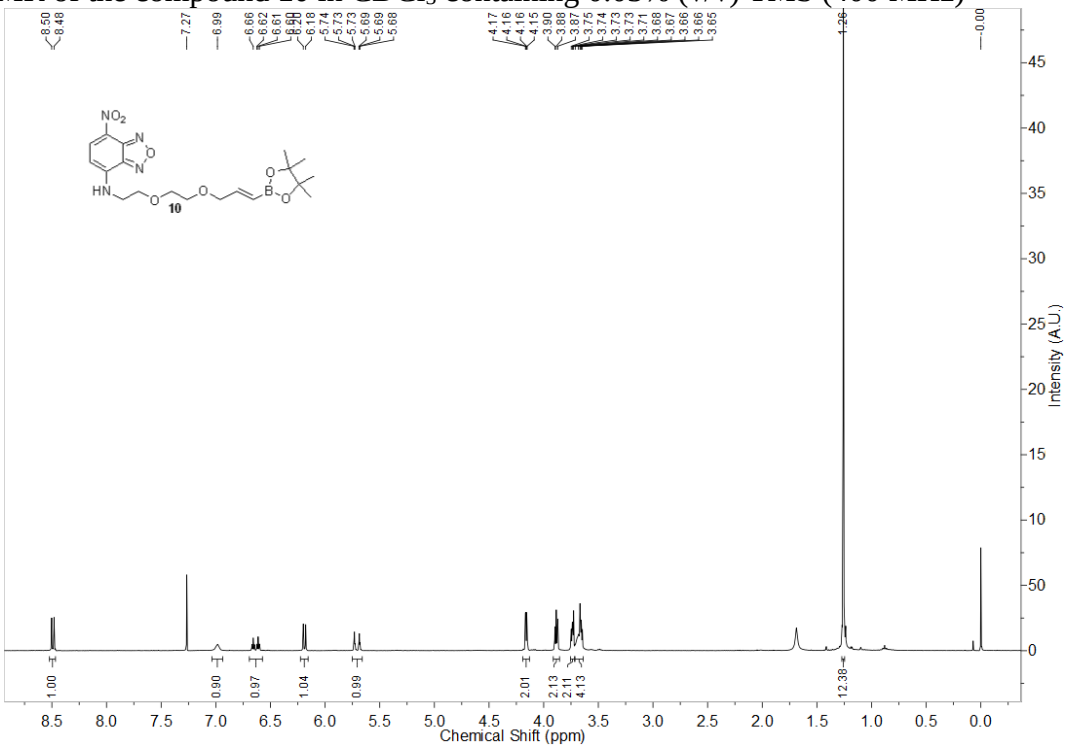

^{13}C NMR of the compound **10** in $CDCl_3$ containing 0.03% (v/v) TMS (100 MHz)

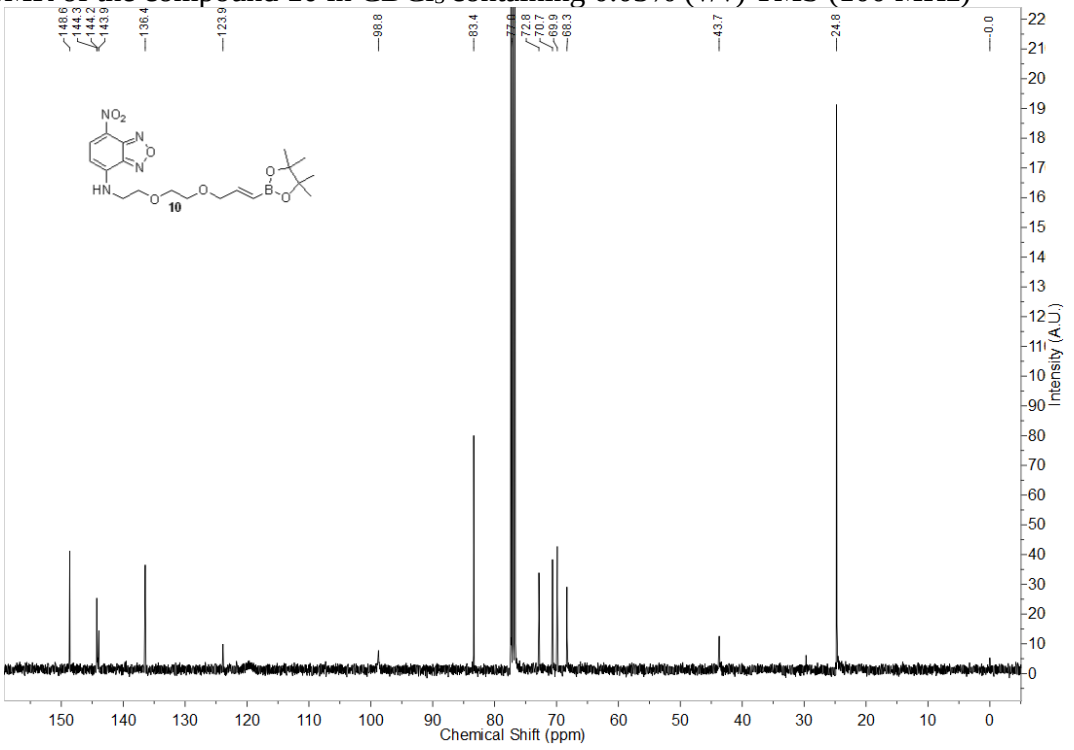

^{1}H NMR of the compound **11b** in d_6-DMSO (400 MHz)

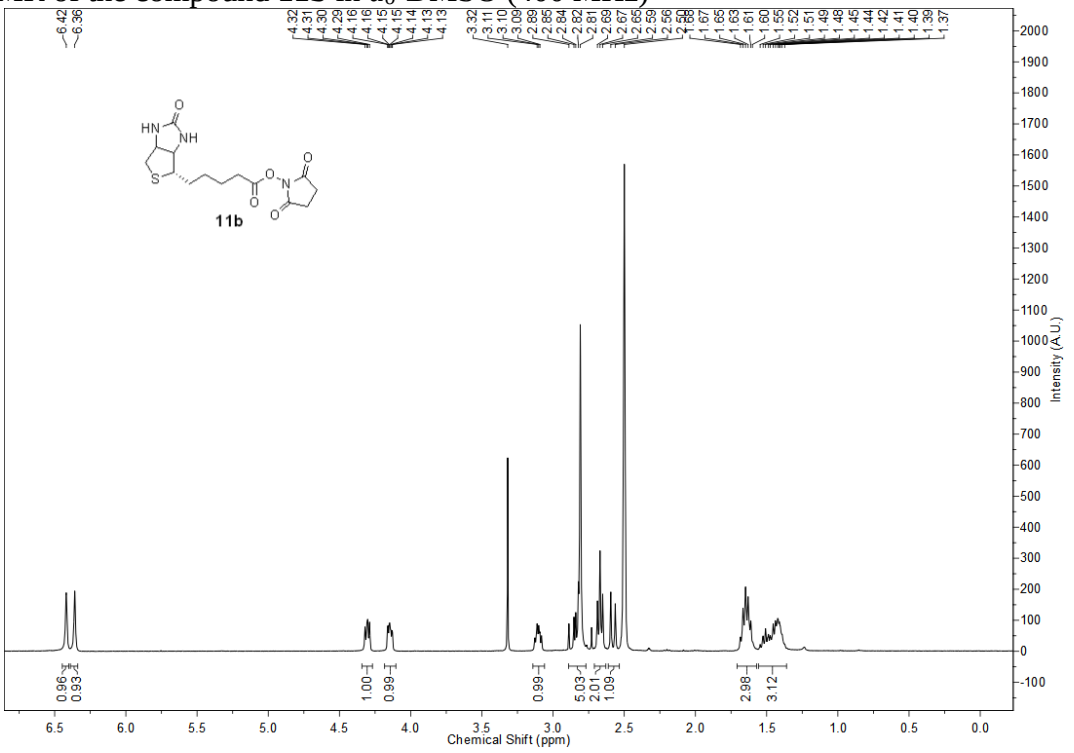

^{13}C NMR of the compound **11b** in d_6-DMSO (100 MHz)

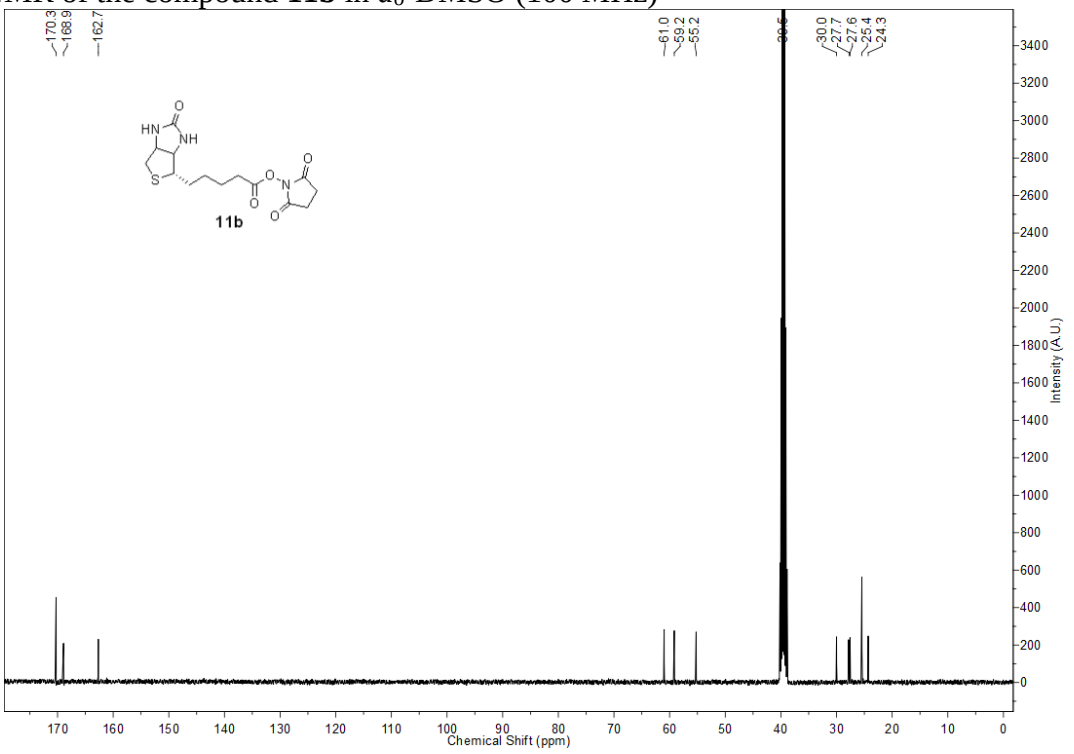

^{1}H NMR of the compound **11** in $CDCl_3$ containing 0.03% (v/v) TMS (400 MHz)

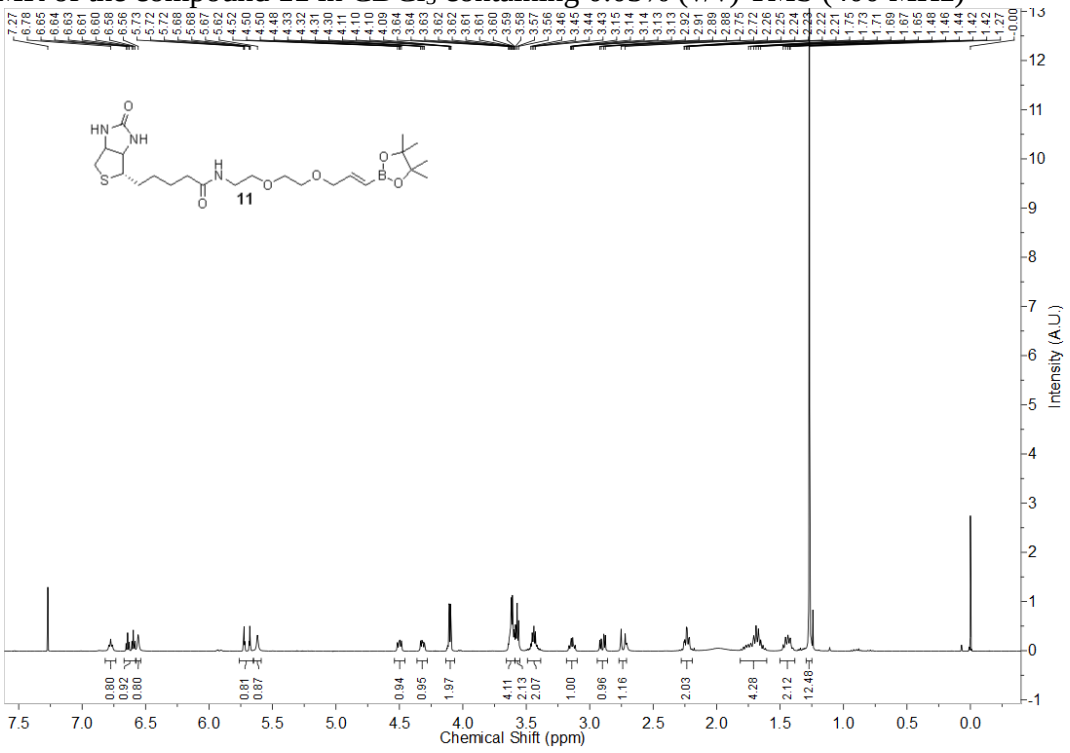

^{13}C NMR of the compound **11** in $CDCl_3$ containing 0.03% (v/v) TMS (100 MHz)

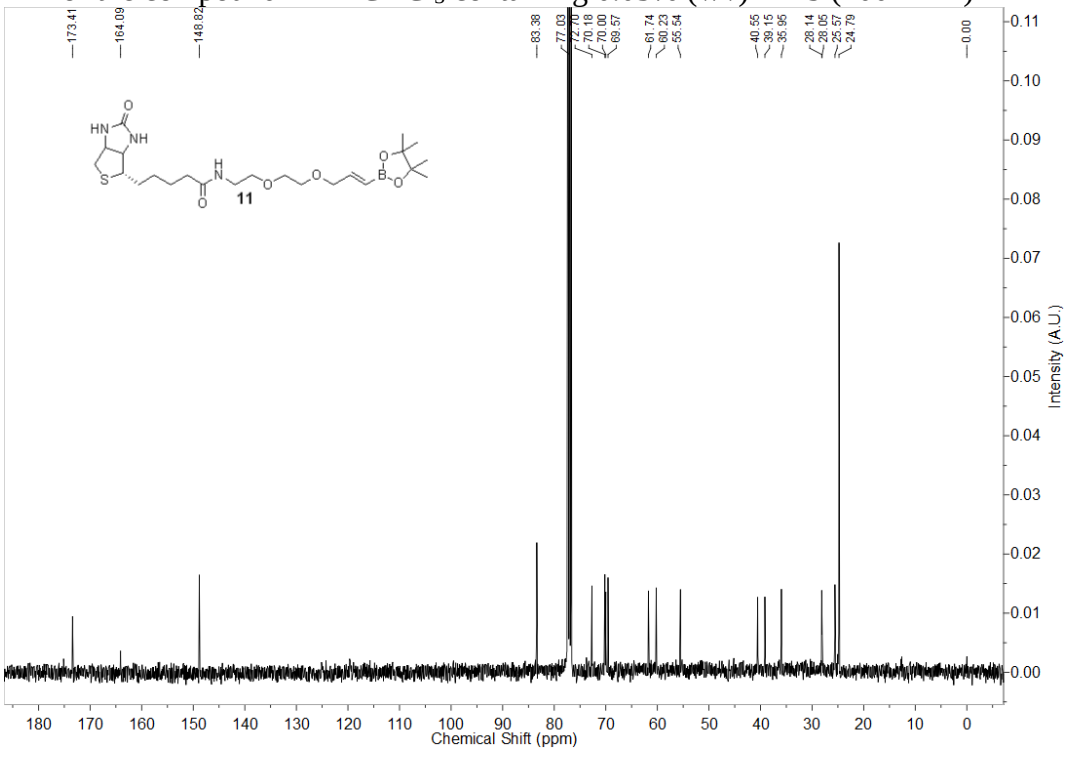

^{1}H NMR of the compound 2-ethynylbenzothiophene in $CDCl_3$ (400 MHz)

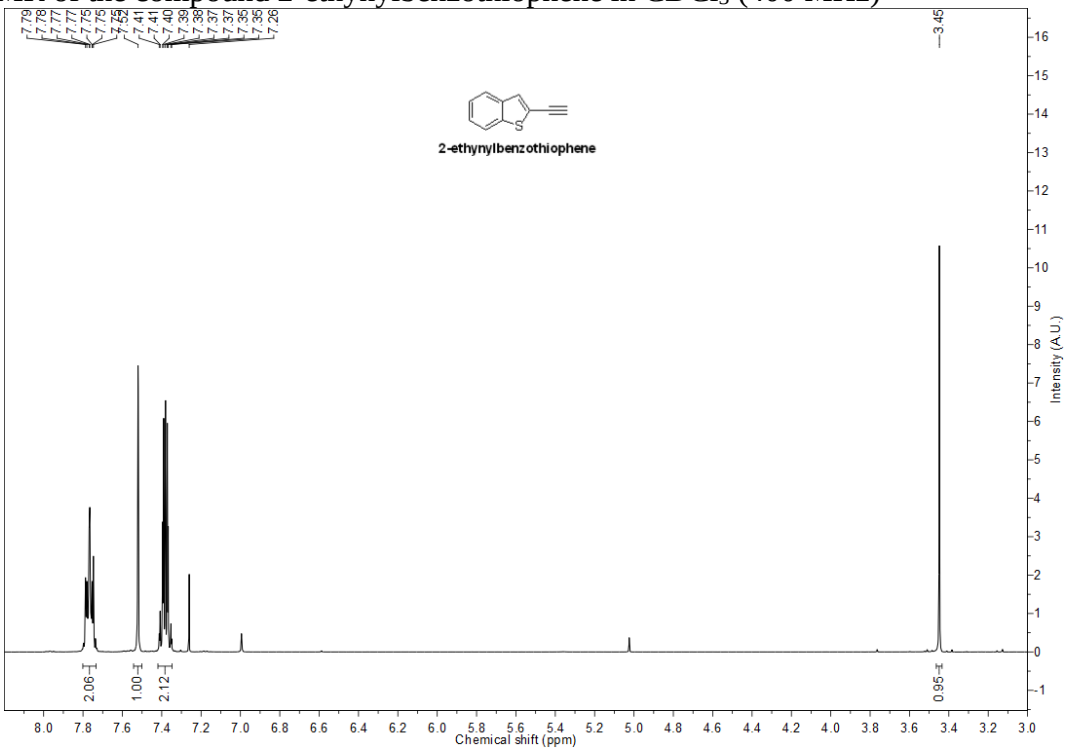

^{1}H NMR of the compound 2-ethynylbenzofuran in $CDCl_3$ (400 MHz)

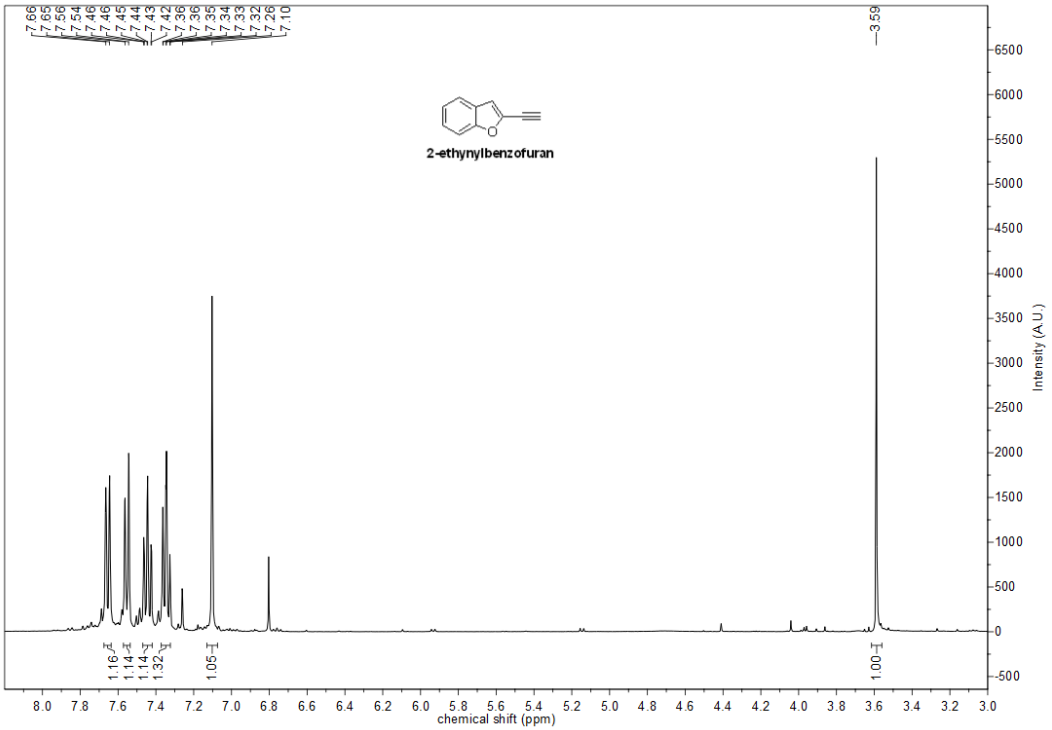

^{1}H NMR of the compound **16** in $CDCl_3$ (400 MHz)

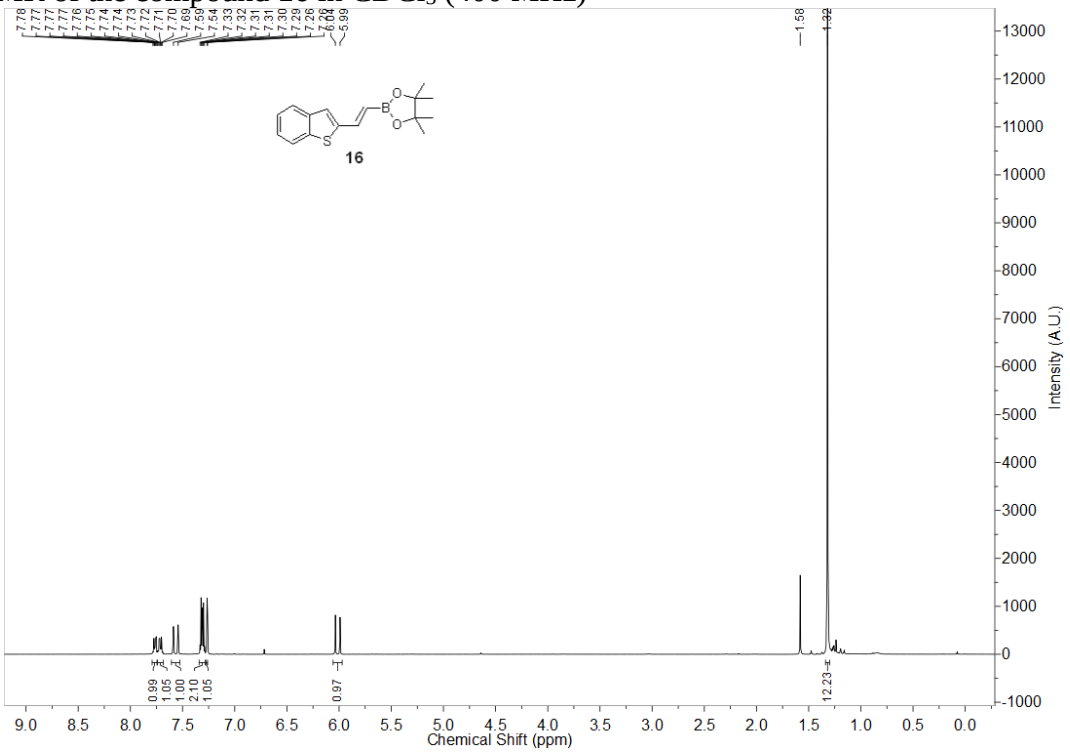

^{13}C NMR of the compound **16** in $CDCl_3$ (100 MHz)

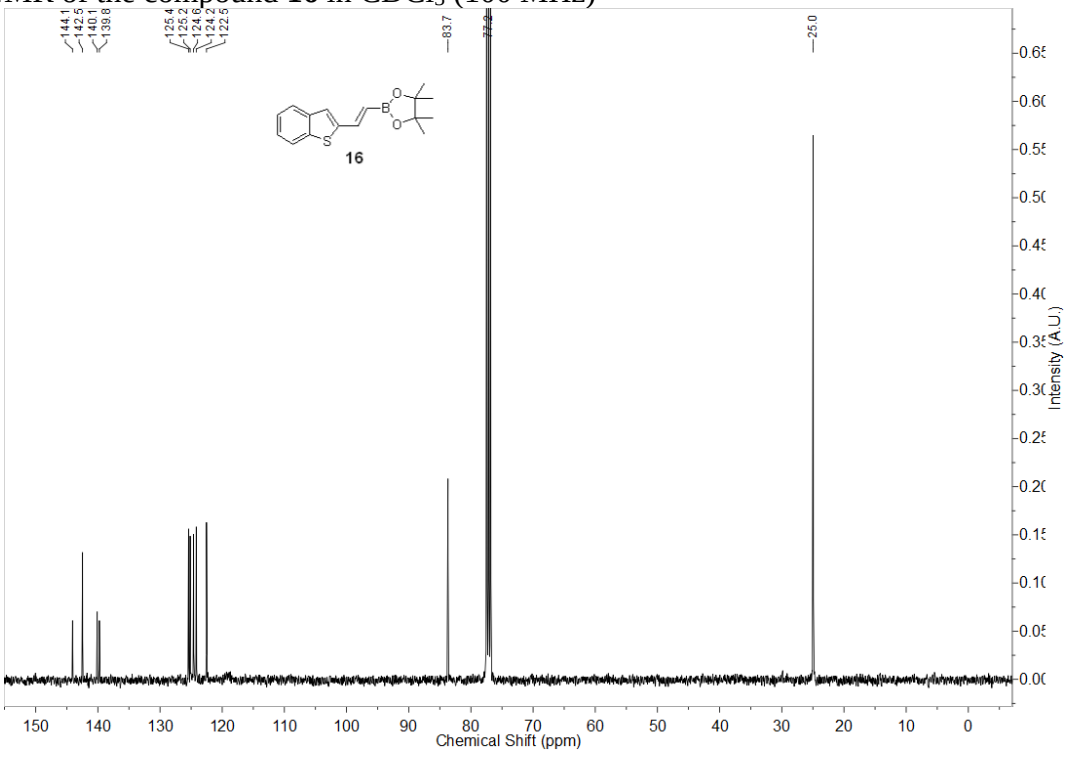

^{1}H NMR of the compound **17** in $CDCl_3$ (400 MHz)

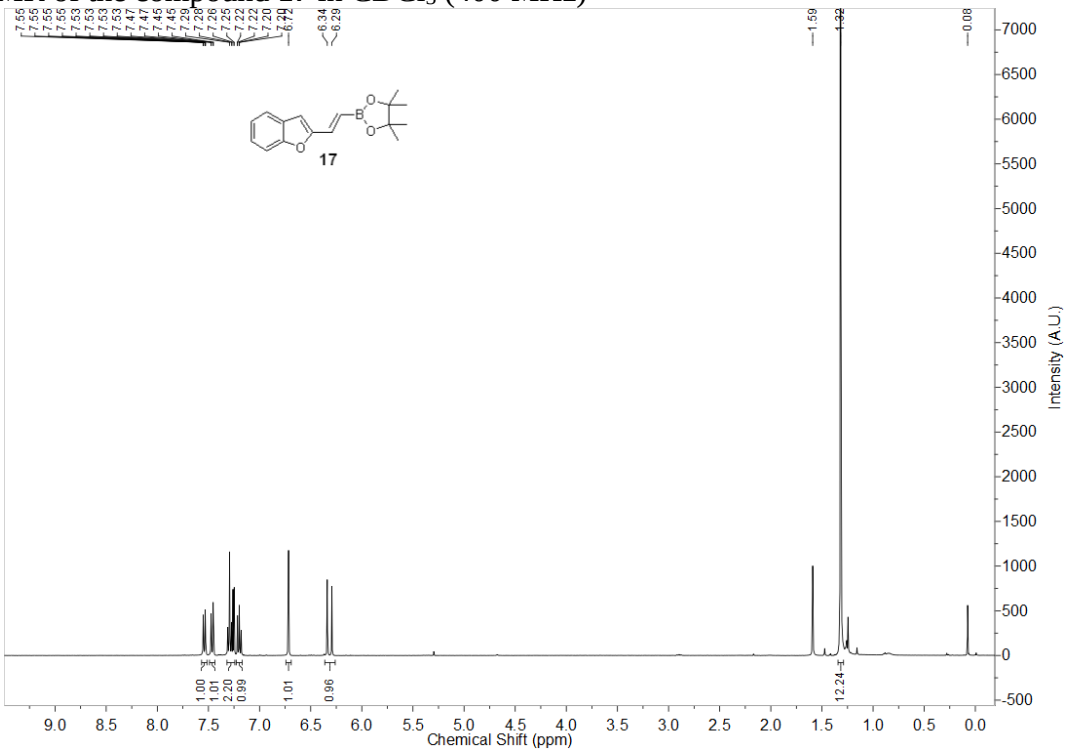

^{13}C NMR of the compound **17** in $CDCl_3$ (100 MHz)

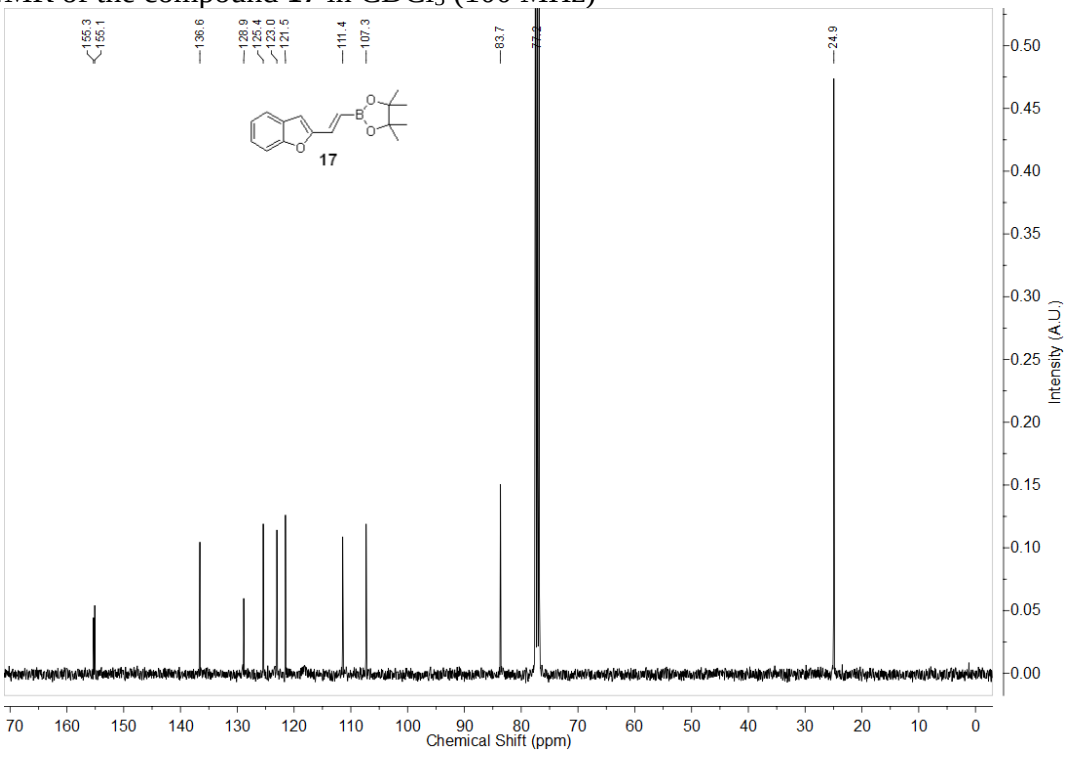

^{1}H NMR of the compound **18** in d_6-DMSO (400 MHz)

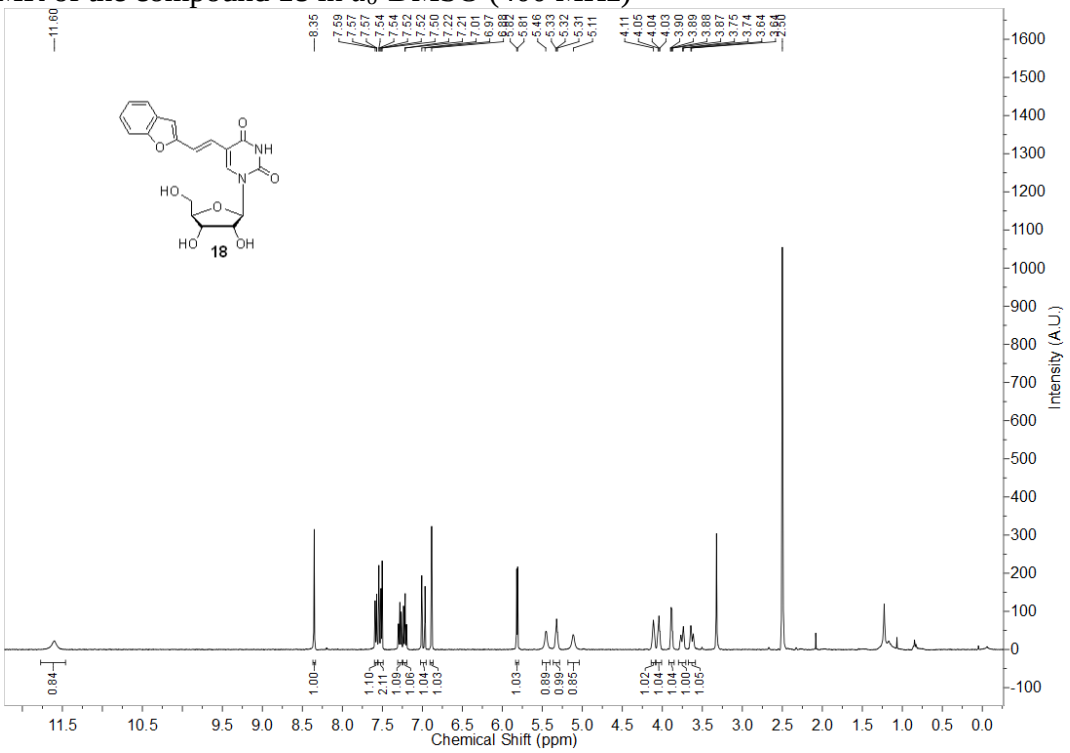

^{13}C NMR of the compound **18** in d_6-DMSO (100 MHz)

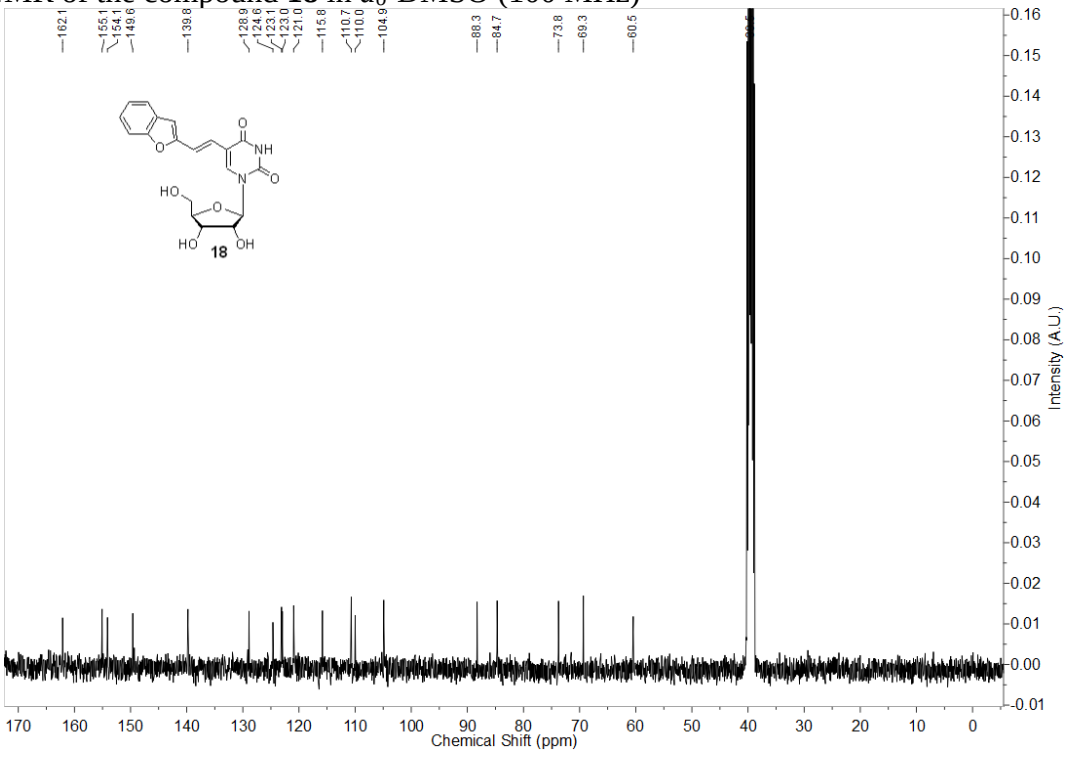

^{1}H NMR of the compound **21b** in $CDCl_3$ containing 0.03% (v/v) TMS (400 MHz)

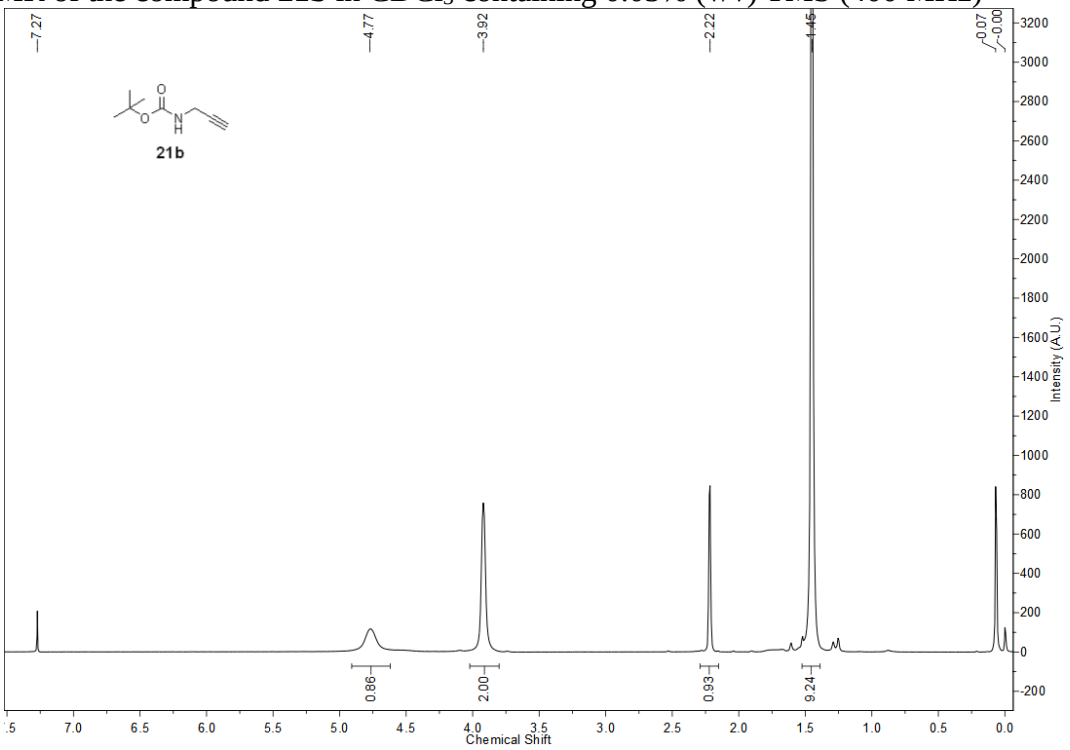

^{13}C NMR of the compound **21b** in $CDCl_3$ containing 0.03% (v/v) TMS (100 MHz)

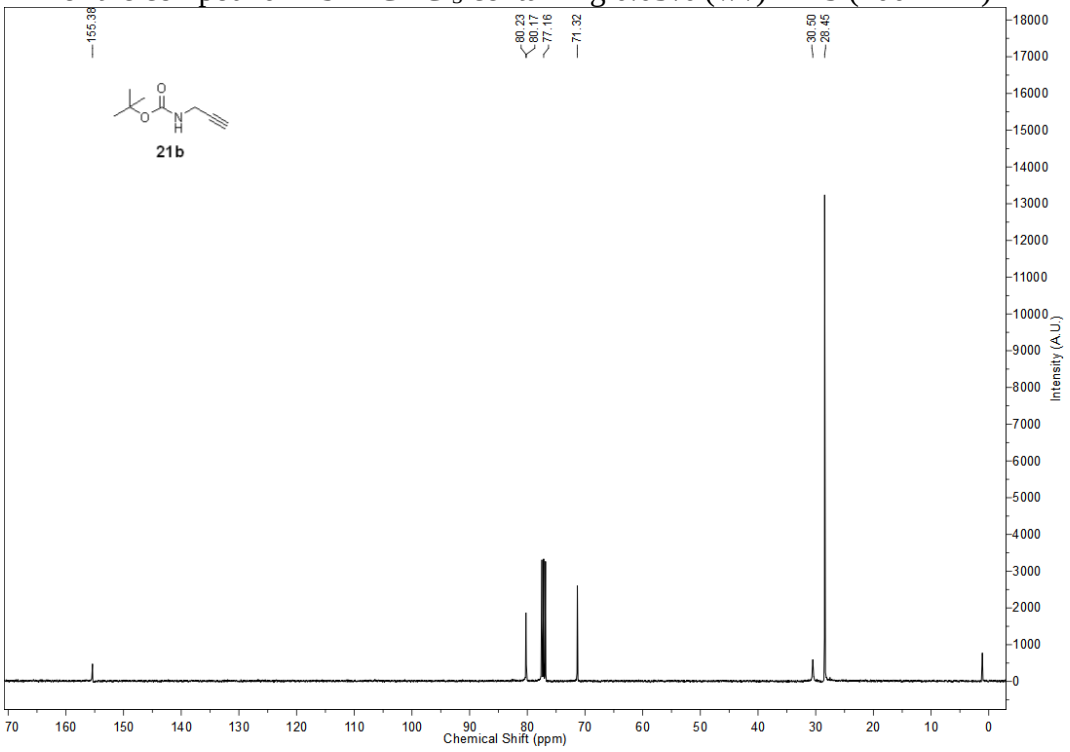

^{1}H NMR of the compound **21c** in $CDCl_3$ containing 0.03% (v/v) TMS (400 MHz)

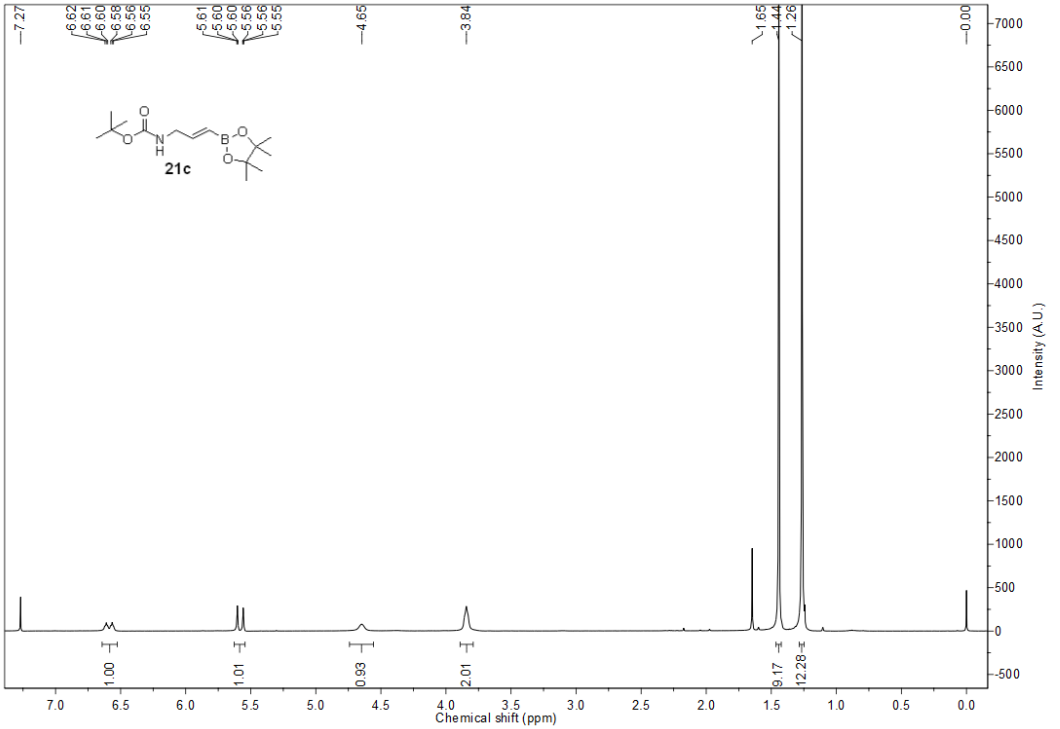

^{13}C NMR of the compound **21c** in $CDCl_3$ containing 0.03% (v/v) TMS (100 MHz)

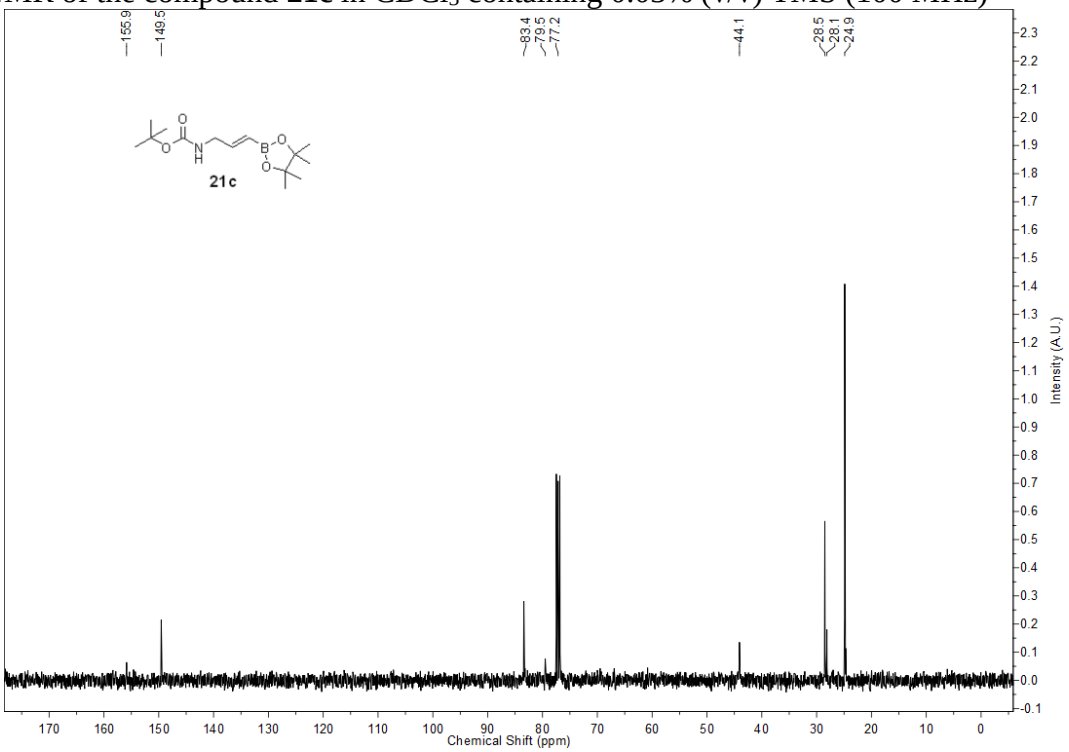

^{1}H NMR of the compound **21d** in $CDCl_3$ containing 0.03% (v/v) TMS (400 MHz)

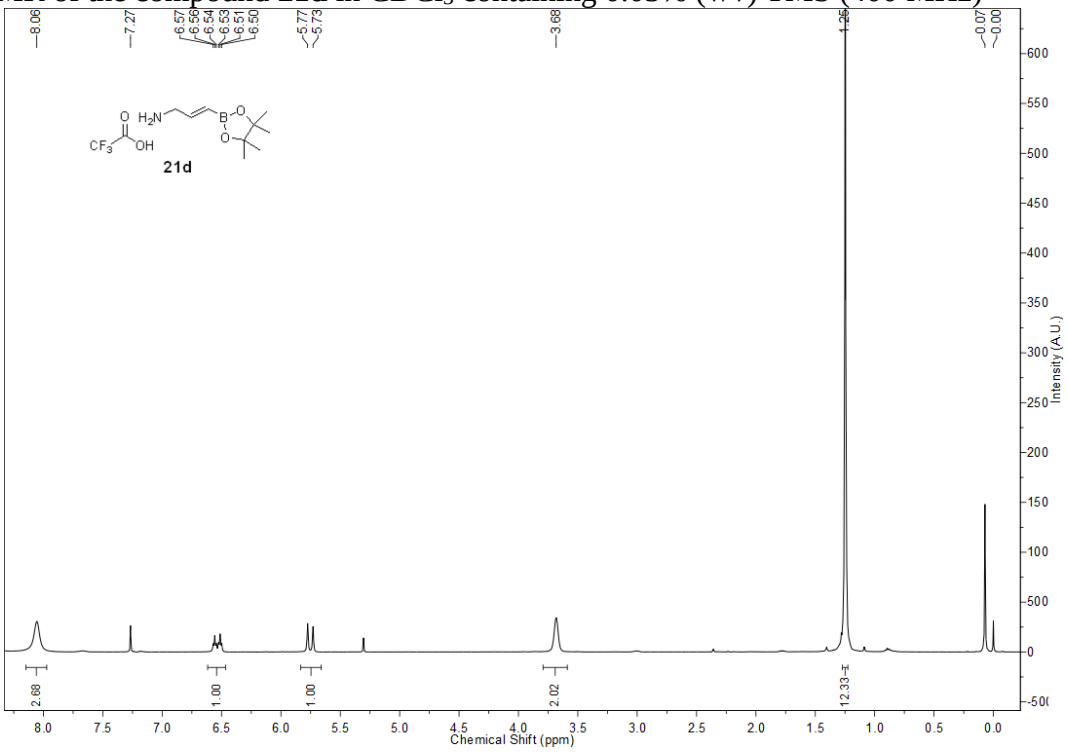

^{13}C NMR of the compound **21d** in $CDCl_3$ containing 0.03% (v/v) TMS (100 MHz)

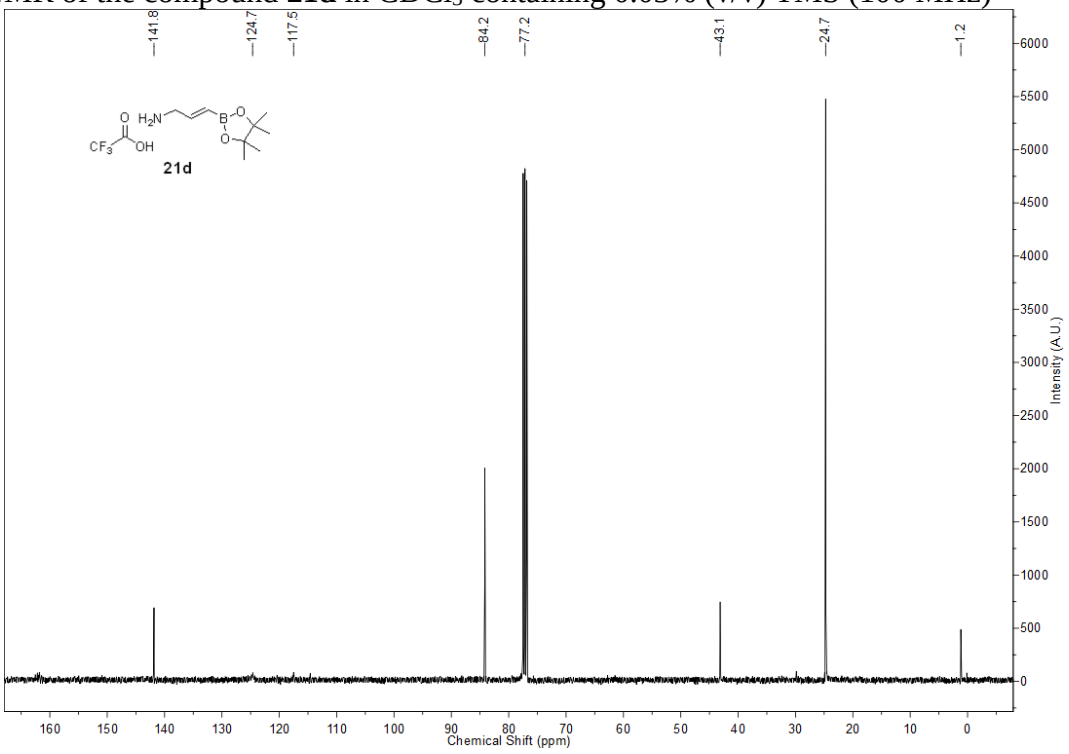

^{1}H NMR of the compound **22b** in $CDCl_3$ containing 0.03% (v/v) TMS (400 MHz)

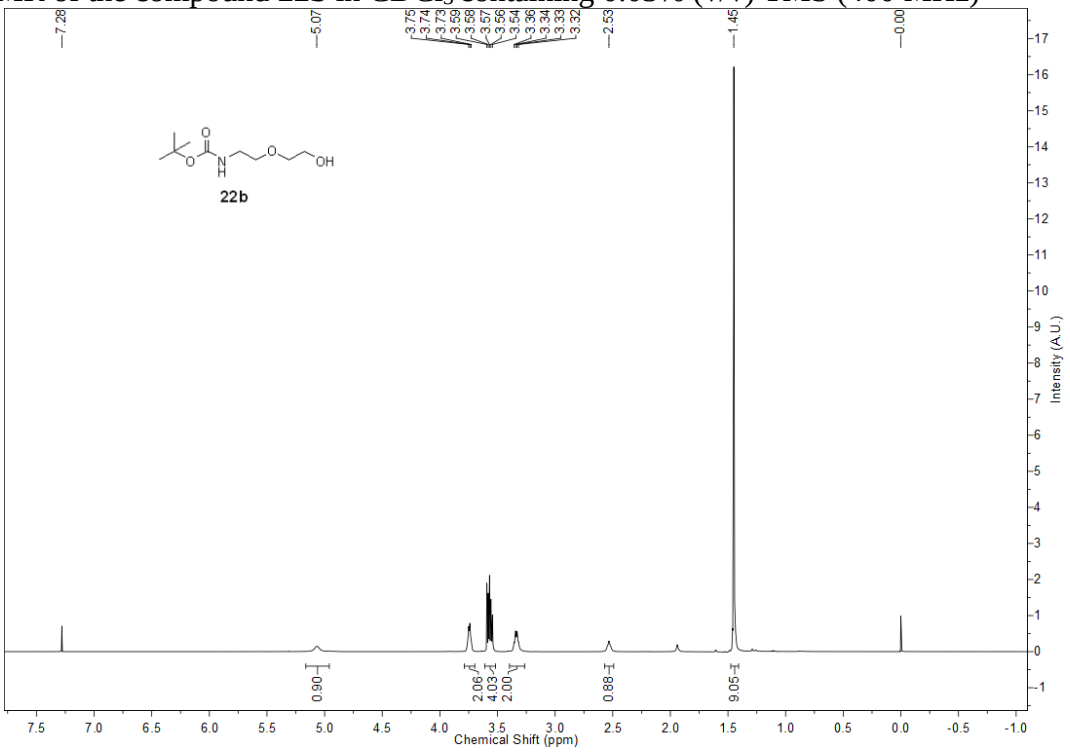

^{13}C NMR of the compound **22b** in $CDCl_3$ containing 0.03% (v/v) TMS (100 MHz)

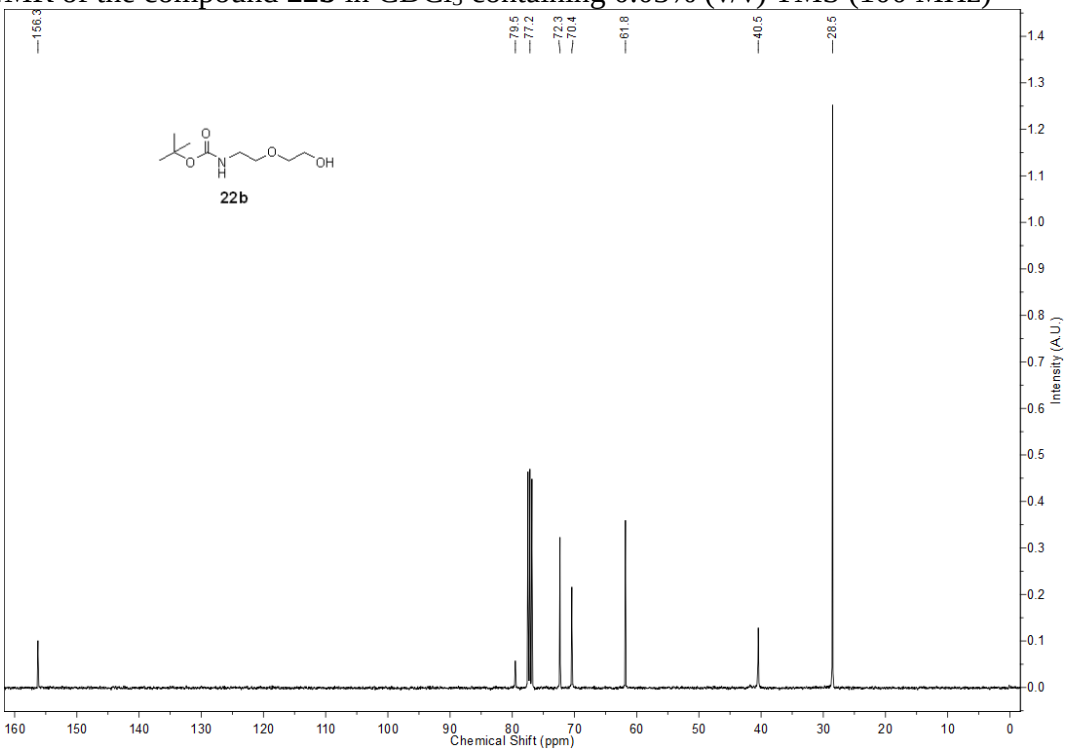

^{1}H NMR of the compound **22c** in $CDCl_3$ containing 0.03% (v/v) TMS (400 MHz)

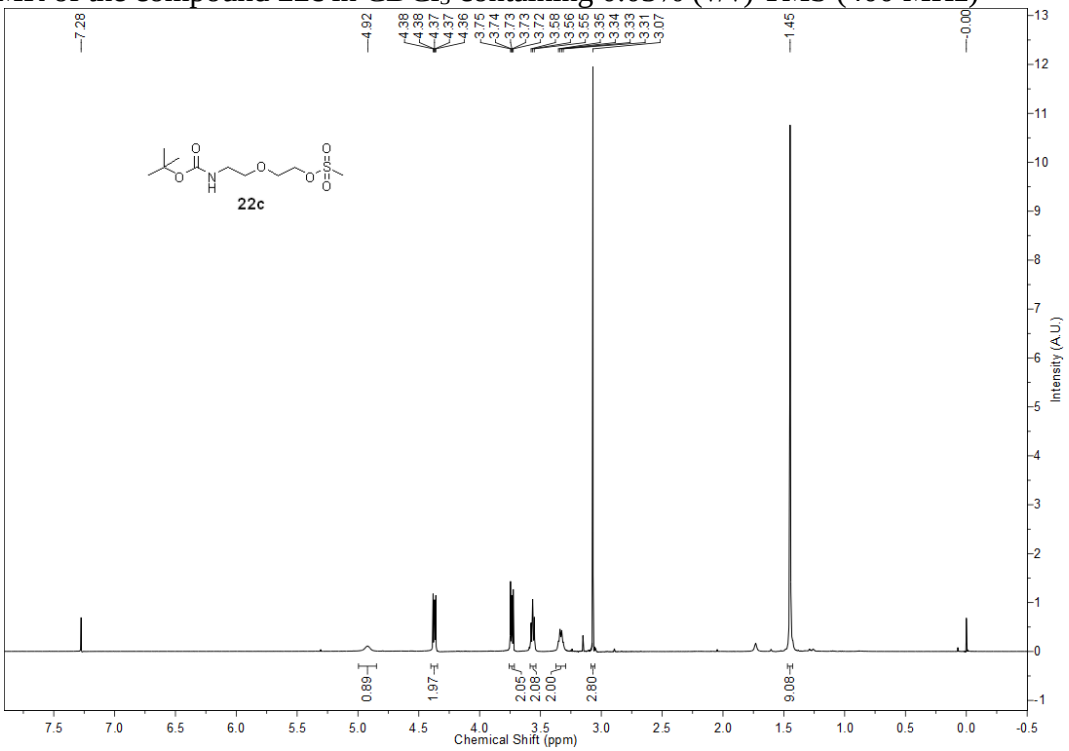

^{13}C NMR of the compound **22c** in $CDCl_3$ containing 0.03% (v/v) TMS (100 MHz)

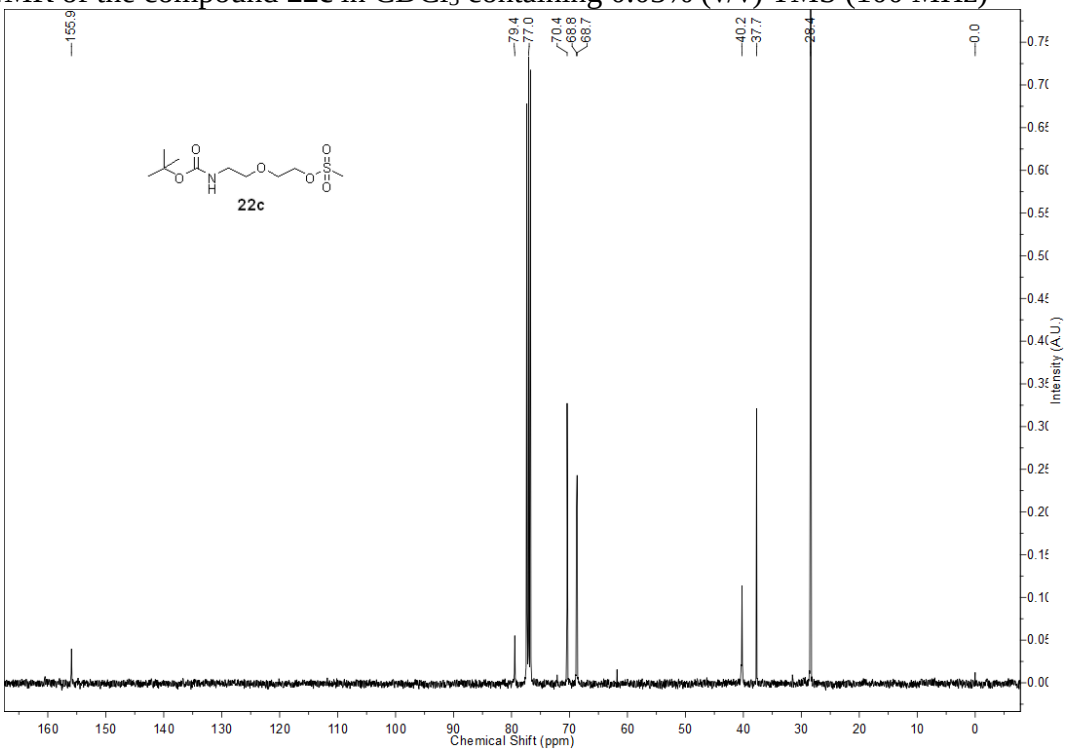

^{1}H NMR of the compound **22d** in $CDCl_3$ (400 MHz)

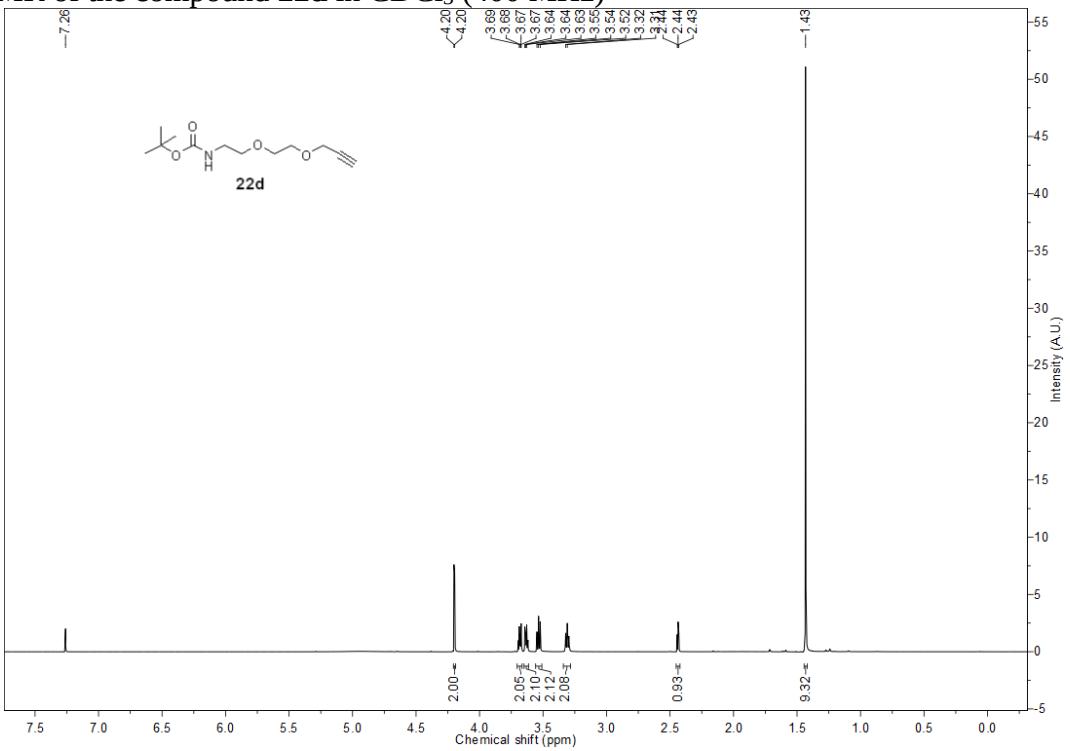

^{13}C NMR of the compound **22d** in $CDCl_3$ (100 MHz)

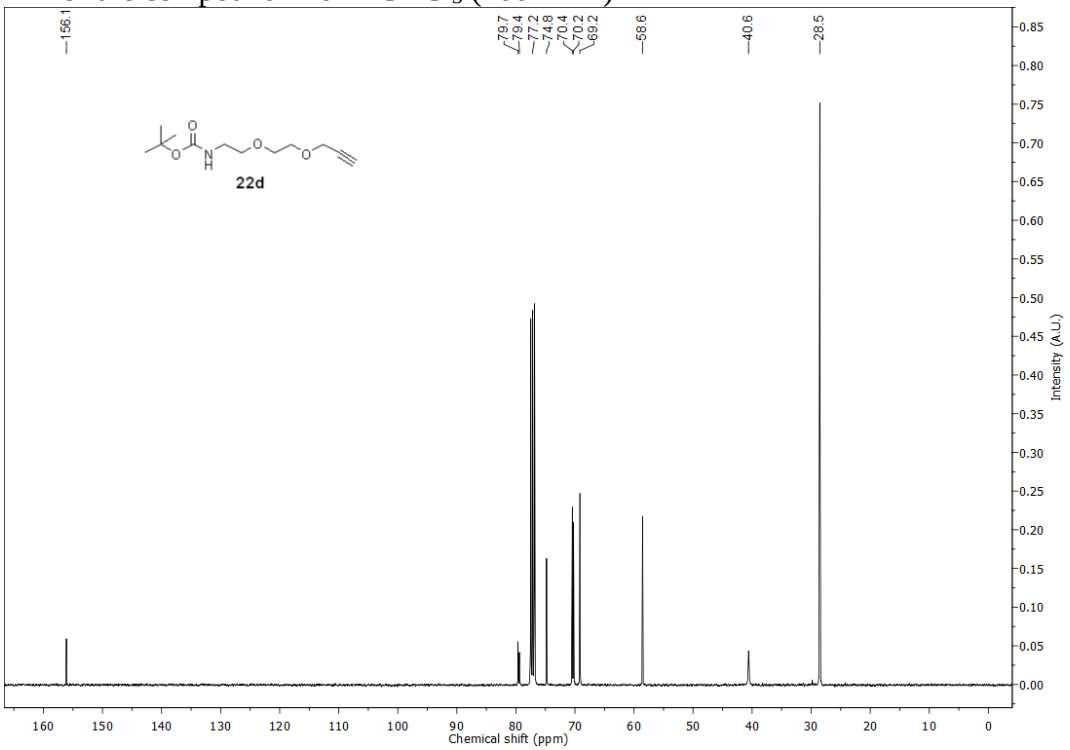

^{1}H NMR of the compound **22e** in $CDCl_3$ containing 0.03% (v/v) TMS (400 MHz)

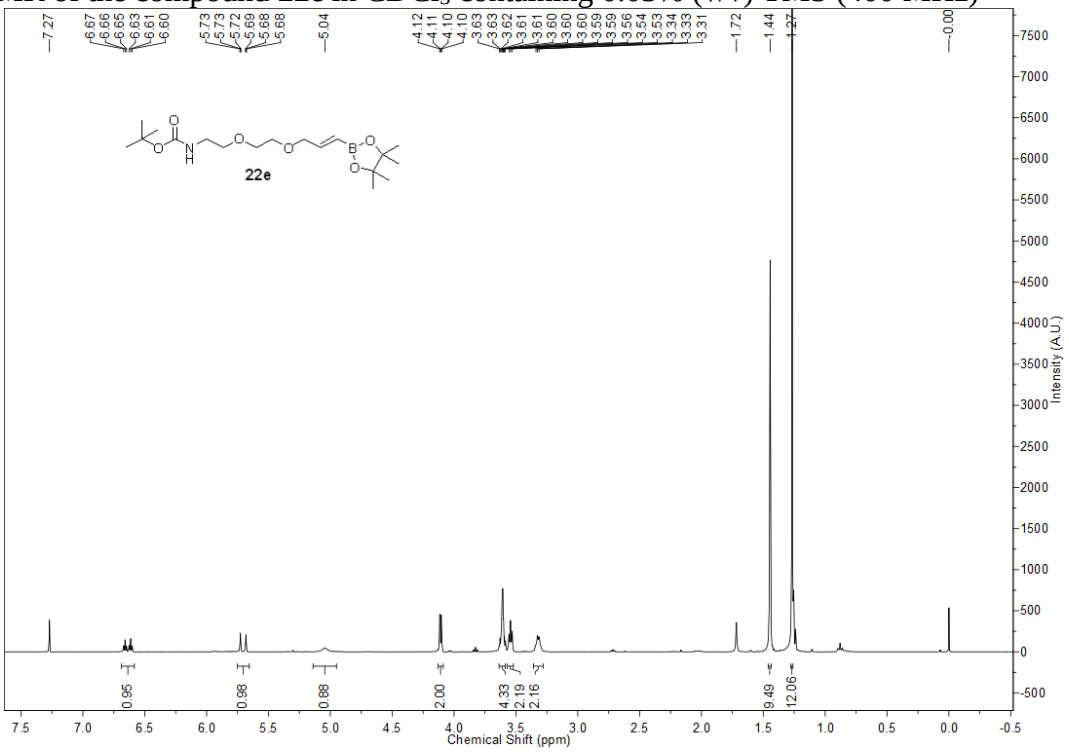

^{13}C NMR of the compound **22e** in $CDCl_3$ containing 0.03% (v/v) TMS (100 MHz)

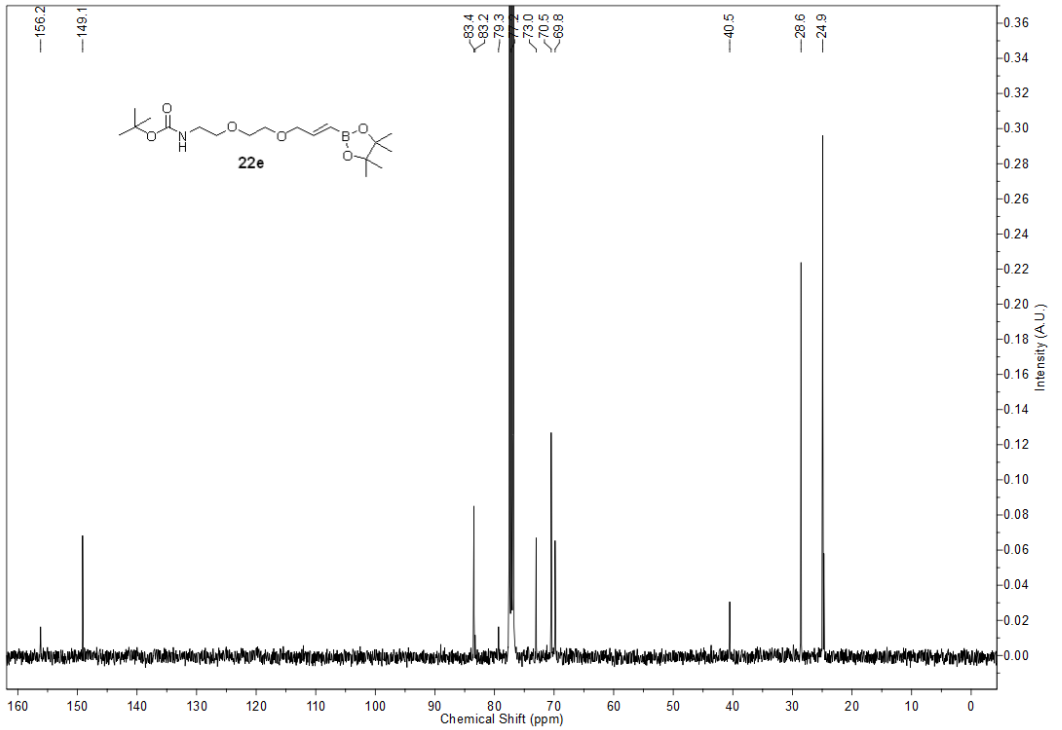

^{1}H NMR of the compound **22f** in $CDCl_3$ containing 0.03% (v/v) TMS (400 MHz)

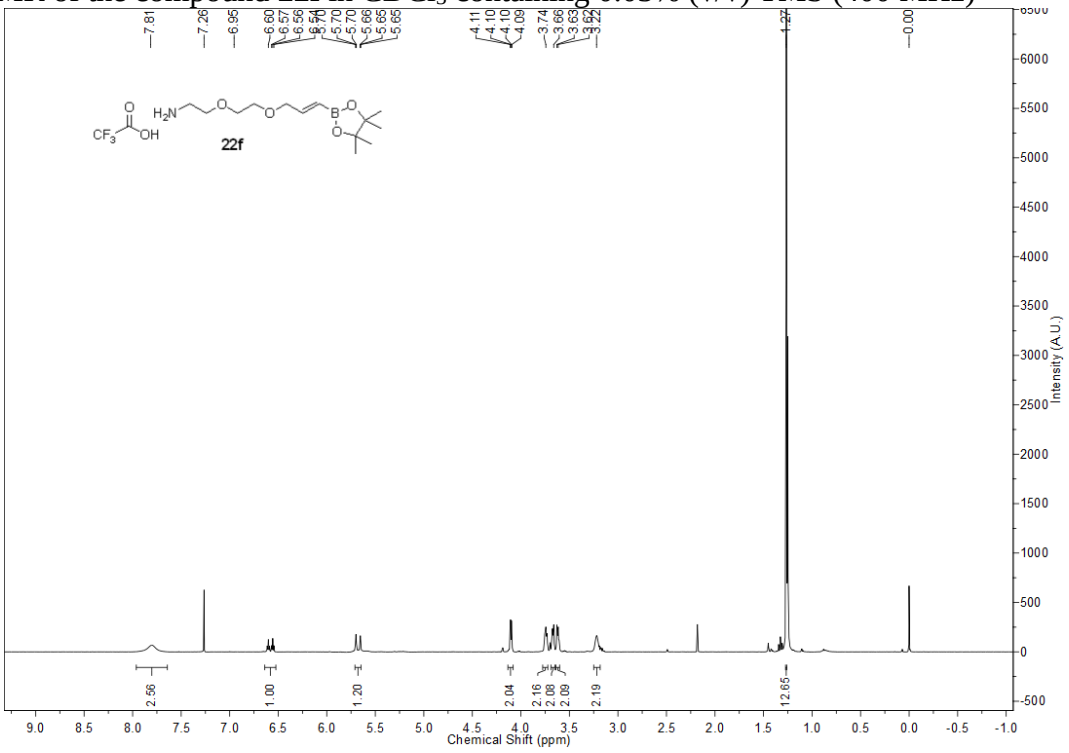

^{13}C NMR of the compound **22f** in $CDCl_3$ containing 0.03% (v/v) TMS (100 MHz)

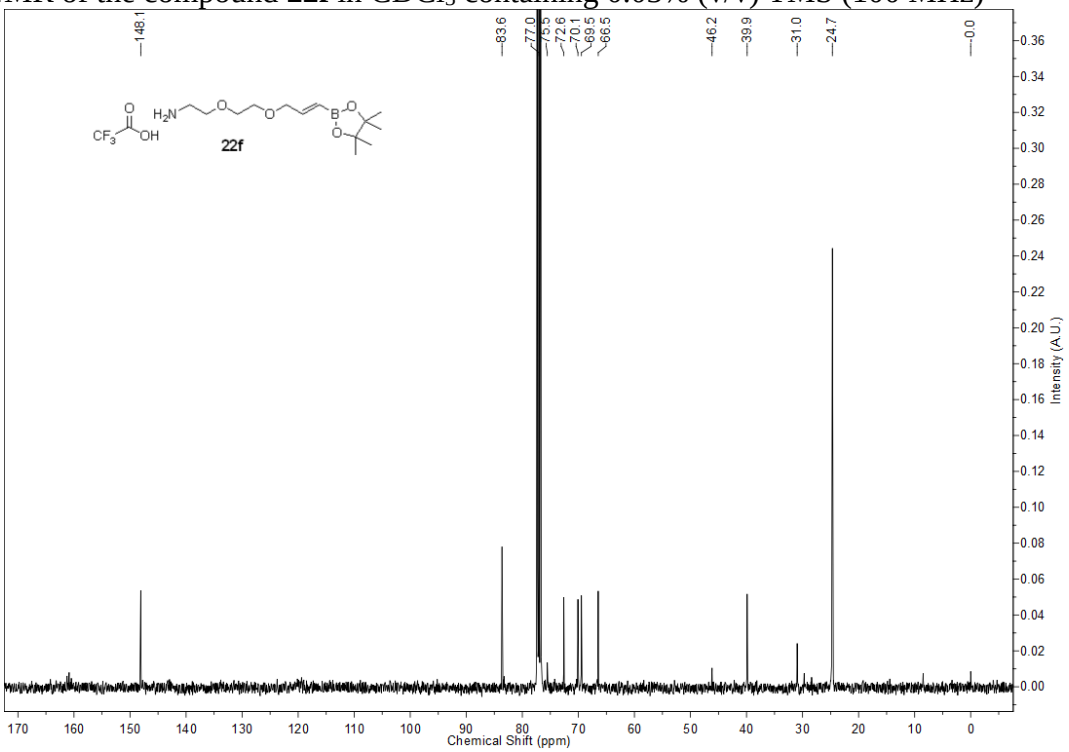

^{1}H NMR of the ligand **L2** in d_6-DMSO (400 MHz)

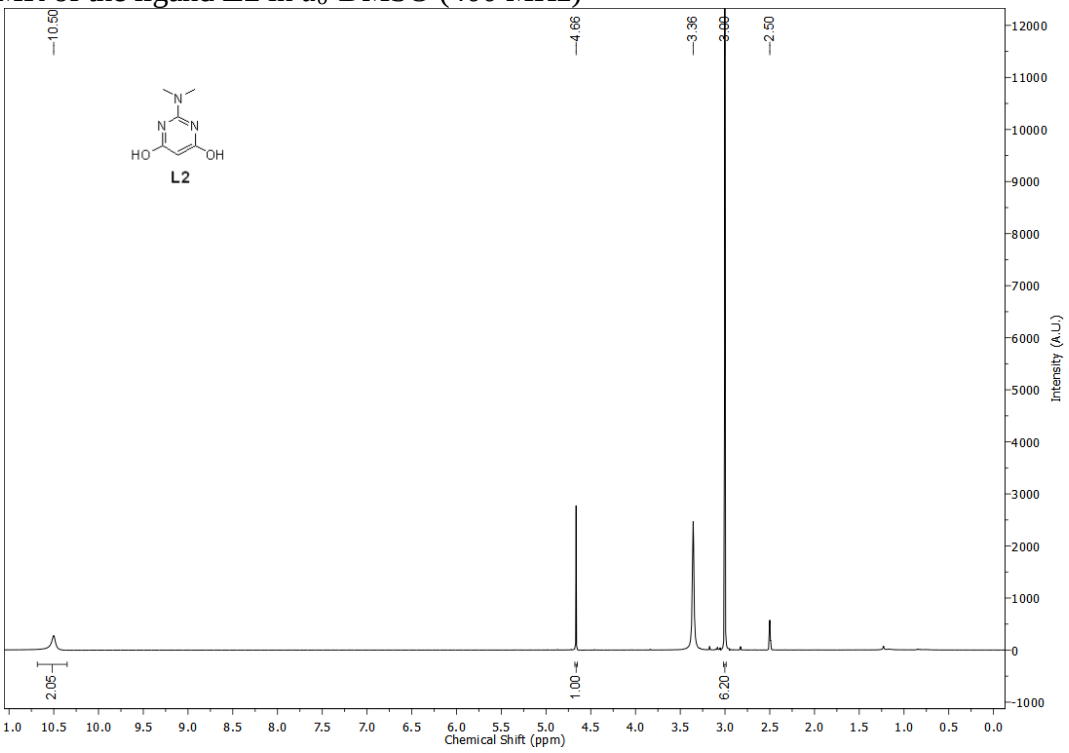

^{13}C NMR of the ligand **L2** in d_6-DMSO (100 MHz)

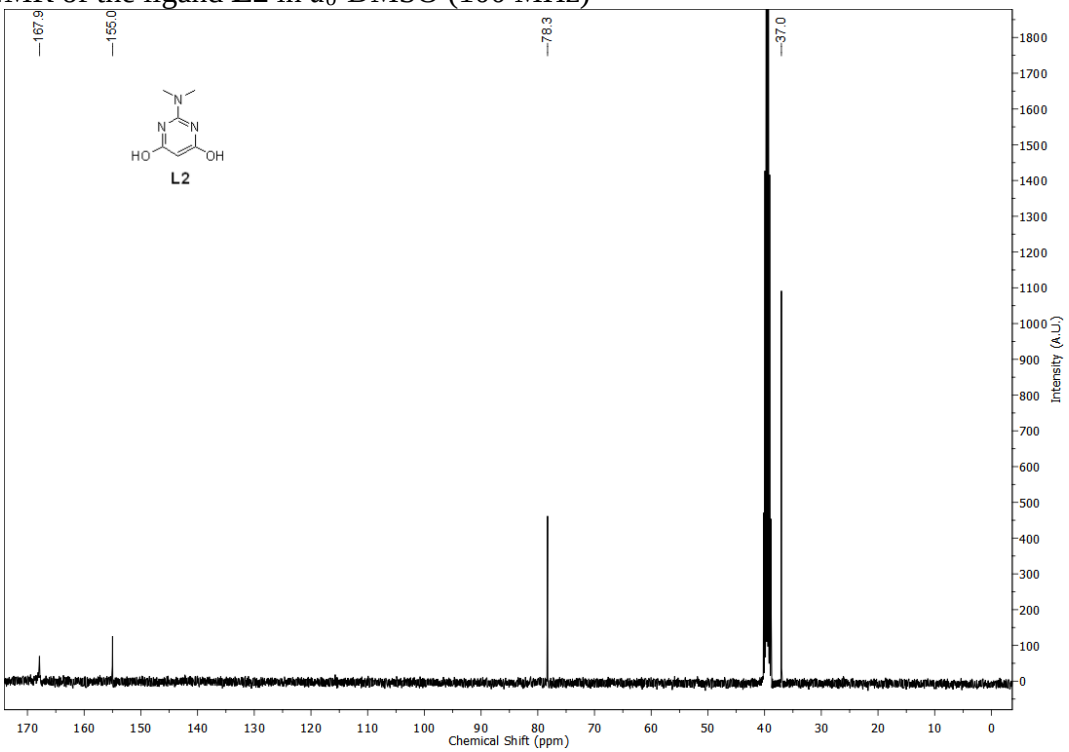

RP-HPLC[a] and corresponding MALDI-TOF[b] spectra for iodo-modified RNA transcripts **19** and **20**.

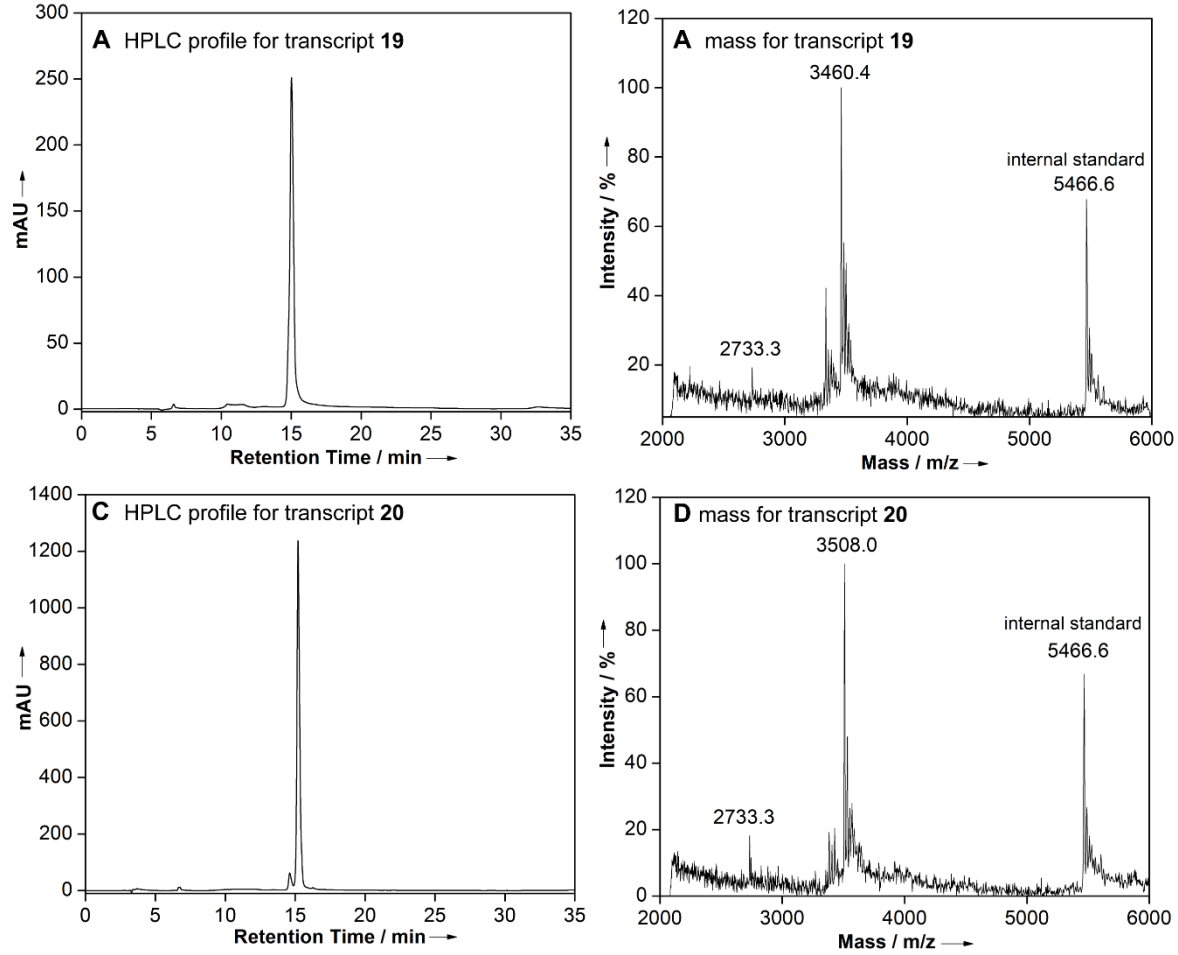

[a] (**A, C**) HPLC chromatogram of PAGE purified IU-labeled RNA transcript **19** and **20** at 260 nm. Mobile phase A = 50 mM triethylammonium acetate buffer (TEAA, pH 7.0), mobile phase B = acetonitrile. Flow rate = 1 mL/min. Gradient = 0−30% B in 35 min, 30−100% B in 10 min and 100% B for 5 min. HPLC analysis was performed using Phenomenex-Luna C18 column (250 x 4.6 mm, 5 micron).

[b] (**B, D**) MALDI-TOF mass spectrum of RNA ON **19** and **20**. Spectrum is calibrated with respect to the +1 and +2 ion of an internal 18-mer DNA ON standard (m/z for +1 and +2 ion are 5466.6 and 2733.3 respectively). Calcd. mass for IU-modified RNA transcript **19**: $[M]^+$ 3460.8; found: $[M]^+$ 3460.4. Calcd. mass for IU-modified RNA transcript **20**: $[M]^+$ 3508.3; found: $[M]^+$ 3508.0.

Chapter 3

Effect of Nucleic Acid Conformation on the Efficiency of Suzuki–Miyaura Cross-Coupling Reaction: Polymorphic G-quadruplex Structure as a Study Model

3.1 Introduction

The ability of nucleic acids to perform various biological roles originates from their ability to adopt different secondary and tertiary structures. Four-stranded DNA structures, popularly known as G-quadruplexes (GQ), are the most studied tertiary structures of nucleic acids formed by guanine-rich sequences. The GQs have drawn significant attention owing to their structural diversity and their crucial roles in many cellular processes. For example, human telomeric (H-Telo) G-rich DNA overhang protects the cell from recombination and degradation.[1,2] The overhang of human telomere is composed of a $(T_2AG_3)n$ repeat, which adopts multiple conformations *in vitro*, which depends on the ionic conditions (Figure 3.1).[3,4] In the presence of K^+ ions, telomeric repeat mainly forms hybrid 1 and hybrid 2 topologies in which the double chain reversal loop is found at the 5′- and 3′-end, respectively.[5,6] On the other hand, the same sequence when crystallized in the presence of K^+ ions and polyethylene glycol (PEG)forms a parallel GQ structure.[7, 8]

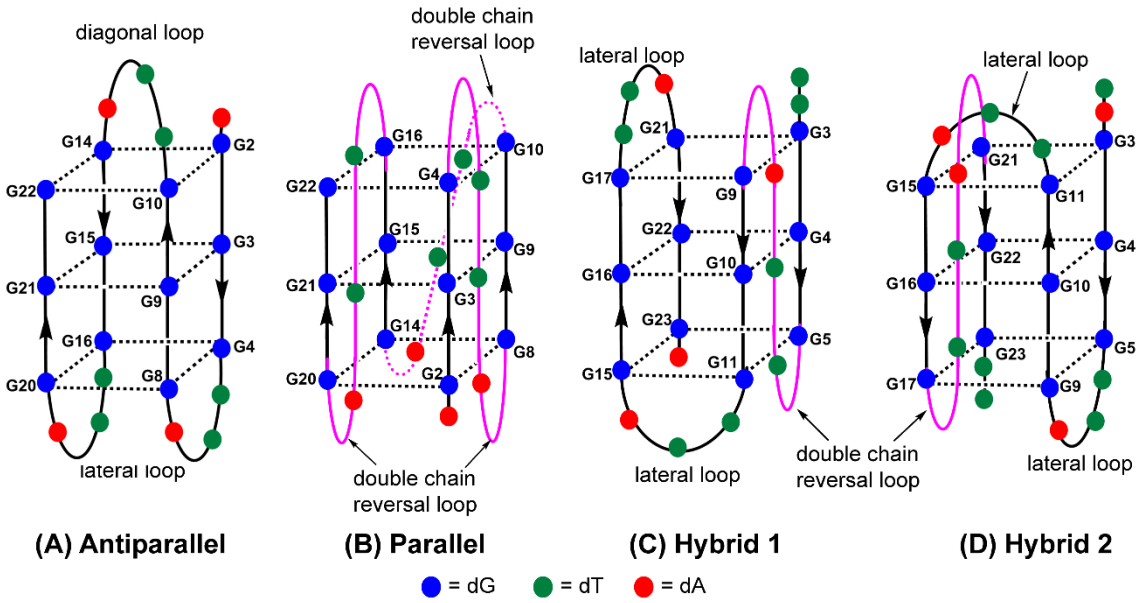

Figure 3.1. GQ topologies formed by telomeric repeat in different ionic conditions. (**A**) Antiparallel GQ conformation of 5′-d[AG_3-$(T_2AG_3)_3$]-3′ in Na^+ solution.[3](**B**) Parallel GQ conformation of 5′-d[AG_3-$(T_2AG_3)_3$]-3′in crystalline conditions or in the presence of PEG 200 containing K^+

solution.[7,8](**C**) Hybrid 1 GQ conformation of 5′-d[T_2G_3-(T_2AG_3)$_3$A]-3′ in K^+ solution.[5] (**D**) Hybrid 2 GQ conformation of 5′-d[TAG_3-(T_2AG_3)$_3T_2$]-3′in K^+ solution.[6]Double chain reversal loops of parallel, hybrid 1 and hybrid 2GQ are shown in the pink color.

Considering the biological importance of G-rich sequences and their ability to fold into different conformations, their identification, isolation, and characterization in the human genome is of great interest. There are several reports, where photochemical approaches have been used to probe different GQs using halo-modified nucleoside.[9–12] In this approach, upon UV light irradiation (280-320 nm), 5-halouracil containing H-Telo G rich sequences gives a highly reactive 5′ uracil radical. This formed radical, further induces conformation-dependent and atom specific hydrogen abstraction of nearby sugar residue leading to 2′-deoxyribonolactone derivatives as well as forms the intra-stand crosslink with nearby purine residue. However, the use of UV light leads to the formation of a major amount of dehalogenated side product. Also, UV light destroys the GQ structure during irradiation which leads to the loss of structural information for further study. Template-assisted click chemistry has also been used as a useful strategy to identify hybrid RNA-DNA G-quadruplexes[13-15], though this strategy has not been well explored for individual GQs and other nucleic acid structures. Recently, Luedke and co-workers utilized the reactivity of a vinyl-modified nucleoside analog and phenyltriazolinedione to study GQ conformations. The vinyl-modified nucleoside was incorporated into GQ forming human telomeric sequences and interestingly, phenyltriazolinedione was found to reasonably reactive with vinyl group of GQ in conformation-selective manner as compared to dsDNA.[16] Although this new bioconjugation strategy is catalyst free, direct attachment of probes to obtain spectrum read-out of the GQ conformation is not straight-forward. Inspired by this strategy, we wanted to explore the influence of nucleic acid conformational space on the efficiency of postsynthetic Suzuki–Miyaura cross-coupling reaction. This endeavour would also enable the direct incorporation of fluorogenic and environment-sensitive nucleoside probe based on the reactivity of different GQ conformations.

In this chapter, we describe the role of GQ conformations on the reactivity of iodo-modified H-Telo DNA sequences towards Suzuki–Miyaura cross-coupling reaction. 5-Iodo-2′-deoxyuridine phosphoramidite was synthesized and incorporated into DNA ONs, which upon annealing in different ionic conditions and in the presence of a synthetic molecular crowding agent (PEG) form different GQ structures (Figure 3.2). Depending on the type of conformation and position of the iodo group within the loop region, the efficiency of Suzuki

reaction varied. Apart from labeling H-Telo DNA GQs with probes, the Suzuki coupling reaction did not work on the corresponding duplex form, suggesting a conformational dependence of the reaction.

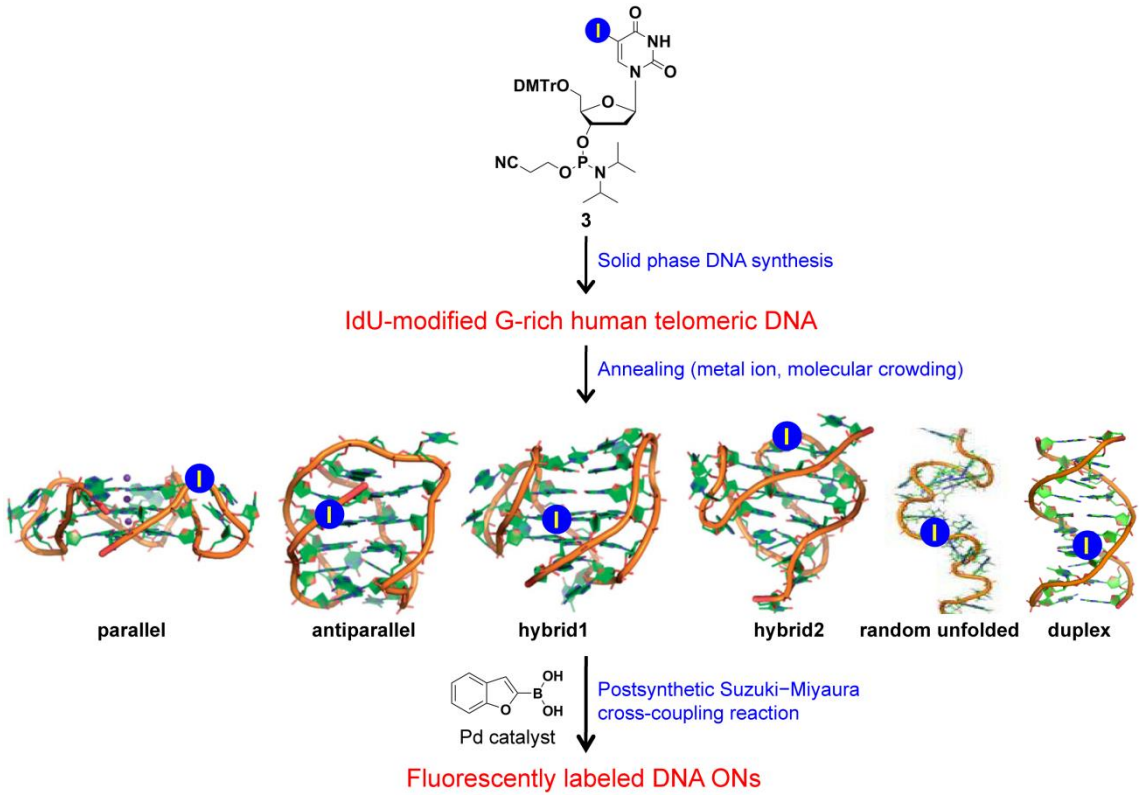

Figure 3.2. Design principle for studying the effect of postsynthetic Suzuki–Miyaura cross-coupling reaction on the various DNA GQ conformations. Here, we have taken polymorphic GQ structures of H-Telo DNA ON repeat as a study model.

3.2 Results and Discussion

3.2.1 Synthesis and incorporation of phosphoramidite 3 into H-Telo DNA ONs: 5-Iodo-2′-deoxyuridine phosphoramidite **3** was synthesized in simples steps as shown in Scheme 1 using analogous reported procedure.[17] 5-Iodo-2′-deoxyuridine**1**was protected with DMTr group to obtain 5′-*O*-DMT-protected 5-iodo-2′-deoxyuridine **2**, was then further reacted with 2-cyanoethyl-*N*,*N*-diisopropylchlorophosphoramidite to give phosphoramidite substrate **3** in good yields. The identity of the product was confirmed by ^{31}P NMR and mass analysis.

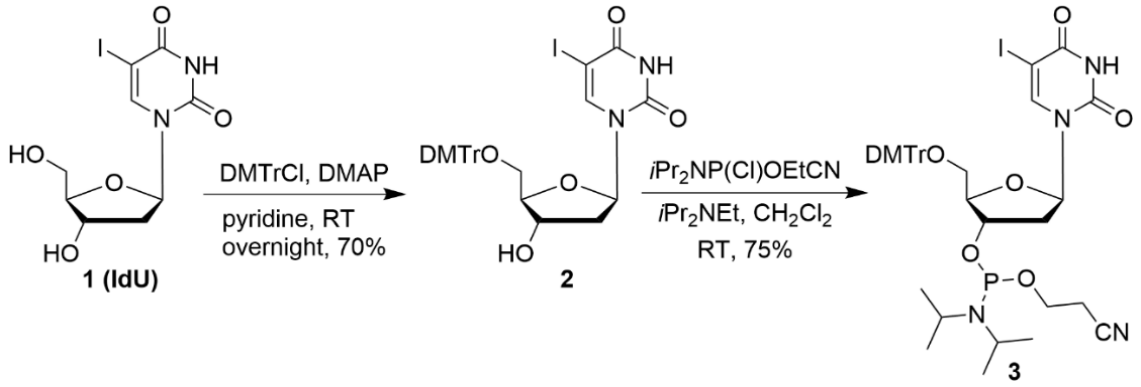

Scheme 3.1. Synthesis of 5-Iodo-2′-deoxyuridine phosphoramidite **3** for the solid-phase synthesis of DNA ONs. DMTr = 4,4'-dimethoxytrityl, DMAP = dimethyl aminopyridine.

The following sequences derived from human telomeric DNA repeat were studied: 5′-d[AG_3-(T_2AG_3)$_3$]-3′ (H-Telo-22), 5′-d[T_2G_3-(T_2AG_3)$_3$A]-3′ (H-Telo-24) and 5′-d[TAG_3-(T_2AG_3)$_3T_2$]-3′ (H-Telo-25), as models for the study (Figure 3.3). H-Telo-22 forms antiparallel GQ in the presence of Na^+ ions, hybrid-type mixed parallel-antiparallel GQs in the presence of K^+ ions and random unfolded form in Li^+ ions. While H-Telo-24 and H-Telo-25 ONs form hybrid type1 and type2 GQs, respectively, in K^+ ionic conditions, in presence of Na^+ H-Telo-24 adopts an antiparallel form and H-Telo-25 does not support the formation of an antiparallel GQ structures. Further, in different GQ structures of H-Telo repeat, there is a reasonable difference in conformation of the loop nucleotides. Hence, to evaluate the effect of nucleic acid conformation on the efficiency of Suzuki reaction, we decided to replace the first and second dT bases in all the three loops of H-Telo DNA with 5-iodo-2′-deoxyuridine (Figure 3.3).The IdU-modified ONs **4**–**17** were prepared by solid-phase DNA ON synthesis protocol and deprotected at room temperature for 48 hand purified by gel electrophoresis. Deprotection at room temperature was necessary for minimizing the deiodination of IdU-modified H-Telo DNA ONs. Purity of the products was ascertained by RP-HPLC and identity was confirmed mass measurements (see 3.6 Appendix-II for HPLC profile, mass spectra, and Table 3.1; see the experimental section for details).

IdU (1) modified H-Telo G-rich DNA ONs 4–17

(**4**) 5' TTGGG**1**TAGGGTTAGGGTTAGGGA 3'
(**5**) 5' TTGGGTTAGGG**1**TAGGGTTAGGGA 3'
(**6**) 5' TTGGGTTAGGGTTAGGG**1**TAGGGA 3'
(**7**) 5' TAGGG**1**TAGGGTTAGGGTTAGGGTT 3'
(**8**) 5' TAGGGTTAGGG**1**TAGGGTTAGGGTT 3'
(**9**) 5' TAGGGTTAGGGTTAGGG**1**TAGGGTT 3'
(**10**) 5' TTGGGT**1**AGGGTTAGGGTTAGGGA 3'
(**11**) 5' TTGGGTTAGGGT**1**AGGGTTAGGGA 3'
(**12**) 5' TTGGGTTAGGGTTAGGGT**1**AGGGA 3'
(**13**) 5' TAGGGT**1**AGGGTTAGGGTTAGGGTT 3'
(**14**) 5' TAGGGTTAGGGT**1**AGGGTTAGGGTT 3'
(**15**) 5' TAGGGTTAGGGTTAGGGT**1**AGGGTT 3'
(**16**) 5' AGGGTTAGGG**1**TAGGGTTAGGG 3'
(**17**) 5' AGGGTTAGGGTTAGGGT**1**AGGG 3'

Control H-Telo G-rich DNA ONs 18–20

H-Telo-24 (**18**) 5' TTGGGTTAGGGTTAGGGTTAGGGA 3'
H-Telo-25 (**19**) 5' TAGGGTTAGGGTTAGGGTTAGGGTT 3'
H-Telo-22 (**20**) 5' AGGGTTAGGGTTAGGGTTAGGG 3'

C-rich H-Telo-22 (21)

5' CCCTAACCCTAACCCTAACCCT 3'

Figure 3.3. IdU-modified H-Telo DNA ONs **4**–**17**: The dT residue in the first (**4**, **7**, **10**, **13**), second (**5**, **8**, **11**, **14**, **16**), and third (**6**, **9**, **12**, **15**, **17**) loops of H-Telo DNA ONs was replaced with iodo-modified nucleoside **1**. ONs **18**–**20**are control, unmodified H-Telo G-rich DNA. ON **21** is C-rich DNA sequence complementary to DNA ONs **4**–**20**.

Table 3.1. ε_{260} and MALDI-TOF/ESI-MS mass data of IdU-modified DNA ONs (**4**–**17**).

IdU-modified DNA	ε_{260} ($M^{-1}cm^{-1}$)[a]	Calculated mass	Observed mass
4	238960	7685.8	7685.8[c]
5	238960	7685.8	7686.0[c]
6	238960	7685.8	7686.6[c]
7	247760	7990.0	7991.0[b]
8	247760	7990.0	7991.7[b]
9	247760	7990.0	7990.7[c]
10	238960	7685.8	7686.6[c]
11	238960	7685.8	7685.4[b]
12	238960	7685.8	7686.0[b]
13	247760	7990.0	7990.7[c]
14	247760	7990.0	7990.5[b]
15	247760	7990.0	7988.7[b]
16	223160	7077.4	7078.4[c]
17	223160	7077.4	7076.8[b]

[a] ε_{260} of modified ONs was determined by using OligoAnalyzer 3.1. The extinction coefficient of nucleoside **1** (ε_{260} = 3360 $M^{-1}cm^{-1}$) was used in place of thymidine (ε_{260} = 8700 $M^{-1}cm^{-1}$).
[b] Mass analysis was done using MALDI-TOF spectroscopy.
[c] Mass analysis was done using ESI-MS.

3.2.2 IdU incorporation and Suzuki–Miyaura coupling reaction conditions did not affect the GQ structure and stability

In the previous chapter, posttranscriptional Suzuki–Miyaura coupling reaction to label short RNA ONs with various biophysical labels under mild conditions was described.[18] The reactions were carried out in Tris-HCl buffer (50 mM, pH = 8.5) containing 20% DMSO. Before performing cross-coupling reaction on different GQ DNA conformations, we studied the effect of iodo modification and coupling reaction conditions on the formation and stability of GQ structures by CD and thermal-melting experiments. As a representative example, IdU-modified (**12**, **15** and **17**) and control unmodified (**18**–**20**) H-Telo DNA ONs were annealed in Tris-HCl buffer (50 mM, pH = 8.5) containing 100 mM KCl or 100 mM NaCl. The CD spectra of both the control and modified H-Telo ONs in K^+ solution were found to be similar and showed a intense positive peak at ~290 nm with a shoulder at ~270 nm and small negative peak at ~235 nm, which is characteristic of hybrid type mixed parallel–antiparallel stranded GQ structures (Figure 3.4). In the presence of Na^+ solution, the control (**18**, **20**) and modified (**12**, **17**) H-Telo ONs displayed a positive peak at ~293nm and a strong negative peak at ~260 nm shows the formation of an antiparallel GQ structure. While, in Na^+ solution 25-nt ONs **15** and **19**, does not support the formation of an antiparallel GQ structure giving a very weak signals in the CD spectrum (Figure 3.4B). UV-thermal melting analysis of the control and modified H-Telo ONs in different ionic conditions (NaCl and KCl) gave a very similar T_m values. Consistent with the previously reported literature,[3–5] CD and Tm data prove that the replacement of thymidine residues in the loops with 5-iodo-2′-deoxyuridine **1** and Suzuki reaction conditions does not perturb the folding of GQ structure.

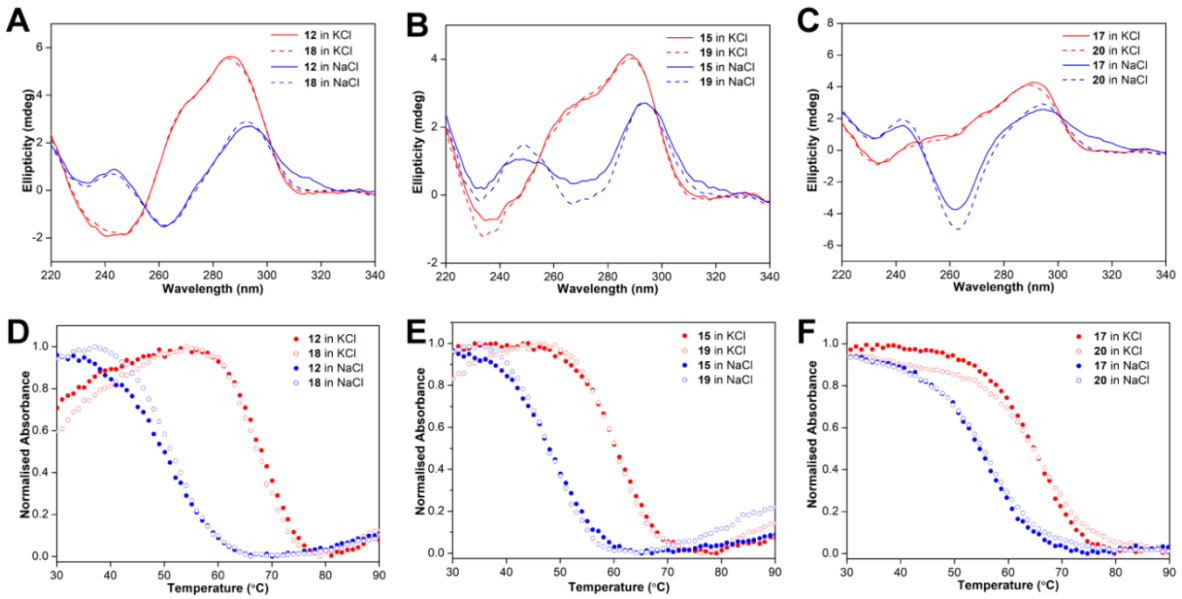

Figure 3.4. (**A**, **B**, **C**)CD spectra of IdU-modified H-Telo ONs**12**, **15** and **17** and control unmodified ONs**18**−**20** in 50 mM Tris-HCl buffer (pH 8.5) containing 100 mM KCl or 100 mM NaCl. (**D**, **E**, **F**) Representative UV-thermal melting profiles of IdU-modified ONs **12**, **15** and **17** and control unmodified ONs **18**−**20** in 50 mM Tris-HCl buffer (pH = 8.5) containing 100 mM KCl or 100 mM NaCl at 295 nm.

Table 3.2. T_m values of iodo-modified and control unmodified GQs in the presence of KCl and NaCl.

IdU-modified GQ	T_m (°C)	Control unmodified GQ	T_m (°C)
12 in KCl	70.5 ± 0.5	**18** in KCl	69.2 ± 0.0
12 in NaCl	51.3 ± 0.6	**18** in NaCl	50.0 ± 1.0
15 in KCl	59.3 ± 0.5	**19** in KCl	61.8 ± 0.7
15 in NaCl	47.7 ± 0.9	**19** in NaCl	48.7 ± 1.3
17 in KCl	66.8 ± 0.7	**20** in KCl	65.3 ± 0.6
17 in NaCl	56.6 ± 0.8	**20** in NaCl	56.2 ± 0.8

3.2.3 Conformation-dependent cross-coupled product formation in H-Telo G-rich DNA sequences

H-Telo DNA ONs were annealed in Tris-HCl buffer containing LiCl/NaCl/KCl and reacted with benzofuran boronic acid (**a**) in the presence of $Pd(OAc)_2L_2$ (Scheme 2). Reaction mixtures were analysed by RP-HPLC and the fraction corresponding to the labeled ON products was isolated (Figure 3.5–3.10, Table 3.3). The identity of the cross-coupled products were confirmed by MALDI-TOF or ESI-MS analysis (see 3.6 Appendix-II for mass data and

Table 4; see the experimental section for details). We have chosen benzofuran boronic acid as a cross-coupling partner because the resultant ONs products will be fluorescent.[19]

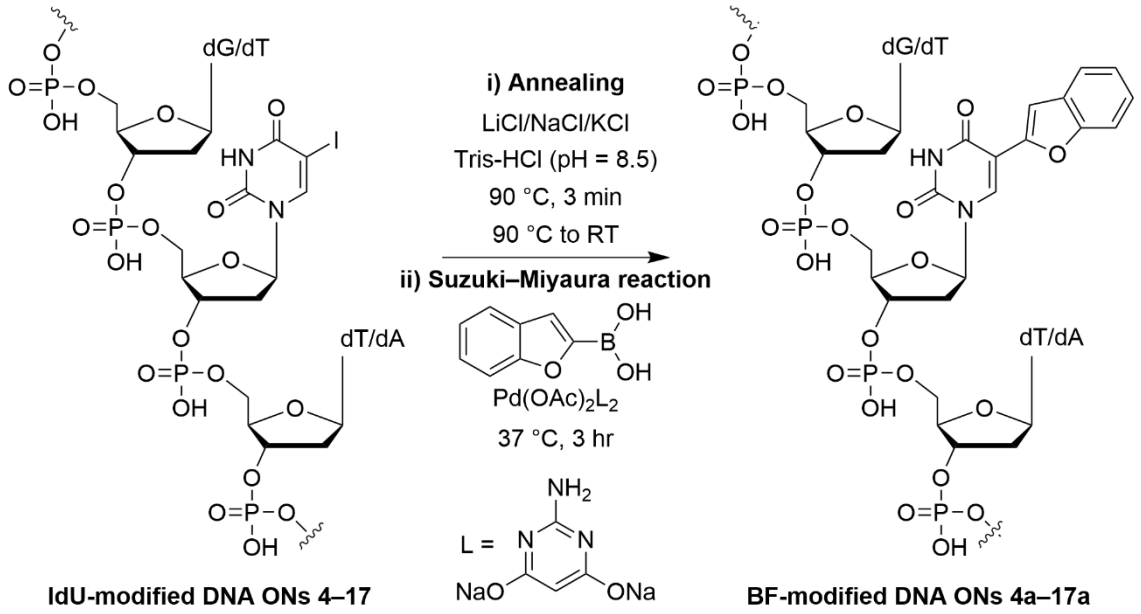

Scheme 3.2. General scheme for the postsynthetic Suzuki–Miyaura coupling reaction on IdU-modified DNA ONs (**4**–**17**).

All the ONs used in this study form a random unfolded structure in the presence of LiCl[20] and respective GQ structures in the presence of NaCl and KCl (Figure 3.4). Rewardingly, when the reactions were performed with G-quadruplex structures the yields of the coupled ON products were considerably higher than when the reactions were performed with the unfolded structures formed by the same sequences (Figure 3.5–3.10, Table 3.3).In case of GQ structure where the modification was replaced at the first thymidine residue of the first, second, or third loop (ONs **4**–**9**) though did not show any conformational selectivity for the cross-coupling reaction, the yields were reasonably good (Figure 3.5–3.7, Table 3.3). For example, in NaCl, the antiparallel GQ topology shows almost similar yield when placed in first (**4**), second (**5**) or third loop (**6**) (Figure 3.5A). Similar results were observed in the case of hybrid 1 (ONs **4**, **5**, **6**) and hybrid 2 (ONs **7**, **8**, **9**) structures in the presence of KCl (Figure 3.5A and 3.5B).

On the other hand, when the modification was placed at the second thymidine residue of the first, second or third loop **(**24-mer ONs **10**–**12**), the reaction efficiency was found to vary with the position of modification. ONs **10**–**12** in Li^+ ionic condition (random unfolded structure) showed low and similar coupling efficiency with the boronic acid substrate (Figure

3.5C). Interestingly, an antiparallel GQ topology formed by ON **12** in which IdU is present in the third loop gave 2 to 3-fold higher yields of the product than ONs **10** and **11** in which the modification is present in the first and second loop, respectively (Figure 3.5C and Table 3.3). For the same set of sequences (ONs **10**–**12**) in the presence of K^+ ions, the yields for the cross-coupled product was very similar irrespective of the position of modification. However, reactions with 25-mer ON sequences **13**–**15** the trend was reversed. In Li^+ and Na^+ ionic conditions, the ONs gave similar amounts of the coupled ON products irrespective of position of modification (Figure 3.5D, Table 3.3). However, the same ONs in the presence of K^+ ions showed difference in coupling efficiency. There was a progressive increase in the product yield as the iodo position was moved from first (**13**) to second (**14**) and to the third loop (**15**).

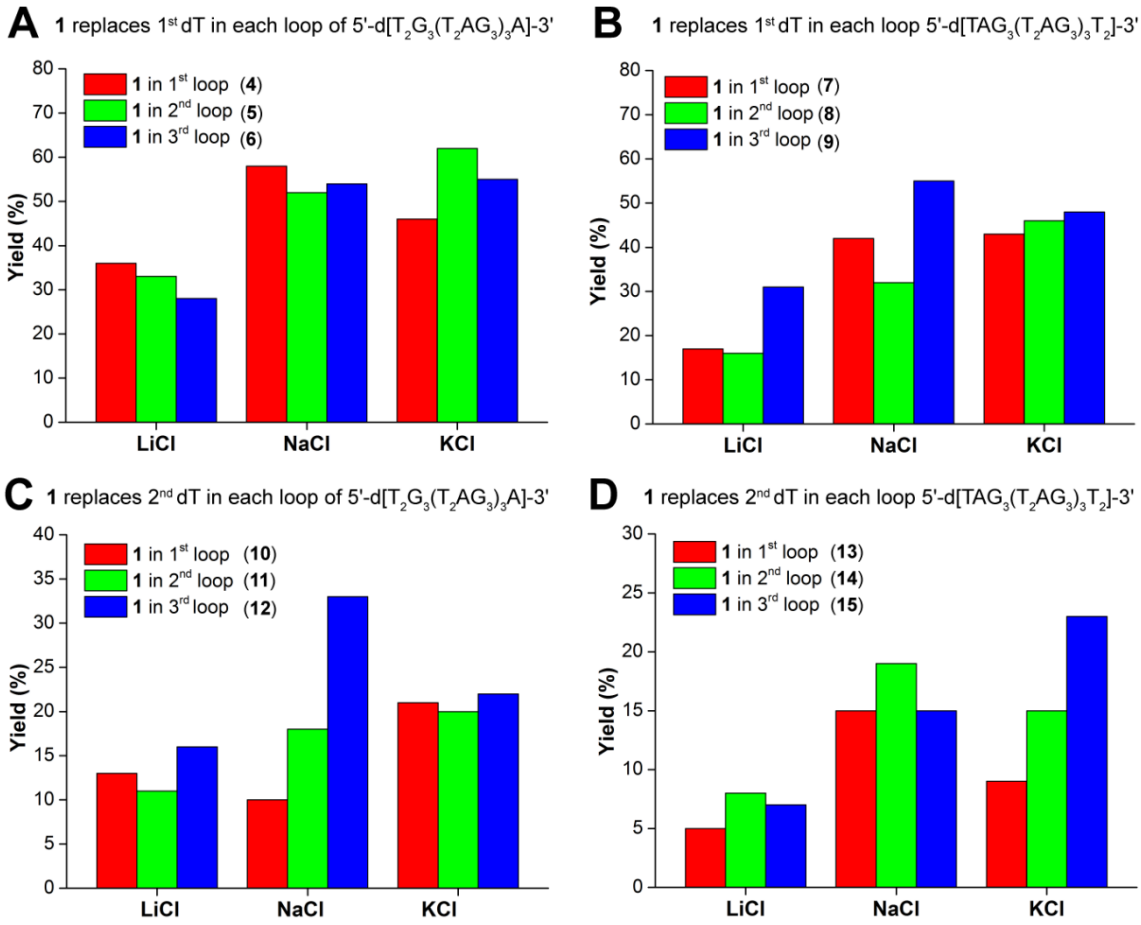

Figure 3.5. Bar diagram for isolated yields of cross-coupled products (**4a**–**15a**) when IdU in first, second and third loop in the presence of LiCl, NaCl and KCl. (**A**) **4**, **5** and **6**. (**B**) **7**, **8** and **9**. (**C**) **10**, **11** and **12**. (**D**) **13**, **14** and **15**.

Figure 3.5C shows the preferential formation of cross-coupled product in the lateral (third) loop of GQ formed by 5′-d[$T_2G_3(T_2AG_3)_3A$]-3′ (H-Telo-24) DNA sequences in Na^+ solution;

Figure 3.5D shows the preferential formation of cross-coupled product in the double chain reversal (third) loop of GQ formed by 5′-d[$TAG3(T_2AG_3)_3T_2$]-3′ (H-Telo-25) DNA sequences in K^+ solution.

Table 3.3. Yields of cross-coupled products (**4a**–**15a**) obtained by Suzuki–Miyaura cross-coupling reaction in different loops of iodo-modified G-quadruplexes sequences in respective ionic conditions (Li^+, Na^+ and K^+).[a]

IdU-modified H-telo DNA ONs	Structure formed by ONs	Isolated yields of cross-coupled product in %		
		First loop	Second loop	Third loop
H-Telo-24 in Li^+ (1^{st} T)[b]	Unfolded	36 (**4a**)	33 (**5a**)	28 (**6a**)
H-Telo-24 in Na^+ (1^{st}T)[b]	Antiparallel	58 (**4a**)	52 (**5a**)	54 (**6a**)
H-Telo-24 in K^+ (1^{st} T)[b]	Hybrid type 1	46 (**4a**)	62 (**5a**)	55 (**6a**)
H-Telo-25 in Li^+ (1^{st} T)[b]	Unfolded	17 (**7a**)	16 (**8a**)	31 (**9a**)
H-Telo-25 in Na^+ (1^{st} T)[b]	Unfolded	42 (**7a**)	32 (**8a**)	55 (**9a**)
H-Telo-25 in K^+ (1^{st} T)[b]	Hybrid type 2	43 (**7a**)	46 (**8a**)	48 (**9a**)
H-Telo-24 in Li^+ (2^{nd} T)[c]	Unfolded	13 (**10a**)	11 (**11a**)	16 (**12a**)
H-Telo-24 in Na^+ (2^{nd} T)[c]	Antiparallel	10 (**10a**)	18 (**11a**)	33 (**12a**)
H-Telo-24 in K^+ (2^{nd} T)[c]	Hybrid type 1	21 (**10a**)	20 (**11a**)	22 (**12a**)
H-Telo-25 in Li^+ (2^{nd} T)[c]	Unfolded	5 (**13a**)	8 (**14a**)	7 (**15a**)
H-Telo-25 in Na^+ (2^{nd} T)[c]	Unfolded	15 (**13a**)	19 (**14a**)	15 (**15a**)
H-Telo-25 in K^+ (2^{nd} T)[c]	Hybrid type 2	9 (**13a**)	15 (**14a**)	23 (**15a**)

[a] All reactions were performed on a 2.5 nmole scale of IdU-modified DNA sequences(**4**–**15**).
[b] Represents **1** replaces first dT residue of loop in GQ sequences (**4**–**9**).
[c] Represents **1** replaces second dT residue of loop in GQ sequences (**10**–**15**).

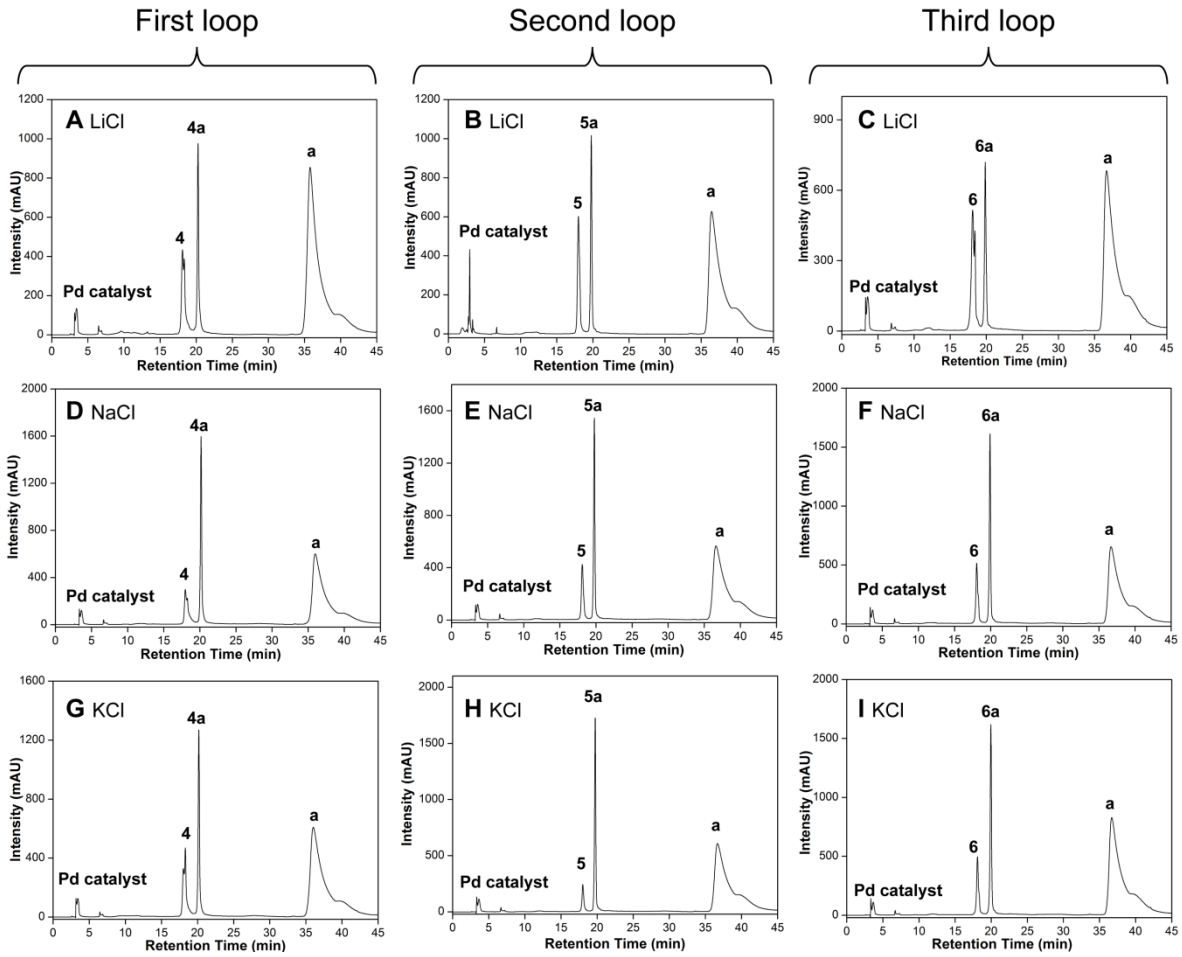

Figure 3.6. RP-HPLC chromatogram of reaction mixture of postsynthetic Suzuki–Miyaura cross-coupling reaction on IdU-modified H-Telo-24 (**1** replaces 1st thymidine in the loop) DNA ON in presence of LiCl (**A**) **4** (first loop), (**B**) **5** (second loop), (**C**) **6** (third loop); in the presence of NaCl (**D**) **4** (first loop), (**E**) **5** (second loop), (**F**) **6** (third loop); in the presence of KCl (**G**) **4** (first loop), (**H**) **5** (second loop), (**I**) **6** (third loop).

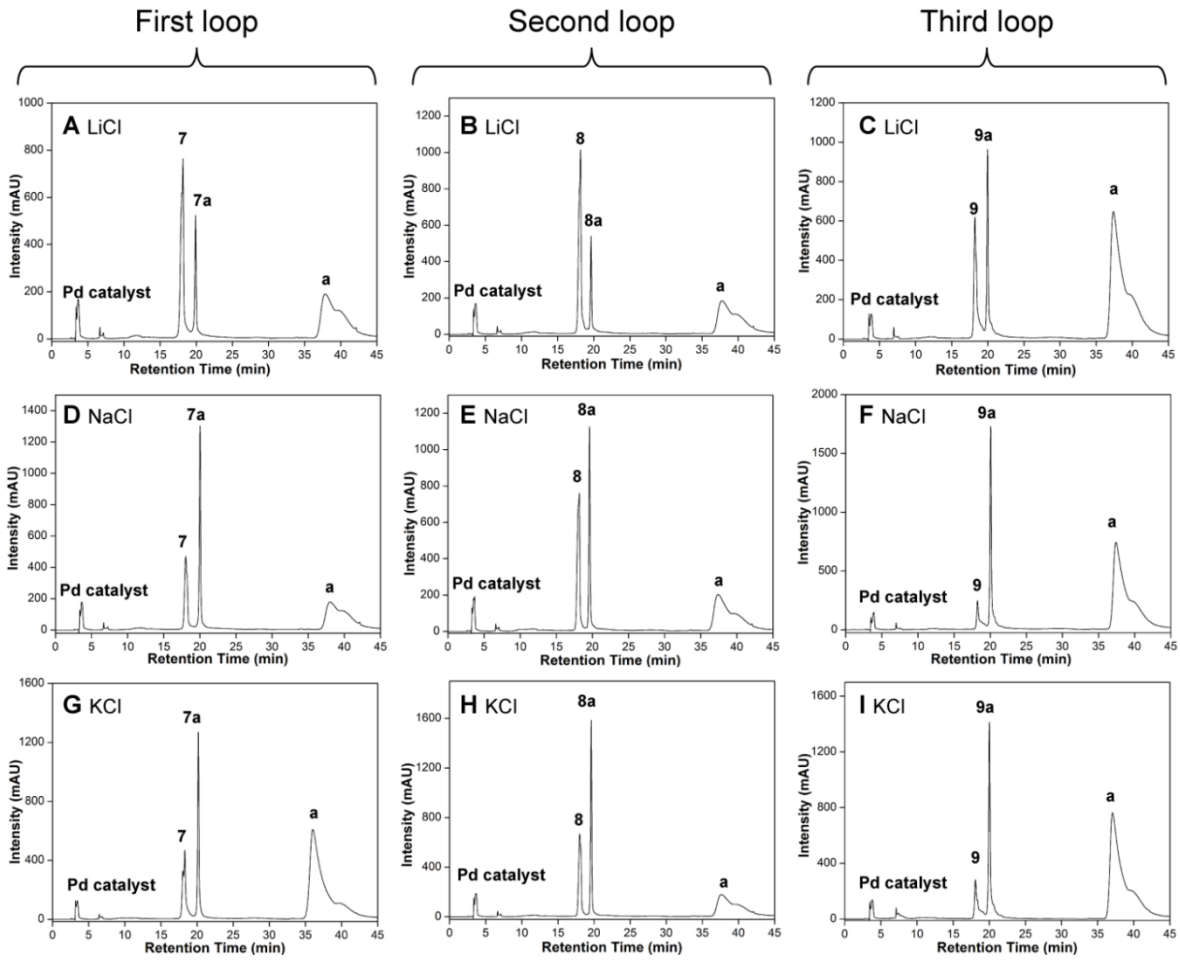

Figure 3.7. RP-HPLC chromatogram of reaction mixture of postsynthetic Suzuki–Miyaura cross-coupling reaction on IdU-modified H-Telo-25 (**1** replaces 1st thymidine in the loop) DNA ON in presence of LiCl (**A**) **7** (first loop), (**B**) **8** (second loop), (**C**) **9** (third loop); in the presence of NaCl (**D**) **7** (first loop), (**E**) **8** (second loop), (**F**) **9** (third loop); in the presence of KCl (**G**) **7** (first loop), (**H**) **8** (second loop), (**I**) **9** (third loop).

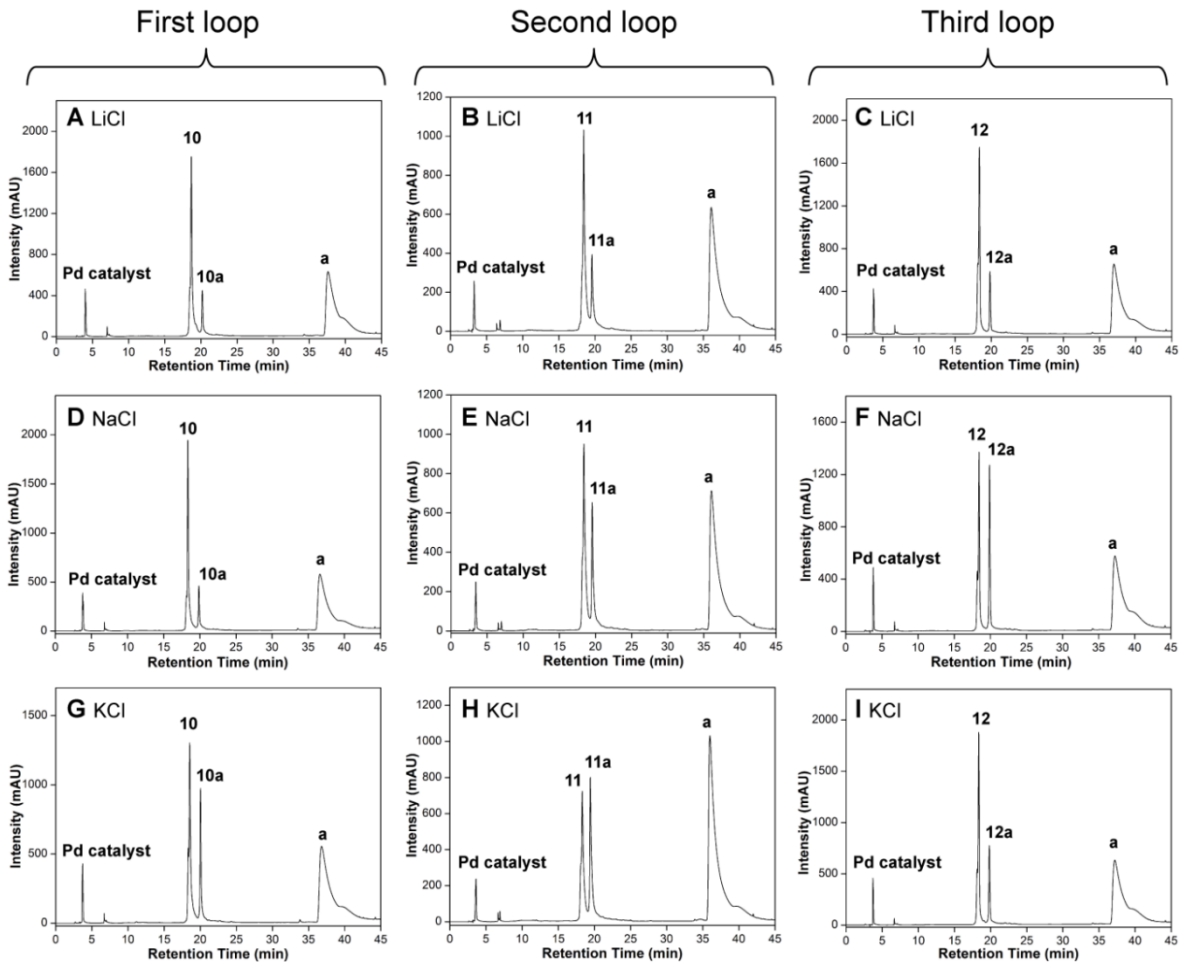

Figure 3.8. RP-HPLC chromatogram of reaction mixture of postsynthetic Suzuki–Miyaura cross-coupling reaction on IdU-modified H-Telo-24 (**1** replaces 2nd thymidine in the loop) DNA ON in presence of LiCl (**A**) **10** (first loop), (**B**) **11** (second loop), (**C**) **12** (third loop); in the presence of NaCl (**D**) **10** (first loop), (**E**) **11** (second loop), (**F**) **12** (third loop); in the presence of KCl (**G**) **10** (first loop), (**H**) **11** (second loop), (**I**) **12** (third loop).

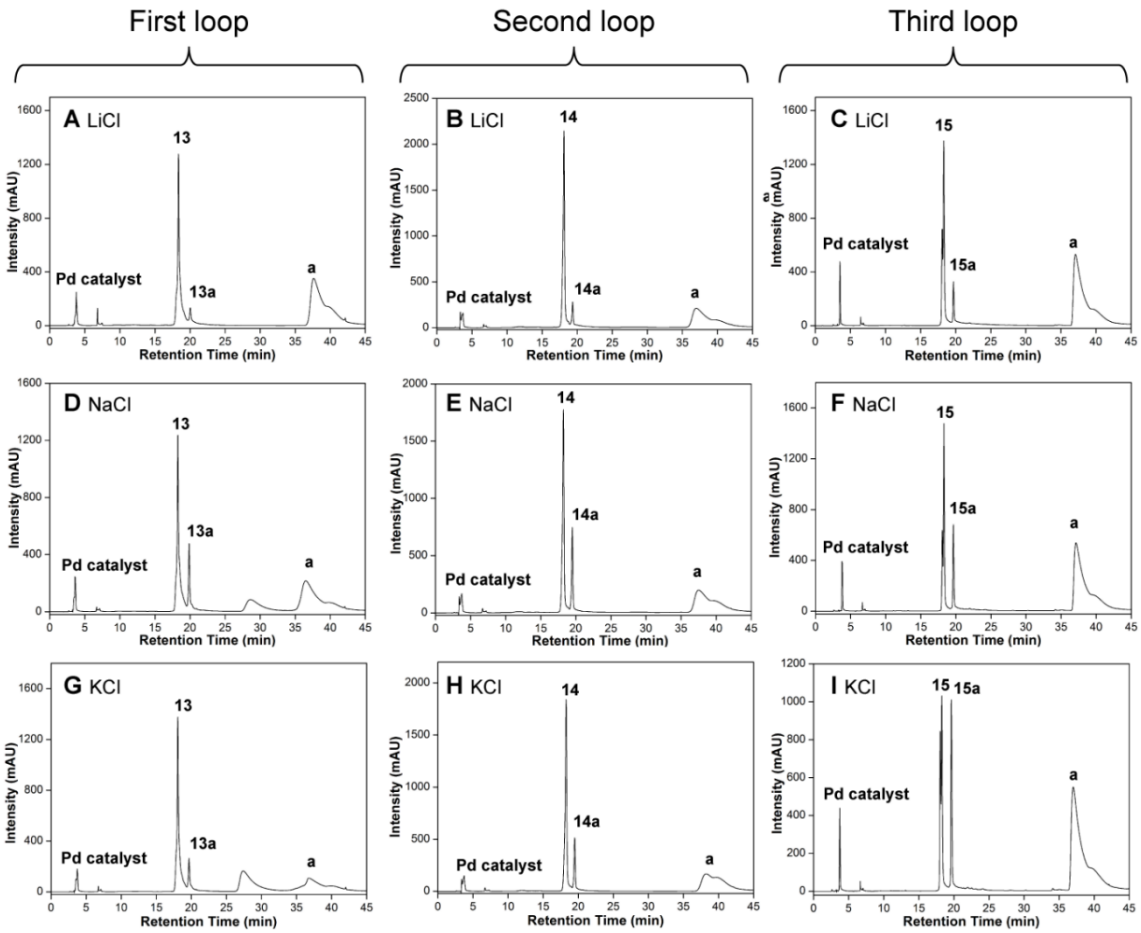

Figure 3.9. RP-HPLC chromatogram of reaction mixture of postsynthetic Suzuki–Miyaura cross-coupling reaction on IdU-modified H-Telo-25 (**1** replaces 2nd thymidine in the loop) DNA ON in presence of LiCl (**A**) **13** (first loop), (**B**) **14** (second loop), (**C**) **15** (third loop); in the presence of NaCl (**D**) **13** (first loop), (**E**) **14** (second loop), (**F**) **15** (third loop); in the presence of KCl (**G**) **13** (first loop), (**H**) **14** (second loop), (**I**) **15** (third loop).

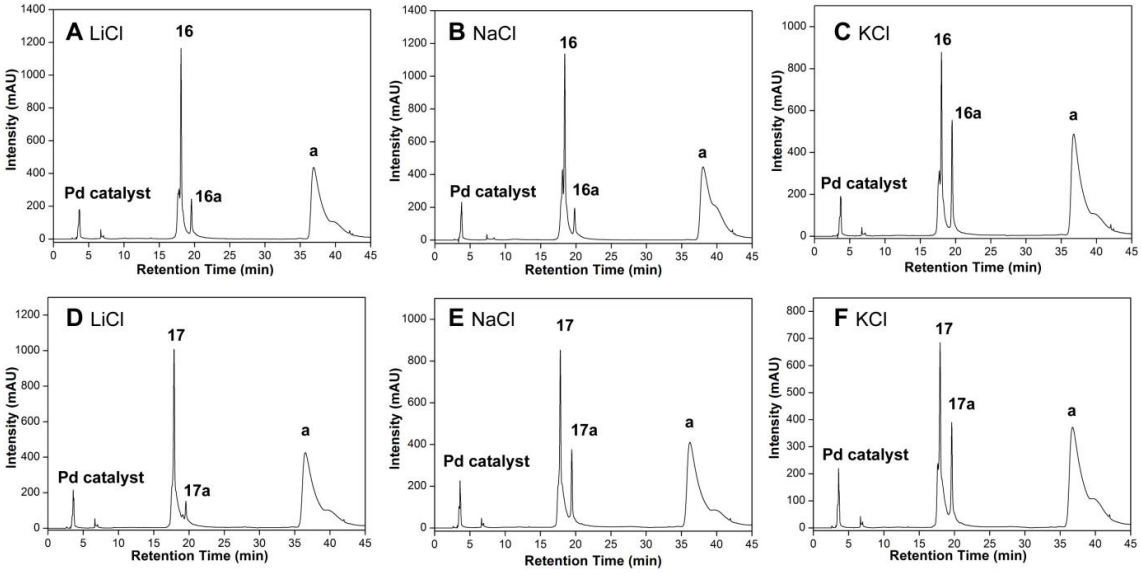

Figure 3.10. RP-HPLC chromatogram of reaction mixture of postsynthetic Suzuki–Miyaura cross-coupling reaction on IdU-modified DNA ON **16** in presence of (**A**) LiCl, (**B**) NaCl, (**C**)KCl and **17** in presence of (**D**) LiCl, **(E**) NaCl, (**F**) KCl.

Table 3.4. ESI-MS and MALDI-TOF mass data of BF-modified DNA.

BF-modified DNA ONs	ε_{260} ($M^{-1}cm^{-1}$)[a]	Calculated mass	Observed mass
4a	248213	7676.0	7676.8[c]
5a	248213	7676.0	7753.0[c] $(M+2K-3H)^-$
6a	248213	7676.0	7752.9[c] $(M+2K-3H)^-$
7a	257013	7980.0	7981.0[c]
8a	257013	7980.0	7981.0[c]
9a	257013	7980.0	7981.0[c]
10a	248213	7676.0	7753.0[c] $(M+2K-3H)^-$
11a	248213	7676.0	7675.7[b]
12a	248213	7676.0	7675.4[b]
13a	257013	7980.0	8057.0[c] $(M+2K-3H)^-$
14a	257013	7980.0	7981.0[c]
15a	257013	7980.0	7979.3[b]
16a	232413	7067.6	7067.6[b]
17a	232413	7067.6	7068.0[b]

[a] Molar absorption coefficient of benzofuran modified ONs was determined by using OligoAnalyzer 3.1, which wasused for the determination of the concentration of modified ONs. The extinction coefficient of nucleoside BFdU (ε_{260} = 12613 $M^{-1}cm^{-1}$)[19] was used in place of thymidine (ε_{260} = 8700 $M^{-1}cm^{-1}$).
[b] Mass analysis was done using MALDI-TOF spectroscopy.
[c] Mass analysis was done using ESI-MS.

Synthetic molecular crowding agents such as PEG can induce G-rich sequences including human telomeric repeat to adopt a parallel-stranded GQ topology.[8] Labeled H-Telo ON **12** and control ON **18** were annealed in Tris-HCl buffer containing 40% PEG (200) and 100 mM KCl. Consistent with earlier reports, CD profiles of the ONs in PEG confirmed the formation of a parallel GQ structure (positive and negative peaks at ~265 nm and ~245 nm, (Figure 3.11A). Suzuki reaction between the parallel form of **12** and benzofuran boronic acid in the presence of Pd $(OAc)_2L_2$ catalyst did produce any detectable coupled product (Figure 3.11B). Closer examination of the HPLC chromatogram revealed considerable reduction in

the peak intensity of the Pd catalyst (retention time ~3.7 min), which could be due to the sequestering effect of PEG. To ascertain this, reactions were performed at different % of PEG (5–30%, Figure 3.12). The formation of cross-coupled product **12a** decreased with increase in the % of PEG (Figure 3.12). Higher amounts of PEG could decrease the diffusion rates and also could coordinate with palladium, thereby reducing the effective concentration of the catalyst.[21]

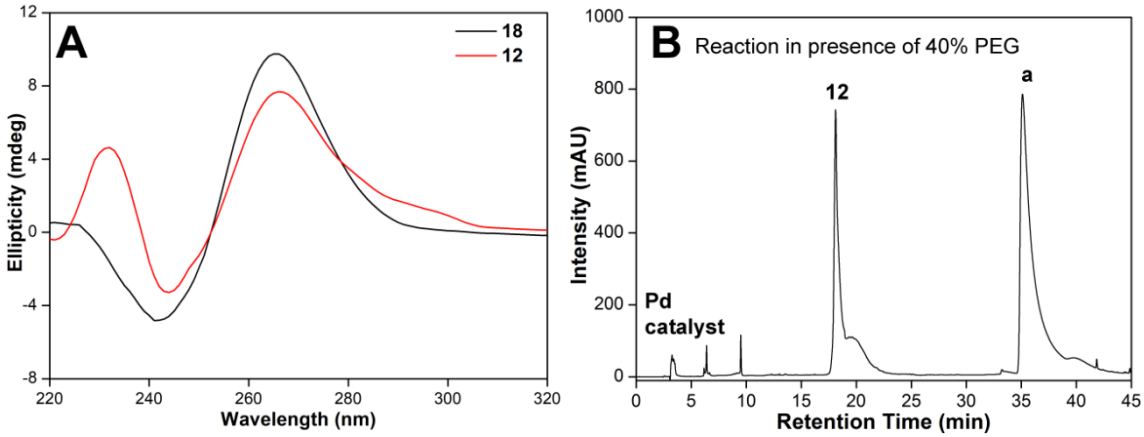

Figure 3.11. (A) CD profile for H-Telo DNA **12** and control unmodified H-Telo DNA **18** in 50 mM Tris-HCl buffer (pH = 8.5) containing 40% PEG (200) and 100 mM KCl. **(B)** HPLC chromatogram for reaction mixture of Suzuki–Miyaura cross-coupling on parallel GQ formed by the DNA ON **12**.

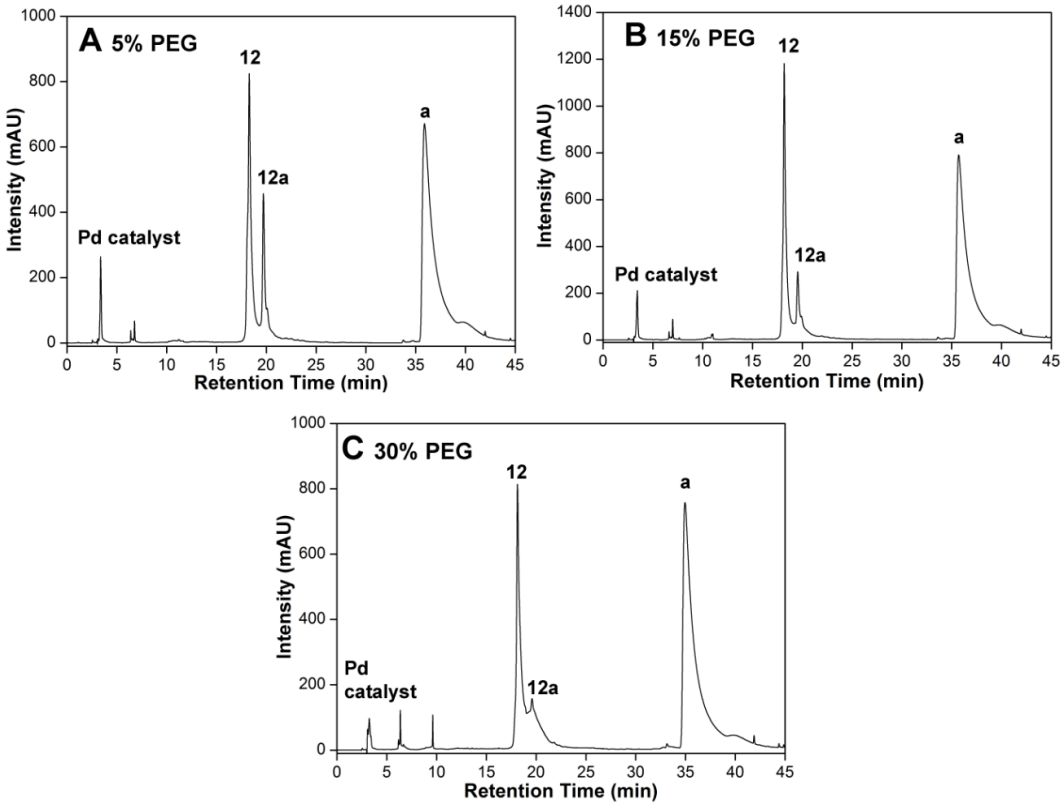

Figure 3.12. HPLC chromatogram for the reaction mixture of Suzuki–Miyaura cross-coupling on parallel GQ topology formed by DNA sequence **12**with an increase in the percentage of PEG (**A**) 5% (**B**) 15% (**C**) 30%.

3.2.4 Suzuki–Miyaura reaction on duplexes formed by using IdU-modified H-Telo DNA ONs

DNA duplexes were prepared by annealing IdU-modified DNA ONs (**12**, **15** and **17**) with 1.1 equivalent of its complementary C-rich DNA ON **21** in Tris-HCl buffer (50 mM, pH = 8.5) containing either 100 mM NaCl or 100 mM KCl (Scheme 3.3). Both control (**18•21**, **19•21**) and modified DNA duplexes (**12•21**, **15•21**) showed similar CD profiles characteristic of B-DNA double helix structure (positive peak at ~270 nm and negative peak at ~240 nm, Figure 3.13).[22] IdU-modified duplexes were reacted with benzofuran boronic acid (50 equiv) in the presence of Pd $(OAc)_2L_2$ catalyst (2 equiv). The reaction mixture was incubated at 37 °C and analysed by HPLC. No cross-coupled product was formed even after 12 h of incubation (Figure 3.14), which also suggests the role of conformation on the reaction efficiency. Next, we have carried out experiments to study the influence of position of IdU modification in double-stranded DNA on the reaction efficiency. We have performed Suzuki reaction on DNA duplex formed by ONs **10**/**11** and complementary C-rich ON **21**. RP-HPLC analysis of the reaction mixture reveals the duplexes formed were completely unreactive. Thus it concludes that position of IdU labeling on the double-stranded DNA does not influence the reactivity of Suzuki reaction.

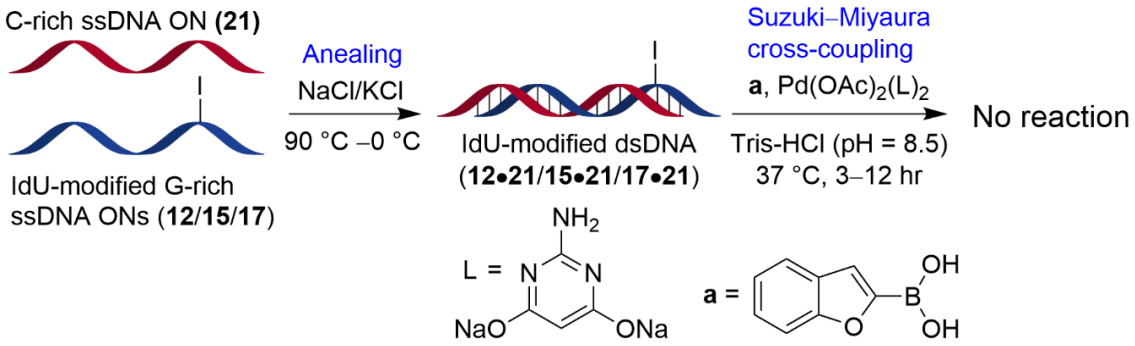

Scheme 3.3. Suzuki–Miyaura cross-coupling reaction on iodo-modified dsDNA with benzofuran boronic acid (**a**) in presence of 100 mM salt (NaCl/KCl).

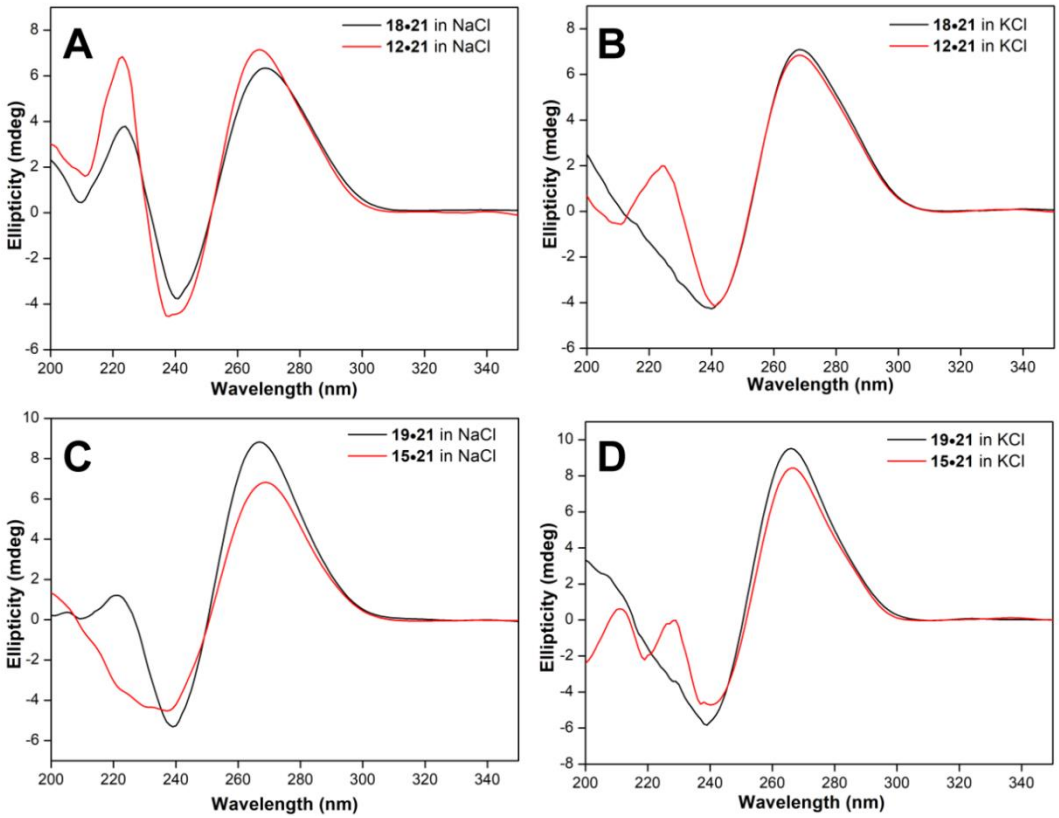

Figure 3.13. CD spectra of control DNA duplexes (**18•21**, **19•21**, 8 μM, black line) and Iodo-modified DNA duplexes (**12•21**, **15•21**, 8 μM, red lines) in aqueous Tris-HCl buffer (50 mM, pH = 8.5) containing either NaCl or KCl.

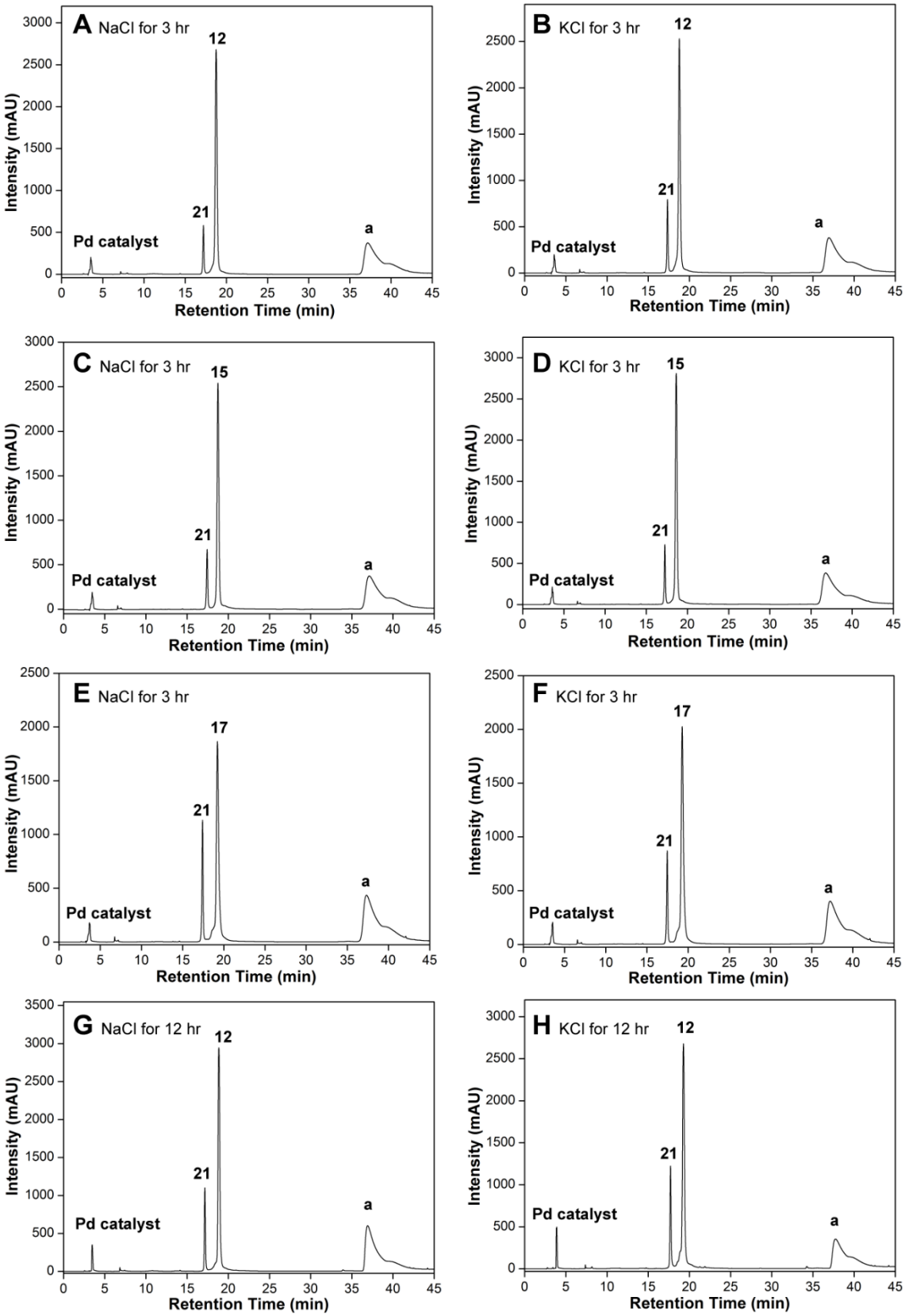

Figure 3.14. RP-HPLC chromatograms illustrating no detectable reaction product between benzofuran boronic acid and iodo-modified dsDNA composed of G-rich DNA ON **12**/**15**/**17** and its

complementary C-rich DNA ON **21**. The reaction contained 50 mM Tris-HCl buffer (pH = 8.5) and 100 mM of NaCl/KCl.

3.2.5 Possible reasons for the differences in the reactivity of unfolded, double stranded and GQ structures

Iodo modification at the C5 position of the nucleoside incorporated into DNA duplexes, should be project in the major grove. The major groove in DNA duplexes is wide (~11.5 Å) but is also deep (~8.5 Å). Probably, this restriction in space puts a constraint on the Pd $(OAc)_2L_2$ catalyst and or the intermediates in the coupling process to attain the right geometry. This restriction is somewhat realised in the random unfolded structures and, hence, we observed reasonable coupling reaction.

The H-Telo ONs used in the study form GQs with three loops formed by TTA bases. IdU-modified GQs in general produced higher yields of the coupled ON products as compared to the random coil structure. When IdU was placed at the first dT in each of the three loops, the coupling efficiency was found to be the best, irrespective the GQ topologies. Based on the 3D structures, the first dT of each of the loops in antiparallel and hybrid structures though show subtle differences in their interaction with neighbouring bases, they are exposed and the C5 iodo group is accessible for coupling reaction (Figure 3.15 and 3.16). On the other hand, IdU placed at the second dT position of the three loops reacted less efficiently with the boronic acid substrate. For example, in the antiparallel form, the second dT in the first loop is almost buried and stacks on the G-tetrad core (Figure 3.15A). While in the second loop the dT is stacked from one side with adjacent dA (Figure 3.15B), dT in the third loop is not stacked but is located in the groove wherein there is void space around the C5 position (Figure 3.15C). Staking interaction can transfer electrons from adjacent guanine to its neighbouring nucleobase, here IdU, thereby potentially increasing its nucleophilicity.[23] Increase in nucleophilicity could decrease the efficiency of IdU to undergo oxidation step in the palladium-catalyzed coupling reaction.[24] Hence, electronic and steric effects originating from the nucleotide conformation results in differences in reactivity exhibited by the ONs adopting different conformations.

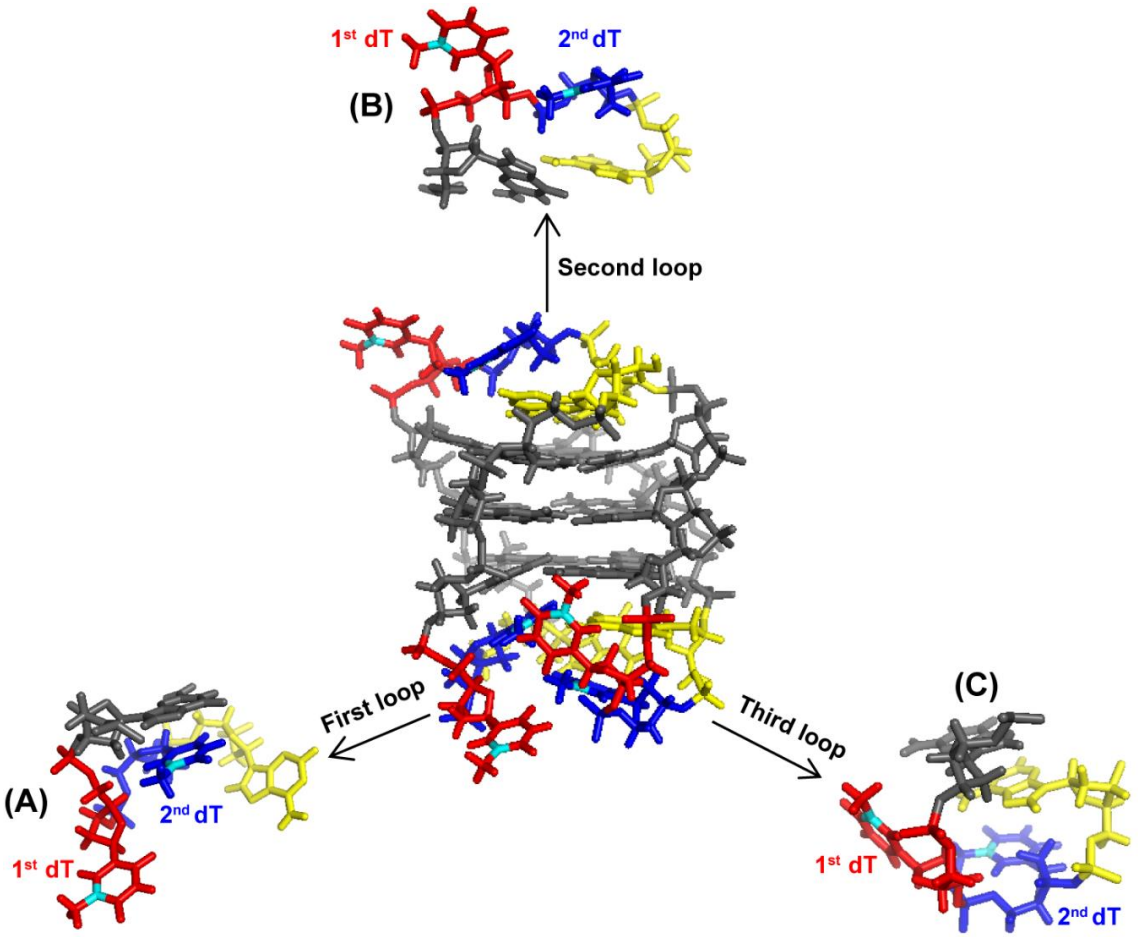

Figure 3.15. Antiparallel G-quadruplex NMR structure of Telo-22 in Na^+ solution (PDB ID: 143D).[3] A close-up view of stacking interactions of nucleobase in the first, second and third loop region. 2′-deoxyguanosines are shown in grey, 2′-deoxyadenosines are shown in yellow, first 2′-deoxythymidines of each loop are shown in red and second 2′-deoxythymidines of each loop are shown in blue. C5 position of the thymidine residues are shown in cyan color.

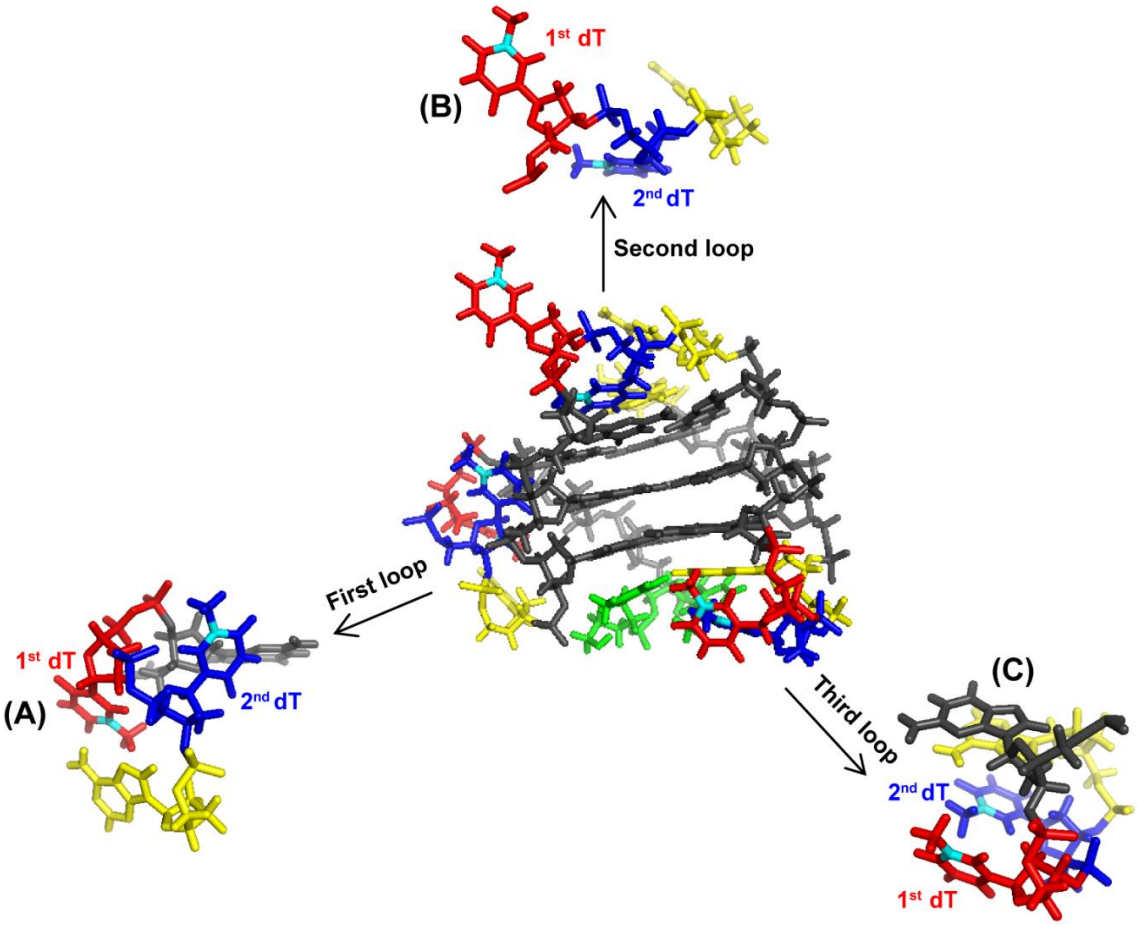

Figure 3.16. Hybrid 1 G-quadruplex structure of Telo-24 in K^+ solution (PDB ID: 2GKU).[5] A close-up view of stacking interactions of nucleobase in the first, second and third loop region. 2′-deoxyguanosines are shown in grey, 2′-deoxyadenosine are shown in yellow, first 2′-deoxythymidines of the loop are shown in red and second 2′-deoxythymidines of each loop are shown in blue. 5′ terminal TT residues are shown in the green. C5 position of the thymidine residues is shown in cyan color.

3.2.6 Changes in ionic conditions do not influence coupling efficiency

It is reported that inorganic salts alter the efficiency of organic reactions such as Suzuki–Miyaura cross-coupling, Diels–Alder cycloaddition, Wittig reactions, to name a few.[25]To test the influence of added salts on the postsynthetic Suzuki–Miyaura cross-coupling of ONs, a short 5-iodouridine-modified RNA ON **22**,[18] which does not form any secondary structure was reacted with benzofuran boronic acid in the presence of LiCl/NaCl/KCl (Scheme 3.4). The added salts did not affect the reaction and yields of the coupled product **22a** were similar in different ionic conditions. This observation indicates that the reaction efficiency is influenced by the conformation adopted by ONs and not due to added salts.

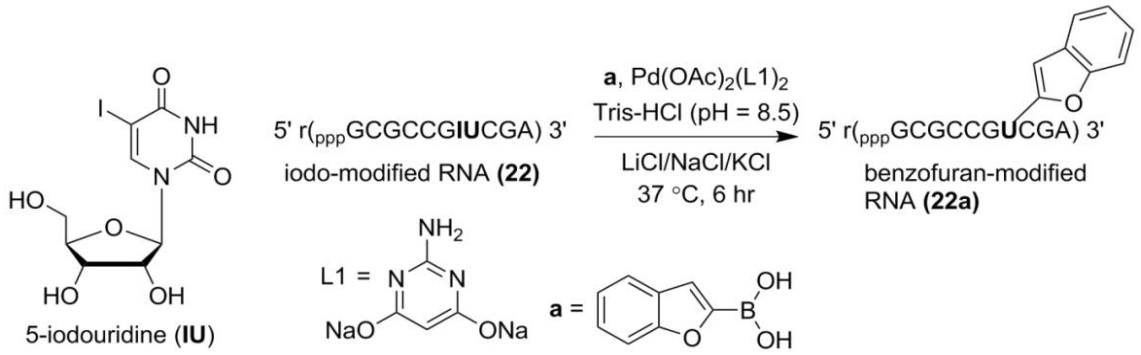

Scheme 3.4. Suzuki–Miyaura cross-coupling reaction on IU-modified RNA **22** with benzofuran boronic acid **(a)** in the presence of salt (LiCl/NaCl/KCl).

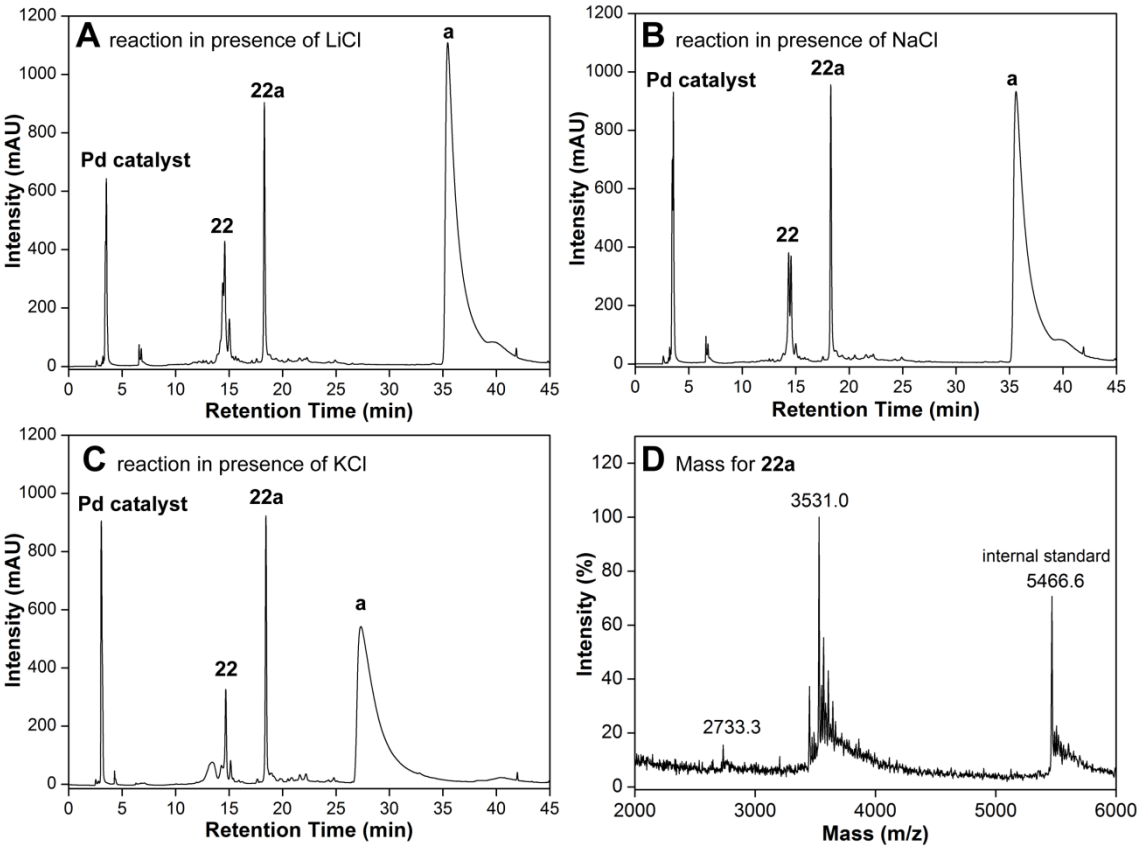

Figure 3.17. RP-HPLC chromatogram of the reaction mixture of Suzuki–Miyaura cross-coupling between IU-modified RNA (**22)** and benzofuran boronic acid (**a**) in presence of LiCl (**A**) NaCl (**B**) KCl (**C**). **22a** correspond to cross-coupled RNA ON product; **a** is excess benzofuran boronic acid.(**D**) MALDI-TOF mass spectrum of cross-coupled RNA ON products **22a**.Calcd. mass for cross-coupled RNA ON products **22a**: $[M]^+$3531.0; found: $[M]^+$ 3531.0.

Table 3.5. Yields for cross-coupled RNA ON product **22a** obtained by Suzuki–Miyaura reaction between IU-modified RNA ON transcripts **22** and benzofuran boronic acid.[a]

Salt	Isolated yield for **22a** (nmol)	Isolated yield for **22a** (%)
LiCl	1.85	37
NaCl	1.97	39
KCl	1.63	33

[a] All reactions were performed on a 5 nmole scale of iodo-modified RNA transcripts **22**. Yields reported are with respect to the RNA products isolated after HPLC purification. Concentration and yield of the product were calculated using the molar absorption coefficient (ε260) of the RNA product **22a** (98553 $M^{-1}cm^{-1}$).

3.2.7. Benzofuran-modification introduced by postsynthetic Suzuki reaction fluorescently distinguishes different GQ topologies: In order to evaluate whether the modified ONs synthesized by Pd-catalyzed reactions are suitable for downstream biophysical analysis, benzofuran-modified H-Telo DNA ON **16a** was subjected to fluorescence analysis. ON **16a** containing the label at the 1st dT base of the second loop formed respective GQ topologies in different ionic conditions without hampering the native fold, which was confirmed by CD analysis (Figure 3.18). We then recorded the fluorescence spectra of the ON in the presence of K^+ or Na^+ ions by exciting the samples at 330 nm. The duplexes made of ON **16a** in KCl and NaCl exhibited very low fluorescence (Figure 3.19). The mixed hybrid-type GQs (hybrid 1 and 2, blue line) formed by **16a** in KCl exhibited ~6-fold enhancement in fluorescence intensity with a red shift in emission maximum (λ_{em} = 434 nm) as compared to the duplex form (λ_{em} for **16a•21** is 427 nm). Antiparallel topology displayed further enhancement in fluorescence intensity (~14-fold, black line) compared to its duplex form. The probe also distinguished between hybrid 1 and hybrid 2 forms (Figure 3.19). While ON **5a**, which predominantly forms a hybrid 1 structure in KCl, displayed an intense emission band (magenta line), nearly 5-fold higher than the hybrid 2 structure formed by ON **8a** (red line). ON **16a**, as before, showed intermediate fluorescence as this sequence forms both hybrid 1 and 2 forms in KCl (blue line). The ability of the probe to fluorescently distinguish different GQ topologies is due to the differences in the microenvironment of the probe in different conformations.[19] Collectively , these results clearly indicate the usefulness of Pd-catalyzed cross-coupling reactions in constructing ONs labeled with functional probes.

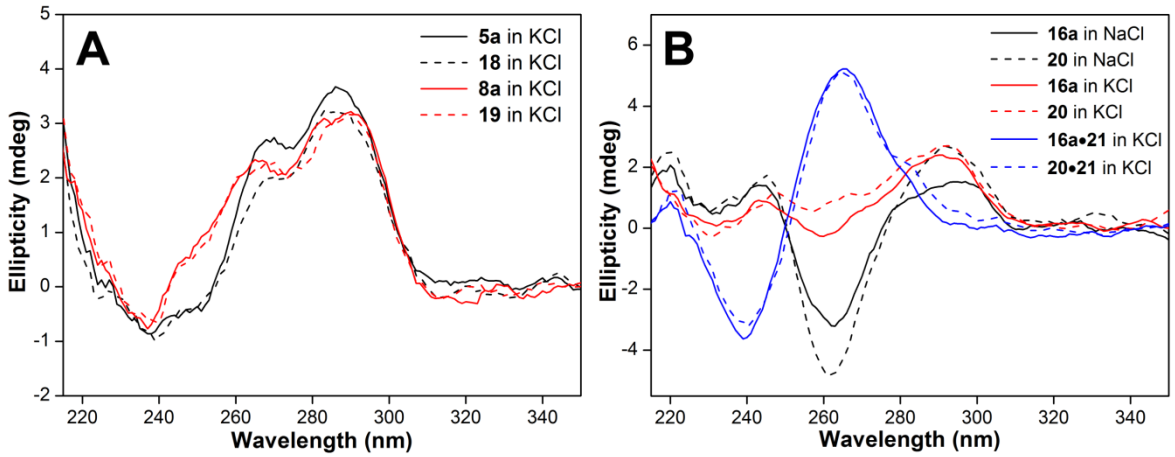

Figure 3.18. CD spectra of (**A**) GQs of BFdU-modified H-Telo DNA ONs **5a** (hybrid 1), **8a** (hybrid 2) and respective unmodified H-Telo DNA ONs **18** and **19** in KCl. (**B**) GQs of BFdU-modified H-Telo DNA ON **16a**, unmodified H-Telo DNA ON **20** and corresponding duplexes (**16a•21**, **20•21**) in different ionic conditions. CD spectra of ON samples (5 μM) were recorded in 10 mM Tris-HCl buffer (pH 7.5) containing 100 mM KCl or 100 mM NaCl. **16a** and **20** in NaCl forms antiparallel GQ structure (black lines) and in KCl hybrid type structures (red lines). Duplexes are shown in blue lines.

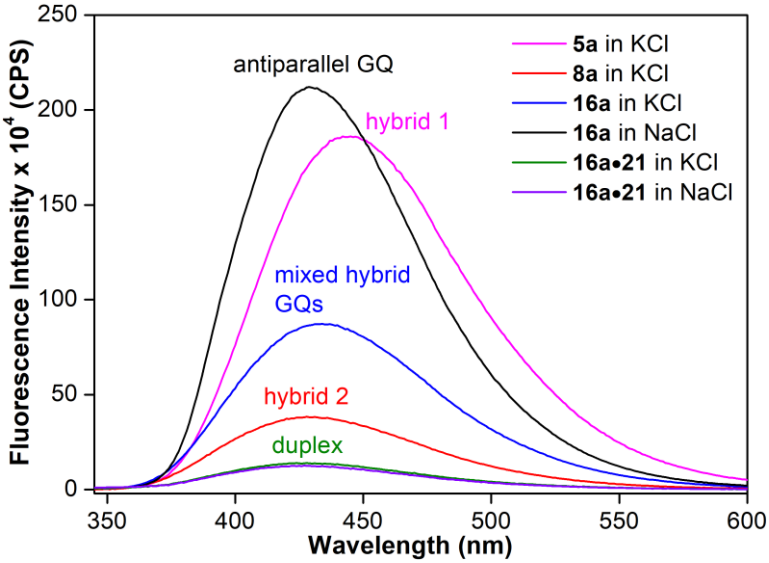

Figure 3.19. Fluorescence spectra of GQs of H-Telo DNA ON **16a** and corresponding duplexes in different ionic conditions. Spectra of GQs of ONs **5a** (hybrid 1), **8a** (hybrid 2) and **16a** (mixed hybrids) in KCl. Samples (0.5 μM) were excited at 330 nm with an excitation and emission slit width of 5 and 6 nm, respectively.

3.3 Conclusion

In conclusion, we have successfully performed the postsynthetic Suzuki–Miyaura cross-coupling reaction on various DNA conformations, including random unfolded, GQs and duplex DNA. The difference in reactivity displayed by different DNA conformations mainly depends on the position of IdU label in the loop and electronic and steric environment around

IdU. Overall this study shows that postsynthetic Suzuki–Miyaura cross-coupling reaction works in a conformation-dependent manner and conformational selectivity of the reaction decreased in the order of: GQ topology > single-stranded DNA and no reaction with double stranded DNA. Given the compatibility of 5-halo-2′-deoxyuridine (e.g., BrdU) with the metabolic machinery of living cells,[26,27] this postsynthetic Suzuki–Miyaura cross-coupling could be potentially used to install probes in a conformation-selective fashion to detect the presence of GQs in cellular environment.

3.4 Experimental section

3.4.1 Materials: 5-iodo-2′-deoxyuridine (**1**) was purchased from TCI Chemicals (India) Pvt. Ltd. DMTr-Cl, *N*,*N*-diisopropylethylamine, benzofuran boronic acid (**a**), 2-cyanoethyl N,N-diisopropylchlorophosphoramidite, 2-aminopyrimidine-4,6-diol (ADHP, L) and $Pd(OAc)_2$ were purchased from sigma aldrich. DMAP was purchased from alfa aesar. *N*-benzoyl-protected dA, dT and *N*,*N*-dimethylformamidine-protected dG phosphoramidite substrates for solid phase oligonucleotide synthesis were purchased from ChemGenes and Proligo. All other reagents and solid-supports required for oligonucleotide (ON) synthesis were purchased either from ChemGenes or from Sigma-Aldrich. Unmodified DNA ONs **18**–**21** were purchased from Integrated DNA Technology, and purified by denaturing polyacrylamide gel electrophoresis (PAGE). ONs were desalted using Sep-Pak Classic C18 cartridges (Waters Corporation). Autoclaved water was used in all biochemical reactions.

3.4.2 Instrumentation: NMR spectra were recorded on a 400 MHz Jeol ECS-400 and Bruker Avance III HD Ascend 400 MHz spectrometer. Modified DNA oligonucleotides were synthesized on an Applied Biosystems RNA/DNA synthesizer (ABI-394).Mass measurements were done using Applied Biosystems 4800 Plus MALDI TOF/TOF analyzer and ESI-MS Waters SYNAPT G2-Si Mass Spectrometry instrument in negative mode. HPLC analysis of ONs was performed using Agilent Technologies 1260 Infinity HPLC. UV-thermal melting analysis of ONs was performed on a Cary 300Bio UV-Vis spectrophotometer. CD spectra were recorded on a JASCO-J-815 CD spectrometer. Absorption spectra were recorded on a PerkinElmer, Lambda 45 UV-Vis spectrophotometer.

3.4.3 Synthesis of 5-iodo-modified uridine phosphoramidite substrate 3

3.4.3.1 5-Iodo-5′-DMT-protected-2′-deoxyuridine 2: 5-Iodo-2′-deoxyuridine **1** (1 g, 2.82 mmol, 1 equiv.), DMAP (172 mg, 1.41 mmol, 0.5 equiv.), DMTrCl (1.43 g, 4.24 mmol, 1.5 equiv.) were taken in a round bottom flask. Dry pyridine (30 mL) was added to it and reaction mixture was stirred at room temperature (RT) overnight. After completion of the reaction, solvent was evaporated under *vacuo*. The crude residue was purified by column chromatography to afford the pure compound **2** as an off-white solid. (1.35 g, 70%). TLC (MeOH:$CHCl_3$ = 5:95 containing few drops of Et_3N); R_f = 0.33; ^{1}H NMR (400 MHz, $CDCl_3$) δ (ppm) 8.11 (s, 1H), 7.42 (d, *J* = 8 Hz, 2H), 7.34–7.28 (m, 6H), 7.23–7.20 (m, 1H), 6.85–6.83 (m, 4H), 6.34 (dd, *J* = 5.8, 7.8 Hz, 1H), 4.57–4.55 (m, 1H), 4.12–4.11 (m, 1H), 3.79 (s, 6H), 3.37 (s, 2H), 2.53–2.48 (m, 1H), 2.29–2.23 (m, 1H); ^{13}C NMR (100 MHz, $CDCl_3$) δ (ppm) = 158.64, 144.42, 144.18, 135.61, 135.60, 135.43, 130.14, 130.10, 128.09, 127.02, 113.37, 86.95, 86.42, 85.51, 72.20, 63.68, 55.29, 41.54. HRMS (m/z): Calculated for $C_{30}H_{29}IN_2O_7Na$ $[M+Na]^+$ = 679.0917, found: 679.0916.

3.4.3.2 5-Iodo-2′-deoxyuridine phosphoramidite substrate 3: 5'-O-(4,4'-Dimethoxytrityl)-2′-deoxy-5-iodo-2′-deoxyuridine(328 mg, 0.5 mmol, 1 equiv) was dissolved in dry DCM (4 mL). To this clear solution diisopropylethylamine (523 µL, 3 mmol, 6 equiv) was added and stirred for 30 min at RT. Next, 2-cyanoethylchloro-N,N-diisopropylphosphoramidite (167 µL, 0.75 mmol, 1.5 equiv) was added slowly under nitrogen. The reaction mixture was stirred for 1 h under nitrogen at RT. After completion of the reaction, reaction mixture was purified by column chromatography to afford the product **3** as a white foamy solid. (316 mg, 75%). TLC (Acetone:cyclohexane=40:60 with few drops of Et_3N);R_f =0.47; ^{1}H NMR (400 MHz, $CDCl_3$) δ (ppm) (diastereomers ratio = 1:0.5); ^{1}H NMR for major diastereomer: 8.14 (s, 1H), 7.42 (br.s, 2H), 7.32 (br.s, 6H), 7.24 (br.s, 1H), 6.86–6.84 (m, 4H), 6.31 (br.s,1H), 4.62 (br.s, 1H), 4.21 (s, 1H), 3.80 (s, 6H), 3.64–3.53 (m, 4H), 3.42–3.31 (m, 2H), 2.70–2.68 (m, 1H), 2.62 (br.s, 2H), 2.31–2.28 (m, 1H), 1.17–1.06 (m, 12H); ^{31}P NMR (162 MHz, $CDCl_3$): δ (ppm) 149.55, 149.09; HRMS (m/z): Calculated for $C_{39}H_{46}IN_4O_8PNa$ $[M+Na]^+$ = 879.1995, found: 879.1996.

3.4.4 Solid-phase synthesis of modified DNA ONs: IdU-modified DNA ONs were synthesized on a 1.0 µmol scale (1000 Å CPG solid support). Phosphoramidite **3** was site-specifically incorporated into the ONs by a standard DNA ON synthesis protocol. After the final detritylation step, the solid support was treated with a 30% aqueous solution of

ammonium hydroxide for 48 h at RT. The aqueous ammonium hydroxide solution was evaporated to dryness on a Speed Vac, and deprotected ON products were purified by 20% polyacrylamide gel electrophoresis under denaturing conditions. Respective modified ON products were visualized by UV shadowing; product bands were excised from the gel and transferred to a Poly-Prep column (Bio-Rad). The gel pieces were crushed with a sterile glass rod, and ONs were extracted in sodium acetate buffer (0.3 M, 4 mL) for 12 h. The resulting solutions were filtered and desalted using Sep-Pak classic C18 cartridges (Waters).

3.4.5 Mass analysis of DNA ONs

3.4.5.1 MALDI-TOF: Sample for mass analysis was prepared by combining 1 µL of the modified DNA ON (~500 µM), 3 µL of DNA standard (100 µM, 18-mer) and 5 µL of a mixture of saturated 3-hydroxy picolinic acid and 100 mM ammonium citrate buffer (pH 9, in the ratio of 9:1). The sample was desalted using ion-exchange resin (Dowex 50W-X8, 100-200 mesh, ammonium cation form), spotted on the MALDI plate, and was air dried. Depending on the peak intensity the ratio of DNA ON and internal DNA standard was varied.MALDI-TOF spectra are calibrated relative to the +1 and +2 ions of an internal 18-mer DNA ON standard (m/z for +1 and +2 ions are 5466.6 and 2733.3, respectively).

3.4.5.2 ESI-MS: ESI-MS analysis was performed in negative mode by injecting DNA oligonucleotide (0.5 nmol) dissolved in 50% acetonitrile in an aqueous solution of 10 mM triethylamine and 100 mM hexafluoro-2-propanol.

3.4.6 CD measurement: The CD spectrum was recorded from 200 to 350 nm on a J-815 CD spectropolarimeter (Jasco, USA) using 1 nm bandwidth at 20 °C. Each CD profile is an average of three scans collected at a scan speed of 100 nm min^{-1}. CD measurements were performed in duplicate and all spectra were corrected using an appropriate blank solution in the absence of ONs.

3.3.6.1 G-quadruplex DNA conformation: Respective DNA conformations were made by annealing IdU-modified DNA ONs **12**/**15**/**17** (8 µM) and control unmodified H-Telo DNA **18**–**20** (8 µM) at 90 °C for 3 min in Tris-HCl buffer (50 mM, pH = 8.5) containing either 100 mM NaCl or 100 mM KCl. To obtain the parallel conformation, IdU-modified DNA ON **12** and unmodified DNA ON **18** were annealed at 90 °C for 3 min in 50 mM Tris–HCl buffer

(pH 8.5) containing 40% PEG 200 and 100 mM KCl. All the solutions were slowly cooled to RT and kept in an ice bath for at least 1 h.

3.3.6.2 Duplex DNA: The corresponding IdU-modified (**12•21**, **15•21**) and unmodified DNA duplexes (**18•21**, **19•21)** were prepared by heating a 1:1.1 mixture of H-Telo DNA ONs **12**/**15**/**18/19** (8 μM) and complementary C-rich DNA ON **21** (8.8 μM) at 90 °C for 3 min in 50 mM Tris-HCl buffer (pH 8.5) containing either 100 mM NaCl or 100 mM KCl. The solutions were slowly cooled to RT and kept in an ice bath for at least 1 h.

3.4.7 Thermal melting analysis: IdU-modified and unmodified DNA ONs (1 μM) were annealed similarly like CD samples and thermal melting analysis was performed usingCary 300 Bio UV-Vis spectrophotometer. The temperature was increased from 20 °C to 90°C at 1 °C/min and the absorbance was measured every 1 °C interval at 295 nm.

3.4.8 Suzuki–Miyaura cross-coupling reaction condition and purification

The percentage of DMSO kept 20% v/v in the reactions and reaction performed at 37 °C temperature. The reaction mixture was filtered using a spin filter (0.45 μm pore size) and was further washed with 50 μL of water. The filtrate was analyzed by RP-HPLC (Phenomenex-Luna C18 column, 250 x 4.6 mm, 5 micron). Mobile phase A: 50 mM TEAA buffer (pH 7.0), mobile phase B: acetonitrile. Flow rate: 1 mL/min. Gradient: 0−30 % B in 35 min, 30−100% B in 10 min and 100% B for 5 min. The run was monitored by UV absorption at 260 nm. Each peak was collected and freeze-dried.

3.4.8.1 Reaction on IdU-modified DNA ON 4–17 in presence of different salt: IdU-modified G-rich DNA ONs **4**–**17** (2.5 nmol, 50 μM, 1 equiv) in 10 μL of Tris-HCl buffer (50 mM, pH 8.5) containing 100 mM salt (LiCl/NaCl/KCl) and 8.75 μL of DMSO was taken in 0.5 mL of eppendorf. Reaction mixture was annealed by heating at 90 °C for 3 min. The samples were cooled to RT and kept in an ice bath for at least 1 h. Further, benzofuran boronic acid **a** (1 nmol, 2.5 mM, 50 equiv) was added to the above solution. The reaction was initiated by adding catalyst $Pd(OAc)_2L_2$ (0.1 mM, 2 equiv).Reaction was incubated at 37 °C for 3 hr.

3.4.8.2 Reaction on duplex DNA: IdU-modified G-rich DNA ONs **12**, **15** and **17** (2.5 nmol, 50 μM, 1 equiv) and complementary C-rich DNA ON **21** (2.75 nmol, 55 μM, 1.1 equiv) in 10

μL of Tris-HCl buffer (50 mM, pH 8.5) containing either NaCl or KCl (100 mM) and 8.75 μL of DMSO was taken in 0.5 mL of eppendorf. Reaction mixture was annealed by heating at 90 °C for 3 min. The samples were cooled to RT and kept in an ice bath for at least 1 h. Further, benzofuran boronic acid **a** (2.5 mM, 50 equiv).The reaction was initiated by adding catalyst $Pd(OAc)_2L_2$ (0.1 mM, 2 equiv). Reaction was incubated at 37 ℃ for 3–12 hr.

3.4.8.3 Reaction on 10-ntiodo-modified RNA 22: IU-modified RNA **22** (5 nmol, 100 μM, 1 equiv) in 10 μL of Tris-HCl buffer (50 mM, pH 8.5), 8.75 μL of DMSO was taken in 0.5 mL of eppendorf. Reaction mixture was annealed by heating at 90 ℃ for 3 min containing 100 mM salt (LiCl/NaCl/KCl). The samples were cooled to RT and kept in an ice bath for at least 1 h. Further, benzofuran boronic acid **a** (5 mM, 50 equiv). The reaction was initiated by adding catalyst $Pd(OAc)_2L_2$ (0.2 mM, 2 equiv). The reaction was incubated at 37 ℃ for 3 h.

3.4.9. Detection of GQ structures by fluorescence. H-Telo ONs **5a**/**8a**/**16a** (0.5 μM) were annealed at 90℃ for 3 min in 10 mM Tris–HCl buffer (pH 7.5) containing either 100 mM KCl or 100 mM NaCl. To obtain a DNA duplex (**16a•21**), ON **16a** and complementary C-rich ON **21** was assembled by heating a 1:1.1 mixture in 10 mM Tris–HCl buffer (pH 7.5) containing either 100 mM KCl or 100 mM NaCl at 90 ℃ for 3 min. All the samples were then cooled slowly to attain RT and placed in an ice bath for 1 h. Each Sample was excited at 330 nm with excitation and emission slit widths of 5 nm and 6 nm, respectively. All fluorescence experiments were performed in triplicate with appropriate blank corrections in a micro fluorescence cuvette (path length 1.0 cm, Hellma) on a Horiba Jobin Yvon, Fluorolmax-4 at 20 °C.

3.5 References

1. J. A. Hackett, D. M. Feldser and C. W. *Cell*, 2001, **106**, 275–286.
2. M. Lei, E. R. Podell, P. Baumann and T. R. Cech, *Nature*, 2003, **426**, 198–203.
3. Y. Wang and D. J. Patel, *Structure*, 1993, **1**, 263–282.
4. A. Ambrus, D. Chen, J. Da, T. Bialis, R.A. Jones andD. Yang, *Nucleic Acids Res.*, 2006, **34**, 2723–2735.
5. K. N. Luu, A.T. Phan, V. Kuryavyi, L. Lacroix and D. J. Patel, *J. Am. Chem. Soc.*, 2006, **128**, 9963–9970.
6. J. Dai, M. Carver, C. Punchihewa, R. A. Jones and D. Yang, *Nucleic Acids Res.*,2007,**35**, 4927–4940.
7. G. N. Parkinson, M. P. H. Lee and S. Neidle, *Nature*, 2002, **417**, 876–880.
8. B. Heddi and A. T. Phan, *J. Am. Chem. Soc.* 2011, **133**, 9824–9833.
9. Y. Xu and H. Sugiyama, *Angew. Chem. Int. Ed.*, 2006, **45**, 1354–1362.
10. G. Lin, J. Zhang, Y. Zeng, H. Luo and Y. Wang, *Biochemistry* 2010, **49**, 2346–2350.
11. A. Saha, S. Bombard, A. Granzhan and M-P. Teulade-Fichou, *Scientific Reports*, 2018 **8**, 15814–15827.
12. Y. Xu and H. Sugiyama,*J. Am. Chem. Soc.*, 2004, **126**, 6274–6279.
13. Y. Xu, Y. Suzuki, and M. Komiyama, *Angew. Chem. Int. Ed.*, 2009, **48**, 3281–3284.
14. Y. Xu, T. Ishizuka, J. Yang, K. Ito, H. Katada, M. Komiyama and T. Hayashi, *J. Bio. Chem.*, 2012, **287**, 41787–41796.
15. Y. Xu, Y. Suzuki, T. Ishizuka, C-D, Xiao, X. Liu, T. Hayashi and M. Komiyama. *Bioorganic & Medicinal Chemistry*, 2014, **22**, 4419–4421.
16. A. Naik, J. Alzeer, T. Triemer, A. Bujalska, and N. W. Luedtke, *Angew. Chem. Int. Ed.*, 2017, **56**, 10850–10853.
17. N. H. Scherberg, *Applied Radiation and Isotopes*, 1993, **44**, 1993, 665–671.
18. M. B. Walunj, A. A. Tanpure and S. G. Srivatsan, *Nucleic Acids Res.*, 2018, e15.
19. A. A. Tanpure and S. G. Srivatsan, *Nucleic Acids Res.*, 2015, **43**, e149
20. A. Dumas and N. W. Luedtke, *Nucleic Acids Res.*, 2011, **39**, 6825–6834.
21. J. Sherwood, J. H. Clark, I. J. S. Fairlamb and J. M. Slattery, *Green Chem.***,** 2019, **21**, 2164-2213.
22. J. Kypr I. Kejnovská, K. Bednářová and M. Vorlíčková, *Compr. Chiropt. Spectrosc.*, 2012, **2**, 575–586.
23. F. D. Lewis, Y. Wu, L. Zhang, X. Zuo, R. T. Hayes and M. R. Wasielewski, *J. Am. Chem. Soc.*2004, **126**, 8206–8215.
24. C. Len, S. Bruniaux, F. Delbecq and V. S. Parmar, *Catalysts*, 2017, 7, 146–168.
25. B. Zhang, J. Song, H. Liu, J. Shi, J. Ma, H. Fan, W. Wang, P. Zhang and B. Han, *Green Chem.***,** 2014, **16**, 1198–1201.
26. H. G. Gratzner, *Science*, 1982, **218**, 474.
27. N.Yan, Y. He, H. Wen, F. Lai, D. Yin and H. Cui, *Analyst*, 2018, **143**, 1224–1233.

3.6 Appendix-II: Characterization data of synthesized compounds

^{1}H NMR (400 MHz) of compound **2** in $CDCl_3$ containing 0.3 v/v% of TMS. Triplet at 1.26 ppm and quartet at 2.90 ppm correspond to Et_3N.

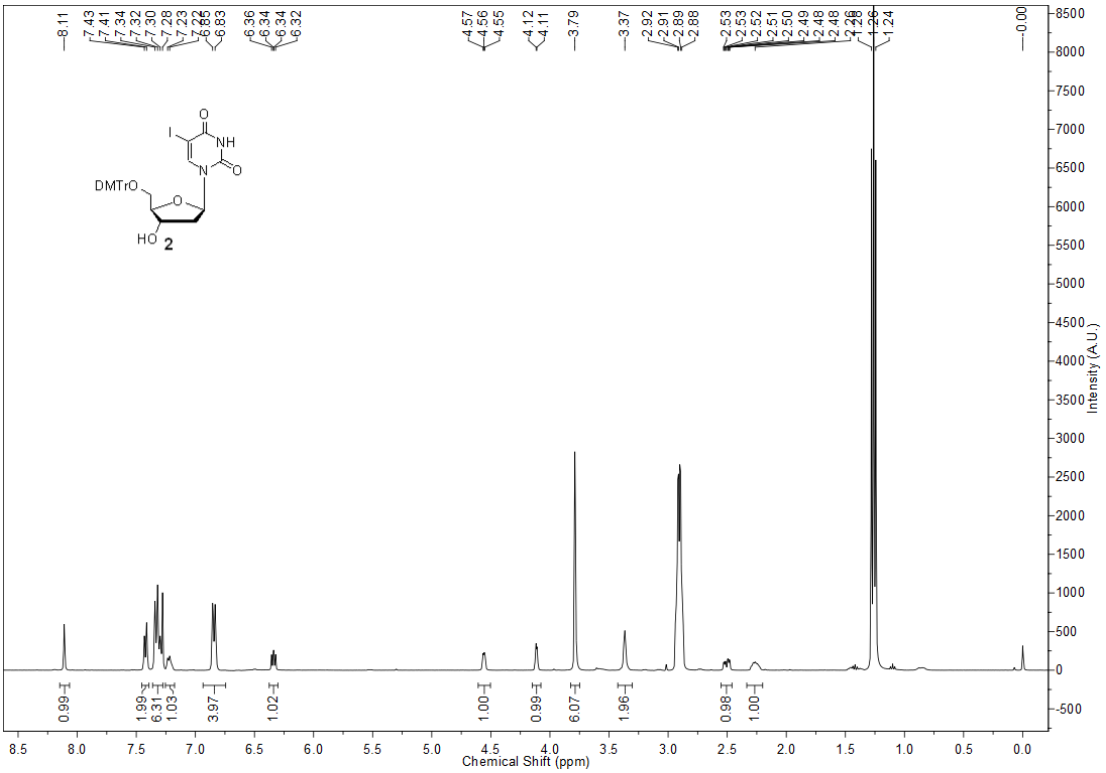

^{13}C NMR (100 MHz) of compound **2** in $CDCl_3$ containing 0.3 v/v% of TMS. Peaks at 9.58 ppm and 45.83 ppm correspond to Et_3N.

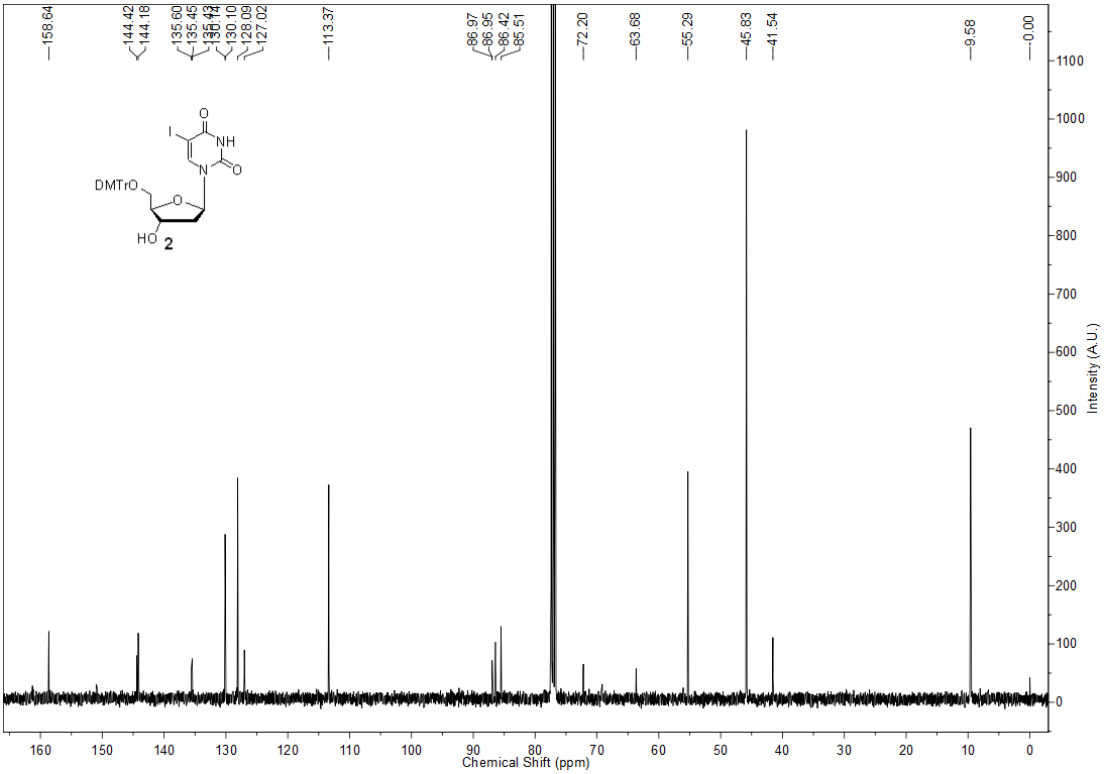

^{1}H NMR (400 MHz) of compound **3** in $CDCl_3$ containing 0.3 v/v% of TMS. (diastereomers ratio = 1:0.5).

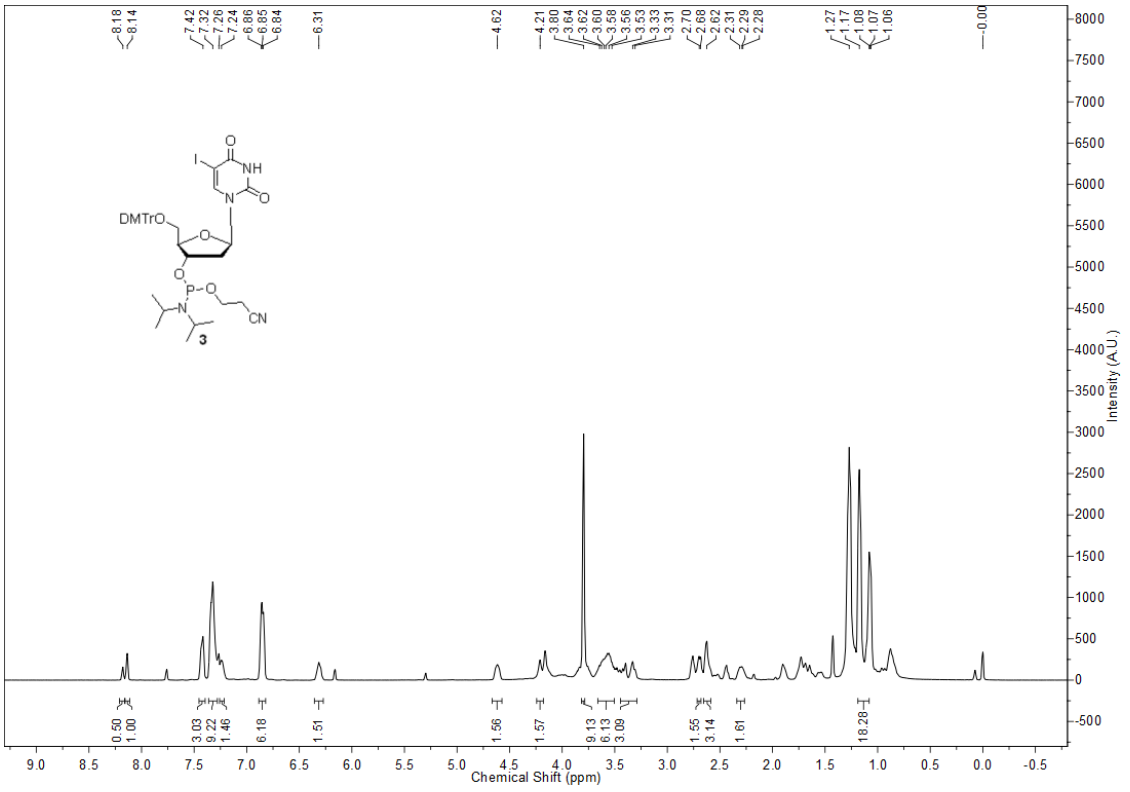

^{31}P NMR (162 MHz) of compound **3** in $CDCl_3$.

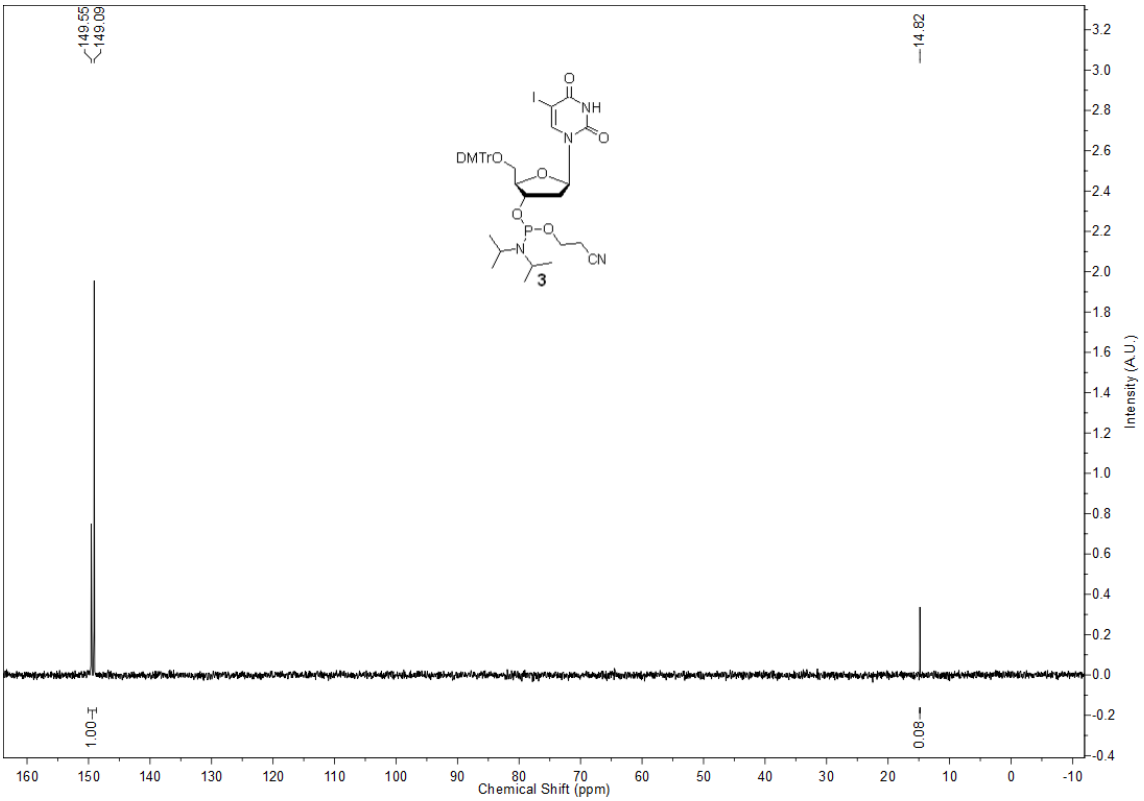

ESI-MS of compound **3**

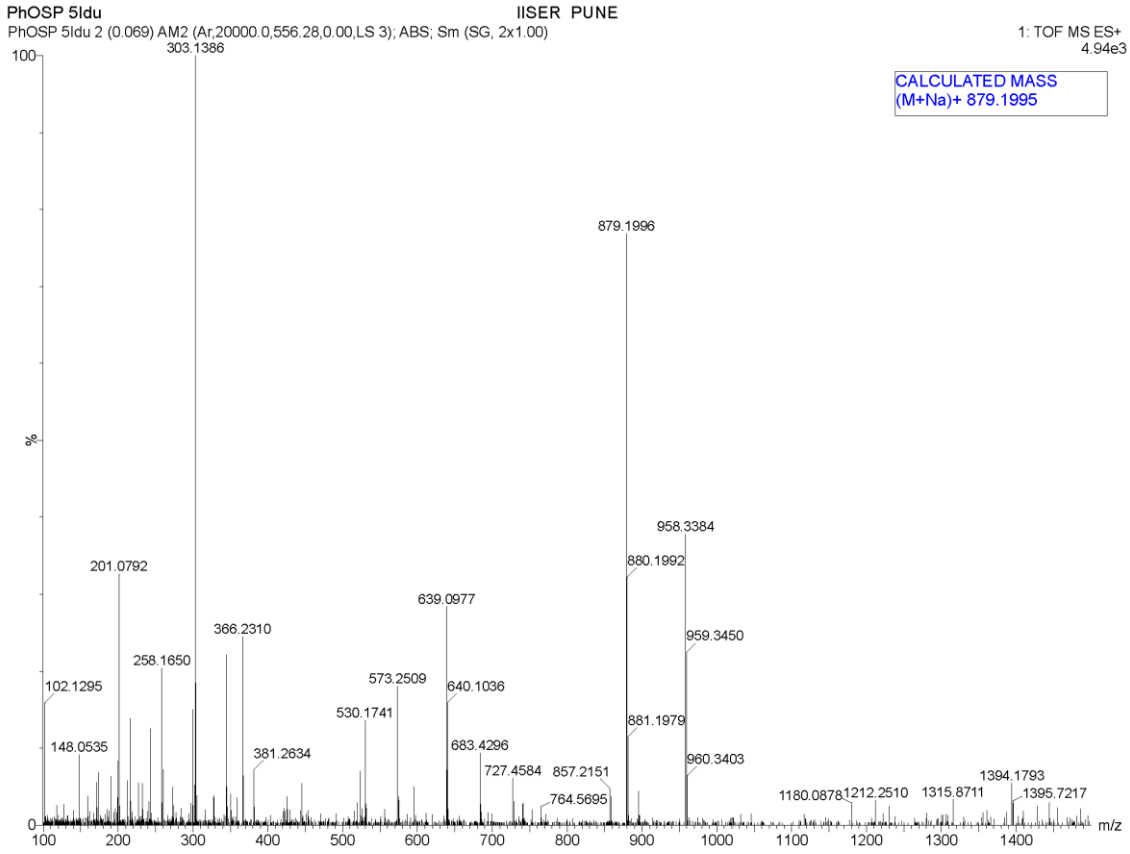

RP-HPLC chromatogram of PAGE purified IdU-modified DNA ONs **4**–**17** at 260 nm.

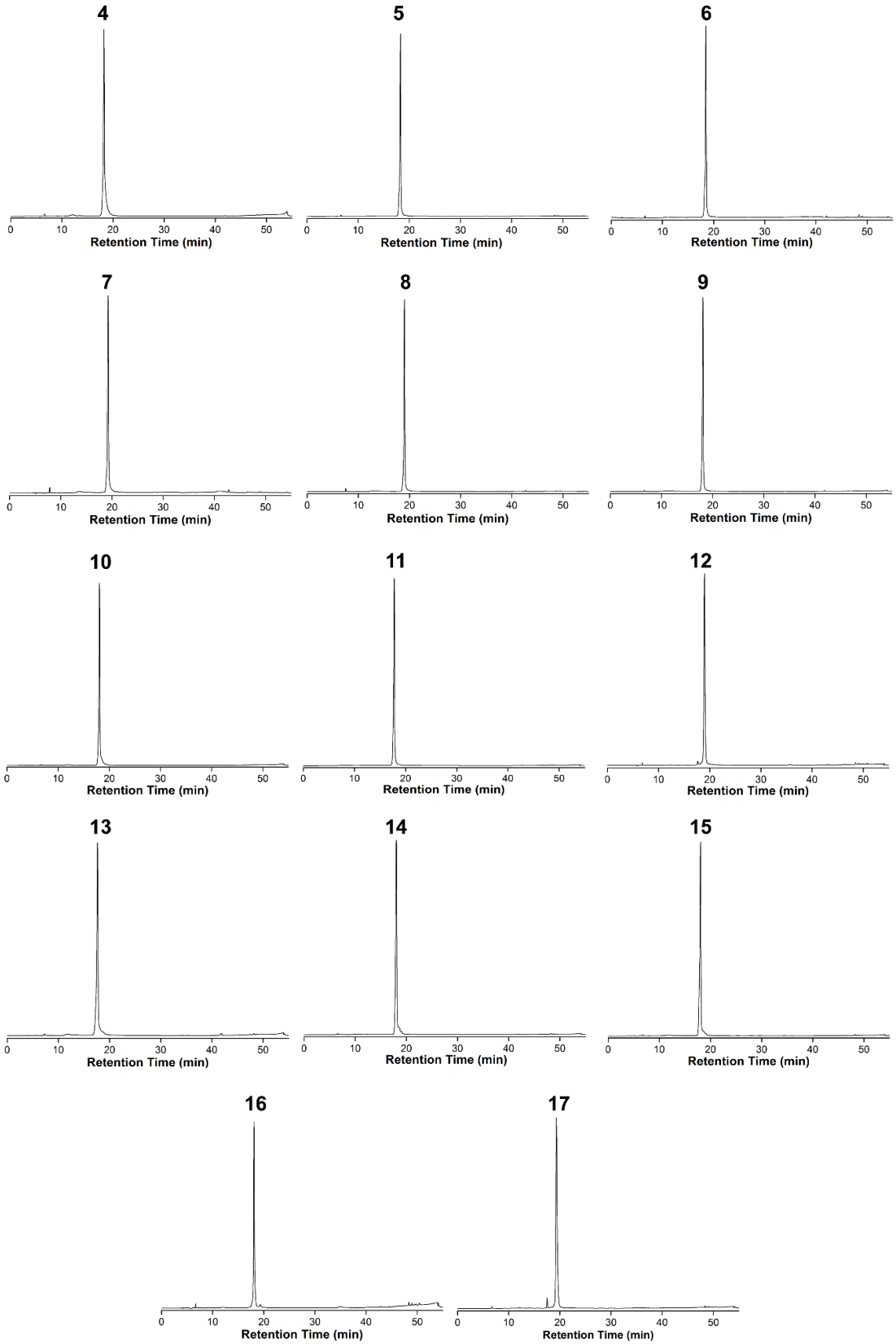

ESI-MS (-ve mode) spectra of IdU-modified H-Telo DNA ONs (**A**) **4**,(**B**) **5,** (**C**) **6**, (**F**) **9**; MALDI-TOF spectra of IdU-modified H-Telo DNA ONs (**D**)**7**, (**E**) **8**. See Table 3.1 for details.

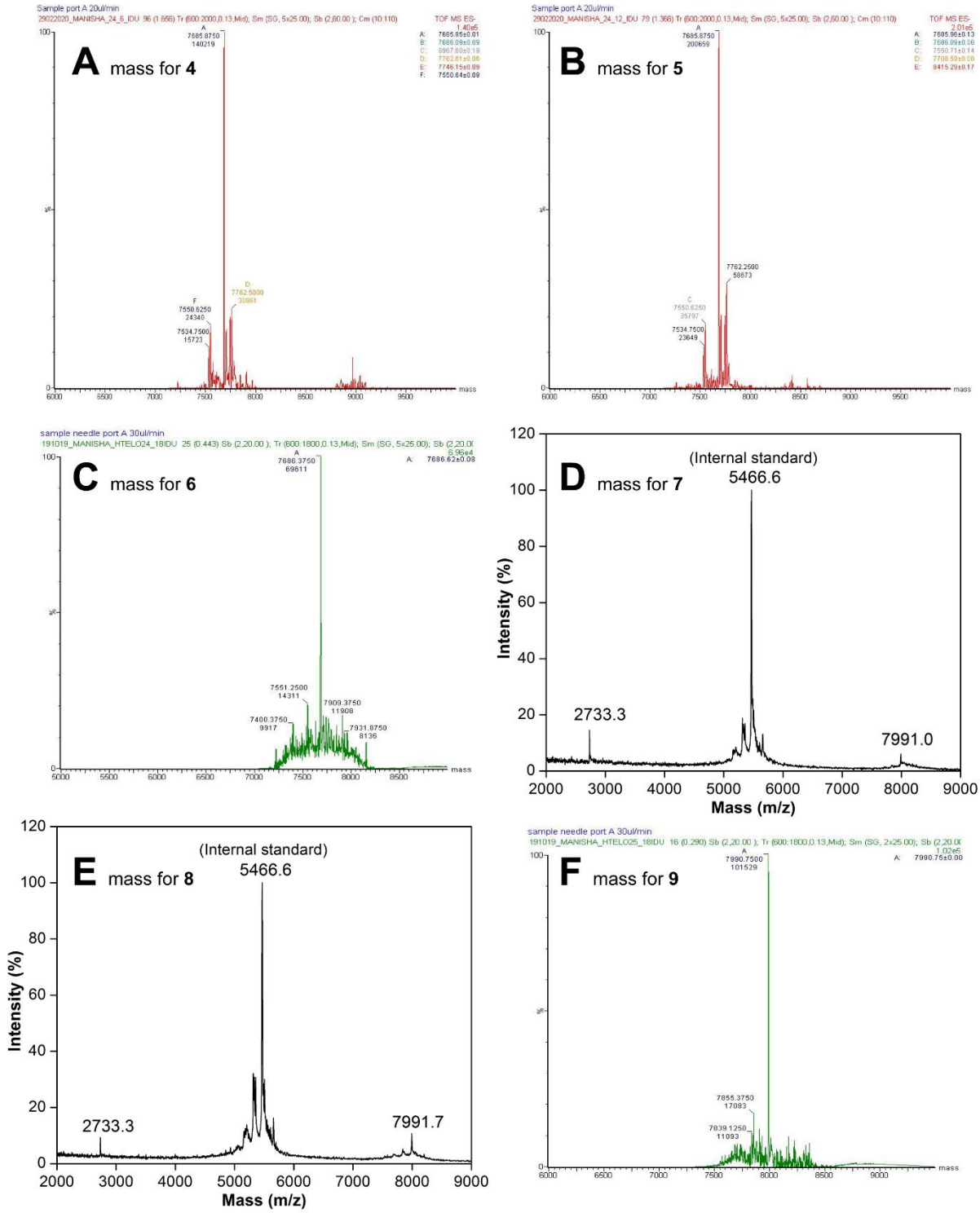

ESI-MS (-ve mode) spectra of IdU-modified H-Telo DNA ONs (**A**) **10**, (**D**) **13**;MALDI-TOF spectra of IdU-modified H-Telo DNA ONs (**B**)**11**, (**C**) **12**, (**E**) **14**,(**F**) **15**.See Table 3.1 for details.

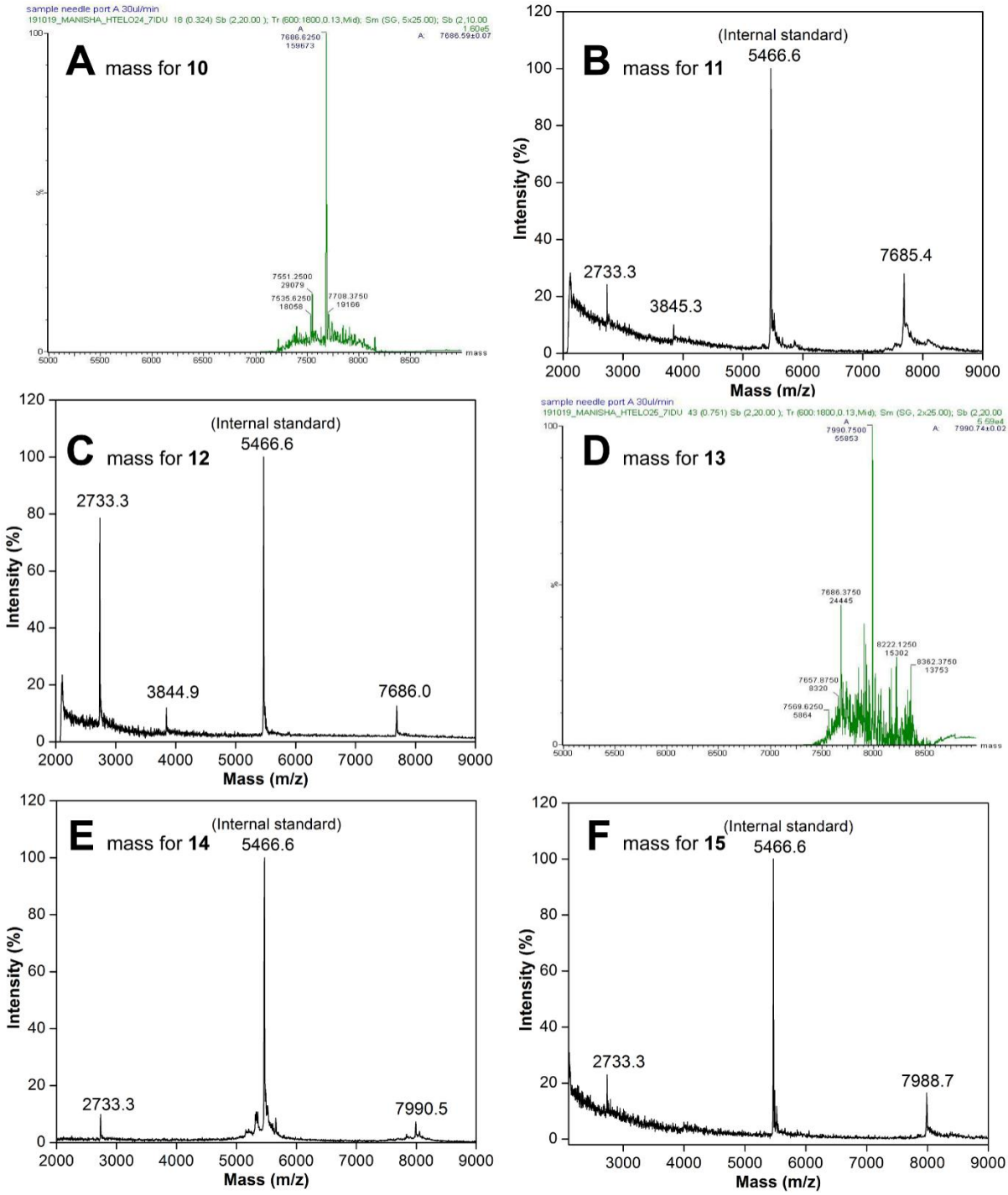

(A) ESI-MS (-ve mode) spectrum of IdU-modified H-TeloDNA ON**16**. **(B)** MALDI-TOF spectrum of IdU-modified H-TeloDNA ON **17**. See Table 3.1 for details.

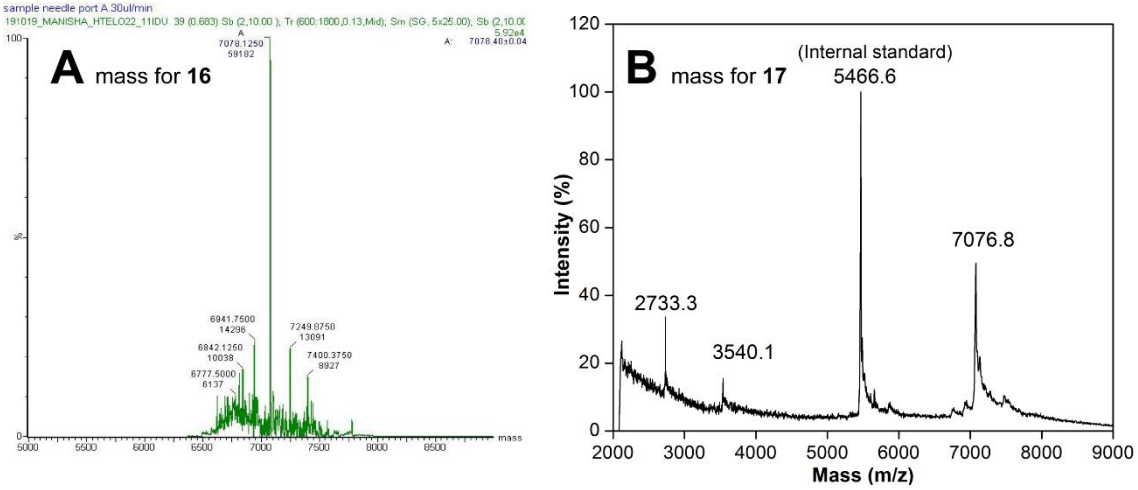

ESI-MS (-ve mode) spectra of BF-modified H-Telo DNA ONs (**A**) **4a**,(**B**) **5a**,(**C**) **6a**, (**D**) **7a**, (**E**) **8**, (F) **9a**.See Table 3.4 for details.

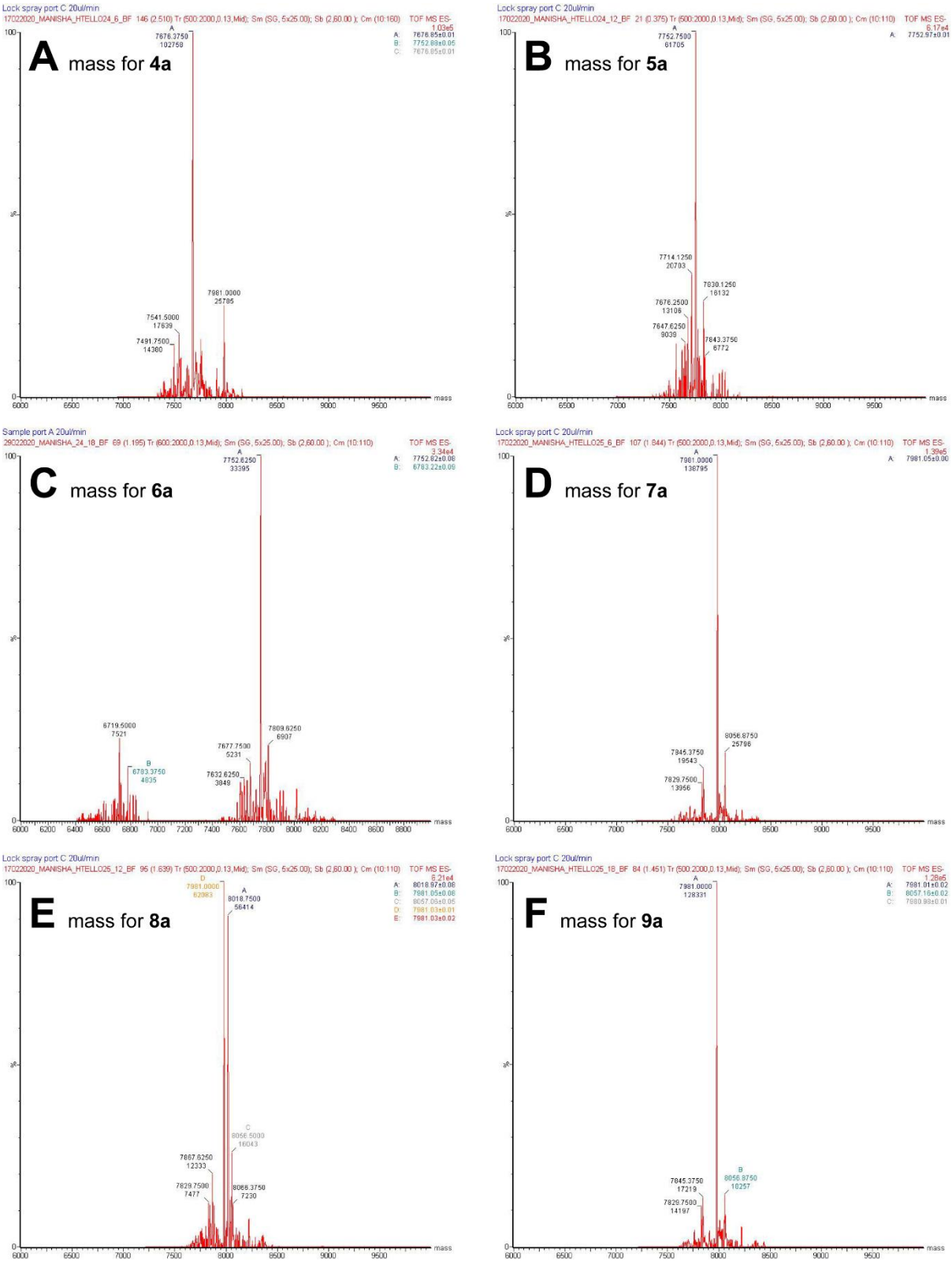

ESI-MS (-ve mode) spectra of BF-modified H-Telo DNA ONs (**A**) **10a**, (**D**) **13a**,(**E**) **14a**. MALDI-TOF spectra of BF-modified H-Telo DNA ONs (**B**) **11a**, (**C**) **12a**, (**F**) **15a**. See Table 3.4 for details.

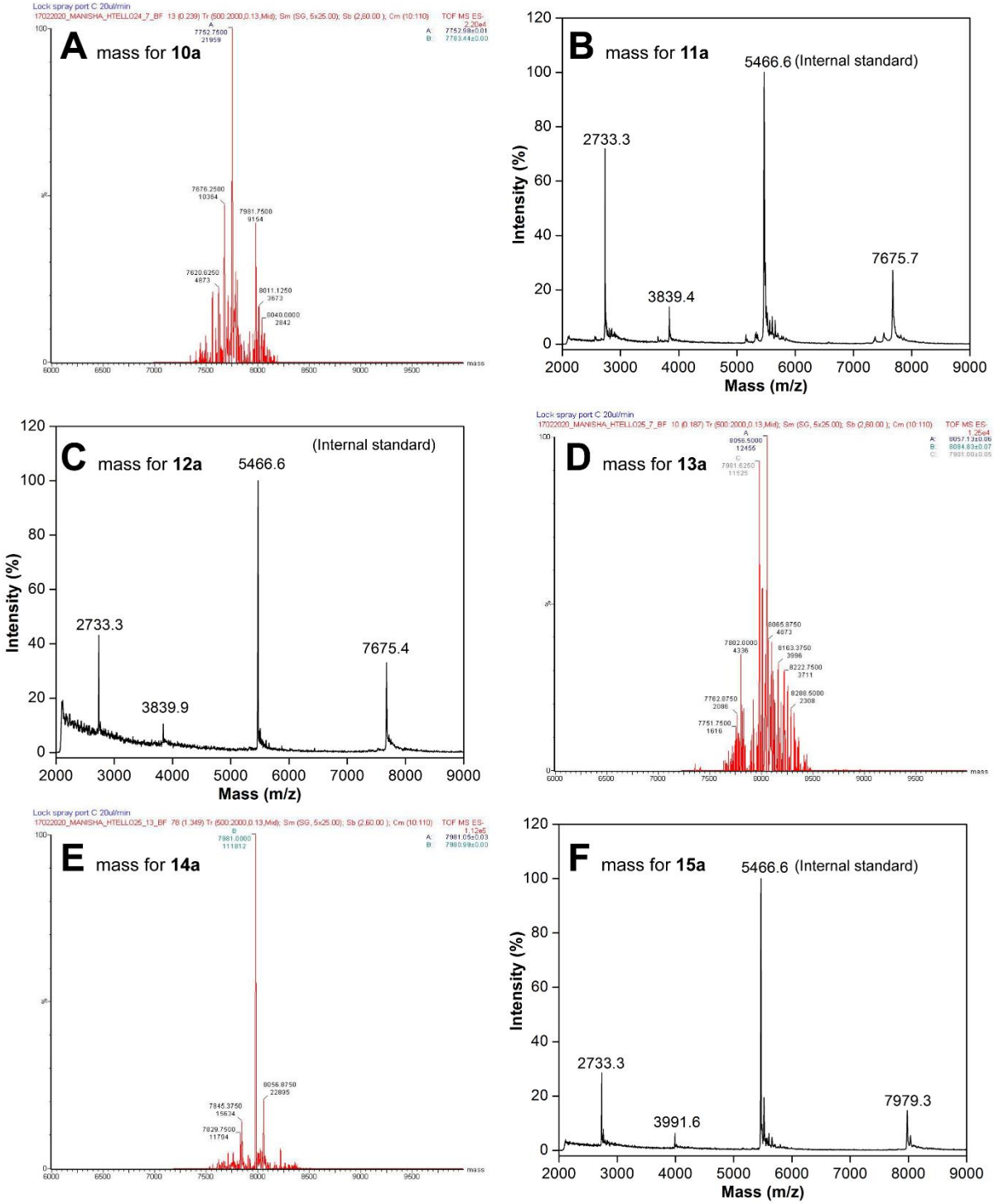

MALDI-TOF spectra of BF-modified H-Telo DNA ONs (**A**) **16a**, (**B**) **6a**.See Table 3.4 for details.

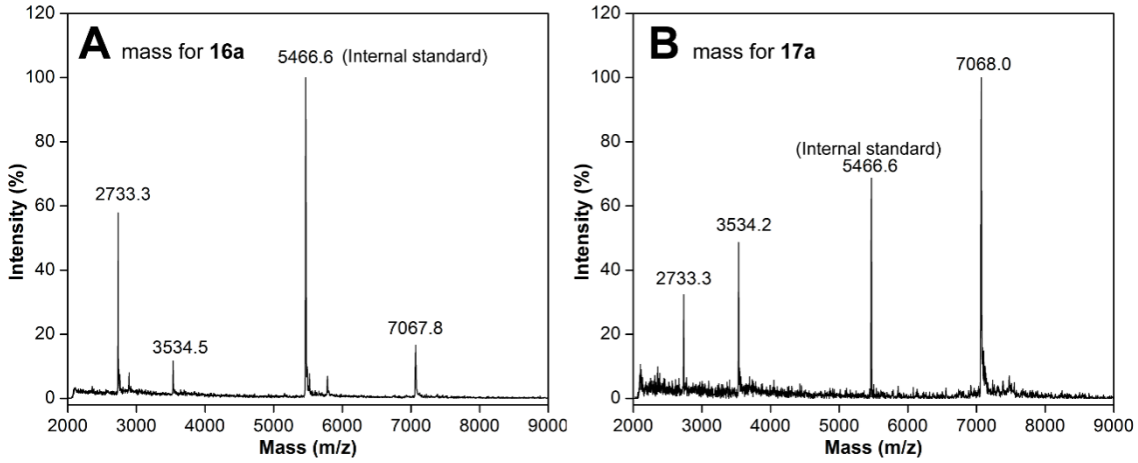

Chapter 4

Supramolecular Synthons Made of an Environment-Sensitive Fluorescent Nucleoside Exhibits Interesting Emission Properties Upon Self-Assembly

4.1 Introduction

Building blocks of nucleic acids such as nucleobase, nucleoside, nucleotides and their derivatives are desirable candidates for developing supramolecular self-assemblies as they retain their recognition feature and are easily scalable.[1] Among the nucleobases, guanine can form variety of self-assemblies because it has two hydrogen bonding faces, namely Watson-Crick and Hoogsteen (Figure 4.1A).[2–4] The most common self-assembly motifs of guanine unit are shown in Figure 1. In the absence of any cation, guanine assembles into G-ribbon I and G-ribbon II architecture (Figure 4.1B). Addition of cations such as K^+, Na^+ allows guanine to adopt planar G4-quartets, composed of four guanine bases, which are noncovalently linked together by eight intermolecular hydrogen bonds (Figure 4.1C).

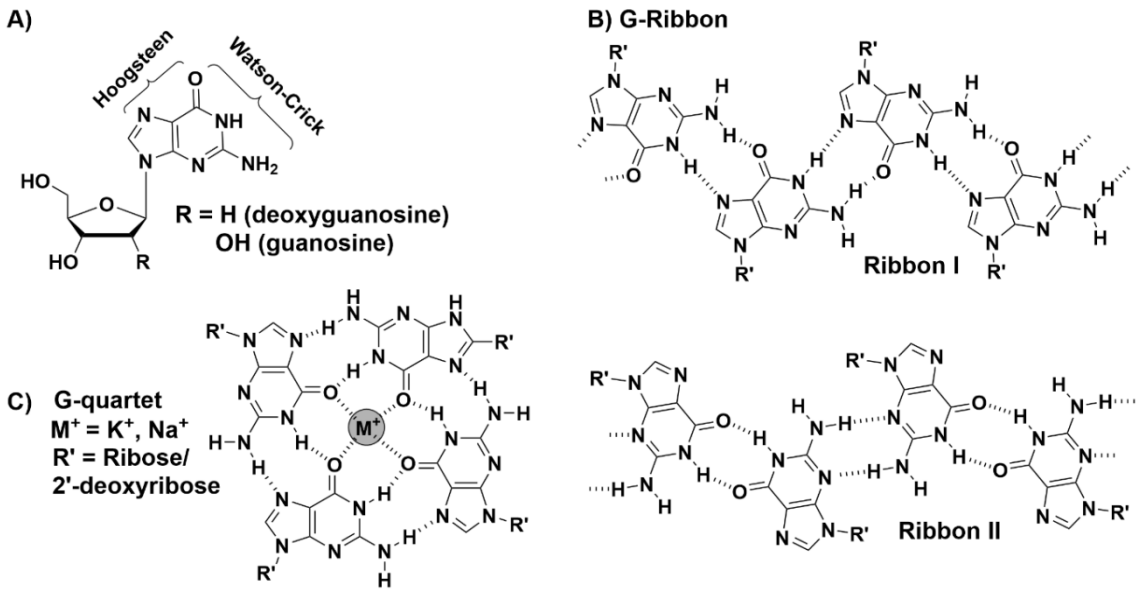

Figure 4.1. Structures of (**A**) guanosine and deoxyguanosine. (**B**) G-Ribbon type I and type II. (**C**) G-quartet.

While lot of work has been done on unsubstituted guanine,[4] sugar substituted lipophilic guanine derivatives have received much more attention in the supramolecular chemistry.[5,6] There are numerous reports where supramolecular behaviour of the lipophilic guanine

derivatives has been well explored in solution[7–9] as well as in gel state.[10–16] Lipophilic guanine derivatives with proper hydrophilic and hydrophobic balance form gel network even in the absence of added cations. Guanine and lipophilic guanine derivatives are especially attractive in the supramolecular field due to their potential applications in drug delivery,[17–20] nanotechnology,[21–24] synthetic ion channels[25–30] and so on.

In spite of the immense development in the area of guanine-based supramolecular self-assemblies, use of fluorescently modified lipophilic guanine derivatives in developing responsive fluorescent organogels has not been well explored. Attachment of aryl groups can be a convenient choice to develop such fluorescently modified synthons for constructing the fluorescent supramolecular assemblies, which can also provide an additional noncovalent interaction such as π–π stacking. To accomplish this, we envision to incorporate a suitable aryl moiety, which could impart fluorescence as well as offer the opportunity to modulate the self-assembly using external stimuli.

In chapter 2, we have gained an understanding of the power of palladium-mediated cross-coupling reaction to generate the environment-sensitive nucleoside analogs. Herein, we have used palladium-mediated cross-coupling reaction to develop a new fluorogenic nucleolipids containing environmentally-sensitive fluorescent deoxyguanosine nucleoside analogs. The fluorophore is based on a (*E*)-8-(2-(benzofuran-2-yl)vinyl)-guanine core (Figure 4.2), which serves as the head group and alkyl chain, attached at 3′-*O* and 5′-*O*-positions of the sugar serves as the lipophilic group. Here we have chosen to attach acyl, myristoyl and palmitoyl group to the sugar residue, which provides lipophilicity to the molecule. The fluorescent deoxyguanosine nucleolipid hinders the crystallization process in guanosine hydrogel, thereby facilitating the formation of a stable co-gel with modulated mechanical properties. Further, the responsiveness of fluorescent deoxyguanosine nucleolipids containing longer fatty acid chain (myristoyl and palmitoyl) was used to develop chemo-and thermo-responsive smart materials.

4.2 Design of fluorescent deoxyguanosine nucleolipids

Recently from our group, we have reported a fluorescent uridine based nucleolipid, which shows excellent supramolecular behavior.[31] Heterobicycles such as benzofuran and benzothiophene were attached at the C-5 position of uracil ring via rotatable aryl-aryl bond, which upon self-assembly show aggregation-induced enhancement in fluorescence. However, such a fluorescent environment-sensitive moiety was not employed in case of other

nucleosides such as deoxyguanosine. In order to address this, we have envisioned to attach 2-vinylbenzofuran moiety at the C-8 position of 2′-deoxyguanosine. We have taken advantage of the power of Pd-mediated Suzuki–Miyaura cross-coupling reaction to develop environment-sensitive fluorescent deoxyguanosine nucleolipids (Figure 4.2). Attachment of aryl moiety could impart fluorescence properties and additional π–π stacking interaction without affecting the Watson-Crick H-bonding of the native nucleoside. Coupling of various fatty acids at 3′-*O*- and 5′-*O*-positions of 2′-deoxyguanosine could facilitate the hydrophobic interaction during the self-assembly process. Interestingly, the presence of a trans double bond (circled in pink color) could provide an extra handle to control the self-assembly process by using light as an external stimulus.

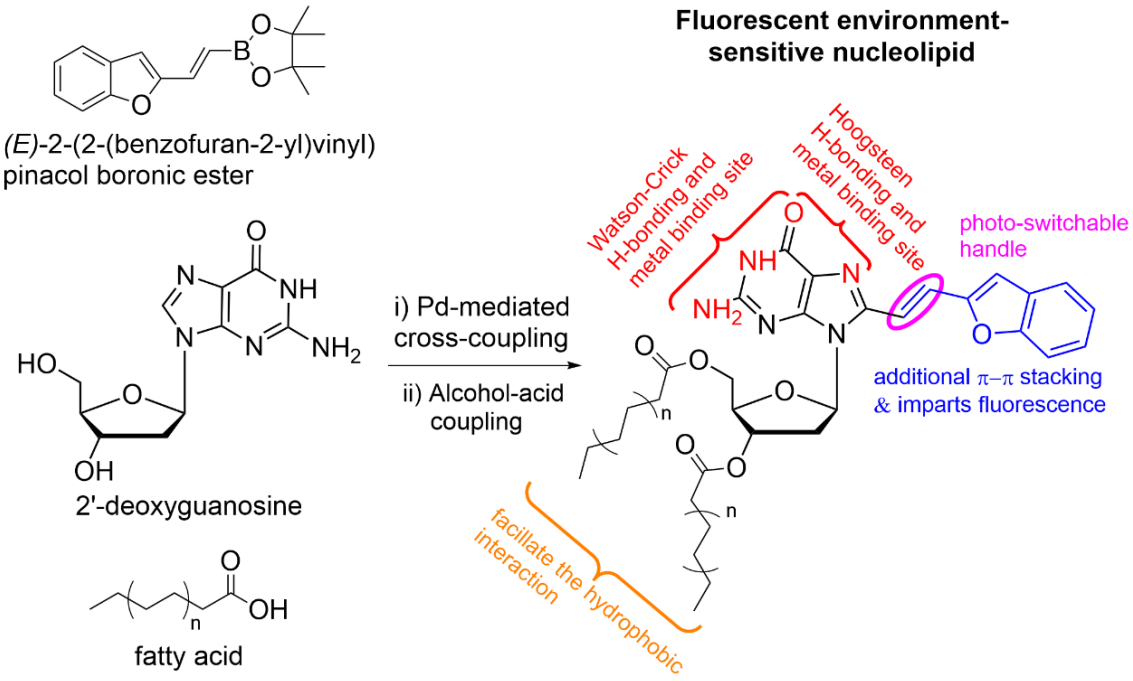

Figure 4.2. Design of self-assembling fluorescent deoxyguanosine nucleolipid.

4.3 Results and discussion

4.3.1 Synthesis and characterization of lipophilic derivatives of (E) 8-(2-(benzofuran-2-yl)vinyl)-2′-deoxyguanosine: Synthesis of the lipophilic derivatives of (*E*) 8-(2-(benzofuran-2-yl)vinyl)-2′-deoxyguanosine (**4**–**5**) was performed in two steps from 8-bromo-2′-deoxyguanosine **1** (Scheme 4.1 and 4.2). Fluorescent nucleoside **3** (trans BFVdG) was prepared by Suzuki–Miyaura cross-coupling reaction between 8-bromo-2′-deoxyguanosine and (*E*)-2-(2-(benzofuran-2-yl)vinyl) pinacol boronic ester (**2**)[32] using $Pd(OAc)_2$ and water-

soluble TPPTS ligand (Scheme 4.1). Further, 3′ and 5′ hydroxyl groups of the sugar residue of nucleoside **3** were reacted with acetic anhydride to yield the acylated product OAcBFVdG (**4**) in good yields. To synthesise lipophilic deoxyguanosines containing longer alkyl chains (**5** and **6**), the hydroxyl groups of the sugar residue of nucleoside **3** were coupled with myristic and palmitic acid using EDC·HCl to yield OmyrBFVdG (**5**) and OpalBFVdG **(6)** (Scheme 4.2). The trans configuration of the double bond in the fluorescent nucleoside derivatives (**3**–**6**) was confirmed by determining the coupling constant between the alkene protons (J = 15.2–15.6 Hz, see ^{1}H NMR data in the experimental section).

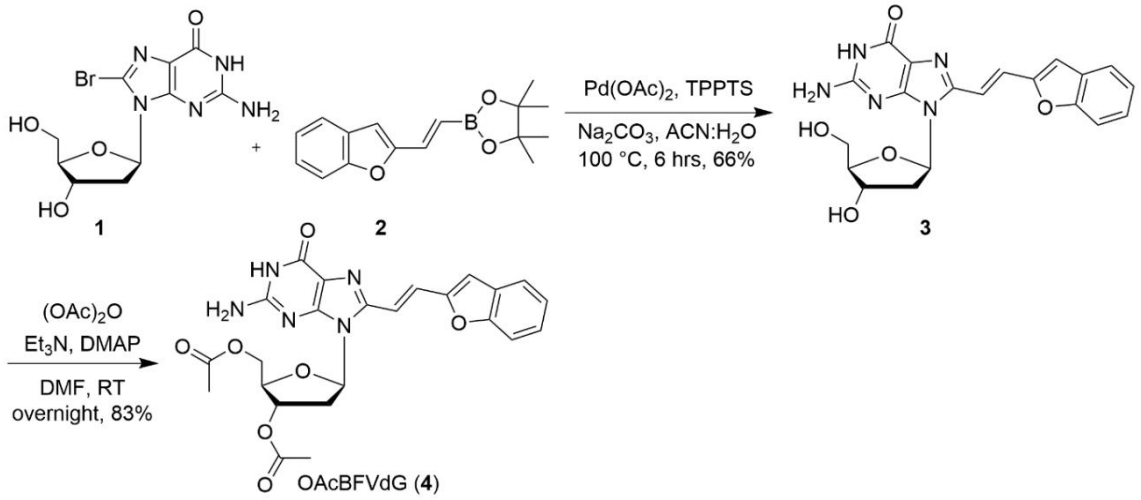

Scheme 4.1. Synthesis of (*E*)-diacetyl 8-(2-(benzofuran-2-yl)vinyl)-2′-dG (OAcBFVdG, **4**), TPPTS = triphenylphosphan-3,3′,3″-trisulfonate; DMAP = 4-dimethylaminopyridine.

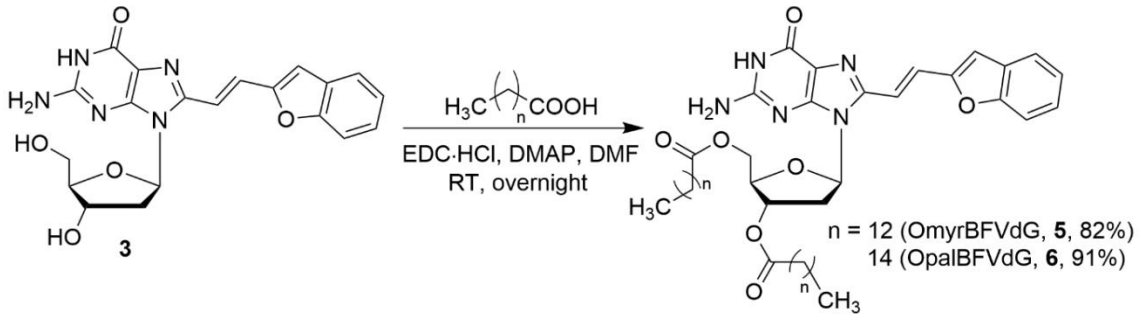

Scheme 4.2. Synthesis of lipophilic derivatives of 8-(2-(benzofuran-2-yl)vinyl)-2′-dG (OmyrBFVdG, **5** and OpalBFVdG, **6**) EDC·HCl = 1-(3-Dimethylaminopropyl)-3-ethylcarbodiimide hydrochloride; DMF = *N*,*N*-dimethylformamide.

Modification at the C-8 position of guanine nucleoside results in anti to syn conformational change about the glycosidic bond (N9-C1′).[33–36] This shift in the conformation is because of the steric clash between the substituent at the C-8 position and 5′

OH group of the sugar residue. This conformational change can be characterized by using NMR spectroscopy. An anti to syn conformational change results in a downfield shift of the ^{1}H2′ signal, but an upfield shift of the ^{13}C2′ signal as compared to that of a native nucleoside.[37,38] According to this analysis, compound **3** and **4** prefers syn conformation (Figure 4.3 and 4.4, Table 4.1 and 4.2). Furthermore, 2D NOESY analysis of compounds **3** and **4** shows, strong cross peak between anomeric proton (H1′) and vinyl proton (Ha) (see appendix III for 2D NMR spectra). These results further confirm the syn glycosidic conformation of **3** and **4**.

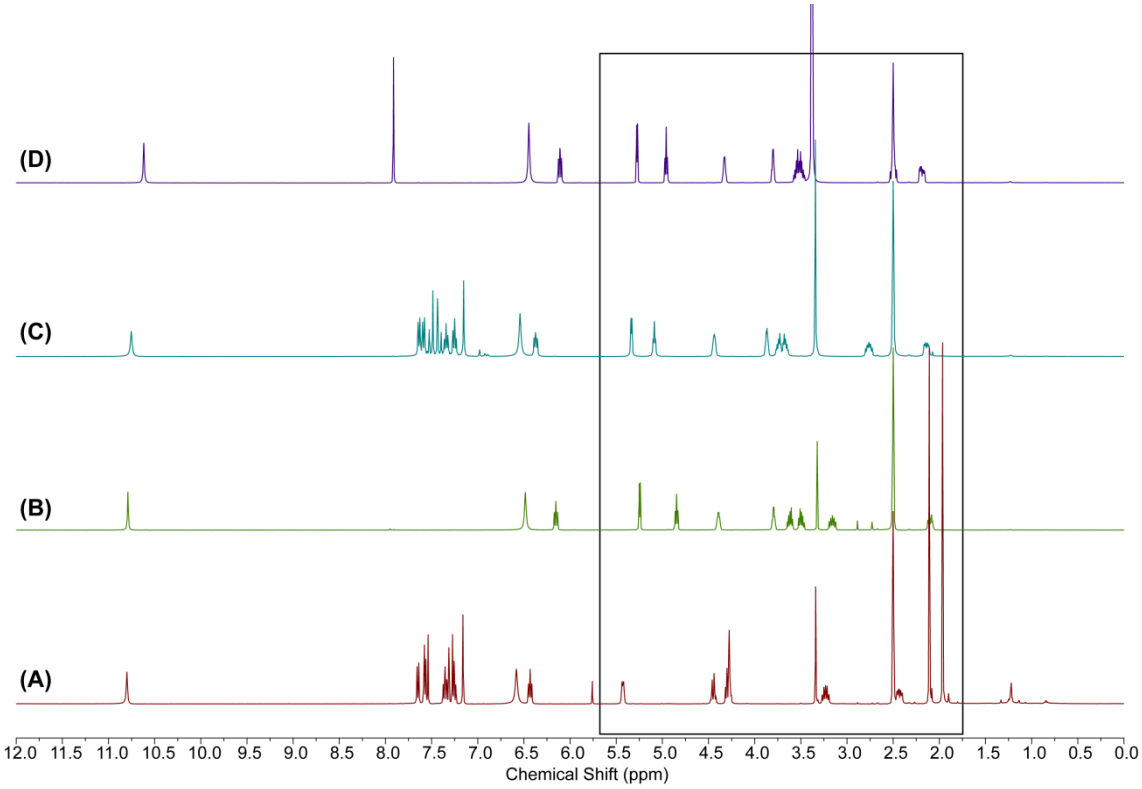

Figure 4.3. ^{1}H NMR spectra for (**A**) (*E*)-diacetyl-8-(2-(benzofuran-2-yl)vinyl)-2′-deoxyguanosine (OAcBFVdG, **4**), **(B)** 8-bromo-2′-deoxyguanosine (BrdG), **(C)** (*E*) 8-(2-(benzofuran-2-yl)vinyl)-2′-deoxyguanosine (*trans* BFVdG, **3**), (**D**) 2′-deoxyguanosine (dG).

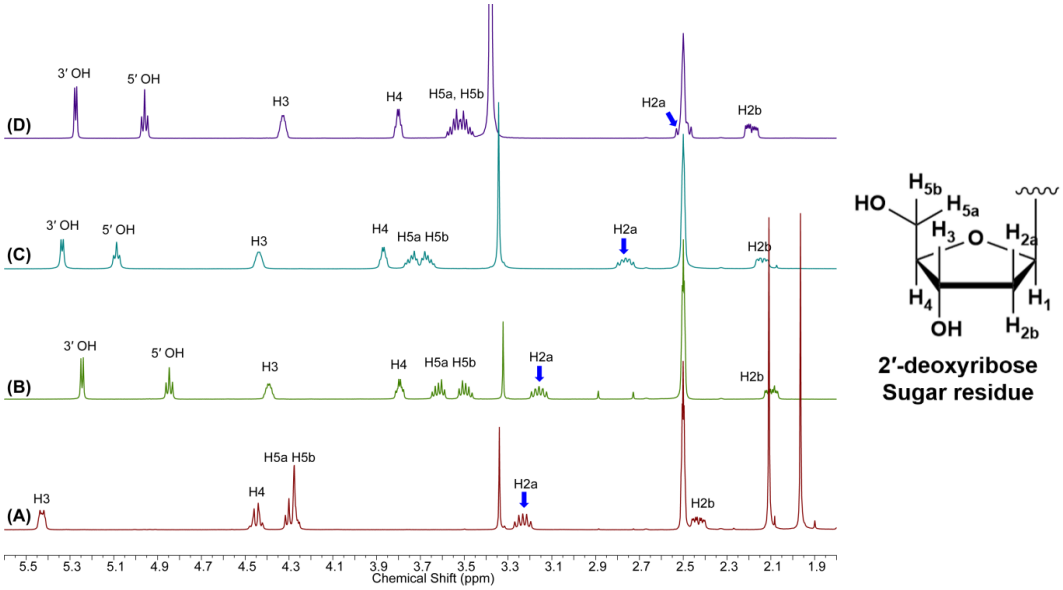

Figure 4.4. Partial ^{1}H NMR spectra (**A**) (*E*)-diacetyl-8-(2-(benzofuran-2-yl)vinyl)-2′-deoxyguanosine (OAcBFVdG, **4**), **(B)** 8-bromo-2′-deoxyguanosine (BrdG), **(C)** (*E*) 8-(2-(benzofuran-2-yl)vinyl)-2′-deoxyguanosine (*trans* BFVdG, **3**), (**D**) 2′-deoxyguanosine (dG). Blue arrow represents H2a proton of sugar residue, which is getting more downfield in case of compounds **3**, **4** and BrdG compared to native nucleoside dG.

Table 4.1. ^{1}H NMR data for compounds **3**, **4**, dG and BrdG.

Compound	N1-H	Vinyl-H	Vinyl-H	N2-H	1′-H	3′-H	4′-H	5′-H	5′-H	2′-H	2′-H
dG	10.62	-	-	6.45	6.11	4.32	3.80	3.55	3.49	2.50	2.18
3	10.75	7.50	7.41	6.54	6.37	4.44	3.87	3.74	3.67	2.76	2.13
BrdG	10.79	-	-	6.48	6.15	4.39	3.79	3.62	3.49	3.16	2.09
4	10.81	7.55	7.29	6.58	6.43	5.43	4.44	4.30	4.27	3.23	2.44

Table 4.2. ^{13}C NMR data for compounds **3**, **4**, dG and BrdG.

Compound	C4′	C1′	C3′	C5′	C2′
dG	87.6	82.6	70.8	61.8	39.6
3	87.6	82.9	70.8	61.8	39.0
BrdG	87.9	85.1	71.0	62.1	36.5
4	83.3	81.5	74.3	63.7	35.2

Proton and carbon signals are in ppm. Spectra were standardized with respect to d_6-DMSO.

4.3.2 Self-assembly of OAcBFVdG (4) in solution

The self-assembly behaviour of acetylated BFVdG **4** was studied by using ^{1}H NMR in deuterated solvents such as DMSO and chloroform at two different concentration. In d_6-DMSO at 5 mM and 30 mM concentration compound **4** shows sharp and well-defined signals for all the protons, which is indicative of the presence of monomeric form (Figure 4.5A and 4.5B).[39,40] Similarly, compound **4** in $CDCl_3$ at 5 mM concentration is in the monomeric form (Figure 4.5C). However, at higher concentration, amino N2-H protons of compound **4**, which resonates at 5.94 ppm in 5 mM solution, shift downfield to 6.43 ppm in a 30 mM solution, (compare figure 4.5C and 4.5D). This shows that amino N2-H protons are hydrogen-bonded only at higher concentration and forms loosely bounded aggregates.[41,42] It is known that guanosine derivatives in the presence of metal ions such as K^+, facilitate the formation of stacked G-tetrad such as octamers, hexadecamers, and higher-ordered aggregates in organic solvents.[43-46] When a weighed amount of KI (~20 equiv) is added to a $CDCl_3$ solution of **4** (5 and 30 mM), we observed a single sharp peak at 13.08 ppm corresponds to imino N1-H proton. The amino N2-H signal becomes unobservable broad at room temperature. Importantly, we did not observe the doubling of signals in the ^{1}H NMR, which is indicative of the formation of D4-symmetric octameric structure (Figure 4.5E, 4.5F, 4.6). This finding is consistent with previously reported literature for such an octameric structure, which eventually forms a columnar aggregate.[5,47]

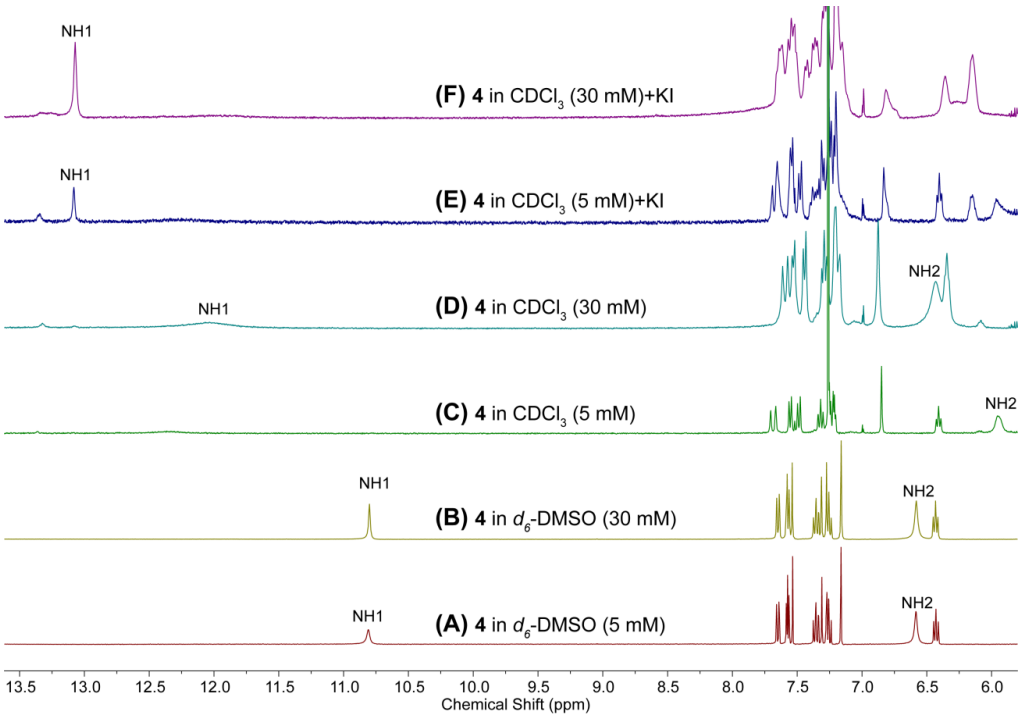

Figure 4.5. Partial ^{1}H NMR of OAcBFVdG **(4)** in different deuterated solvents solvent. **(A)** d_6-DMSO (5 mM). **(B)** d_4-MeOH-*d4* (5 mM). **(C)** $CDCl_3$ (5 mM) **(D)** $CDCl_3$ (30 mM) **(E)** $CDCl_3$ (5 mM) + KI **(F)** $CDCl_3$ (30 mM) + KI. ~ 20 equivalent of KI is used in this study and sample was equilibrated for 4 h at room temperature.

Table 4.3. ^{1}H NMR (400 MHz) chemical shifts (ppm) for solutions of **4** in different deuterated solvents at room temperature (See the figure 4.5 for details).

Solvent	Concentration of **4** (mM)	NH(1) ppm	NH(2) ppm
d_6-DMSO	5	10.81	6.58
d_6-DMSO	30	10.80	6.58
$CDCl_3$	5	n.d	5.94
$CDCl_3$	30	12.07 (br.s)	6.43
$CDCl_3$ + KI	5	13.08	n.a.
$CDCl_3$ + KI	30	13.08	n.a.

Further, the NMR spectrum of **4** (30 mM) in $CDCl_3$ was recorded as a function of increasing concentration of KI, which resulted in the gradual formation of the D4-symmetric octameric structure (Figure 4.6 and Figure 4.7).

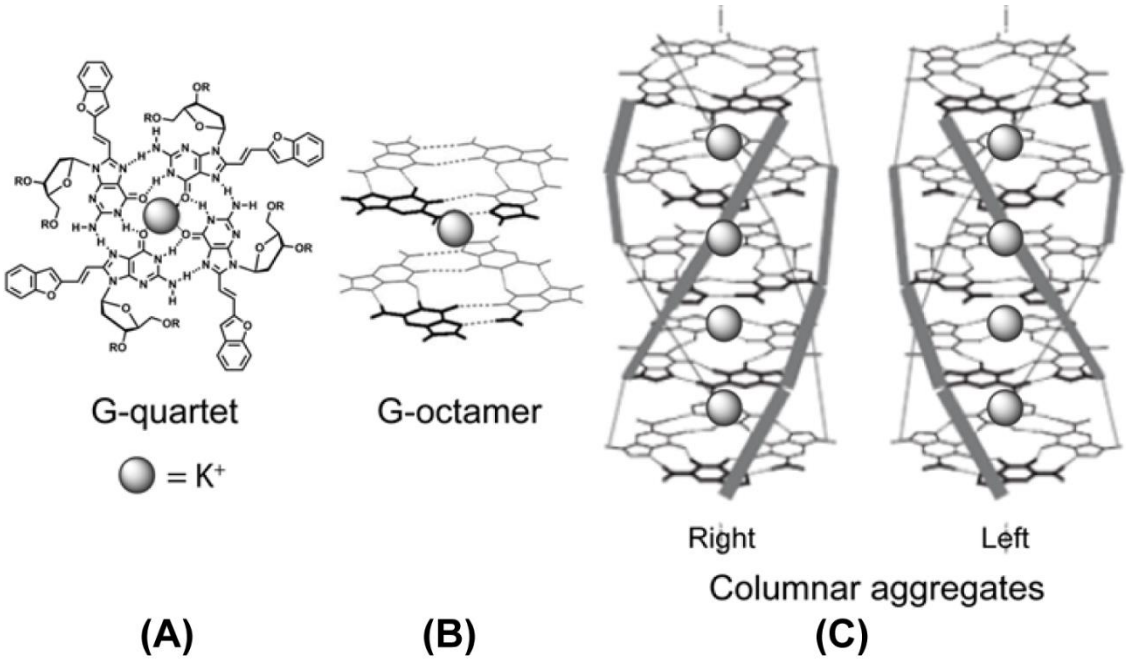

Figure 4.6. Self-assembly of lipophilic guanine derivatives. **(A)** The G-quartet formed by **4**, (**B**) Representation ofthe octameric $G8{\cdot}M^+$, (**C**) polymeric chiral columnar aggregates $(G4{\cdot}M^+)_n$ formed by a stack of G-quartets held together by K^+ (shadowed spheres).

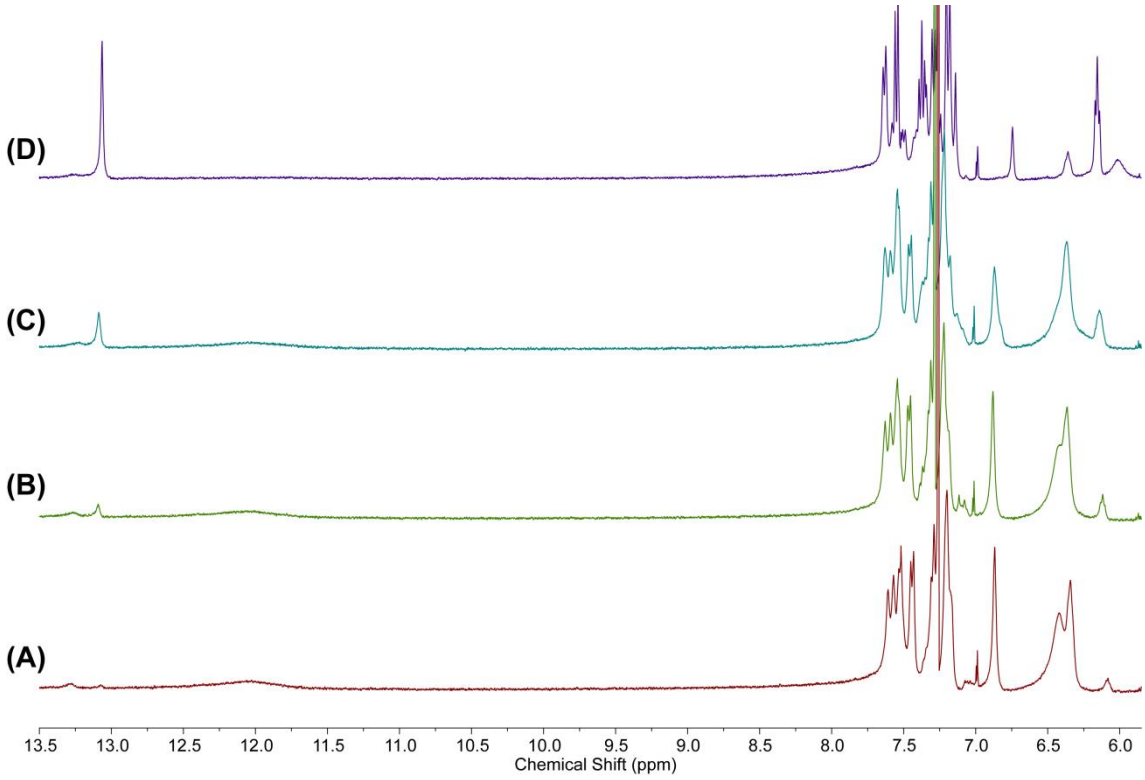

Figure 4.7. Partial ^{1}H NMR of OAcBFVdG (**4**,30 mM**)** with increase in molar equivalent of potassium iodide (KI) in $CDCl_3$. **(A)** 0, **(B)** 0.13, (**C**) 0.5, (**D**) 2. Each sample was equilibrated for 4 h at room temperature.

CD technique is ideal for following the process of the association from the isolated molecules to the formation of supramolecular aggregate, and also it allows the determination of the handedness of the cholesteric superhelix.[48–51] We have performed CD analysis of compound **4** in chloroform at two different concentration. Compound **4** at 5 mM concentration shows a positive peak around 420 nm and a weak negative peak around 410 nm. While at 30 mM concentration, it shows the negative peak at 440 nm and weak positive peak at 430 nm (Figure 4.8A). This shows that compound **4** is possibly in a random assembled state as seen in 1H NMR (Figure 4.5).[41] When KI was added to a solution of compound **4 (**5 mM and 30 mM**)** in chloroform, the spectrum gradually changes to a much stronger monosignate spectrum which is characteristic of the cholesteric phase (Figure 4.8B).[52,53] A cholesteric phase is formed by the chiral arrangement of chiral columnar aggregates (Figure 4.6C).[54] Interestingly, compound **4** at 5 mM and 30 mM concentration in the presence of KI shows a strong monosignate positive peak (430 nm), and strong monosignate negative peak (440 nm), respectively. This indicates that, in presence of KI, compound **4** at 5 mM shows the formation of right-handed cholesteric phase, whereas at 30

mM it adopts left-handed cholesteric phase (Figure 4.8B). These results are quite surprising to us, as changing the concentration of 5 mM to 30 mM, we observed change in the handedness of the cholesteric phase, from right-handed to left-handed.

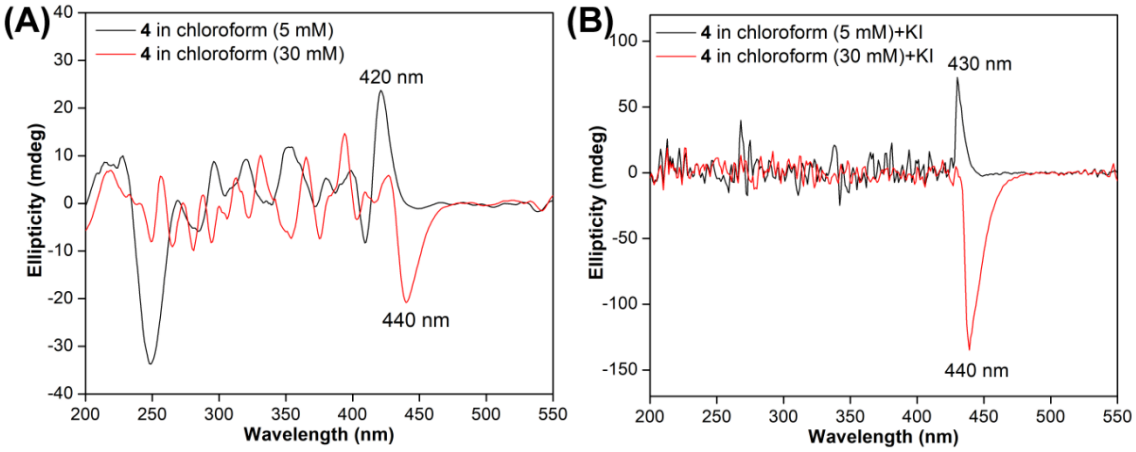

Figure 4.8. CD spectra for compound **4**. (**A**) at 5 and 30 mM in chloroform. (**B**) at 5 and 30 mM in chloroform in the presence of 20 equivalent of potassium iodide (KI). Spectra were collected from 500 to 220 nm on a Jasco J-815 CD spectrometer using 1 nm bandwidth at 25°C. Experiments were performed in duplicate wherein each spectrum was an average of three scans. The spectrum of chloroform without lipophilic deoxyguanosine and KI was subtracted from all the sample spectra.

4.3.3 Addition of OAcBFVdG (4) stabilizes guanosine gel

Despite the long history of guanosine hydrogels, the major limitation associated with such gels is their poor stability.[55,56] For example, crystallization occurs over a period of time (24 h), which collapses the gel (Figure 4.9). This crystallization happens because the gel-forming assemblies are generally kinetically trapped and are not the thermodynamically trapped inside the gel network. Addressing this drawback is very important to advance the utility of guanosine-based hydrogel gels for biomedical and material applications. In this context, non-gelling additives (e.g., acylated guanosine) have been used to prevent the crystallization process and hence, increase the stability of the gel or even provide additional functional properties.[57] Therefore, we hypothesized that mixing guanosine with OAcBFVdG**4**, which has the same recognition feature of the native base could provide a heterogeneity to disfavour the crystallization while still allows the formation of supramolecular self-assembly for gelation to take place.

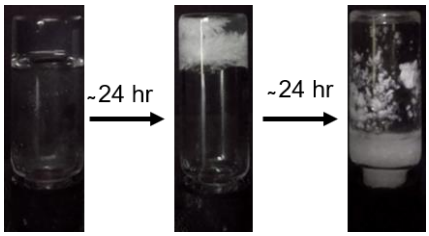

Figure 4.9. Picture showing the crystallization process in guanosine hydrogel (2 wt%).

Fluorescent guanosine derivative **4** does not show any gelation ability in DMSO in the absence and presence of metal ions (K^+ and Na^+). However, it supports the formation of a stable gel when mixed with guanosine in the presence of 500 mM KCl. 35 wt% of non-gelator is the maximum concentration that results in a stable gel, and beyond this concentration, the gel collapses (Figure 4.10A, Table 4.4). It is important to mention here that even in the gel state, we could observe fluorescence, and the gel was stable for few months (Figure 4.10B).

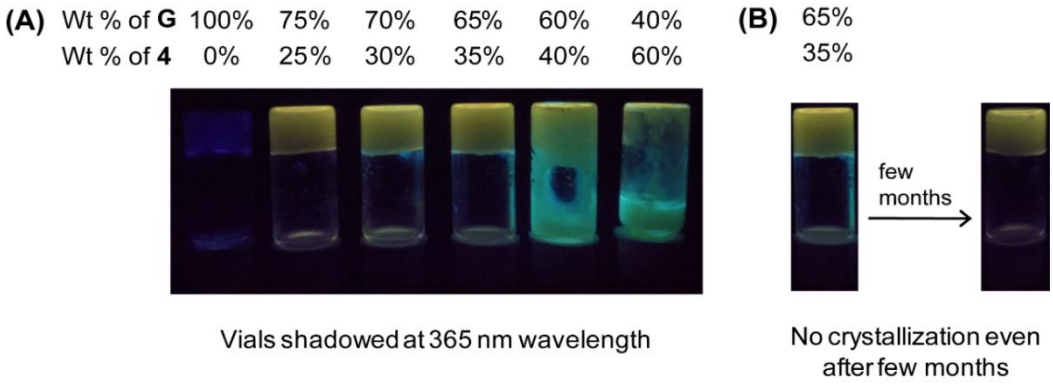

Figure 4.10. (**A**)Visual appearance of 2 wt% co-gel made from varying ratios of OAcBFVdG (**4**) and Guanosine (G) in 500 mM potassium chloride (KCl). (**B**) Vial showing 2 wt% co-gel (35:65, **4**:G) is stable and no crystallization was observed after a few months.

Table 4.4. Amount of OAcBFVdG (**4**), guanosine, and DMSO:H_2O proportion required for co-gel formation.

Wt% of OAcBFVdG **(4)**	Wt% of guanosine **(G)**	v/v% of DMSO in H_2O
0	100	0 % DMSO in H_2O
25	75	40% DMSO in H_2O
30	70	50% DMSO in H_2O
35	65	50% DMSO in H_2O
40	60	60% DMSO in H_2O
60	40	60% DMSO in H_2O

Next, we checked the fluorescence of the co-gel in assembled and disassembled states**.** Interestingly, guanosine gel in the presence of 4, though exhibited a weak fluorescence, its emission maximum was markedly red-shifted (~510 nm, yellowish color) as compared to the free analog **4** (λ_{em} = 474 nm) (Figure 4.11). Expectedly, the mixture in solution state obtained by heating the gel displayed a significant enhancement in fluorescence intensity with a blue-shifted emission (λ_{em} = 474 nm**,** cyan color). It is well documented that guanosine quenches the fluorescence of several fluorophores. Hence, here we believe that the fluorescent additive **4** is involved in the formation of a fibrous gel network, which results in the quenching of fluorescence by guanosine and aggregation-induced quenching. However, it is not clear how the gel formed by this mixture shows significantly red-shifted emission.

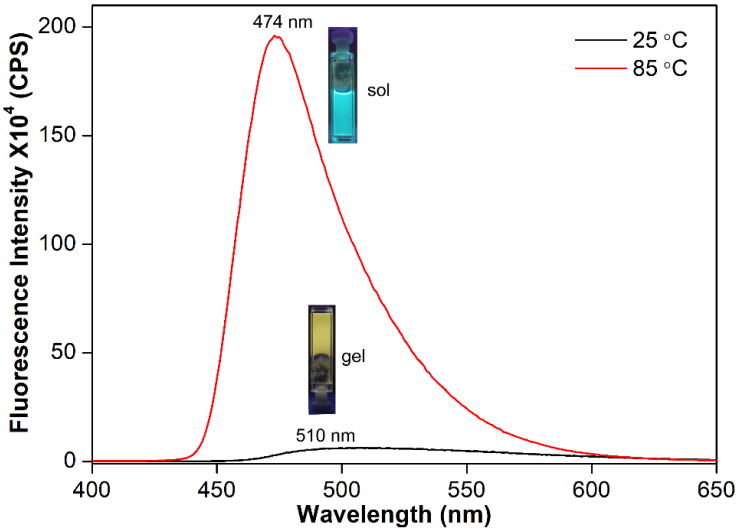

Figure 4.11. Fluorescence spectra for cogel made up 2 wt% gel (35:65, **4**:G) in DMSO:H_2O containing 500 mM KCl at two different temperature 25 °C (gel state, λ_{em} = 510 nm) 85 °C (sol state, λ_{em} = 474 nm). The samples were excited at 387 nm with an excitation and emission slit width of 1 nm and 2 nm, respectively.

4.3.4 Percentage of incorporation 4 in co-gel

Next, we wanted to find out the percentage of gelator guanosine and nongelator (**4**) into the cogel. For most of the LMWG, it can be expected that not all of the gelator molecules are incorporated into a gel network, and some may remain in the solution phase.[58,59] NMR spectroscopy can be used to measure the amount of each component, which is incorporated into the gel network during the assembly process.[60–63] When the components are in the solution phase, peaks correspond to 100% molecules can be observable by ^{1}H NMR. When the components start to assemble, molecules get incorporated into the gel network, and

broadening of the peaks can be observed in the gel state. Hence, the component which is not incorporated into the gel network can only be seen in the NMR spectrum. We have performed variable temperature ^{1}H NMR experiment with the expectation that higher temperature guanosine and **4** are in the sol phase should be observable by ^{1}H NMR. When the temperature is decreased from 85 °C to 25 °C in steps (with 10 °C increment, 15 min equilibration time) guanosine and **4** starts to assemble leaving behind some amount of components in sol phase, which can be detected by ^{1}H NMR (Figure 4.12).

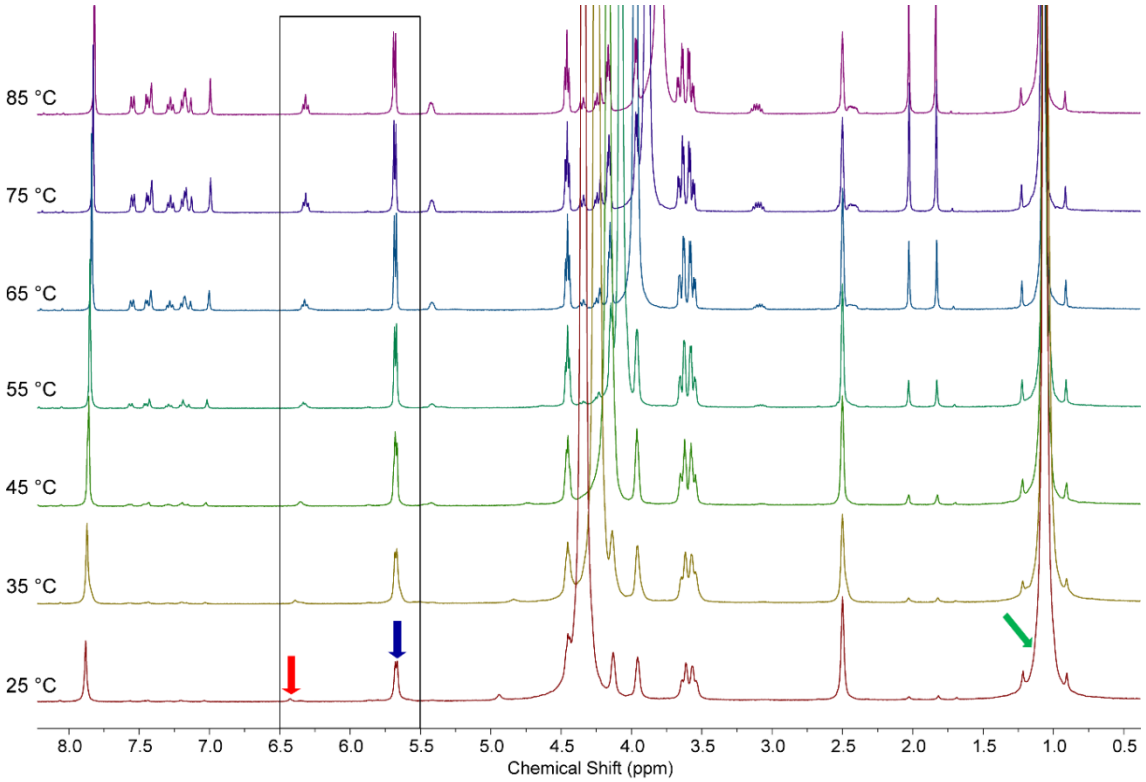

Figure 4.12. Variable temperature ^{1}H NMR spectrum of 2 wt% co-gel (35:65, **4**:G) in the presence of 500 mM KCl. The integration of the internal standard (t-BuOH) peak (green arrow) was compared with the integration of the G (blue arrow) and **4** (red arrow) anomeric proton (H1′) peaks to determine the percentage of incorporation of each component at the given temperature.

Table 4.5. Peak integration values for the variable temperature ^{1}H NMR experiment. t-BuOH is an internal standard.

Temp	**4** Peak integration	G Peak integration	t-BuOH peak integration	Percentage gelation according to **4**	Percentage gelation according to G
85 °C	0.096	0.354	9	0%(assumed)	0% (assumed)
75 °C	0.080	0.314	9	17%	11%
65 °C	0.047	0.301	9	50%	15%
55 °C	0.025	0.297	9	74%	16%
45 °C	0.016	0.291	9	83%	18%
35 °C	0.008	0.277	9	91%	22%
25 °C	0.004	0.197	9	96%	44%

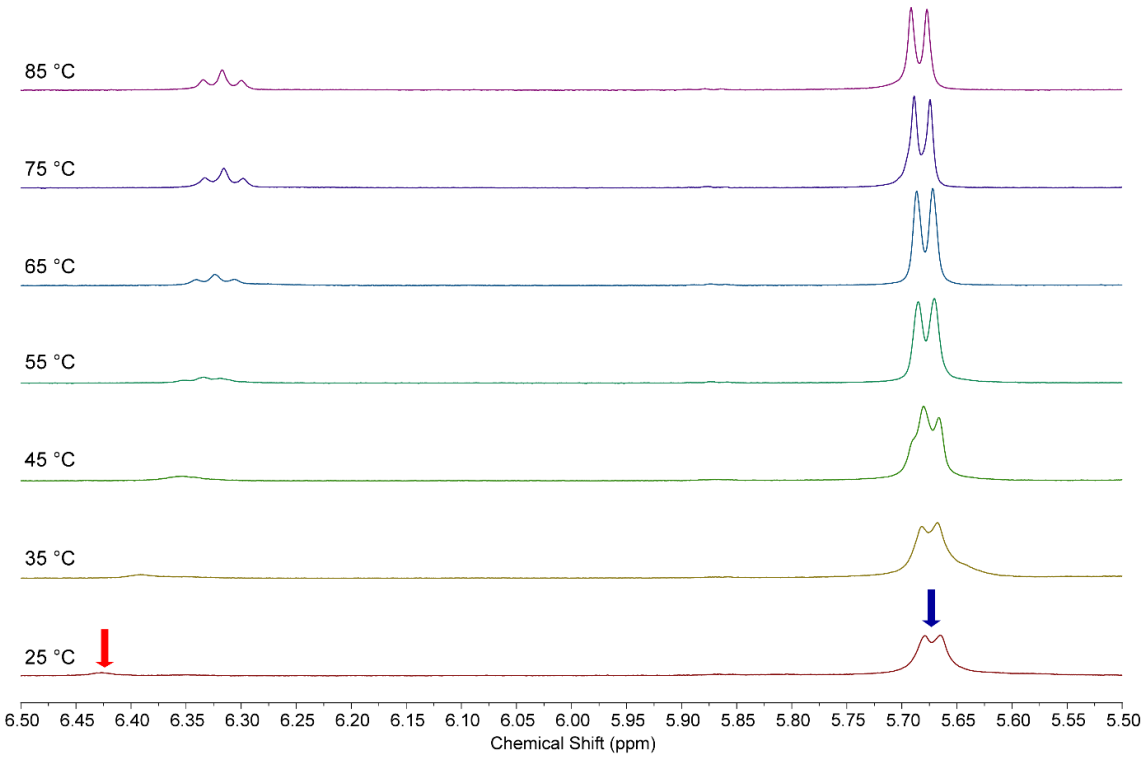

Figure 4.13. Zoomed in spectrum from boxed region in Figure 15. The integration of the internal standard (t-BuOH) peak was compared with the integration of the guanosine (blue arrow) and **4** (red arrow) anomeric proton (H1′) peaks to determine the percentage of gelation for the given temperature.

The amount of the components left in the sol phase was estimated using the integration of anomeric protons (H1′, 5.68 ppm for guanosine and 6.32 ppm for **4**) w.r.t. an internal tert-butyl alcohol standard (singlet at 1.07 ppm for three CH_3, Table 4.5, Figure 4.12 and 4.13). This experiment shows that at room temperature *ca.* 44% of available guanosine

and *ca.* 96% of available **4** participate in the gel network formation. This indicates that compound **4** is incorporated into the gel roughly two times as much as that of guanosine. Although **4** is non-gelator, still it has more incorporation efficiency into the gel network compared to guanosine. The reason behind the incorporation preference for the **4** is its preference to adopts a *syn*-conformation over the *anti* (Figure 4.14).[5,60] Previously, it is reported that *syn*-conformation helps in gelation process by forming the effective cation-templated H-bonded self-assembly of stacked G-quartet.[18,64] While *anti*-conformation of guanosine derivatives hinders the process of gelation. Hence, the *syn*-conformation of non-gelator **4** is helping guanosine to form the stable co-gel by forming the effective G-quartet.

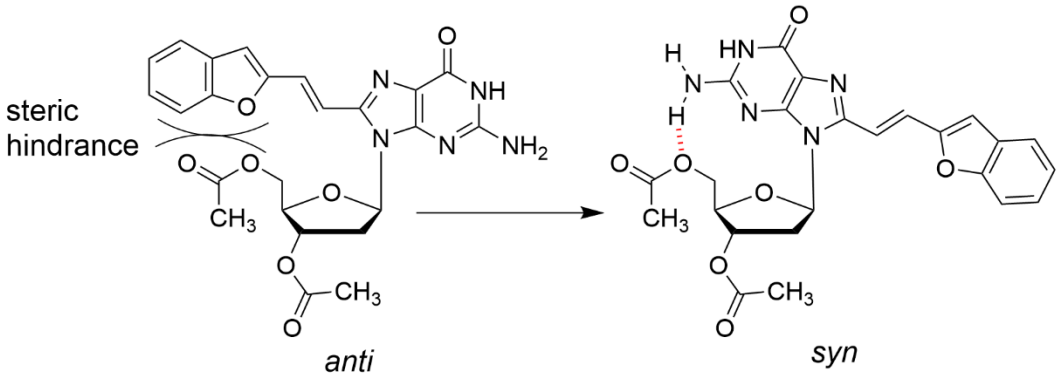

Figure 4.14. Conformational changes in 8-aryl deoxyguanosine from *anti* to *syn* due to steric clash between aryl at the C-8 position and acetyl moiety at 5′ position. A hydrogen bond between amino proton and oxygen of the acetyl group is shown in red dotted line. The steric effect between aryl and 5′ -OH group, and the possibility of a hydrogen bond between N2H and acetyl moiety are the main forces for molecule **4** to adopt the syn conformation.

4.3.5 Morphology of Guanosine and cogel

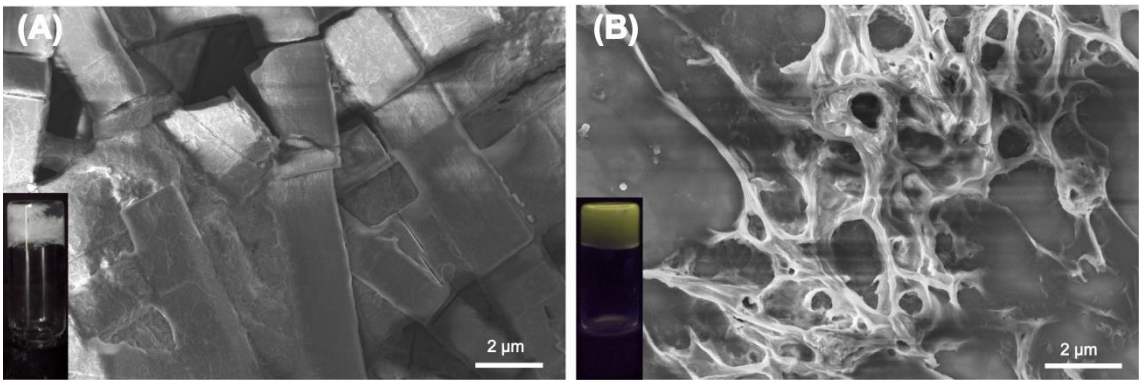

Figure 4.15. FESEM images of xerogel of (**A**) 2 wt% guanosine and (**B**) 2 wt% co-gel (35:65, **4**:G).

The morphological insight of guanosine gel and co-gel (35:65 wt%, G:**4**) was characterized using field emission scanning electron microscopy (FESEM). Xerogel of

guanosine and co-gel shows completely distinct morphology. Xerogel of guanosine itself crystallizes and form discontinuous thick sheets having a width around 1 µm (Figure 4.15A). However, in the presence of nongelator**4**, the formation of an interconnecting fibrous network was observed (Figure 4.15B). This dramatic change in morphology can occur on account of a change in the crystallization kinetics of native gel and thus forming the thermodynamically stable co-gel. Similar kind of changes in morphology after addition of non-gelator is observed in the previously reported literature.[65]

4.3.6 Rheological measurement of co-gel

Next, we investigated how varying ratios of co-monomers **4** and G affect the viscoelastic properties of the co-gel. Strain sweep experiment shows that these co-gels are stable till 1% of strain (Figure 4.16). We observed a drastic decrease in storage modulus (G') and loss modulus (G") with increase in the amount of nongelator **4** (25 to 40 wt%). It is possible that the tetrads formed by heterogeneous combination of guanosine and acetylated guanosine analog **4** do not stack efficiently on each other and not support long range ordering resulting in fibrous gel network with lower mechanical strength.[60,61,66] This observation is also in line with the FESEM images of xerogels made of guanosine and a mixture of guanosine and **4**.

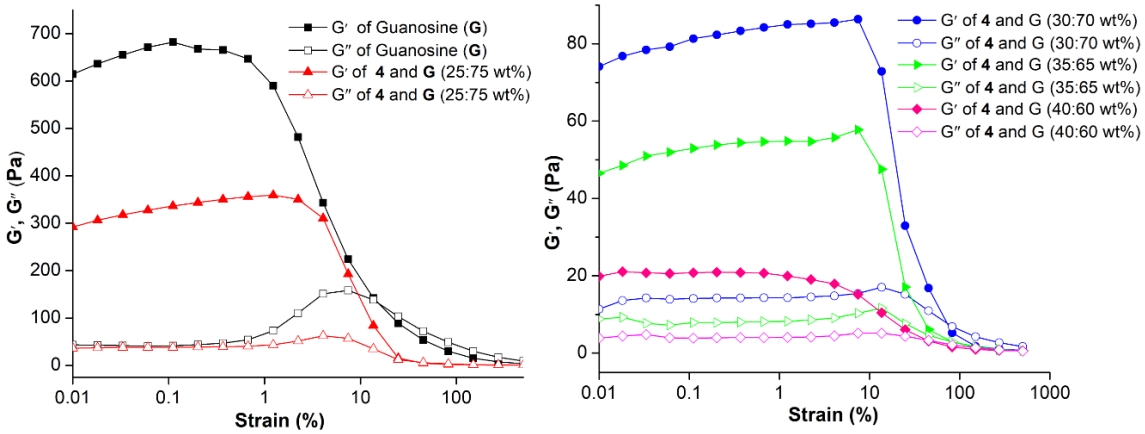

Figure 4.16. Strain sweep measurement for guanosine (G) and cogel with varying ratio of **4** and guanosine performed at constant angular frequency 10 rad/sec.

4.3.7 Self-assembly of fluorescent deoxyguanosine containing longer fatty acid chains

4.3.7.1 Gelation ability of nucleolipid 5 and 6

Unlike OAcBFVdG **4**, myristoyl and palmitoyl-attached nucleolipids **5** and **6** supported the formation of organogels in DMSO. The nucleolipids were dissolved in DMSO by heating and were left to come to room temperature. Rewardingly, nucleolipid **5** and **6** formed stable

fluorescent gels at room temperature even in the absence of any cations such as K^+, Na^+ (Figure 4.17). The gel-sol interconversion was found to be thermo-reversible over several cycles of heating and cooling steps. All gels were stable at room temperature for several months. Ultrasound waves can promote rapid gelation by facilitating the conversion of intramolecular interactions into intermolecular interactions.[67] A hot solution of nucleolipid in DMSO was subjected to ultrasonication for approximately 1 min, which resulted in the rapid formation of gels. The gelation ability of nucleolipid was found to depend on alkyl chain length. Critical gelation concentration (CGC) for nucleolipid **5** containing C14 myristoyl chain was found to be higher as compared to nucleolipid **6** containing C16 palmitoyl chain (CGC for **5** = 1 wt%, CGC for **6** = 0.7 wt%). Importantly, in the gel state also nucleolipids exhibited high fluorescence, which is in contrast to the majority of LMWGs, which lose their fluorescence upon self-assembly (Figure 4.17).

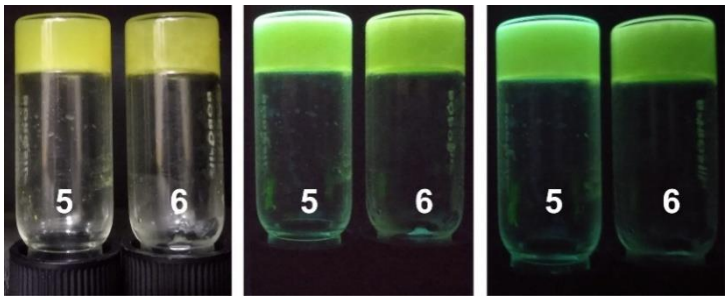

Figure 4.17. Left pair: photograph of organogels of 2-vinylbenzofuran-modified nucleolipids **5** and **6** in DMSO at the respective CGC values. **Middle pair:** the same samples under UV illumination (254 nm). **Right pair:** the same samples under UV illumination (365 nm).

4.3.7.2 Morphology and rheology measurements of nucleolipid gels

FESEM images of xerogel of nucleolipids revealed entangled ribbon-like structures (Figure 4.18). The mechanical properties of organogels of **5** and **6** were investigated by rheological measurements under constant oscillating frequency with the varying shear strain (Figure 4.19A). At low strain values, storage modulus (G′) of **5** and **6** (2825 and 1720 Pa) was significantly greater than its loss modulus (G″: 366 and 241 Pa). Further, crossover point of G′ and G″ for **5** and **6**, where gel transforms into the sol, was observed at around 45% and 20% of the strain, respectively. The effect of variation in angular frequency at a constant strain (0.05 %) on G′ and G″ of the nucleolipid gels was studied. Though frequency sweep did not significantly affect the G′ and G″, the G′ values were found to be considerably higher than the G″ values (Figure 4.19B). These results indicate that nucleolipid gel **5** containing

C14 myristoyl chain exhibits more mechanical strength in terms of viscoelastic character compared to **6** containing C16 palmitoyl chain.

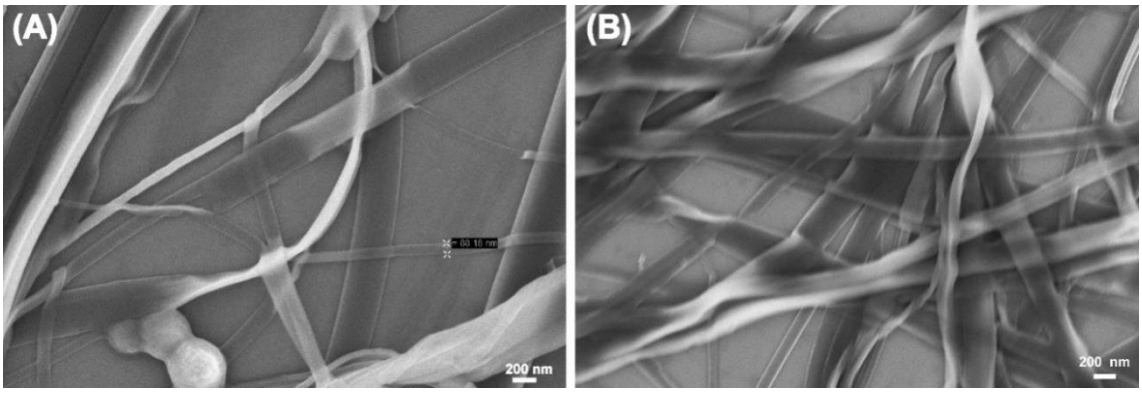

Figure 4.18. FESEM images of xerogels of nucleolipid **5 (A)** and **6 (B)**.

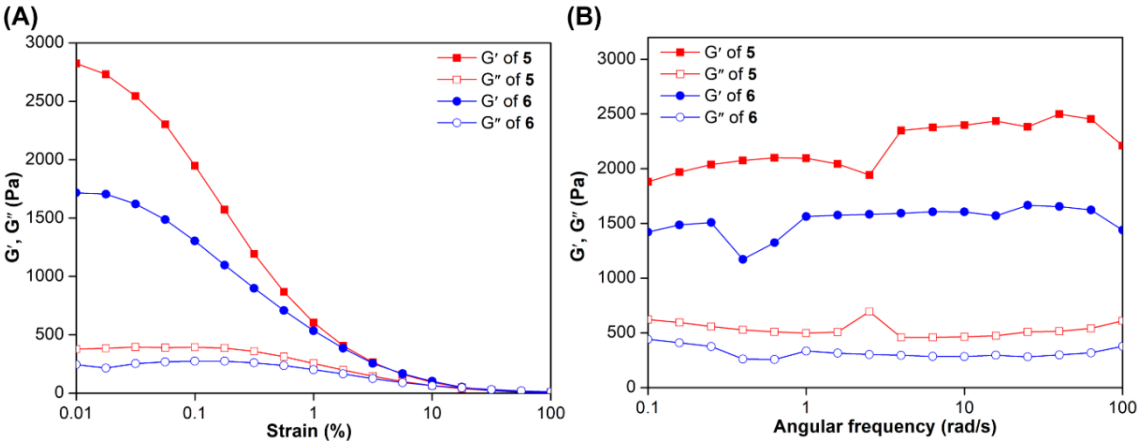

Figure 4.19. Rheological studies for nucleolipid gel **5** and **6** at respective CGC in DMSO. (**A**) Strain sweep measurement at a constant angular frequency of 10 Hz. (**B**) Angular sweep measurement at a constant strain of 0.05 %.

4.3.7.3 Driving force for the self-assembly

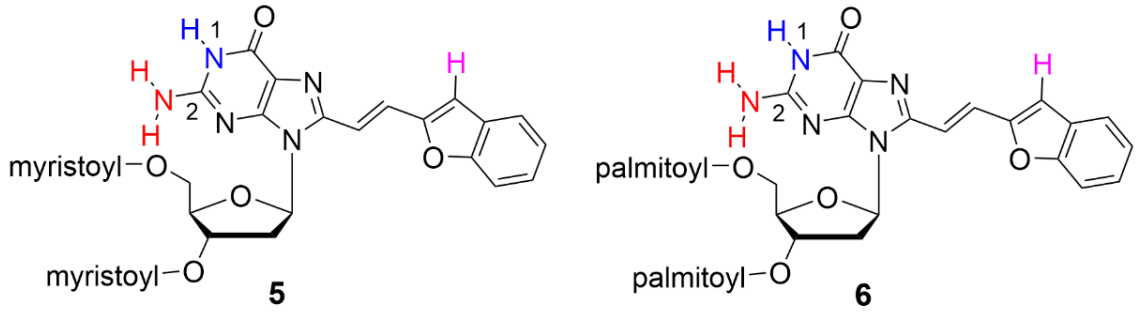

Figure 4.20. Structure of nucleolipid **5** and **6** showing the N1 imino H (represented in blue color) and N2 amino H (represented in red color) and aromatic C-H (represented in pink color) which participated in hydrogen bonding.

To evaluate the type of hydrogen bonding interactions that drive the gelation process, variable temperature ^{1}H NMR experiment using **5** and **6** at their CGC values was performed. For organogel **5,** as the temperature of the gel was increased from 25 °C to 75 °C, the N1 imino H (represented in blue color, Figure 4.20) and N2 amino H (represented in red color) exhibited a significant upfield shift in their signal in the sol state ($\Delta\delta$ = 0.19, $\Delta\delta$ = 0.20 ppm, respectively Figure 4.21). Aromatic C-H (represented in pink color, Figure 24) of benzofuran moiety also showed small upfield shift and sharper signal during the gel-sol transition ($\Delta\delta$ = 0.04, Figure 4.21). Similar kind of shift in the protons was also observed in previously reported organogels.[31] Importantly, in the case of organogel **5**, at 25 °C we observed peak at 11.95 ppm corresponds to N1 imino H characteristic for G-tetrad formation (Figure 4.21A). This peak disappears as temperature increases from 25 °C to 75 °C. The progressive change in the NMR signals of the protons mentioned above is possibly due to loosening or breaking of the respective H-bonds as the gel is transformed into the sol phase. Collectively, these results indicate that N1-H and N2-H of guanine base and to some extent C-H of benzofuran ring drives the self-assembling process by possibly forming G-tetrad as the basic unit. This notion is further substantiated by CD analysis of nucleolipids in gel and sol states (Figure 4.22). CD spectrum of organogels of **5** and **6** recorded at 25 °C revealed two opposite signed bands at 269 nm and 256 nm, which suggests the presence of G-tetrad motif in the gel network. A negative peak at 446 nm corresponds to the 2′-vinylbenzofuran chromophore. Upon transforming the gel to sol by increasing the temperature to 75 °C, the CD signals almost disappeared indicating the disassembling of the chiral gel network

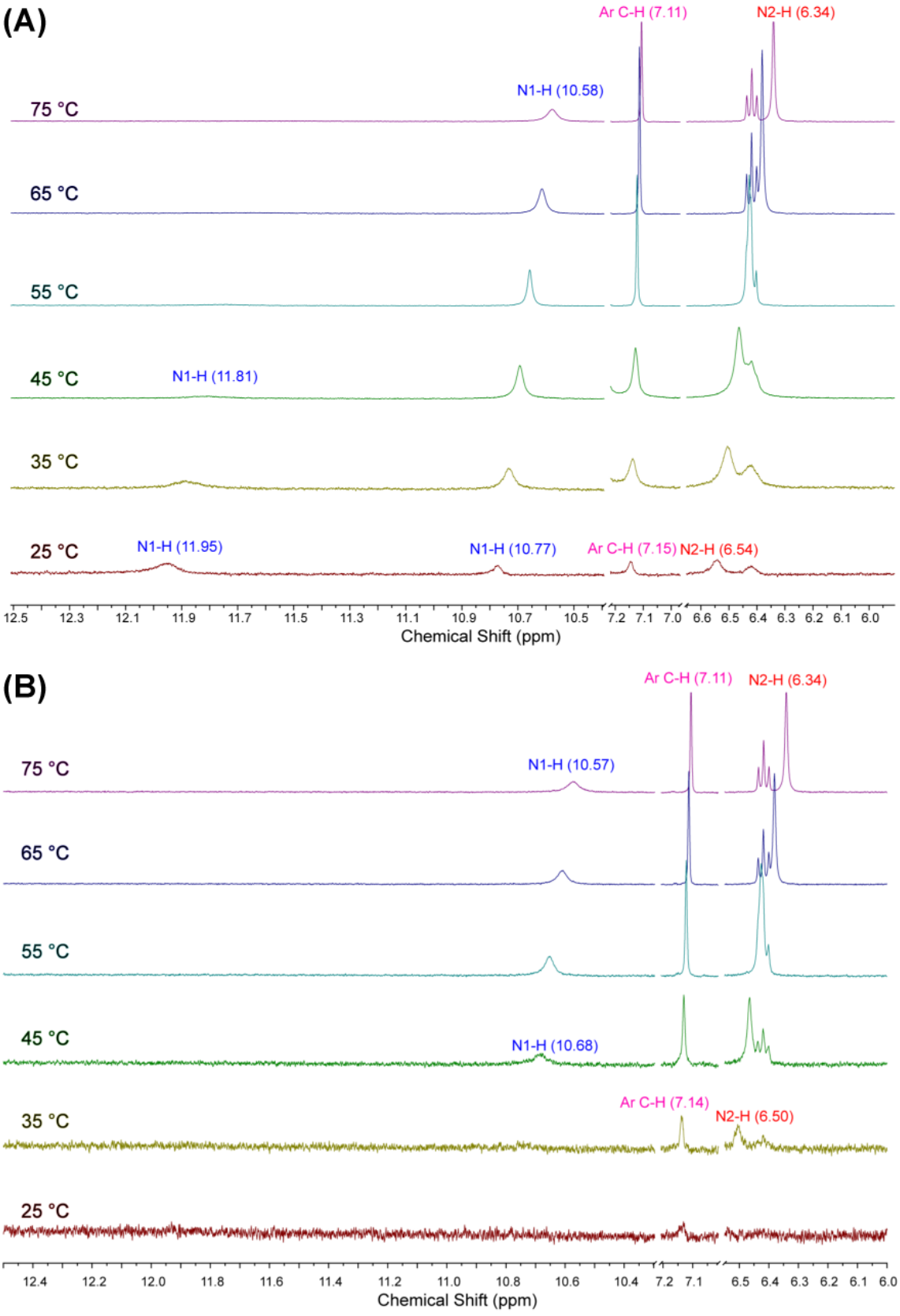

Figure 4.21. Partial ^{1}H NMR spectra of nucleolipid organogels **5** (**A**) and **6** (**B**) in d_6-DMSO as a function of increasing temperature. N1-H and N2-H, which participated in strong hydrogen bonding, exhibited a significant upfield shift in their proton signals during the gel-sol transition. Aromatic C-H

proton of benzofuran may have participated in weak intramolecular hydrogen bonding, also showed small upfield during gel-sol transition.

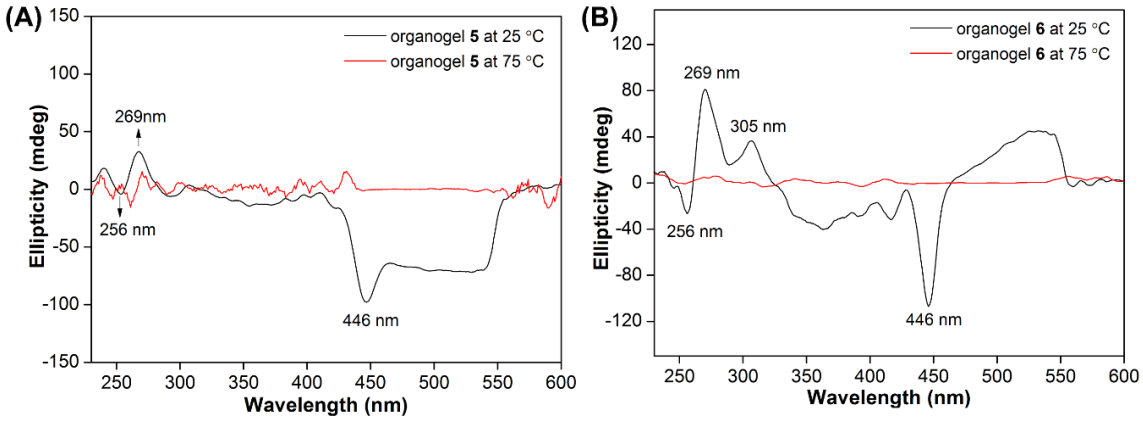

Figure 4.22. (**A**) and (**B**) CD spectra for organogel **5** and **6**, respectively. All CD spectra were taken at CGC value of nucleolipids. Spectra were collected from 600 to 230 nm on a Jasco J-815 CD spectrometer using 1 nm bandwidth at 25 °C. Experiments were performed in duplicate wherein each spectrum was an average of three scans. The spectrum of chloroform without nucleolipid was subtracted from all the sample spectra.

4.3.7.4 Powder X-ray diffraction (PXRD) analysis

Further insights on the molecular arrangement of nucleolipids in the gel network was obtained by PXRD analysis. PXRD spectrum of xerogels of nucleolipid **5** and **6** displayed a prominent diffraction peak corresponding to an interplanar distance of 4.04 nm and 3.75 nm, respectively (Figure 4.23). Notably, xerogel of nucleolipid **5** containing myristoyl chain showed diffraction peaks corresponding to layer spacings in the ratio of 1:1/2:1/3:1/4:1/6, which is indicative of an ordered lamellar arrangement (Figure 4.23A).[31,68–70] However, in the case of xerogel of nucleolipid **6** containing palmitoyl chains, PXRD pattern did not reveal a lamellar packing arrangement (Figure 4.23B). Layer spacing in the range of 3.8 and 4.1 Å was also observed, which could arise due to tetrads held by stacking interaction. Collectively, results from NMR, CD and PXRD experiments suggest a hierarchical self-assembling process, wherein nucleolipids come together to form a G-tetrad by a coordinated H-bonded network, which stacks and propagates into a lamellar arrangement, resulting in fibers and then entangled ribbons.

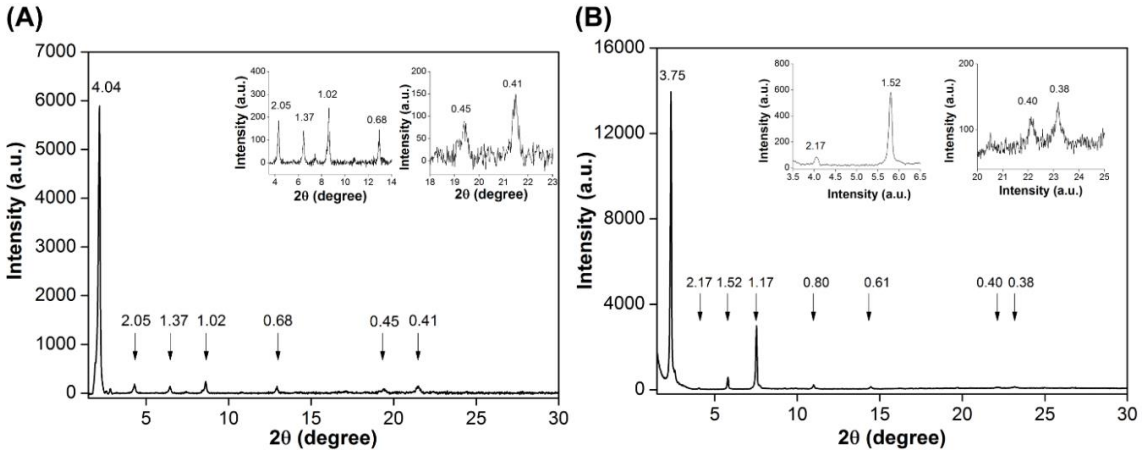

Figure 4.23.PXRD spectra of xerogels of **5 (A)** and **6 (B)**. Inset in **(A)**: peaks in the 2θ values range of 3.5–14° and 18–23° and inset in **(B)**: peaks in the 2θ values range of 3.5–6.5° and 20–25°have been magnified. Layer spacing (nm) for prominent diffraction peaks are also given.

4.3.7.5 Aggregation induced enhancement in the fluorescence

Most often LMWG used as synthons in constructing supramolecular assemblies lose their strong fluorescence upon self-assembly, which restricts their practical applications.[71] Therefore self-assembling organic fluorophores that retain or exhibits enhanced fluorescence upon aggregation are promising candidates for the fabrication of optical materials and sensor.[72–75] Nucleolipids **5** and **6** contains a heteroaryl moiety, which is attached to the guanine ring via an aryl-vinyl bond. This bond could undergo rotation in the excited state and lead to quenched fluorescence. However, if rigidified in the gel state, then it could show enhancement in the fluorescence intensity.[76] To test this, the fluorescence of nucleolipids at respective CGC was recorded in the assembled (25 °C) and dissembled states (75 °C). When the temperature of the gel is increased from 25 °C to 75 °C, the gel disassembles and shows a decrease in fluorescence intensity (Figure 4.24A). Nucleolipids **5** and **6** in gel state displayed almost 4.5-fold and 3-fold higher fluorescence intensity as compared to in sol state, respectively. Along with fluorescence intensity, we have also observed changes in emission wavelength in the gel as well as in sol state. In DMSO monomeric nucleolipid **6** (2 μM) shows emission wavelength at 474 nm (Figure 4.24B). In the gel state, at CGC nucleolipids **5** and **6** show a bathochromic shift (23 nm) corresponding to an emission maximum of 497 nm. When the temperature of the gel increased from 25 °C to 75 °C, gel dissembles and this dissembled state displayed hypsochromic shift from 497 nm to 484 nm (Figure 4.24A). This result indicates, in disassemble or sol state, chromophore loses its

rigidification which leads to the decrease in emission wavelength as well as emission intensity.

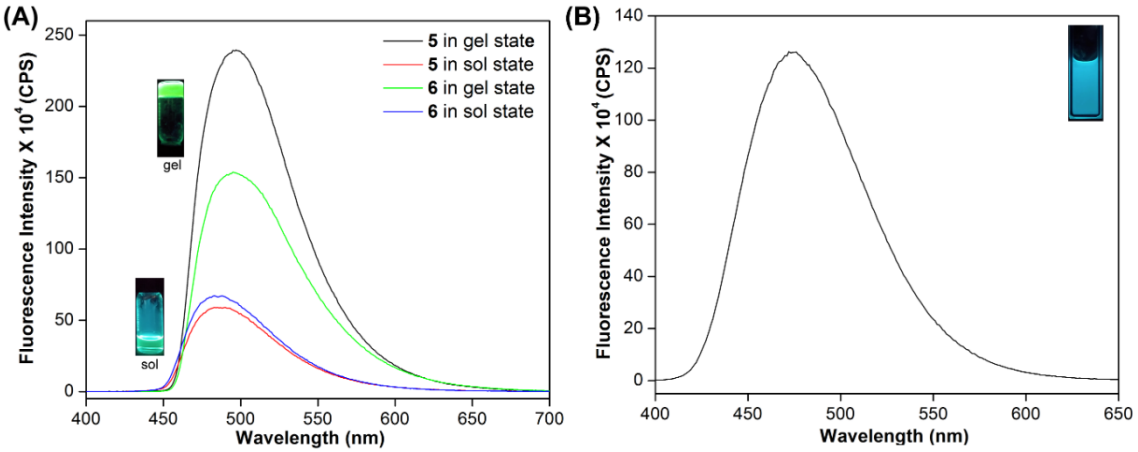

Figure 4.24. Fluorescence spectra for **(A)** Nucleolipid **5** and **6** in DMSO (at CGC concentration) at two different temperature 25 °C (gel state, λ_{em} = 497 nm) 75 °C (sol state, λ_{em} = 484 nm). **(B)** Nucleolipid **6** in DMSO (2 μM concentration, monomeric state, λ_{em} = 474 nm) at 25 °C. The samples were excited at 387 nm with an excitation and emission slit width of 1 nm and 1 nm, respectively.

4.3.7.6 Chemo- and thermo-responsive supramolecular material

The ability of guanine base to form a Watson-Crick base pair with cytosine promoted us to study the self-assemblies of two-component mixtures made of nucleolipid **5** and complementary nucleoside cytidine and its dimyristate derivative (Figure 4.25A).

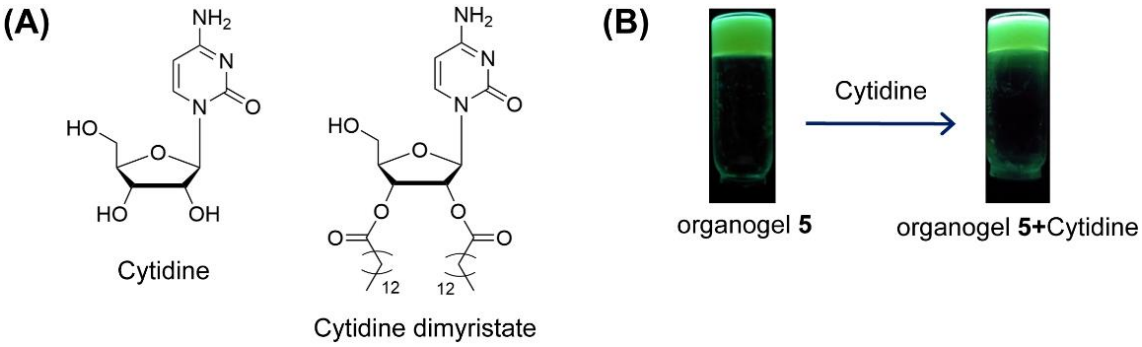

Figure 4.25. (A) Structure of Cytidine and its dimyristate derivative. **(B)** Picture of vials showing the addition of cytidine (5 equiv) into organogel **5**.

Addition of even 5 equivalents of cytidine to nucleolipid **5** did not affect the gel formation and its fluorescence (Figure 4.25B). On the other hand, the addition of 2′, 3′-*O*-dimyristoyl-substituted cytidine to guanosine nucleolipid **5** resulted in interesting observation. Addition of 5 equivalents of 2′, 3′-*O*-dimyristoyl-substituted cytidine did not disrupt the organogel formed by **5**, but exhibited remarkable red-shift in emission maximum

(497 nm to 543 nm), thereby converting the green fluorescence gel to yellow fluorescent gel, albeit with reduced fluorescence intensity (Figure 4.26A). When the yellow fluorescent co-gel was disassembled by heating at 75 °C, it showed a blue shift in the emission band (486 nm) corresponding to free nucleolipid **5** (Figure 4.26B). This change in emission wavelength and emission intensity with the addition of complimentary nucleolipid shows the chemo-responsive property of organogel **5**. Also, changes in the emission wavelength and intensity upon heating shows the thermochromic behaviour of the co-gel. Altogether, chemo and thermochromic behaviour of this organogel **5** can be possibly applied in constructing the chemical and temperature sensor material.[77,78]

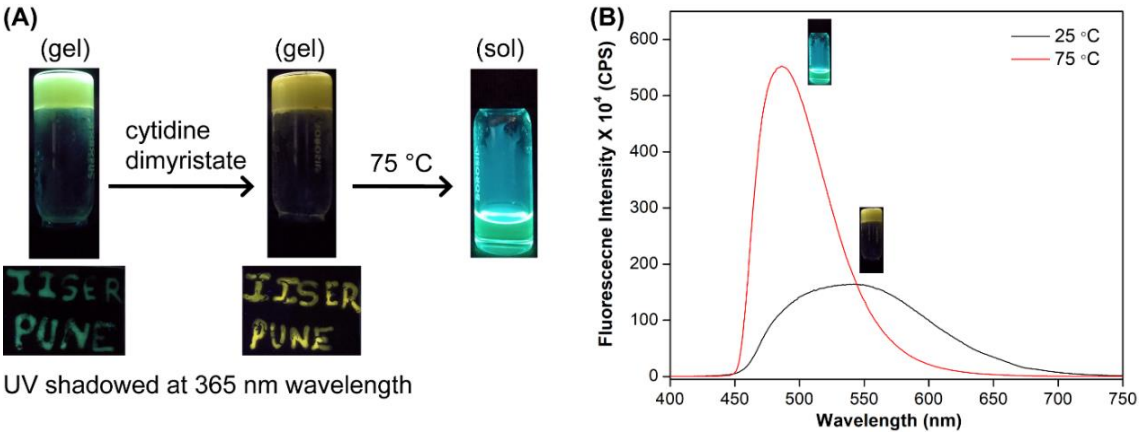

Figure 4.26. (**A**) Picture of vials showing changes in emission color after the addition of cytidine dimyristate. (**B**) Fluorescence spectra for cogel made up of nucleolipid **5** and cytidine dimyristate (1:5 millimolar ratio) in DMSO (at CGC concentration of nucleolipid **5**) at two different temperature 25 °C (gel state, λ_{em} = 543 nm) 75 °C (sol state, λ_{em} = 486 nm). The samples were excited at 387 nm with an excitation and emission slit width of 2 nm and 3 nm, respectively.

4.3.8 Cis–trans isomerization of fluorescent nucleoside BFVdG

In the field of photochemistry, there has been great interest in developing photo-switchable compounds including stilbene and azobenzene derivatives, which reversibly undergoes *E–Z* photoisomerization by external light stimuli.[79,80] Compounds **3–6** (derivatives of stilbene) contains trans double bond, which can potentially undergo photoisomerization into cis double bond. Derivatives of 8-vinyl guanosine, including 8-styryl-2′-deoxyguanosine, 8-vinylpyrene-2′-deoxyguanosine, 8-(2-pyridyl)-2′-deoxyguanosine were reported to be cis-trans photoisomerizable switches capable of influencing DNA conformation[81–83]

Along the same line, we also wanted to examine the photoisomerization of compound **3**. For this, we have synthesized *Z*-isomer **9** in two steps.[84] Sonogashira cross-coupling reaction of **1** and ethynylbenzofuran (**7**)[85] gave compound **8**. Hydrogenation of

8 using 5% Pd/C at room temperature for 16 h gave the cis isomer **9** in moderate yields (Scheme 4.3). The geometry of double bond in compound **9** was confirmed by calculating coupling constant between vinyl protons in ^{1}H NMR spectrum (J = 13.6 Hz, See ^{1}H NMR data in the experimental section). 1D NMR analysis indicates that compound **8** and **9** also adopt *syn* conformation (Table 4.7 and 4.8). Furthermore, 2D NOESY analysis of compound **9** shows strong cross peak between anomeric proton (H1′) and vinyl proton (Ha) (see appendix for the 2D NMR spectra). These results indicate a *syn* conformational preference for compound **9** over *anti*.

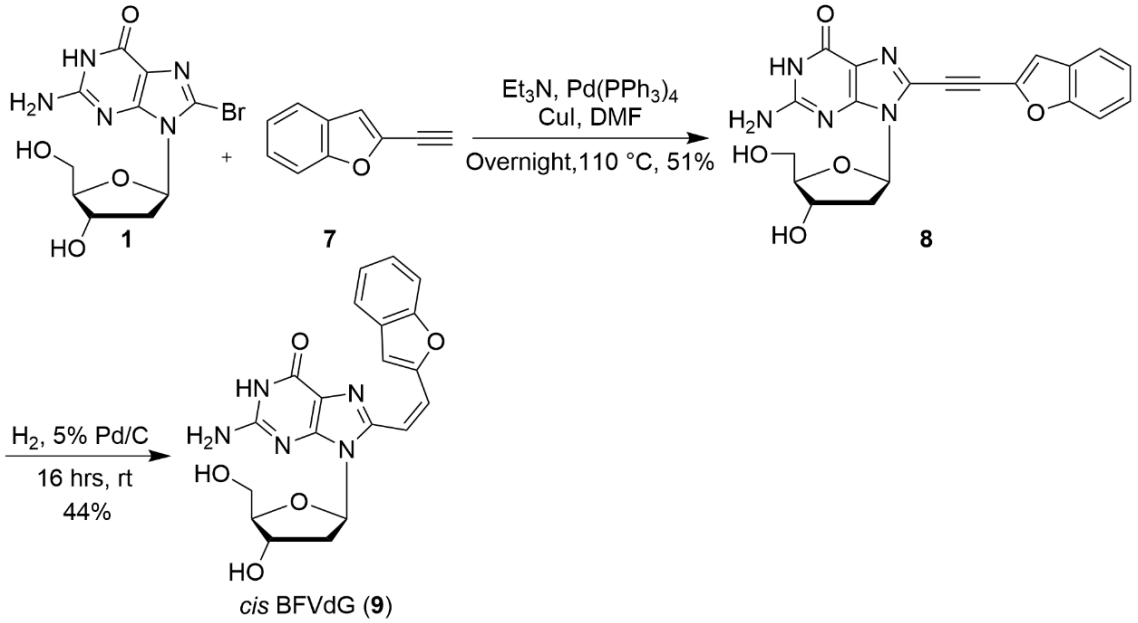

Scheme 4.3. Synthesis of (Z) 8-(2′′-vinylbenzo[b]furan)-2′-dG (BFVdG, **9**).

Table 4.7. Proton signals in ppm, spectra was standardized with respect to d_6-DMSO (2.5 ppm)

Compound	N1-H	Vinyl -H	Vinyl -H	N2-H	1′-H	3′-H	4′-H	5′-H	5′-H	2′-H	2′-H
dG	10.62	-	-	6.45	6.11	4.32	3.80	3.55	3.49	2.50	2.18
9	10.88	6.98	6.72	6.60	6.34	4.39	3.81	3.66	3.60	2.72	2.05
8	10.92	-	-	6.68	6.31	4.41	3.82	3.64	3.54	3.04	2.20
BrdG	10.79	-	-	6.48	6.15	4.39	3.79	3.62	3.49	3.16	2.21

Table 4.8. Carbon signals in ppm, spectra was standardized with respect to d_6-DMSO (39.5 ppm)

Compound	C4′	C1′	C3′	C5′	C2′
dG	87.6	82.6	70.8	61.8	39.6
9	87.4	82.9	70.6	61.6	38.0
8	87.9	83.0	71.1	62.1	37.5
BrdG	87.9	85.1	71.0	62.1	36.5

Photoisomerization of compounds **3** and **9** was examined using HPLC and UV spectroscopy. Isomer *E* (**3**) and *Z* (**9**) have distinct UV absorbance (Figure 4.27A) and retention time in HPLC chromatogram (Figure 4.27B). Trans isomer absorbs at λ_{max}= 360 nm, and cis-isomer absorbs at λ_{max} = 285 nm in water containing 5% DMSO (Figure 4.27A).

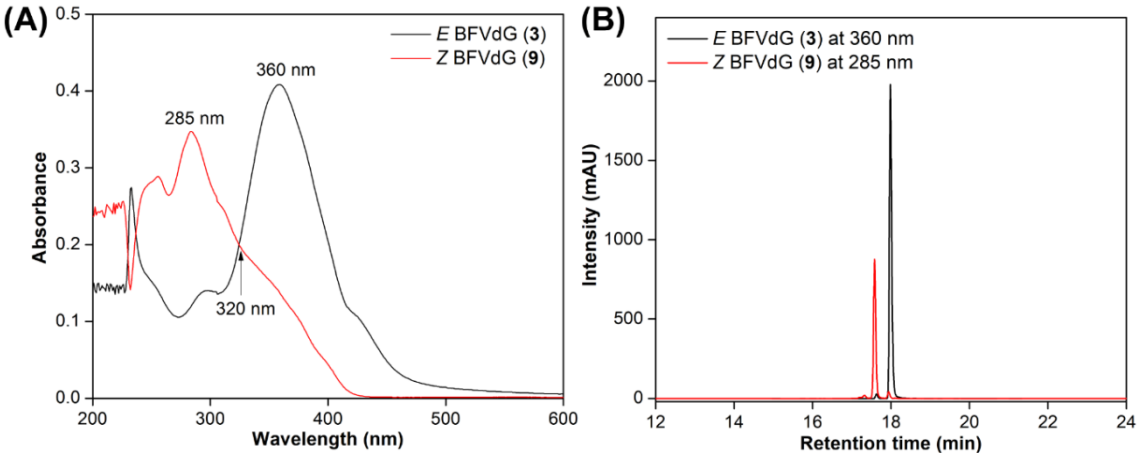

Figure 4.27. A) UV profile for compound trans BFVdG (**3**) and cisBFVdG (**9**) having concentration 25 µM in water (5% DMSO). 320 nm is the isobestic point. (**B**) HPLC profile for compound trans BFVdG (**3**) and cisBFVdG (**9**). Mobile phase A: 50 mM TEAA buffer (pH 7.0); mobile phase B: acetonitrile. Flow rate: 1 mL/min. Gradient: 0−50% B in 10 min, 50−100% B in 10 min and 100% B for 5 min.

The photoisomerization of compound **3** and **9** was examined in an aqueous solution containing 20% DMSO. HPLC analysis of *E*–*Z* photoisomerization was done with UV detection at the isosbestic point (320 nm). When *E* isomer trans BFVdG (**3**) was exposed to 365 nm UV lamp for 15 min, a new peak emerged matching the retention time of the authentic *Z* isomer cis **9** (Figure 4.28). Exposure of *E* isomer trans **3** for 60 min gave almost 86% of *Z* isomer cis **9**. When the *Z* isomer **9** was irradiated using 254 nm UV light, a peak corresponding to the *E* isomer **3** was observed (Figure 4.29). Exposure of *Z* isomer **9** for 15 min at 254 nm wavelength gave almost 91% of *E* isomer **3**. Reversibility of the

photoisomerization process was evaluated by alternatingly irradiating the sample with 365 nm and 254 nm light source (Figure 4.30). Both HPLC and UV absorption profiles confirmed the exchange of isomers upon irradiation.

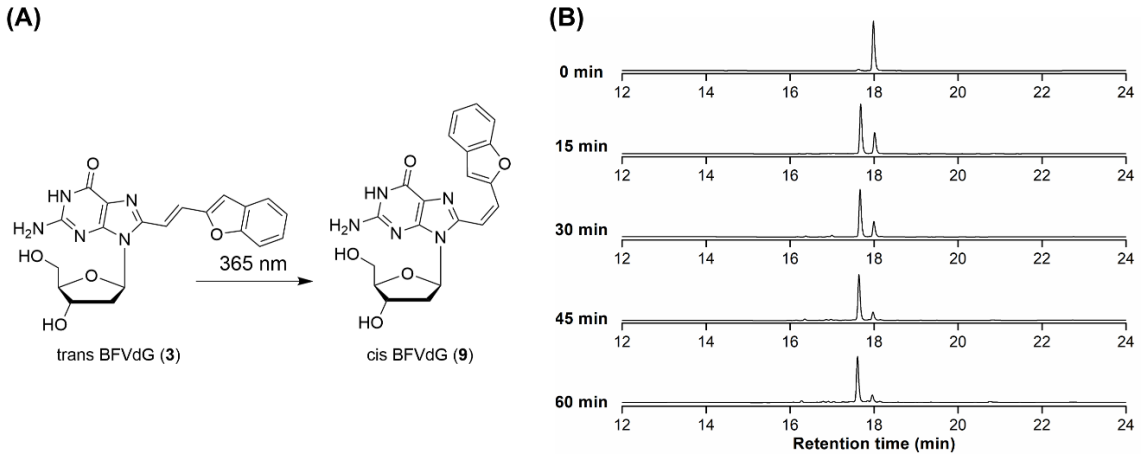

Figure 4.28. (A) Scheme for *E* to *Z* isomerization at 365 nm wavelength. (**B**) HPLC profile for the same at 0, 15, 30, 45 and 60 min Mobile phase A: 50 mM TEAA buffer (pH 7.0); mobile phase B: acetonitrile. Flow rate: 1 mL/min. Gradient: 0−50% B in 10 min, 50−100% B in 10 min and 100% B for 5 min.

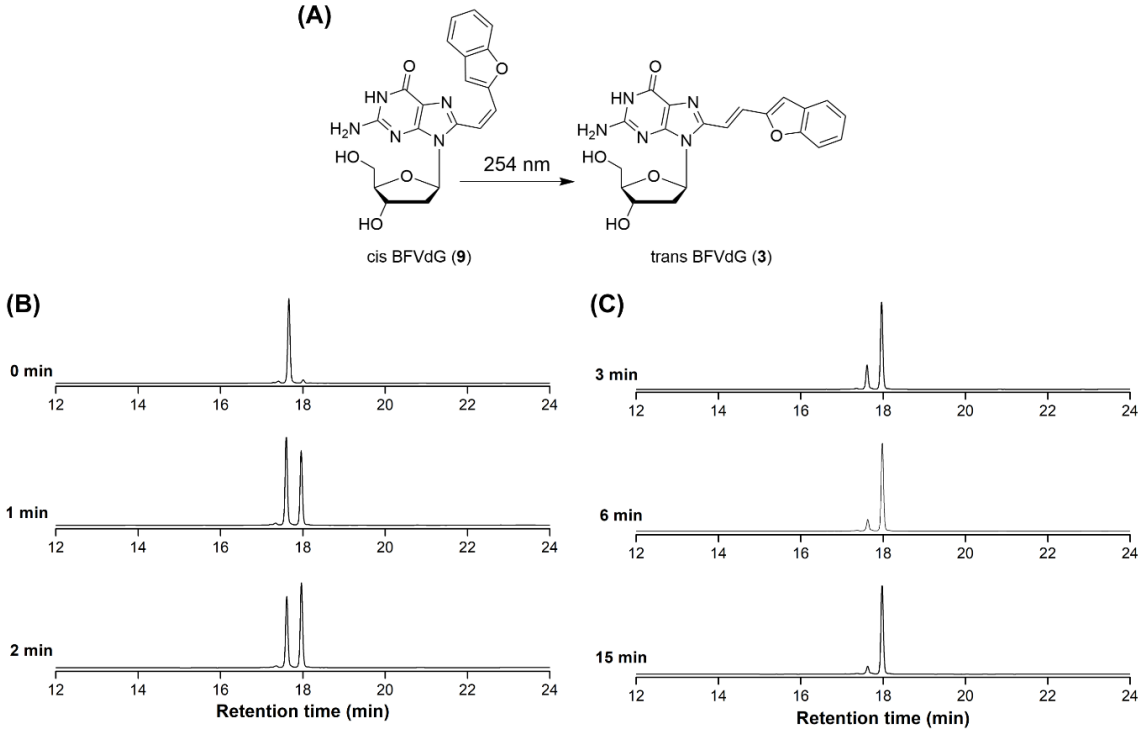

Figure 4.29. (A) Scheme for cis to trans isomerization at 254 nm wavelength. (**B**) HPLC profile for the same at 0, 1, 2, 3, 6 and 15 min Mobile phase A: 50 mM TEAA buffer (pH 7.0); mobile phase B: acetonitrile. Flow rate: 1 mL/min. Gradient: 0−50% B in 10 min, 50−100% B in 10 min and 100% B for 5 min.

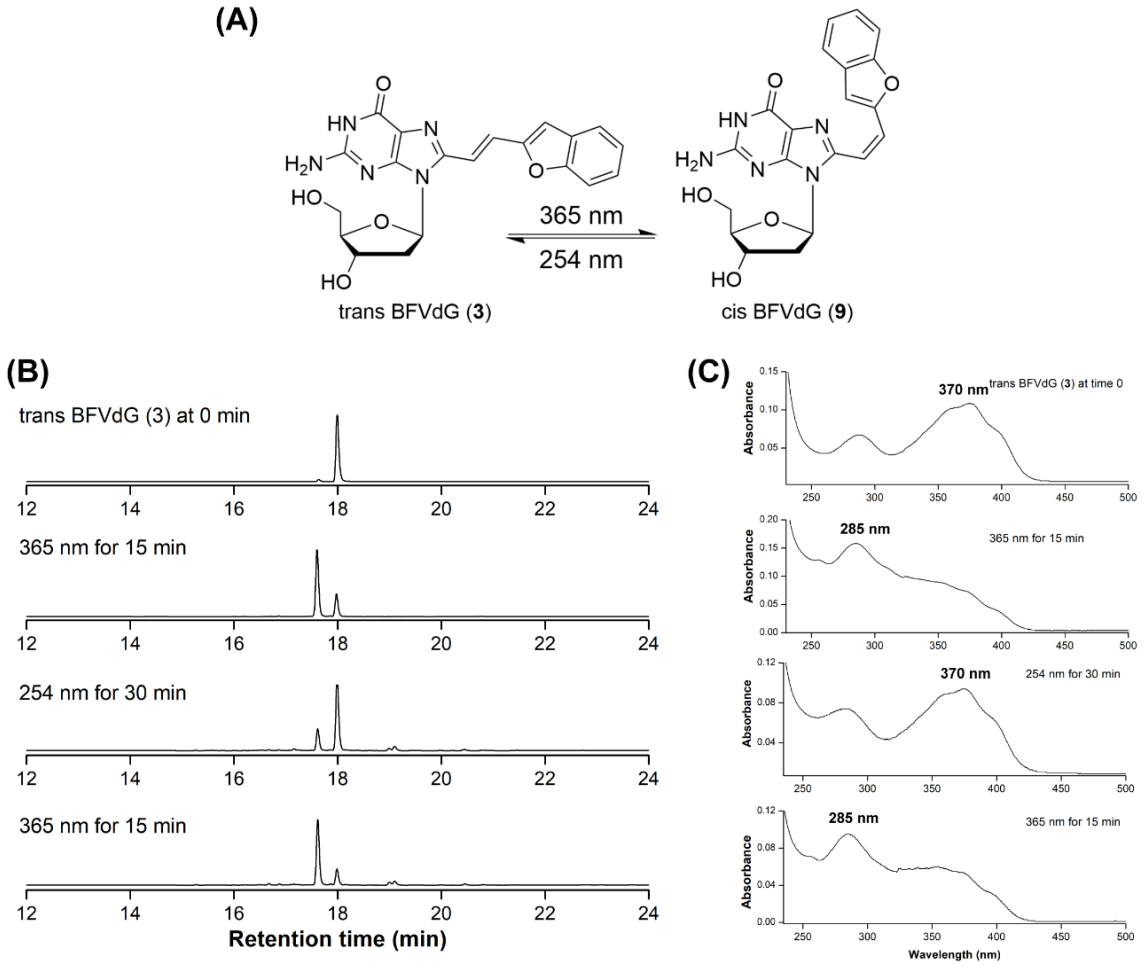

Figure 4.30. (A) Scheme for reversible photoisomerization of BFVdG at respective wavelength. (**B**) HPLC profile for the same. Mobile phase A: 50 mM TEAA buffer (pH 7.0); mobile phase B: acetonitrile. Flow rate: 1 mL/min. Gradient: 0−50% B in 10 min, 50−100% B in 10 min and 100% B for 5 min. (**C**) UV profile for the respective reaction mixture after exposure of particular wavelength.

Inspired by this photo reversible behaviour of the nucleoside **3**, we sought to use this *E–Z* photoisomerization process to control the self-assembly of nucleolipid **5** and **6** inside the gel network. The idea is, after irradiation of organogel **5** and **6** with appropriate wavelength, trans double bond present in the nucleolipids **5** and **6** would get isomerizes to the cis double bond. This formed Z isomer containing cis double bond is no longer planar and shows the less effective ability of the molecule to pack into a one-dimensional network thus could inhibit the effective π–π stacking interaction inside the gel network. This changes in packing efficiency and could result in the changes in mechanical or morphological properties of the organogel. Unfortunately, we did not observe any changes in the properties as mentioned above, and the gel was still intact after irradiation of light even after 2 h (data is shown). This

could be because of trans to cis isomerization process is less favourable in the gel state, which is more rigid compared to the solution phase.[86]

4.5 Conclusion

In summary, we have synthesized fluorescent environment-sensitive deoxyguanosine supramolecular synthons, which shows the interesting self-assembly behaviour and emission properties. We have demonstrated that mixing of the nongelator **4** into the guanosine gelator, hinders the crystallization process of guanosine gel, which results to the formation of thermodynamically stable gel. This ability to access the cogel of guanosine with nongelator **4** may open the new gate for tailoring the properties of guanosine gels like morphology and visco-elastic nature. We have also developed the organogels based on fluorescent deoxyguanosine-fatty acid hybrids. In particular, addition of the complimentary cytidine dimyristate nucleolipid to the fluorescent organogel **5** resulted in remarkable changes in emission wavelength and emission intensity, i.e., the green fluorescence gel transitioned to yellow fluorescent gel. Moreover, the emission properties of cogel of nucleolipid **5** and dimyristate cytidine are responsive to the temperature change. Thus, organogel **5** exhibits responsiveness to the heat as well as complementary nucleolipid. This dual responsiveness of the fluorescent nucleolipids can open the new opportunity in the supramolecular field for sensing application.

4.6 Experimental section

4.6.1 Materials: 8-Bromo-2′-deoxyguanosine was purchased from ChemGenes. Palmitic acid, $Pd(OAc)_2$, $Pd(PPh_3)_4$, CuI and 5% palladium on carbon were purchased from Sigma-Aldrich. EDC (1-(3-dimethylaminopropyl)-3-ethyl carbodiimide hydrochloride) and 4-dimethylaminopyridine were obtained from Avra synthesis private limited. Myristic acid was procured from Fluka.TPPTS (triphenylphosphan-3,3′,3″-trisulfonate) were purchased from alfa aesar. 8-vinylbenzo[b]furan boronic ester (**2**)[32] and 2-ethynylbenzofuran (**7**)[85] were synthesized by previously reported procedure. Silicon wafers (N-type without dopant) were purchased from Sigma-Aldrich.

4.6.2 Instrumentation: NMR spectra were recorded on 400 MHz Jeol ECS-400 spectrometer and Bruker 500 MHz spectrometer. Mass measurements were recorded on Applied Biosystems 4800 Plus MALDI TOF/TOF analyzer and Water Synapt G2 High

Definition mass spectrometers. Steady state fluorescence experiments were carried out in a micro fluorescence cuvette (Hellma, path length 1.0 cm) on Fluoromax- 4 spectrophotometer (Horiba Jobin Yvon). The morphology of gels was analyzed by using Zeiss Ultra Plus field-emission scanning electron microscope (FESEM). Powder X-ray diffraction (PXRD) spectra were obtained at room temperature using Bruker D8 Advance diffractometer (CuKα radiation, λ = 1.5406 Å). CD spectra were recorded on a JASCO-J-815 CD spectrometer. Rheology measurements were carried out in Anton Paar MCR 302 instrument.

4.6.3 Synthesis

4.6.3.1 (*E*) 8-(2-(benzofuran-2-yl)vinyl)-2′-deoxyguanosine (trans BFVdG, 3): 8-bromo-2′-deoxyguanosine (**1**) (410 mg, 1.19 mmol, 1 equiv), $Pd(OAc)_2$ (13.4 mg, 6 mmol%), TPPTS(170 mg, 30 mmol%), Na_2CO_3 (380 mg, 3.58 mmol, 2 equiv),and 8-vinylbenzo[b]furan boronic ester (**2**)[32] (420 mg, 1.55 mmol, 1.3 equiv) were placed in a round bottomed flask fitted with a condenser and reverse filled with argon. Degassed 2:1 H_2O:CH_3CN (24 mL) solution was added and the solution was heated to reflux for 6 h. Following completion the mixture was diluted with 50 mL of H_2O and pH was adjusted to 7.5 with 1M aqueous HCl. The mixture was then cooled to 0°C, filtered, washed with DCM to yield 365 mg of **3** (75%) as yellow powder. TLC (MeOH:CH_2Cl_2 = 20:80); R_f = 0.80; ^{1}H NMR (400 MHz, *d*$_6$-DMSO) δ (ppm) 10.75 (br.s, 1H), 7.64 (d, *J* = 7.8 Hz,1H), 7.59(d, *J* = 7.8 Hz,1H), 7.50 (d, *J* = 15.6 Hz, 1H), 7.41 (d, *J* = 15.6 Hz, 1H), 7.36–7.32 (m, 1H), 7.25 (t, *J* = 7.4 Hz, 1H), 7.15 (s, 1H), 6.54 (br. s, 2H), 6.37 (dd, *J*= 8.4, 6.4 Hz, 1H), 5.34 (d, *J* = 4 Hz, 1H), 5.09 (t, *J* = 5.4 Hz, 1H), 4.44 (s, 1H), 3.88–3.85 (m, 1H), 3.77–3.72 (m, 1H), 3.69–3.64 (m, 1H), 2.80–2.73 (m, 1H), 2.17–2.11 (m, 1H); ^{13}C NMR (100 MHz, *d*$_6$-DMSO) δ = 156.5, 154.4, 154.1, 153.4, 151.9, 143.5, 128.7, 125.3, 123.3, 121.3, 120.0, 117.1, 116.6, 111.0, 107.3, 87.6, 82.8, 70.8, 61.8; HRMS calcd for $C_{20}H_{20}N_5O_5$ $[M+H]^+$410.1464; found 410.1458.

4.6.3.2 (*E*)-diacetyl 8-(2-(benzofuran-2-yl)vinyl)-2′-deoxyguanosine (4): Compound **3** (305 mg, 0.75 mmol) Et_3N (0.27 mL, 1.95 mmol, 2.6 equiv), acetic anhydride (0.17 mL, 1.8 mmol, 2.4 equiv) and a catalytic amount of DMAP (9.16 mg, 7.5 mmol%) were added to anhydrous DMF (10 mL). The resulting solution was stirred overnight at room temperature. The crude, after evaporation in vacuo of the solvent, was applied to a silica gel column and eluted with a mixture of dichloromethane-methanol (96:4). The product was obtained as a

yellow solid (306 mg, 83% yield). TLC (MeOH:CH_2Cl_2 = 10:90); R_f= 0.64; ^{1}H NMR (400 MHz, d_6-DMSO) δ (ppm) 10.81 (br. s, 1H), 7.65 (d, *J* = 7.2 Hz, 1H), 7.58–7.54 (m, 2H), 7.38–7.33 (m, 1H), 7.31–7.24 (m, 2H), 7.16 (s, 1H), 6.58 (br. s, 2H), 6.43 (t, *J* = 7.2 Hz, 1H), 5.44–5.41 (m, 1H), 4.48–4.42 (m, 1H), 4.31–4.25 (m, 2H), 3.27–3.17 (m, 1H), 2.46–2.44 (m, 1H), 2.11 (s, 3H), 1.96 (s, 3H); ^{13}C NMR (100 MHz, d_6-DMSO) δ = 170.2. 170.1, 156.4, 154.5, 153.9, 153.3, 151.8, 143.4, 128.6, 125.5, 123.3, 121.4, 120.4, 117.4, 115.4, 110.9, 108.4, 83.3, 81.5, 74.3, 63.7,35.2, 20.9, 20.5; HRMS calcd for $C_{24}H_{24}N_5O7$ $[M+H]^+$ 494.1675; found 494.1670.

4.6.3.3 Synthesis of 3′, 5′-*O*-disubstituted deoxyguanosine nucleolipids (5 and 6): Compound **4** (1.0 equiv), fatty acid (myristic acid/palmitic acid 2.4 equiv), EDC (2.4 equiv) and DMAP (2.4 equiv) were dissolved in anhydrous DMF. The reaction mixture was stirred for overnight at room temperature under nitrogen atmosphere. After completion of the reaction, the reaction mixture was diluted with dichloromethane and extracted using 5% $NaHCO_3$ solution and dried over sodium sulfate. Then dichloromethane layer was dried over anhydrous Na_2SO_4, filtered. The filtrate was removed *in vacuo* to afford the crude product which was purified by silica gel column chromatography to obtain the deoxyguanosine nucleolipids (**5** and **6**). Characterization data for **5** and **6** is provided below.

Compound (*E*)-dimyristoyl 8-(2-(benzofuran-2-yl)vinyl)-2′-deoxyguanosine (5):
Compound **3** (300 mg, 0.73 mmol, 1 equiv,), myristic acid (402 mg, 1.76 mmol, 2.4 equiv), EDC·HCl (337 mg, 1.76 mmol, 2.4 equiv) and DMAP (215 mg, 1.76 mmol, 2.4 equiv) yielded **5** as a yellow solid (500 mg, 82%) TLC (MeOH:CH_2Cl_2 = 10:90); R_f= 0.88; ^{1}H NMR (400 MHz, $CDCl_3$) δ (ppm) 12.32 (br.s, 1H), 7.68 (d, *J* = 15.2 Hz, 1H), 7.55 (d, *J* = 7.8 Hz, 1H), 7.49(d, *J*= 7.8 Hz, 1H), 7.32 (t, *J*= 7.6 Hz,1H), 7.26–7.20 (m, 2H), 6.85 (s, 1H), 6.41 (t, *J*= 7.2 Hz, 1H), 6.02 (br.s, 2H), 5.55–5.53 (m, 1H), 4.72–4.68 (m, 1H), 4.43–4.39 (m, 1H), 4.36–4.34 (m, 1H), 3.43–3.36 (m, 1H), 2.41–2.33 (m, 3H), 2.28 (t, *J* = 7.4 Hz, 2H) 1.69–1.62 (m, 2H), 1.57–1.52 (m, 2H), 1.29–1.18 (m, 40H), 0.89–0.84 (m, 6H); ^{13}C NMR (100 MHz, $CDCl_3$) δ (ppm) = 174.00, 173.32, 155.37, 155.34, 153.99, 152.84, 152.58, 139.44, 132.02, 129.05, 125.76, 123.32, 121.46, 118.09, 114.24, 111.24, 108.78, 84.36, 82.49, 74.63, 63.75, 34.39, 34.19, 33.97, 32.06, 29.83, 29.80, 29.75, 29.65, 29.59, 29.50, 29.46, 29.38, 29.32, 29.23, 25.02, 24.94, 22.83,14.26; HRMS calcd for $C_{48}H_{72}N_5O7$ $[M+H]^+$ 830.5432; found 830.5430.

Compound (*E*)-dipalmitoyl 8-(2-(benzofuran-2-yl)vinyl)-2′-deoxyguanosine (6):

Compound **3** (300 mg, 0.73 mmol, 1 equiv,), palmitic acid (452 mg, 1.76 mmol, 2.4 equiv), EDC·HCl (337 mg, 1.76 mmol, 2.4 equiv) and DMAP (215 mg, 1.76 mmol, 2.4 equiv) yielded **6** as a yellow solid (590 mg, 91%) TLC (MeOH:CH_2Cl_2 = 10:90); R_f = 0.80; ^{1}H NMR (400 MHz, $CDCl_3$ containing 0.03 v/v % TMS) δ (ppm) 12.38 (br. s, 1H), 7.70 (d, *J* = 15.6 Hz, 1H), 7.55 (d, *J* = 7.8 Hz, 1H), 7.49(d, *J* = 7.8 Hz, 1H), 7.34–7.30 (m, 1H), 7.26–7.20 (m, 2H), 6.84 (s, 1H), 6.42 (t, *J*= 7.2 Hz, 1H), 5.96 (br.s, 2H), 5.55–5.53 (m, 1H), 4.73–4.69 (m, 1H), 4.44–4.40 (m, 1H), 4.37–4.33 (m, 1H), 3.43–3.35 (m, 1H), 2.42–2.33 (m, 3H), 2.28 (t, *J* = 7.6 Hz,2H) 1.71–1.64 (m, 2H), 1.55–1.51 (m, 2H), 1.29–1.19 (m, 48H), 0.89–0.85 (m, 6H); ^{13}C NMR (100 MHz, $CDCl_3$ containing 0.03 v/v % TMS) δ = 173.83, 173.15, 155.19, 153.85, 128.91, 128.58, 123.17, 121.31, 117.94, 111.09, 108.62, 84.16, 82.33, 74.49, 63.59, 35.67, 34.25, 34.05, 31.93, 29.77, 29.71, 29.67, 29.62, 29.52, 29.46, 29.37, 29.32, 29.24, 29.19, 29.10, 24. 89, 24.80, 22.70, 14.13, HRMS calcd for $C_{52}H_{80}N_5O7$ $[M+H]^+$ 886.6058; found 886.6051.

4.6.3.4 8-(2-(benzofuran-2-yl)ethynyl)-2′-deoxyguanosine (8): To solution of 8-bromo-2′-deoxyguanosine (**1**) (200 mg, 0.49 mmol, 1 equiv), 2-ethynylbenzofuran (**7**, 105 mg, 0.74 mmol, 1.5 equiv), and Et_3N (205 µL, 1.5 mmol, 3 equiv) in 5 mL of DMF were added $Pd(PPh_3)_4$(15 mg, 2.5 mmol%) and copper(I)iodide (5 mg, 5 mmol%) under nitrogen. The mixture was stirred at 110 °C for overnight. The resulting mixture was concentrated *in vacuo* and washed with chloroform and crude product was purified by reversed phase combi-flash chromatography to yield **5** (101 mg, 51%) as yellow powder. TLC (MeOH:CH_2Cl_2 = 10:90); R_f = 0.44; ^{1}H NMR (400 MHz, d_6-DMSO) δ (ppm) 10.92 (br.s, 1H), 7.73 (d, *J* = 8 Hz,1H), 7.66–7.64 (m,1H), 7.57 (d, *J* = 0.8 Hz, 1H), 7.49–7.45 (m, 1H), 7.37–7.33 (m, 1H), 6.68 (br.s, 2H), 6.31 (m, 1H), 5.34 (d, *J* =4.4 Hz, 1H), 4.89 (t, *J* = 5.6 Hz, 1H), 4.43–4.39(m, 1H), 3.84–3.81 (m, 1H), 3.67–3.61 (m, 1H), 3.57–3.51 (m, 1H), 3.07–3.00 (m, 1H),2.23–2.17 (m, 1H); ^{13}C NMR (100 MHz, d_6-DMSO) δ = 156.2, 154.7, 154.3, 151.2, 136.4, 127.8, 127.0, 126.9, 124.0, 122.1, 118.0, 114.5, 111.5, 87.9, 85.6, 83.6, 83.0, 71.1, 62.1, 48.7, 37.5; HRMS calcd for $C_{20}H_{18}N_5O_5[M+H]^+$408.1308 ; found 408.1305.

4.6.3.5 (*Z*) 8-(2-(benzofuran-2-yl)vinyl)-2′-deoxyguanosine (cis BFVdG, 9): To the above obtained 8-(2′′-ethynyl benzo[b]furan)-2′-dG (88 mg, 0.23 mmol, 1 equiv) in20 mL of ethanol was added, dissolved and stirred for 10 minutes at 50 °C. After hydrogen substitution

in the system, 5% palladium/carbon (10.6 mg) was added, stirred for 48hr at room temperature and catalytic hydrogen reduction was performed. After the reaction, solvent was concentrated *in vacuo* and crude product was purified by reversed phase combi-flash chromatography to yield **9** (38 mg, 43%) as a yellow solid. TLC (MeOH:CH_2Cl_2 = 10:90); R_f= 0.50; ^{1}H NMR (400 MHz, d_6-DMSO) δ (ppm) 10.88 (br.s, 1H), 8.58 (s, 1H) 7.69 (d, *J* = 8 Hz, 1H), 7.53 (d, *J* = 8 Hz 1H), 7.36–7.32 (m, 1H), 7.26 (t, *J* = 7.2 Hz, 1H), 6.98(d, *J* = 13.6, 1H), 6.72 (d, *J* = 13.4, 1H), 6.60 (br.s, 2H), 6.34 (dd, *J* = 8.4, 6.4, 1H), 5.27 (d, *J* = 4 Hz, 1H), 5.04 (t, *J* = 5.2 Hz, 1H), 4.39(s, 1H), 3.81 (dd, *J* = 7.2, 4.0 Hz, 1H), 3.69–3.59 (m, 2H), 2.75–2.68 (m, 1H), 2.08–2.02 (m, 1H). ^{13}C NMR (100 MHz, d_6-DMSO) δ : 156.49, 153.92, 153.75, 153.39, 151.44, 142.41, 128.66, 125.42, 123.16, 121.67,119.89,116.90, 116.87,110.91, 109.27, 87.43, 82.91,70.56,61.57; MALDI ToF calcd for $C_{20}H_{19}N_5O_5K$ $[M+K]^+$ 448.50 ; found 448.08.

4.6.4 Gelation test

4.6.4.1 Cogel made up of OAcBFVdG (4) and guanosine (G): A weighed amount of OAcBFVdG**4** and guanosine in a glass vial was dissolved in DMSO:H_2O system by heating. The samples were cooled to room temperature and the gel formation was confirmed by inverting the vial. Together **4** and guanosine within 30 minutes formed stable cogels. Repeated heating and cooling steps were performed to confirm the thermo-reversibility of the formed gels. All experiments were performed at least in duplicate.

4.6.4.2 Organogel made up of nucleolipid 5 and 6: A weighed amount of deoxyguanosine nucleolipids in a glass vial was dissolved in dimethyl sulfoxide by heating. The samples were cooled to room temperature and the gel formation was confirmed by inverting the vial. Nucleolipids **5** and **6** within 30 minutes formed stable gels. Repeated heating and cooling steps were performed to confirm the thermo-reversibility of the organogels. All experiments were performed at least in triplicate.

For all the experiments detailed below, fresh gels were made just prior to use.

4.6.5 FESEM analysis. The morphology of assemblies formed by individual nucleolipids and different mixtures of nucleolipids and nucleosides was characterized by FESEM. Gel samples in respective solvents were drop-casted on a silicon wafer and dried in a vacuum

desiccator for ~15 h. Samples were gold-sputtered to minimize sample charging before FESEM analysis. The FESEM images were analyzed by using ImageJ 1.46r software.

4.6.6 Rheological studies: Rheology measurements were carried out in Anton Paar MCR 302 instrument by using 15 mm diameter parallel plate. Measurements were carried out at 25 °C. For all the experiments, around 200 μL of the hot solution was placed on the parallel.

4.6.6.1 Cogel made up of OAcBFVdG (4) and guanosine (G): A strain sweep experiment at a constant frequency (10 rad/sec) was performed in the 0.01–500% range to determine the linear viscoelastic region of the gel sample. A hot solution of the gel was loaded on to the plate. The hot solution was allowed to form the stable gel for 30 min prior to the measurement. The gap was fixed at 500 μm for the parallel plate apparatus.

4.6.6.2 Organogel made up of nucleolipid 5 and 6: A strain sweep experiment at a constant frequency (10Hz) was performed in the 0.01–100% range to determine the linear viscoelastic region of the gel sample. Frequency sweep experiment at constant strain (0.05 %) was performed in the 0.1–100 rad/sec range. A hot solution of the gel was loaded on to the plate. The hot solution was allowed to form the stable gel for 30 min prior to the measurement. The gap was fixed at 1 mm for the parallel plate apparatus.

4.6.7 Variable temperature ^{1}H NMR: ^{1}H NMR was recorded on aJeol 400 MHz NMR instrument as a function of temperature.

4.6.7.1 Cogel made up of OAcBFVdG (4) and guanosine (G): A 2 wt% mixture of **4** and guanosine (35:65) containing 500 mM KCl in 0.5 mL mixture of *d6*-DMSO:D_2O (1:1) was warmed to obtain a clear solution and to this hot solution internal standard tBuOH (2 μL) was added. Then the solution was transferred into a hot NMR tube, which was immediately transferred into a Jeol 400 MHz NMR instrument at 85 °C and was allowed to equilibrate for 15 min. NMR spectra were recorded at 85 °C, after which the sample was cooled to 75 °C and again allowed to equilibrate for 15 min. This process was repeated until the final measurement (at 25 °C) was completed.

4.6.7.2 Organogel made up of nucleolipid 5 and 6: Gels of **4** (1 w/v %) and **5** (0.7 w/v %) in d_6-DMSO at respective CGC were formed in individual NMR tubes by heating and cooling

steps. The temperature of the sample was elevated from 25 °C to 75 °C with an increment of 10 °C and equilibration time of 15 min. The spectrum was recorded at every 10 °C interval.

4.6.8 Powder X-ray diffraction (PXRD) analysis of deoxyguanosine nucleolipids 5 and 6: Gels of **5** and **6** in DMSO at respective CGC were formed on a glass slide by drop-casting method. The glass slide was placed in a vacuum desiccator and dried under vacuum for nearly 15 h to obtain the xerogels. PXRD spectrum was recorded using Bruker D8 Advance diffractometer with CuKα source (1.5406 Å). Diffraction data were collected at 2θ angle from 1° to 30° using a 0.01° step size and 0.5 s per step. Low angle diffraction data was collected by keeping the motorized divergence slit in automatic mode so as to maintain the X-ray beam footprint on the sample to 12 x 12 mm. Further, the position sensitive detector (Lynxeye) channels were reduced to minimize the background X-ray scattering entering the detector.

4.6.9 Variable temperature circular dichroism for organogel 5 and 6: Spectra were collected from 600 to 200 nm on a Jasco J-815 CD spectrometer using 1 nm bandwidth at 25 °C and 75 °C. Sample kept for 10 min at each temperature for equilibration. Experiments were performed in duplicate wherein each spectrum was an average of three scans. The spectrum of DMSO without nucleolipid was subtracted from all the sample spectra.

4.6.10 Variable temperature Fluorescence: Spectra for were recorded in a micro fluorescence cuvette (Hellma, path length 1.0 cm) using TCSPC Fluoromax-4 fluorescence spectrometer (Horiba Jobin Yvon).

4.6.10.1 Cogel made up of OAcBFVdG (4) and guanosine (G): A hot solution of a 2 wt% mixture of **4** and guanosine (35:65) containing 500 mM KCl in 0.5 mL mixture of DMSO:H_2O (1:1) was taken in a micro fluorescence cuvette and was allowed to stand at RT until a stable cogel was formed, cuvette was inverted to test the gel formation. Fluorescence spectra of gel samples were recorded at two different temperature 25 °C and 85 °C. Sample was excited at 387 nm with an excitation slit width of 1 nm and emission slit width of 2 nm with equilibration time 15 min.

4.6.10.2 Organogel 5 and 6: A hot solution of the nucleolipid at respective CGC was taken in a micro fluorescence cuvette and was allowed to stand at RT until a stable gel was formed,

cuvette was inverted to test the gel formation. Fluorescence spectra of gel samples were recorded at two different temperature 25 °C and 75 °C. Sample was excited at 387 nm with an excitation slit width of 1 nm and emission slit width of 1 nm with equilibration time 15 min

4.6.11 *E–Z* photoisomerization:Photo irradiation to observe *trans* to *cis* isomerization was performed in a 100 uL of aqueous solution (20% DMSO) containing 50 µM of nucleoside BFVdG (**3** and **9**) using a handheld UV lamp (Spectroline® E-Series UV lamp, 8 W) at 365 nm wavelength. Conversion from the cis to trans isomer was carried outby irradiation using at 254 nm wavelength.

4.7 References

1. S. Sivakova and S. J. Rowan, *Chem. Soc. Rev.,* 2005, **34**, 9–21.
2. W. Guschlbauer, J. -F. Chantot and D. Thiele, *J. Biomol. Struct. Dyn.,* 1990, **8**, 491–511.
3. J. T. Davis, *Angew. Chem. Int. Ed.,* 2004, **43**, 668–698.
4. J. T. Davis and G. P. Spada, *Chem. Soc. Rev.,* 2007, **36**, 296–313.
5. S. Masiero, S. Pieraccini and G .P. Spada, The self-assembly of lipophilic guanosine derivatives. In Molecular Self-Assembly: Advances and Applications; Li, A. D., Ed.; Pan Stanford: Singapore, 2012, 93–122.
6. L. Stefan and D. Monchaud, *Nat. Rev. Chem*, 2019, **3**, 650–668.
7. M. d. C. Rivera-Sánchez, I. Andújar-de-Sanctis, M. García-Arriaga, V. Gubala, G. Hobley and J. M. Rivera, *J. Am. Chem. Soc.*, 2009, **131**, 10403–10405.
8. D. *González-Rodríguez,* J .L. *J. van Dongen, M.Lutz, A. L. Spek, A. P. H. J. Schenning and* E. W. *Meijer, Nat. Chem., 2009*, **1**, 151.
9. G. Gottarelli, S. Masiero and G. P. Spada, *J. Chem. Soc.Chem.Commun.*, 1995, **24**, 2555–2557.
10. L. Meng, K. Liu, S. Mo, Y. Mao and T. Yi, *Org. Biomol. Chem.*, 2013, **11**, 1525–1532.
11. K. Araki, R. Takasawa and I. Yoshikawa, *Chem. Commun.*, 2001, 1826–1827.
12. T. Sato, M. Seko, R. Takasawa, I. Yoshikawa and K. Araki, *J. Mater. Chem.*, 2001, ***11***, 3018–3022.
13. I. Yoshikawa, J. Li, Y. Sakata and K. Araki, *Angew. Chem. Int. Ed.*, 2004, ***43***, 100–103.
14. I. Yoshikawa, S. Yanagi. Y. Yamaji and K. Araki, *Tetrahedron*, 2007, ***63***, 7474 –7481.
15. L. Simeone, D. Milano, L. De Napoli, C. Irace, A. Di Pascale, M. Boccalon, P. Tecilla and D. Montesarchio, *Chem. – Eur. J.,* 2011, **17** , 13854–13865.
16. X. Wang, L. Zhou, H. Wang, Q. Luo, J. Xu and J. Liu, *J. Colloid Interface Sci.,* 2011, **353** , 412–419.
17. T. N. Plank and J. T. Davis, *Chem. Commun.*, 2016, **52**, 5037–5040.
18. R. N. Das, Y. P. Kumar, S. Pagoti, A. J. Patil and J. Dash, *Chem. – Eur. J.,* 2012, **18**, 6008–6014.
19. B. Buchs, W. Fieber, F. Vigouroux-Elie, N. Sreenivasachary, J.-M. Lehn and A. Herrmann, *Org. Biomol. Chem.*, 2011, **9**, 2906–2919.
20. N. Sreenivasachary and J.-M. Lehn, *Chem. – Asian J.*, 2008, **3**, 134–139.

21. D. González-Rodríguez, P. G. A. Janssen, R.Martín-Rapún, I .D. Cat, S. D.Feyter, A. P. H. J. Schenning and E. W. Meijer, *J. Am. Chem. Soc.*, 2010, **132**, 4710–4719.
22. Z. Li and C. A. Mirkin, *J. Am. Chem. Soc.*, 2005, **127**, 11568–11569.
23. F. Pu, L. Wu, X. Ran, J. Ren, and X. Qu, *Angew. Chem. Int. Ed.*, 2005, **54**, 892–896.
24. Y.-L. Wu, N. E. Horwitz, K.-S. Chen, D. A. Gomez-Gualdron, N. S. Luu, L. Ma, T. C. Wang, M. C. Hersam, J. T. Hupp, O. K. Farha, R. Q. Snurr and M. R. Wasielewski, *Nat. Chem.*, 2016, **9**, 466–472.
25. N. Sakai, Y. Kamikawa, M. Nishii, T. Matsuoka, T. Kato and S. Matile, *J. Am. Chem. Soc.*, 2006, **128**, 2218.
26. L. Simeone, D. Milano, L. De Napoli, C. Irace, A. Di Pascale, M. Boccalon, P. Tecilla and D. Montesarchio, *Chem. – Eur. J.*, 2011, **17**, 13854.
27. M. S. Kaucher, W. A. Harrell, Jr. and J. T. Davis, *J. Am. Chem. Soc.*, 2006, **128**, 38.
28. J. Dash and P. Saha, *Org. Biomol. Chem.*, 2016, **14**, 2157–2163.
29. F. W. Kotch, V.Sidorov, Y.-F.Lam, K. J. Kayser, H.Li, M. S.Kaucher and J. T. Davis, *J. Am. Chem. Soc.*, 2003, **125**, 15140–15150.
30. L. Ma, M. Melegari, M. Colombini and J. T. Davis, *J. Am. Chem. Soc.*, 2008, **130**, 2938–2939.
31. A. Nuthanakanti and S. G. Srivatsan, *Nanoscale*, 2016, **8**, 3607–3619.
32. M. B. Walunj, A. A. Tanpure and S. G. Srivatsan, *Nucleic Acids, Res*., 2019, **e15**.
33. G. I. Birnbaum, P. Lassota and D. Shugar, *Biochemistry*, 1984, **23**, 5048–5053.
34. E. Dias, J. L. Battiste and J. R. Williamson, *J. Am. Chem. Soc.*,1994, **116**, 4479–4480.
35. Y. Xu and H. Sugiyama, *Nucleic Acids Res.*, 2006, **34**, 949–954.
36. A. Dumas and N. W. Luedtke, *Nucleic Acids Res.*, 2011, **39**, 6825–6834.
37. S. Uesugi and M. Ikehara, *J. Am. Chem. Soc.*, 1977, **99**, 3250–3253.
38. R. Stolarski, C. E. Hagberg and D. Shugar, *Eur. J. Biochem.*, 1984, **138**, 187–192.
39. V. Gubala, J. E. Betancourt and J. M. Rivera, *Org. Lett.*, 2004, **6**, 4735–4738.
40. L. Meng, K. Liu, S. Mo, Y. Mao and T. Yi, *Org. Biomol. Chem.***,** 2013**, 11**, 1525–1532.
41. S. Pieraccini, T. Giorgi, G. Gottarelli, S. Masiero and G. P. Spada, *Molecular Crystals and Liquid Crystals*, 2003, 398:1, 57–73.
42. S. Lena, G. Brancolini, G. Gottarelli, P. Mariani, S. Masiero, A. Venturini, V. Palermo, O. Pandoli , S. Pieraccini, P. Samorì and G. P. Spada, *Chem. – Eur. J.*, 2007, **13** , 3757 –3764.
43. X. Shi, K. M. Mullaugh, J. C. Fettinger, S. A. Hofstadler and J. T. Davis, *J. Am. Chem. Soc.*, 2003, **125**, 10830–10841.
44. R. Rinaldi, G. Maruccio, A. Biasco, V. Arima, R. Cingolani, T. Giorgi, S. Masiero, G. P. Spada and G. Gottarelli, *Nanotechnology* 2002, **13**, 398–403.
45. X. Shi, J. C. Fettinger and J. T. Davis, *Angew. Chem., Int. Ed.*, 2001, **40**, 2827–2831.
46. E. Mezzina, P. Mariani, R. Itri, S. Masiero, S. Pieraccini, G. P. Spada, F. Spinozzi, J. T. Davis and G. Gottarelli, *Chem. – Eur. J.*, 2001, **7**, 388–395.
47. S. Lena, P. Neviani, S. Masiero, S.Pieraccini and G. P. Spada, *Angew. Chem. Int. Ed.*, 2010, **49**, 3657–3660.
48. G. Gottarelli, S. Masiero and G. P. Spada,*Enantiomer A Journal of Stereochemistry* 1998, **3**, 429–438.
49. G. Gottarelli, S. Lena, S. Masiero, S. Pieraccini and G. P.Spada,*chirallity*, 2008, **20**, 471–485.
50. S. Bonazzi, M. Capobianco, M. M. De Morais, A. Garbesi, G. Gottarelli, P. Mariani, M. G. P. Bossi, G. P. Spada and L. Tondelli, *J. Am. Chem. Soc.*,1991, **113**, 5809– 5816.
51. L. Simeone, D. Milano, L. D. Napoli, C. Irace, A. D. Pascale, M. Boccalon, P. Tecilla and D. Montesarchio, *Chem. – Eur. J.*, 2011, **17**, 13854–13865.

52. S. Pieraccini, G. Gottarelli, P. Mariani, S. Masiero, L. Saturni and G. P. Spada, *chirality*, 2001, **13**, 7–12.
53. G. P. Spada , S. Bonazzi , A. Garbesi, S. Zanella, F. Ciuchi P. Mariani, *Liquid Crystals*, 1997, **22**, 341–348.
54. G. Gottarelli, and G. P. Spada, *The Chemical Record*, 2004, **4**, 39–49.
55. B. Adhikari, A. Shah and H.-B Kraatz, *J. Mater. Chem. B*, 2014, **2**, 4802–4810.
56. M. Chen, L. Weimin, L. Hong, N. Ji and H. Zhao, *BioMed Research International*, vol. 2019, Article ID 6258248, 18 pages, 2019. https://doi.org/10.1155/2019/6258248.
57. L. E. Buerkleand S. J. Rowan, *Chem soc rev* 2012, **41**, 6089–6102.
58. A. R. Hirst, I. A. Coates, T. R. Boucheteau, J. F. Miravet, B. Escuder, V. Castelletto, I. W. Hamley and D. K. Smith, *J. Am. Chem. Soc.*, 2008, **130**, 2948– 2949.
59. Y. E. Shapiro, *Prog. Polym. Sci.*, 2011, **36**, 1184–1253.
60. L. E. Buerkle, H. A. von Recum and S. J. Rowan,*Chem. Sci.*, 2012, 3, 564.
61. L.E. Buerkle, Z. Li, A. M. Jamieson and S. J. Rowan, *Langmuir*, 2009, **25**, 8833–8840**.**
62. B. Escuder, M. LLusar and J. F. Miravet, *Org. Chem.*, 2006, **71**, 7747–7752.
63. A. E. Way, A. B. Korpusik, T. B. Dorsey, L. E. Buerkle, H. A.vonRecum and S. J. Rowan, *Macromolecules*, 2014, **47**, 1810–1818.
64. J.-F. Chantot and W. Guschlbauer, *FEBS Letters*, 1969, **4**, 173–176.
65. X. Y. Liu, P. D. Sawant, W. B. Tan, I. B. M. Noor, C. Pramesti and B. H. Chen, *J. Am. Chem. Soc.*, 2002, **124**, 15055–15063.
66. L. Zheng, L. E. Buerkle, M. R. Orseno, K. A. Streletzky, S. Seifert, A. M. Jamieson and S.J. Rowan, *Langmuir* 2010, **132**, 12051−12058.
67. X. Yu, L. Chen, M. Zhang and T. Yi, *Chem. Soc. Rev.***,** 2014, **43**, 5346−5371.
68. A. Ajayaghosh, V. K. Praveen, *Acc. Chem. Res.*, 2010, **40**, 644−656.
69. S. Basak, J. Nanda and A. J. Banerjee, *Mater. Chem.*, 2012, **22**, 11658−11664.
70. S. Bhattacharjee, B. Maiti and S. Bhattacharya, *Nanoscale*, 2016, **8**, 11224−11233.
71. J. B. Birks, *photophysics of aromatic molecules*, Wiley, London,1970
72. A. Pérez, J. L,. Serrano, T. Sierra, A. Ballesteros, D. de Saá and J. Barluenga, *J. Am. Chem. Soc.*,2011, **133**, 8110– 8113.
73. J. Zhao, D. Yang, Y. Zhao, X.-J. Yang, Y.-Y, Wang and B. Wu, *Angew. Chem. Int. Ed.*, 2014, **53**, 6632–6636.
74. R. Hu, N. L. C. Leung and B. Z. Tang, *Chem. Soc. Rev.*, 2014, **43**, 4494–4562.
75. L. Zhang, N. He and C. Lu, *Anal. Chem.* 2015, **87**, 1351–1357.
76. Z. Zhao, J. W. Y. Lam and B. Z. Tang, *J. Mater. Chem.*, 2012, **22**, 23726–23740.
77. X. D. Wang, O. S. Wolfbeis and R. J. Meier, *Chem. Soc. Rev.* 2013, **42**, 7834−7869.
78. A. Pucci, A, R. Bizzarri and G. Ruggeri, *Polymer SoftMatter* 2011, **7**, 3689−3700.
79. H. Meier,*Angew. Chem. Int. Ed.* 2001, **40**, 1851–1853.
80. H. M. D. Bandara, and S. C. Burdette, *Chem. Soc. Rev.*, 2012, **41**, 1809–1825.
81. S. Ogasawara and M. Maeda, *Angew. Chem. Int. Ed*, 2008, **47**, 8839–8842.
82. Y. Saito, K. Matsumoto, Y. Takeuchi, S. S. Bag, S. Kodate, T. Morii and I. Saito, *Tetrahedron Lett*., **2009**, *50*, 1403–1406.
83. S. Ogasawara and M. Maeda, *Angew Chem. Int. Ed*., 2009, **48**, 6671–6674.
84. S. Ogasawara, I. Saito, and M. Maeda, *Tetrahedron Lett*., 2008, **49**, 2479–2482.
85. H. Zang, H. and R. C. Larock, *J. Org. Chem.*, 2002, **67**, 7048–7056.
86. R. Wang, C. Geiger, L. Chen, B. Swanson and D. G. Whitten, *J. Am. Chem. Soc.*, 2000, **122**, 2399–2400.

4.8 Appendix III: Characterization data of synthesized compounds

^{1}H NMR of the compound **3** in d_6-DMSO (400 MHz)

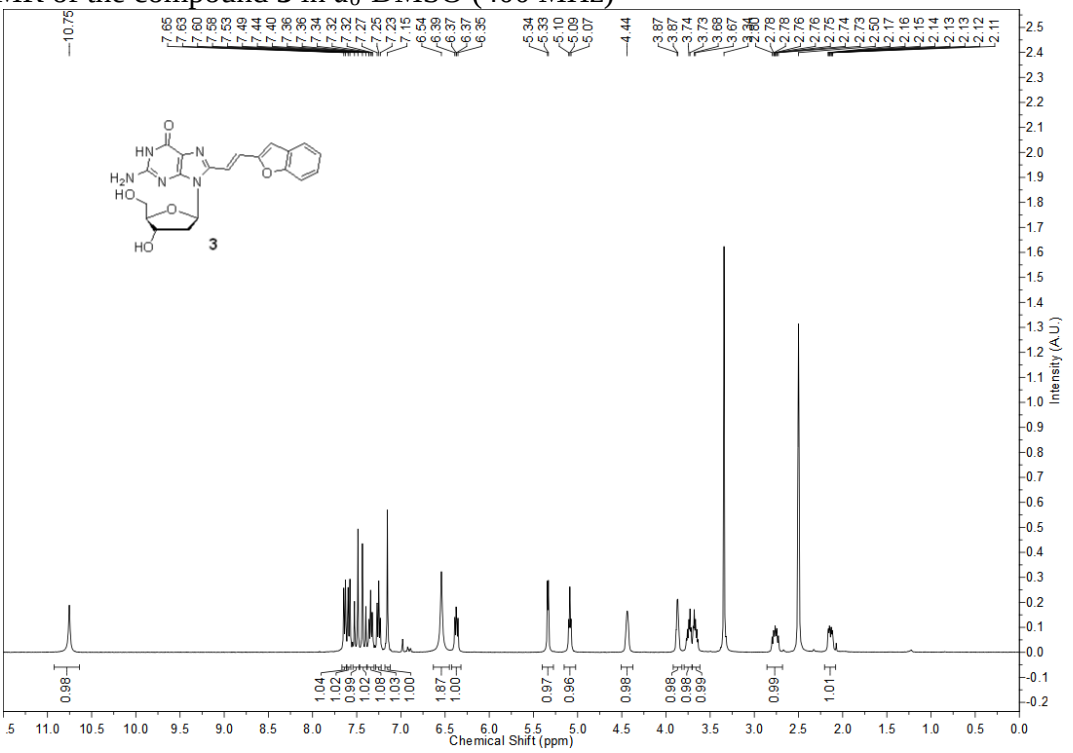

^{13}C NMR of the compound **3** in d_6-DMSO (100 MHz)

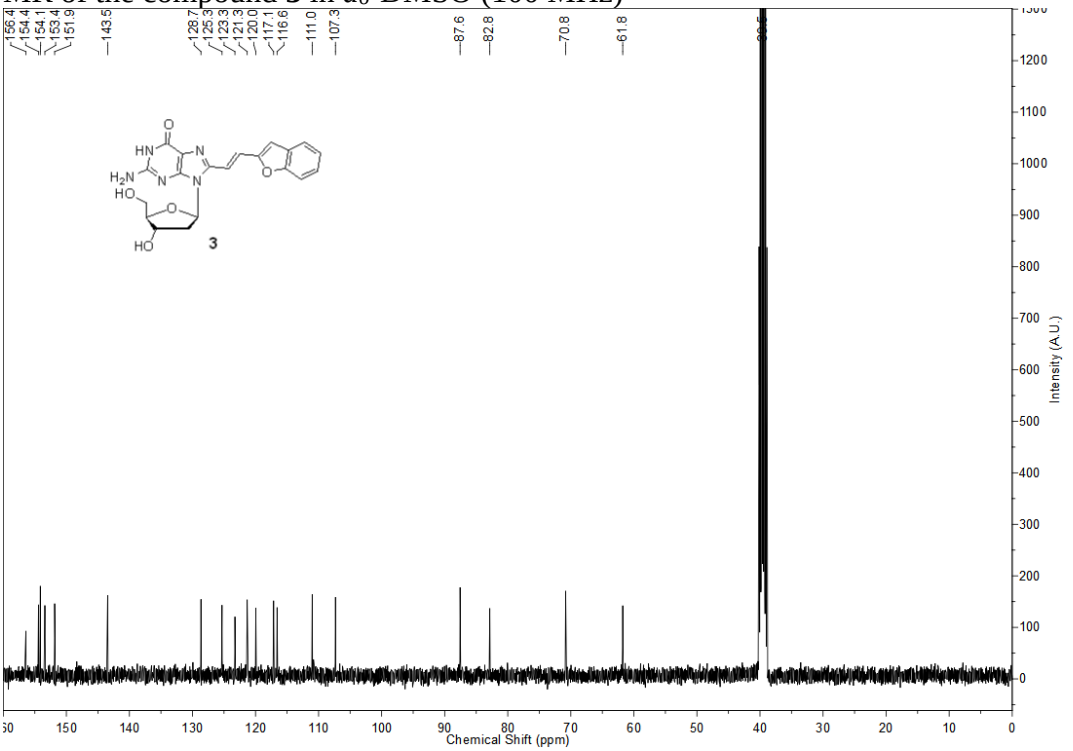

^{1}H NMR of the compound **4** in d_6-DMSO (400 MHz)

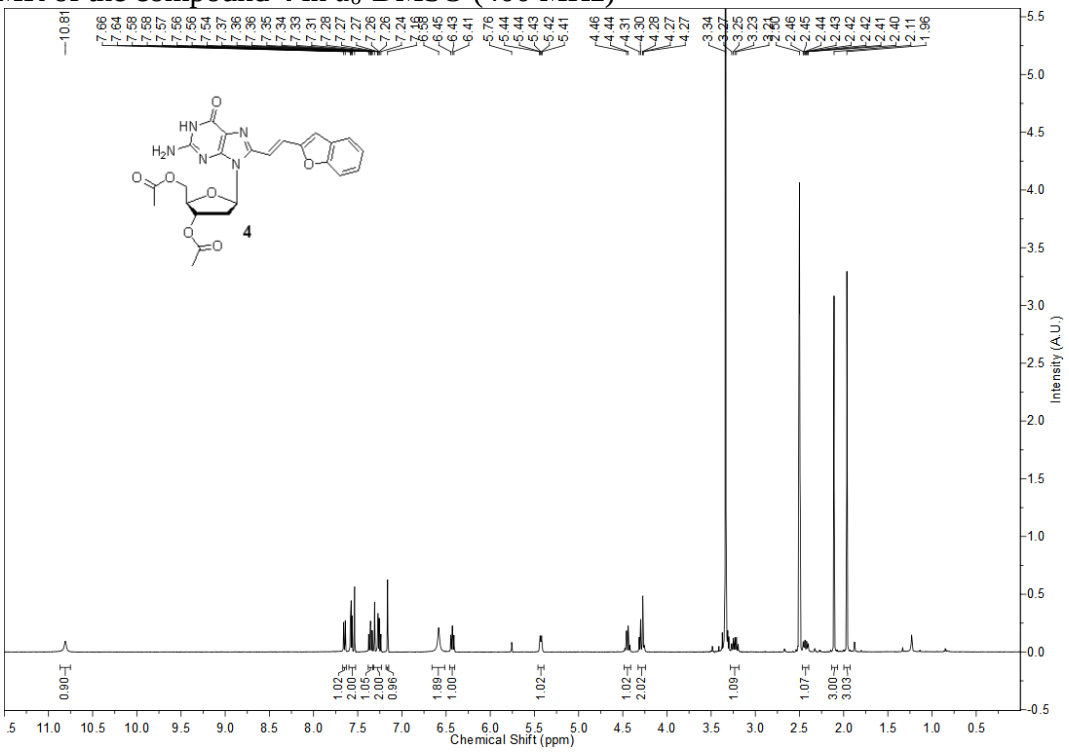

^{13}C NMR of the compound **4** in d_6-DMSO (100 MHz)

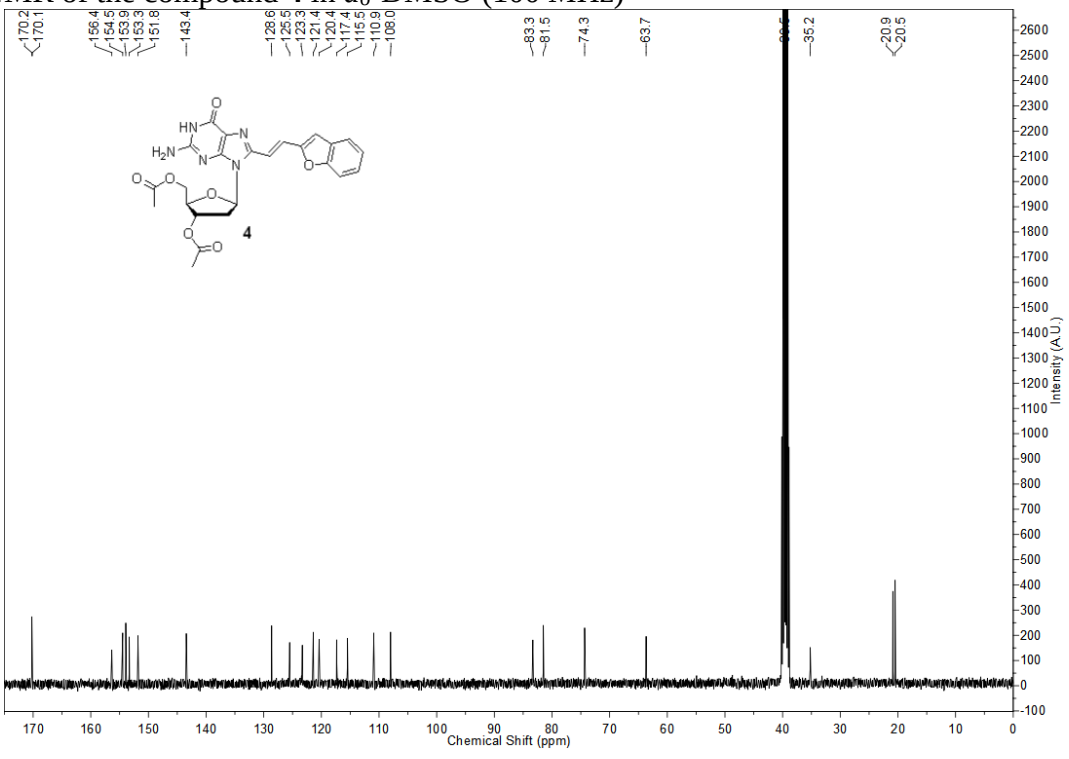

^{1}H NMR of the compound **5** in $CDCl_3$ (400 MHz)

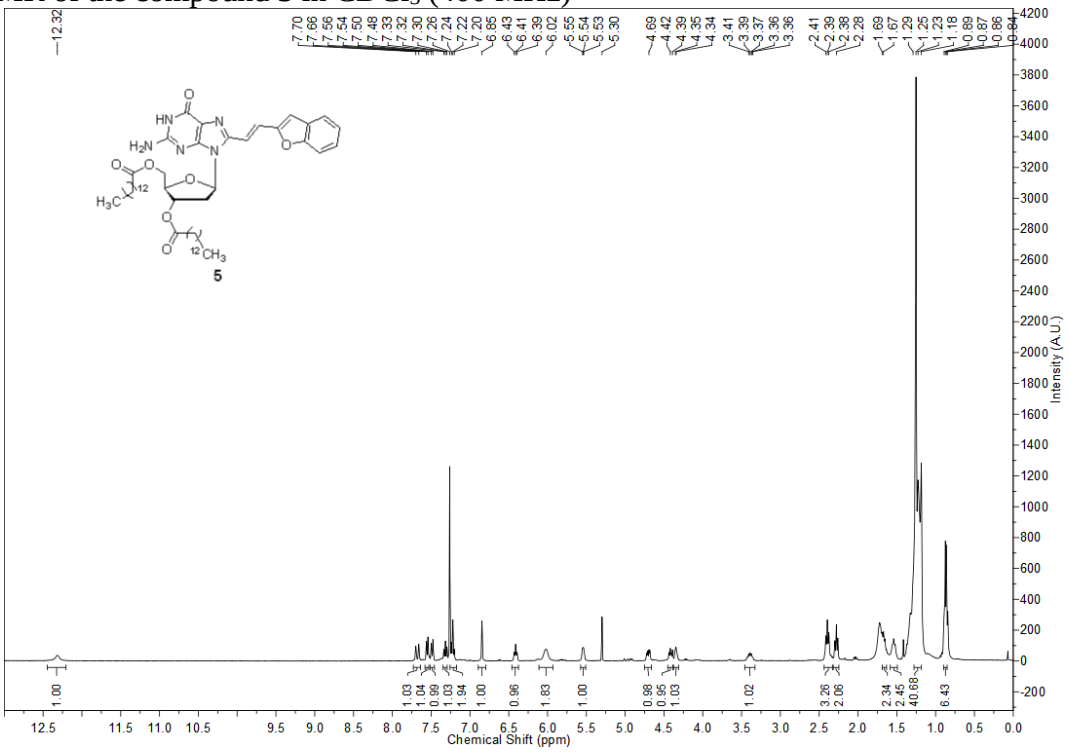

^{13}C NMR of the compound **5** $CDCl_3$ (100 MHz)

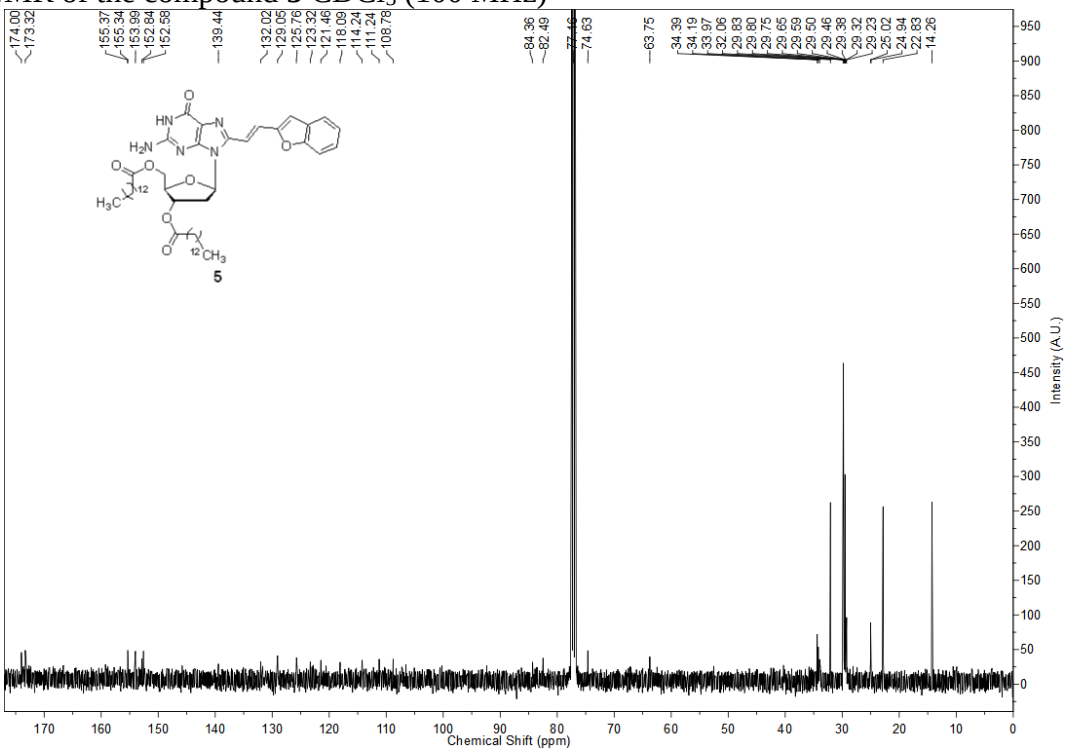

^{1}H NMR of the compound **6** in $CDCl_3$ containing 0.03% (v/v) TMS (400 MHz)

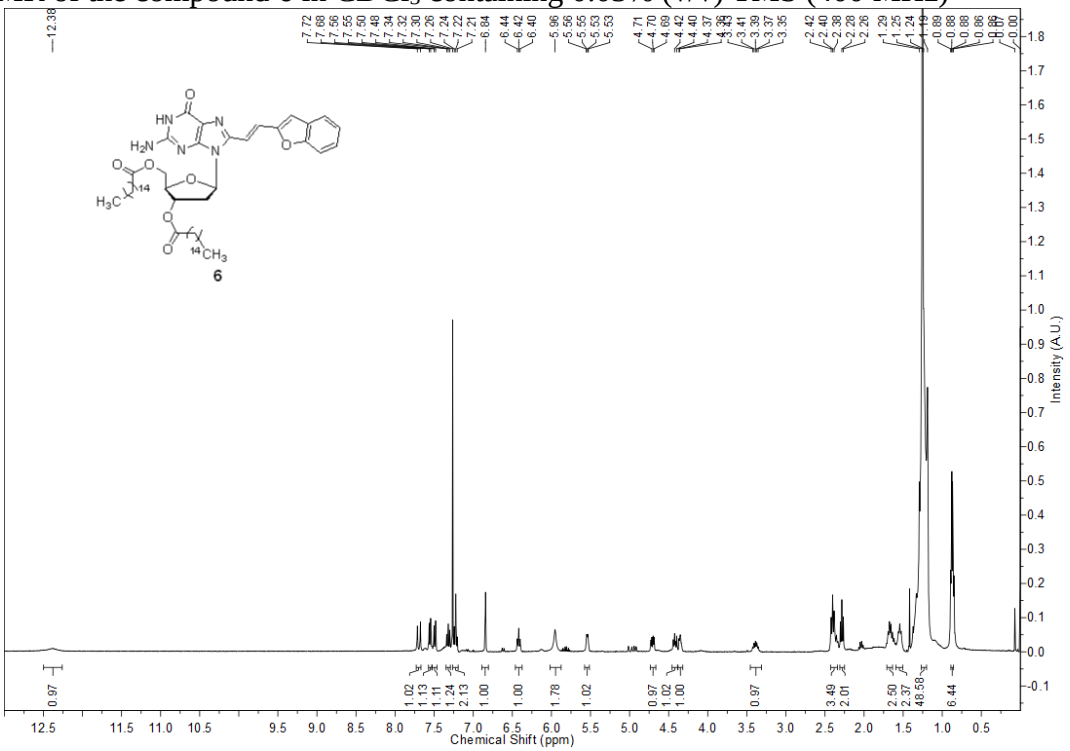

^{13}C NMR of the compound **6** in $CDCl_3$ containing 0.03% (v/v) TMS (100 MHz)

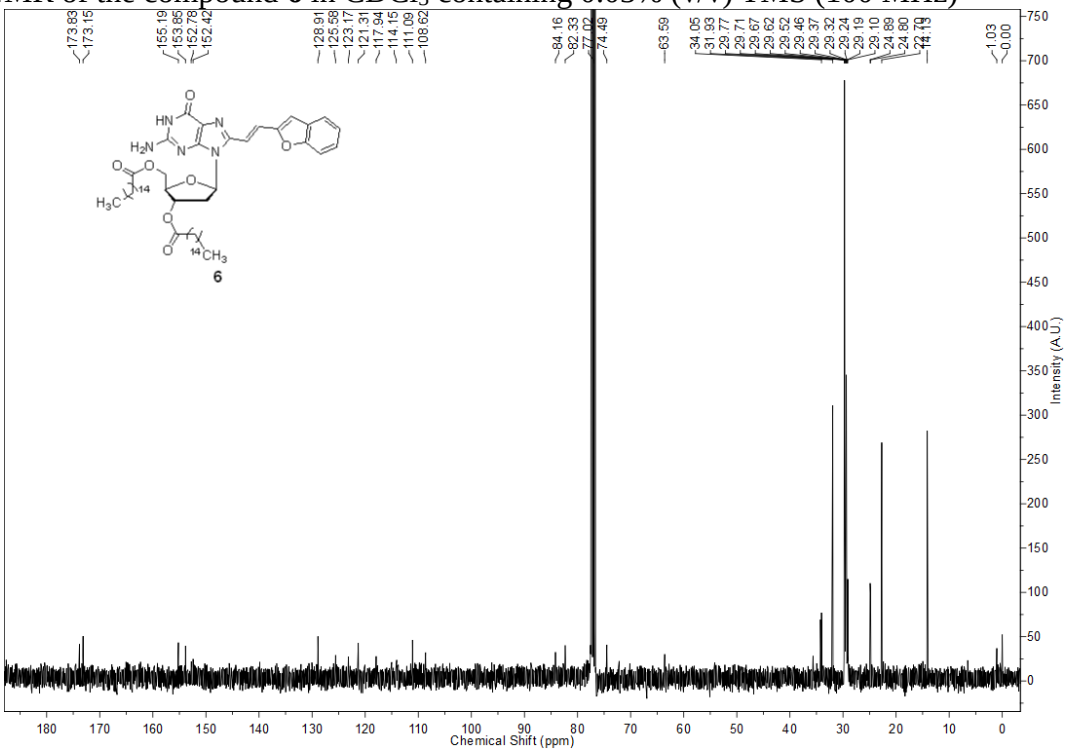

^{1}H NMR of the compound **8** in d_6-DMSO (400 MHz)

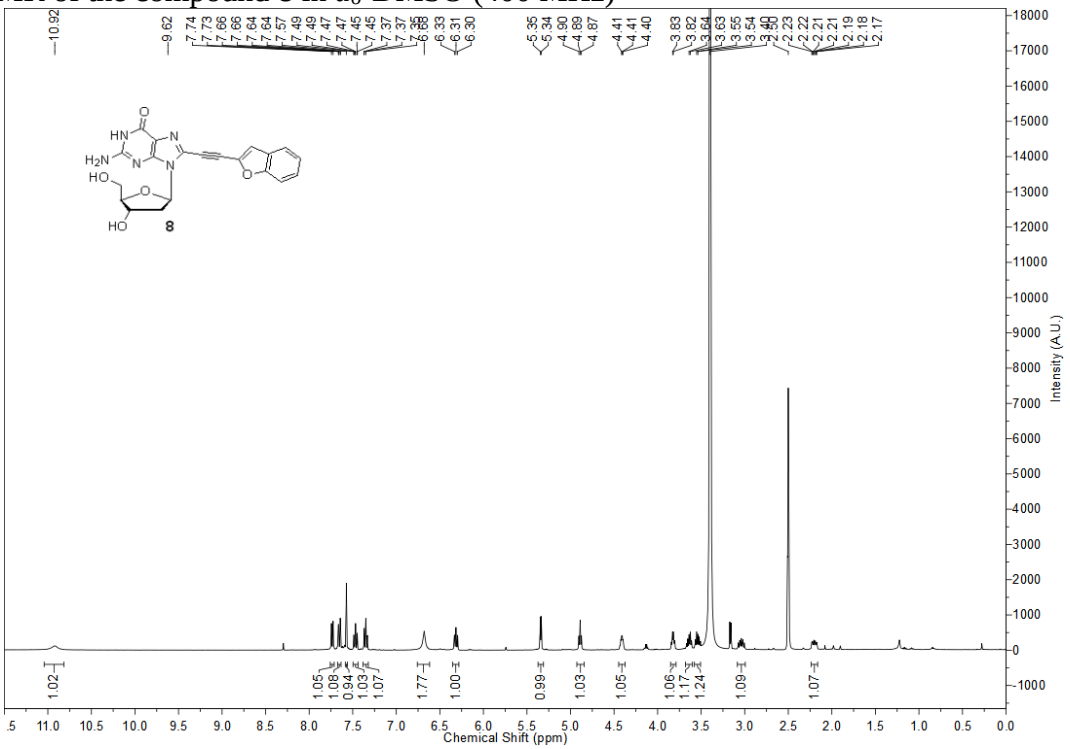

^{13}C NMR of the compound **8** in d_6-DMSO (100 MHz)

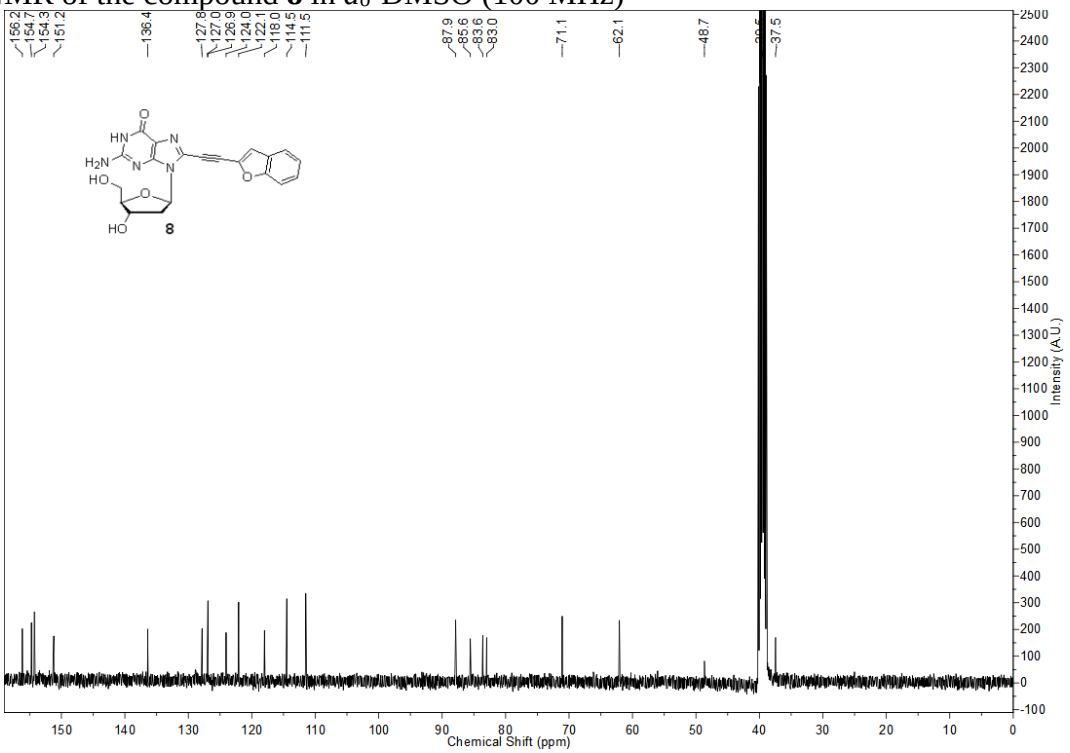

^{1}H NMR of the compound **9** in d_6-DMSO (400 MHz). Peak at 8.32 ppm is for $CHCl_3$.

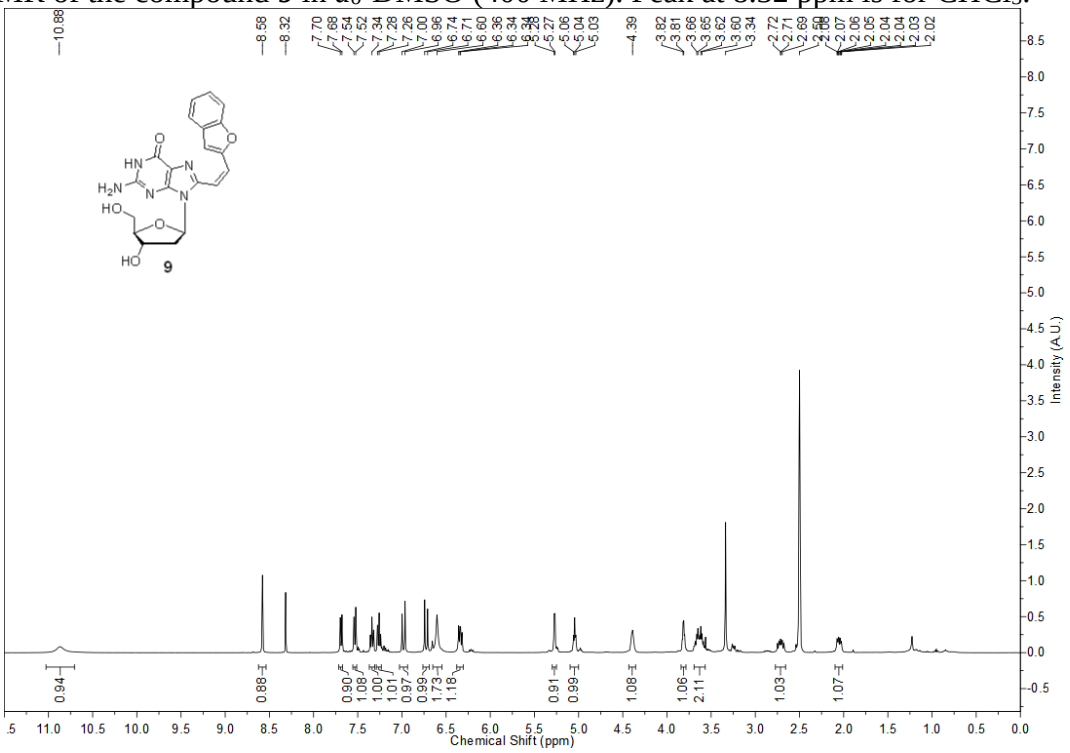

^{13}C NMR of the compound **9** in d_6-DMSO (100 MHz). Peak at 79.17 ppm is for $CHCl_3$.

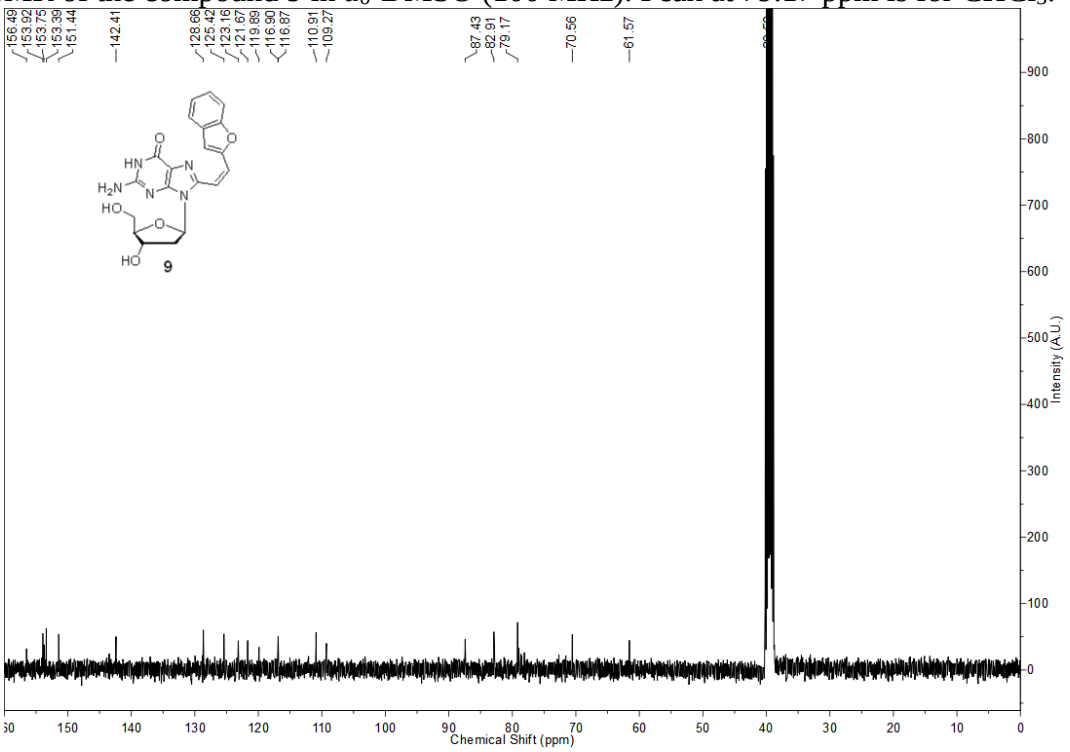

2D NOESY spectra for compound **3** in d_6-DMSO. Mixing time = 300 ms.

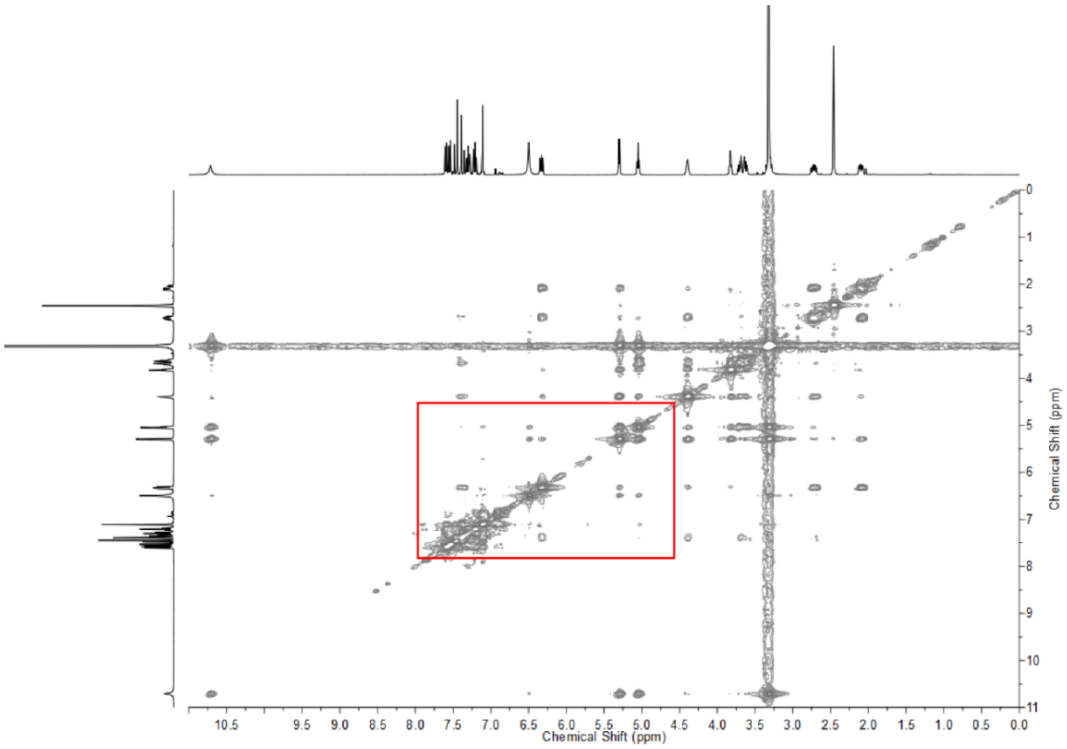

Zoomed in spectrum from boxed region

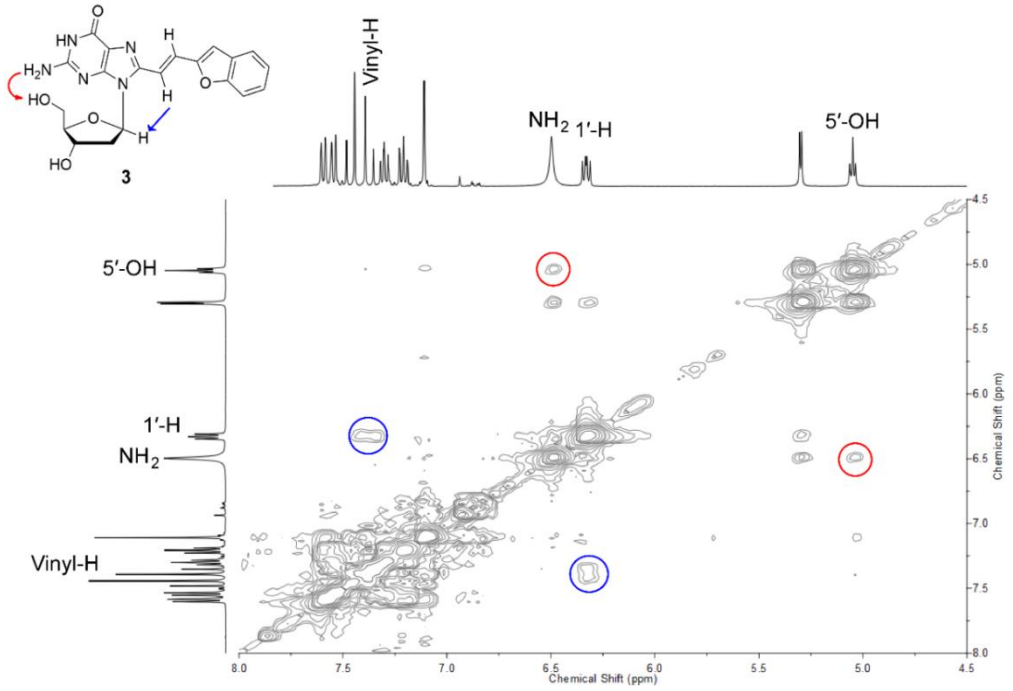

2D NOESY spectra for compound **4** in d_6-DMSO. Mixing time = 300 ms.

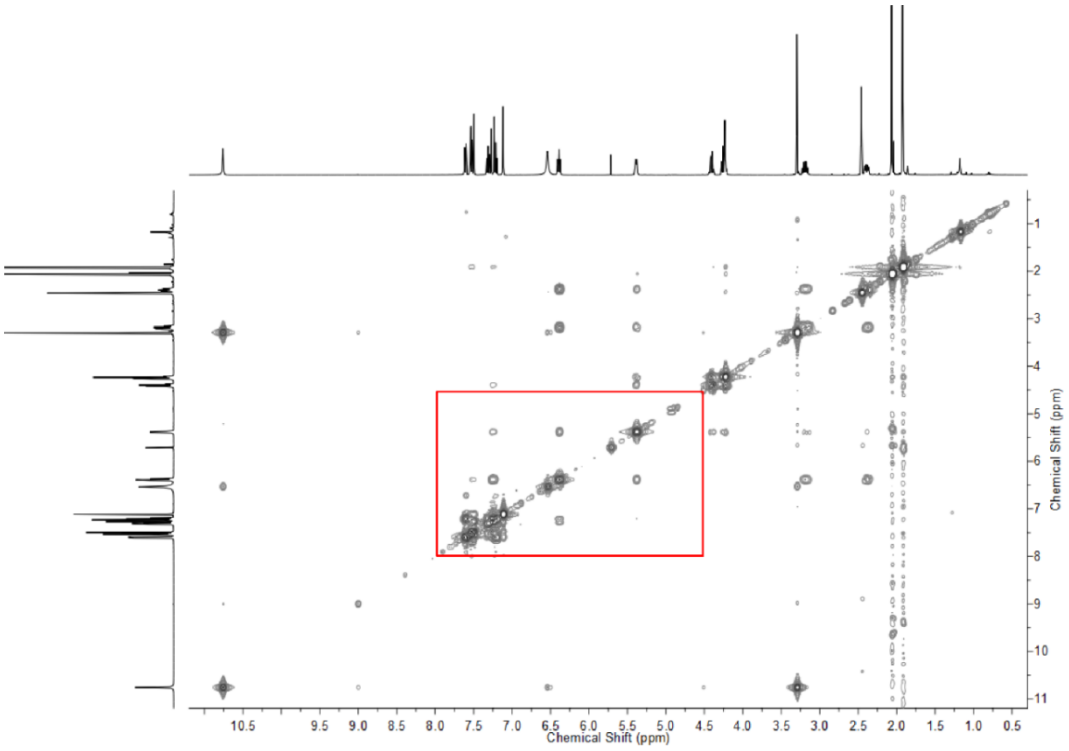

Zoomed in spectrum from boxed region.

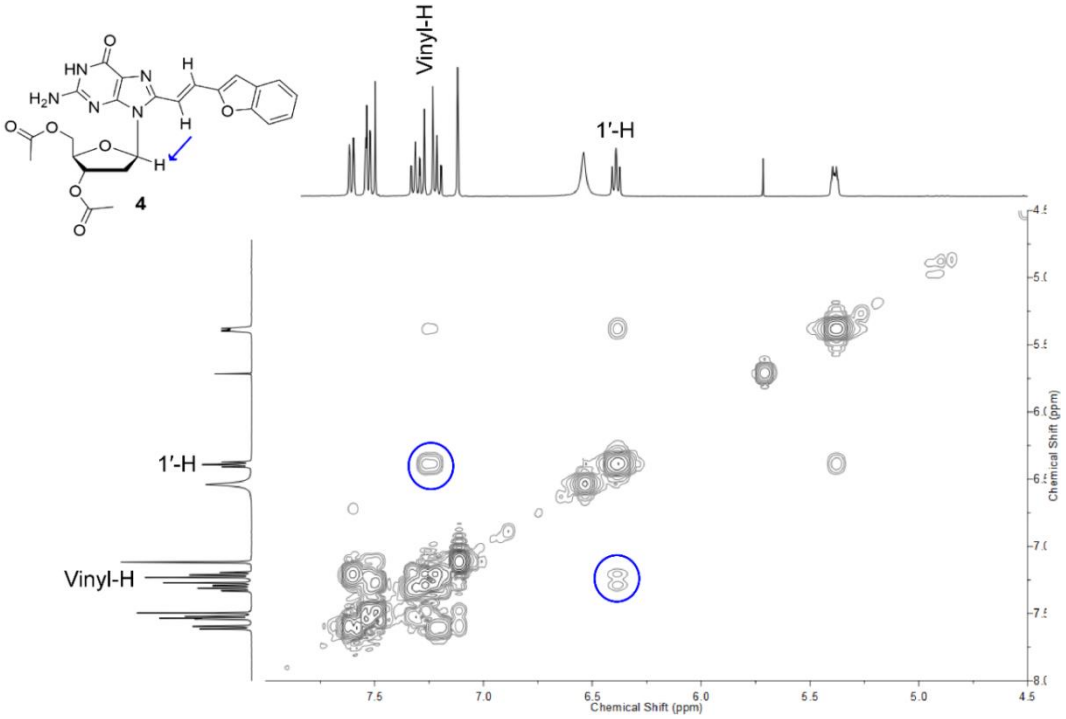

2D NOESY spectra for compound **9** in d_6-DMSO (2.5 ppm) 300 ms.

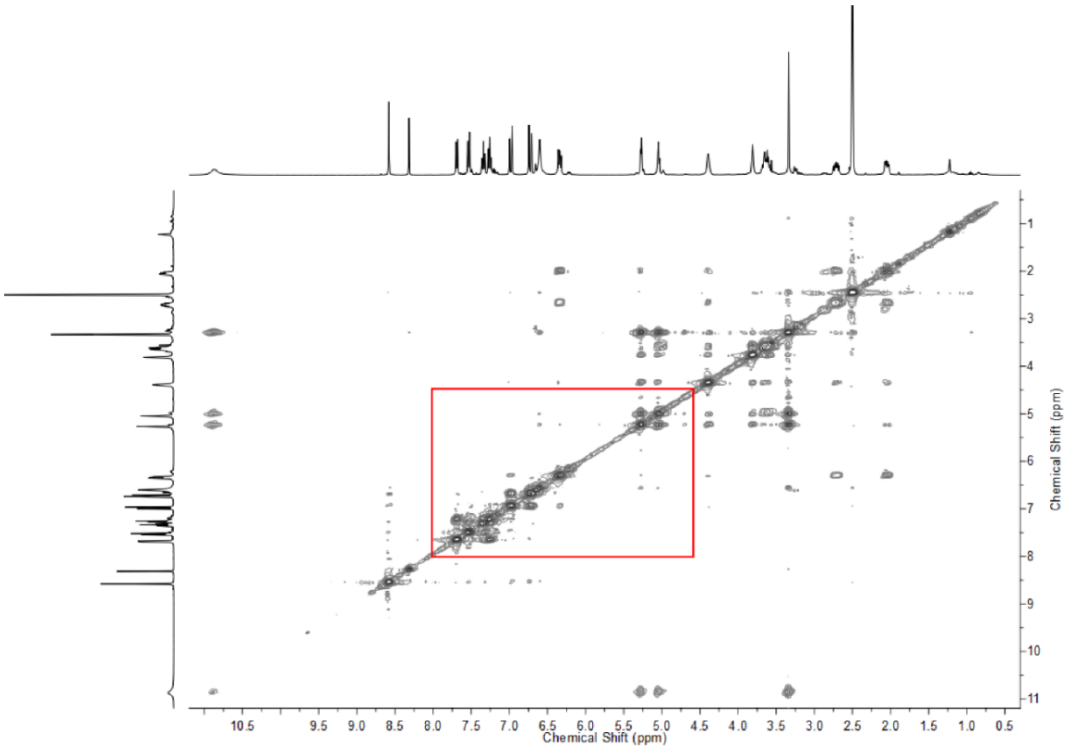

Zoomed in spectrum from boxed region.

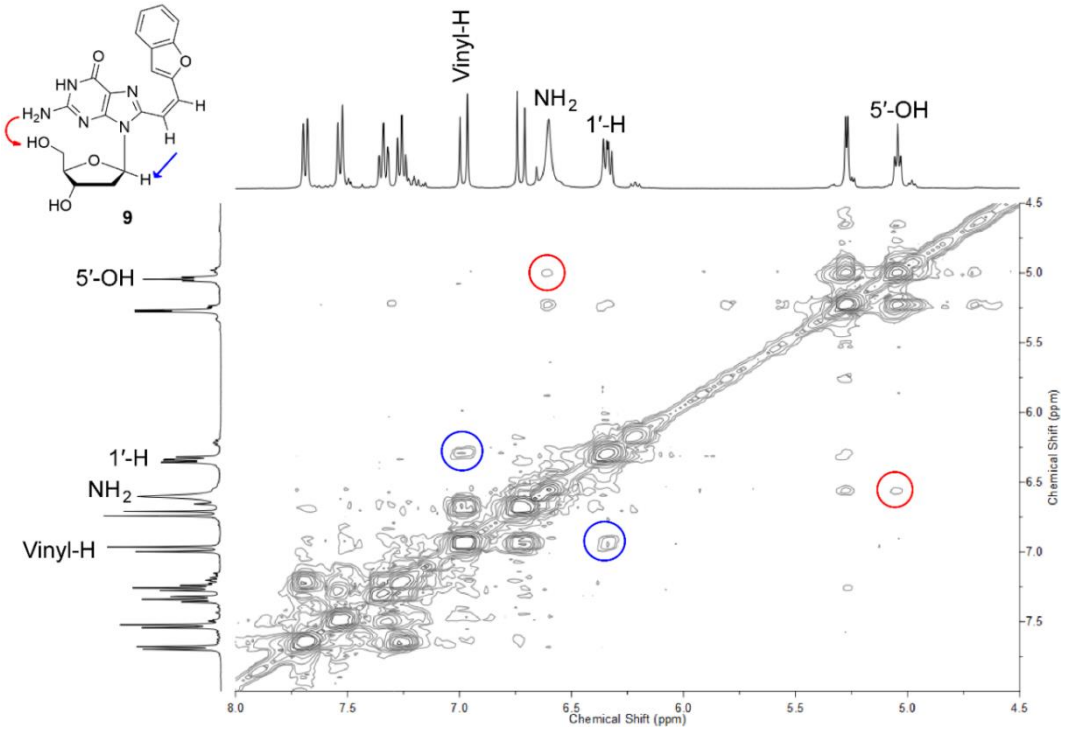

Final Conclusions and Outlook

In this doctoral dissertation, we have developed palladium-mediated cross-coupling reactions for postsynthetic modification of nucleic acids and generation of fluorescent nucleoside supramolecular synthons. We demonstrated the incorporation of iodo group into RNA transcript by means of *in vitro* transcription reaction followed by Pd-mediated posttranscriptional Suzuki–Miyaura cross-coupling reaction to label RNA with various biophysical probes. This method is highly chemoselective and enabled the direct access of RNA oligonucleotides labeled with commonly used fluorescent and affinity tags and new fluorogenic environment-sensitive nucleoside probes in a ligand-controlled stereoselective fashion. Further, we explored the influence of nucleic acid conformations on the Suzuki–Miyaura cross-coupling reaction using polymorphic G-quadruplex forming sequences as the study model. We observed that the cross-coupling reaction works in a conformation-dependent manner and conformational selectivity of the reaction decreased in the order of – GQ topology > single-stranded DNA and no reaction with double-stranded DNA. This developed postsynthetic Pd-mediated cross-coupling is versatile and provides an access to attach vast number of fluorescent probes to generate a fluorogenic nucleic acid *via* direct C-C bond formation. This power of Pd-mediated chemistry to generate a fluorogenic nucleic acid could be potentially used in fluorescent labeling of nucleic acid *in vivo* with background-free signal. Also, we are currently in the process of studying the effect of different conformations of RNA on postsynthetic Suzuki reaction.

Along the same line, we have used Pd-mediated cross-coupling reaction to develop environment-sensitive fluorescent deoxyguanosine nucleolipids. We demonstrated how the variations in the aliphatic chain length attached to 3′ and 5′ hydroxyl groups of the sugar residue could serve two purpose in guanine-based self-assembly process. Attaching acetyl moiety to the hydroxyl group, hinders the crystallization process of guanosine gel, which results to the formation of thermodynamically stable gel. While, myristoyl and palmitoyl containing fluorescent nucleolipids supports the organogel formation and show interesting chemo- and thermo-responsive behaviour upon self-assembling.

Taken together, our results demonstrate that appropriately tailored nucleosides can serve as useful tools in establishing new postsynthetic nucleic acid labeling technology and develop fluorescent supramolecular assemblies exhibiting unique properties.